The Use of Sol-Gel Technology for Adhesive and Structural Durability Applications

Mousa. M PhD 2010

The use of sol-gel technology for adhesive and structural durability applications

Mousa May

A thesis submitted in partial fulfilment of the requirements of
Sheffield Hallam University
for the degree of Doctor of Philosophy

August 2010

Abstract

The use of adhesives for joining metallic and non-metallic substrates is widely accepted in various structural engineering applications, such as aerospace, automobiles. In order to meet the industry requirements, the ability to achieve good mechanical properties under a wide variety of conditions should be considered. A major advantage of adhesive bonding over conventional mechanical fastening such as bolts and rivets is that it enables dissimilar materials to be joined. However, these materials (i.e. cured epoxy resins) are brittle and have poor resistance to cracks which indicate low capability to absorb the external energy therefore limiting their application in fields requiring high adhesive and impact strength. The incorporation of secondary components or modifiers into the epoxy system can overcome these issues. Sol-gel technology is finding increasing applications, for example, as hydrophobic self-cleaning and decorative colour coatings, formation of low-temperature cure high purity optical components and biomedical applications. The basic advantage of the sol-gel process is its ability to form inorganic structures and hybrid organic and inorganic network structures at relatively low temperatures using conventional coating techniques such as dip coat, spin coat or spraying. The present work is based upon the use of sol-gel technology to produce an adhesive which can be used to bond aluminum 2024-T3 and mild steel substrates. A novel adhesive material is produced from the combination of a hybrid silica sol-gel system, nano-inorganic particles and an epoxy polymer. The adhesive strength was investigated using a universal tensile test machine. The percentage of the bond strength of the material formed through the hybrid silica-base sol-gel is found to be related to the condensation reaction of sol-gel or via a formation of Si-O-Si networks in the adhesive. The effects of adding different concentrations of organic and inorganic materials on sol-gel adhesive strength were studied. For example, by doping a DGEBA epoxy resin, TiO_2, γ-Al_2O_3, MWCNT and mixture of PANI and γ-Al_2O_3 into the sol-gel, an increase in bond strength via the enhancement of the cross-linking among a hybrid sol-gel system was observed. The effects of cure process were investigated and it was observed that an increase in cure temperature/time led to an increase of the adhesive strength. In addition, the adhesive strength was increased as the specimen surface roughness increased due to a mechanical keying effect. Lap shear strength was also increased as bond geometry of the joint increased. The strength of the sol-gel adhesive joint has found to decrease on increasing the test temperature, being related to a softening of the sol-gel adhesive. Furthermore the adhesive strength decreased as the immersion time in 3.5%NaCl increased as a result of water absorption and the formation of corrosion products along the interfacial bond line. A study of sol-gel adhesive performance subjected to cyclic loading showed fatigue behaviour, as reported in the literature, notably increasing fatigue life with decreasing fatigue load. No significant effects in the fatigue behaviour of the lap joints were noted for different loading frequencies. FTIR, Raman and XPS analysis confirmed that improvements in the strength of the hybrid epoxy/sol-gel materials were related to the formation of different covalent bonds in the adhesive matrix, i.e. Si-O-Si, Si-O-Al and Si-O-C.

Acknowledgments

Foremost, I would like to express my most sincere appreciation and gratitude to my supervisor Prof. R. Akid to whom I am deeply indebted. I offer my special thanks to Dr H. Wang for his support and cooperation. I would also like to thank Dr. D. Greenfield for his invaluable advice.

I furthermore wish to extend my appreciation to M. Ward and A. Walton at the University of Leeds for their help and hospitality during support with TEM and XPS analysis.

I wish to express my sincere feelings to my laboratory and Office mates for their help at various stages of my work and for keeping a congenial atmosphere during my stay in the department.

Above all, I wish to acknowledge from the depth of my heart the untiring sacrifices made by my family to achieve the highest degree in the field of education.

My special thanks go to my wife Asma and children, Heba and Mohammed, for their love, patience, support and encouragement.

Last, but not least, the Libyan Higher Education Committee is acknowledged for sponsoring me to join the Sheffield Hallam University.

Advanced studies

As part of the course of study I attended the following conferences and taught lectures

Conferences;

1- 43rd Conference on Adhesion & Adhesives – Automotive and Aerospace Applications, Oxford Brookes University, Wheatley Campus – 4 July '07.

2- The UK Corrosion conference and Corrosion Science Symposium, Sheffield Hallam University, 3-5 Sep 2007.

3- 8th International conference on Multiaxial Fatigue and Fracture, 10-14 June 2007, Sheffield, UK.

Taught lecture:

Prof J. Atkinson, "Fracture and fatigue".
School of engineering, Sheffield Hallam University.

Papers published and preparation:

1- M. May, H. Wang and R. Akid, "Effects of inorganic nanoparticles on the adhesive strength of a hybrid sol-gel epoxy system". Published "International Journal of Adhesion and Adhesives". International Journal of Adhesion & Adhesives, 30 (2010) 505–512.

2- M. May, H. Wang and R. Akid, "Assessment an adhesive strength of hybrid sol-gel materials on Al2024-T3 substrates". In preparation.

Table of contents

List of Abbreviations

AA	Aluminium Alloy
MS	Mild steel
S1#	Silica-base sol-gel
SG	Sol-gel material
SG/Al	Sol-gel on aluminium substrate
SG/MS	Sol-gel on mild steel substrate
TEOS	Tetraethoxysilane
MTMS	Methyltrimethoxysilane
SiO_2	Silicon dioxide
PANI	Polyaniline
γ-Al_2O_3	Gamma alumina
TiO_2	Titanium dioxide
CNTs	Carbon nano-tubes
MWCNTs	Multi-walled carbon nano-tubes
DGEBA	Diglycidyl ether of bisphenol-A resin
DETA	Diethylenetriamine
TETA	Triethylenetriamine
AD2#	Mixture of polyaniline and sol-gel
AD3#	Mixture of gamma alumina and sol-gel
AD4#	Mixture of titanium dioxide and sol-gel
AD5#, AD6#, AD6#	Different mixtures of gamma alumina , polyaniline and sol-gel
PE	DGEBA epoxy resin cured by adding DETA
SG1	Mixture of DGEBA and silica base sol-gel
SG2	Mixture of DGEBA, γ-Al_2O_3 and silica base sol-gel
SG3	Mixture of DGEBA, γ-Al_2O_3 , MWCNTs and silica base sol-gel
SEM	Scanning Electron Microscopy
EDX	Energy Dispersive X-ray analysis
XPS	X-Ray Photoelectron Spectroscopy
IFM	Infinite Focus Microscope
FTIR	Fourier Transformation Infrared Spectroscopy
Raman	Raman spectroscopy
TGA	Thermo-gravimetric analysis
Tg	Glass transition temperature

HT	High temperature
AD	Adhesive failure mode (interfacial)
CO	Cohesive failure mode
AD+CO	Mixed failure mode
τ	Shear strength, MPa
τ_{max}	Max shear strength, MPa
τ_y	Shear strength at yielding
σ	Tensile strength, MPa
σ_{max} , σ_{min}	Maximum and minimum stress
R	Stress ratio (σ_{min} /σ_{max})
R_a	Average surface roughness profile

List of Figures

List of Tables

CHAPTER 1 Introduction

1.1 SUBJECT OF THE THESIS

In recent years, sol-gel technology has been used in a wide variety of engineering applications such as coatings and adhesives [1,2], and is attracting greater interest due to the advantages of low temperature processing without the need for ultra low or high pressure environments to produce materials with good thermal, electrical and mechanical properties [3,4]. Many novel organic-inorganic hybrid materials have been developed via the sol-gel method in recent years, providing highly homogeneous network structures that combine both organic functional groups and an inorganic matrix. The combination of rigidity and high stability of inorganic materials with the flexibility, ductility and processibility of organic polymers is a major reason for the improvement in the mechanical performance of sol-gel materials [4]. A potential application for sol-gel coatings on metals is that of the replacement of conventional chromate anticorrosion conversion and primer coatings [5]. To form a superior anticorrosion system for the protection of the substrate would require the coating to provide excellent adhesion both to the metal and to the topcoat. For example, sol-gel methods are already also used to treat aerospace alloys (e.g. Al2024 alloys) as a pre-treatment, promoting the adhesion of the subsequent primer coating [6,7].

The use of sol-gel coatings in the optical and electronic industries for use as an intermediate layer to bond two materials has been widely studied [8] as they offer the advantage of providing an active, uniform and homogeneous bonding layer due to a strong interaction both with the substrate and the epoxy-resin-based adhesive primer [9]. However, no reports appear to have been published on the use of a sol-gel method for the modification of a hybrid silica-based sol-gel formulation to produce novel adhesives for bonding two metallic substrates.

The present work will focus on the exploration of a hybrid sol-gel method to produce novel adhesives for the bonding of metallic materials. This work will study the changes in bond strength (shear and tensile) and adhesive structure

following the modification of the hybrid sol-gel material by the addition of a variety of components into the formulation, including different inorganic nano-particles, organic polymers, and organic-inorganic combined components.

A potential advantage in using a sol-gel adhesive is that it is possible to combine the barrier anticorrosion properties with that of the adhesion pre-treatment features to the bonded metallic materials [9]. This research project has led to the successful development of a novel sol-gel/epoxy hybrid adhesive. This novel adhesive and its strength performance on Al 2024-T3 alloys and mild steels are reported in this thesis.

1.2 ADHESIVE BONDING APPLICATIONS

The significance of adhesive bonding as an alternative to riveting, bolting, or welding is increasing in many industries, e.g. automotive and aircraft, because of its numerous advantages [10], for example, low weight, homogeneous stress distribution, low cost, high corrosion resistance, ease of application and excellent thermal and insulation properties. Adhesives can be used to join many different materials including metals, composites, ceramics, films and damage-sensitive materials, singly and in combination. It has the valuable capability of joining and fabricating complicated shapes to produce a smooth aerodynamic surface that gives an improvement in corrosion and/or fatigue resistance [11]. Due to their visco-elastic properties adhesives can reduce the vibration of the bonded parts compared with conventional joining techniques. All these features have encouraged scientists to investigate the production of new adhesives.

Currently, one of the mostly widely used types of adhesive used in producing composites, coatings, and structural adhesives is an epoxy-based organic polymer, produced from the modification of epoxy resins based on diglycidylether of bisphenol-A (DGEBA). These have particularly good adhesion performance on different metallic surfaces but have some limitations on their application due to, for example the brittleness of cured bisphenol-A (DGEBA) [12]. Two general routes have been reported to improve the toughness (total energy required to cause failure in the joint) of an epoxy resin: (i) the introduction of a second phase of dispersed rubber particles into the epoxy

matrix to increase its ductile properties, and (ii) the modification of epoxy structures by introducing functional groups into the main or side chain of the epoxy resin [12,13]. Extensive research has investigated the mechanisms of the chemical reactions between the neat epoxy and the curing agent in order to form a highly cross-linked structure, and it is well known that different curing agents (hardeners) have been used to fabricate a wide class of organic polymers based on epoxy resins [14]. The modified physical and chemical properties of the cured epoxy resins, including excellent chemical and heat resistance, high adhesive strength, low shrinkage, good impact resistance, high strength, high electrical insulation, etc, are related to the chemical structures and properties of the curing agents and cure processing parameters such as temperature and duration.

1.3 AIM AND OBJECTIVES

The aim of this work is to develop a novel hybrid sol-gel adhesive and investigate the influence of formulation chemistry on the adhesive strength of bonded joints (using various modified sol-gel adhesives).

To achieve this aim, the properties of a silica-base sol-gel formulation, as an adhesive material, were modified by introducing organic and/or inorganic components into the sol-gel matrix. Several major objectives were assigned to assess the role of sol-gel chemistry on adhesive performance, including;

1) Assessment of the effect of doping inorganic nano-materials (i.e. TiO_2 and Al_2O_3) and multi-wall carbon nano-tubes (MWCNTs) into the hybrid sol-gel formulation on adhesive strength.
2) Assessment of the effects of introducing organic materials such as polyaniline, or epoxy resin, and nano-particles (Al_2O_3) and MWCNTs in the hybrid sol-gel formulation on adhesive strength.
3) Evaluation of the effect of different environmental conditions (i.e. at room and high temperatures, and under dry and wet conditions) on the bond strength of the hybrid sol-gel system using Al2024-T3 and mild steel substrates.

4) Characterisation of structure changes of the hybrid sol-gel adhesive using a Scanning Electron Microscope (SEM), Infinite Focus Microscope (IFM), Fourier Transform Infrared (FTIR), Raman spectroscopy, X-ray Photoelectron Spectroscopy (XPS) and Thermogravimetric Analysis (TGA) techniques.

1.4 ORGANISATION OF THE THESIS

The thesis is organised as follows.

Chapter 2, presents a literature review discussing various issues concerned with adhesive materials, sol-gel processes and introduces the characterisation techniques used in the experimental programme.

Chapter 3, describes the experimental work conducted to evaluate the substrate materials, surface preparation, formulation of sol-gel adhesives, mechanical tests and chemical and structural analysis.

Chapter 4, presents the results on the application of sol-gel material as a potential adhesive, including effects of sol-gel composition, cure conditions, surface roughness, bond geometry, the external environment and the hybrid epoxy/sol-gel structure.

Chapter 5, provides a discussion of the experimental results.

Chapter 6, presents the overall conclusions. The possible future work resulting from this study is given in Chapter 7.

CHAPTER TWO

2. Literature review

This chapter is divided into ten sections; section 2.1 introduces the background information on the benefit of using structural adhesives in industry to assemble engineering parts, and provides further information on adhesive manufacturing and properties. Section 2.2 introduces several theories in adhesion science. Section 2.3 provides brief information on the structure of adhesives, and 2.4 deals with adhesive joint design. The types of stress in joints and failure modes are introduced in section 2.5 and 2.6, respectively. The influence of various factors on adhesive bond strength and adhesive performance under cycling loading (fatigue), all are discussed in section 2.7 and 2.8, respectively. Sol-gel technology and its application in engineering is presented in 2.9. Finally, the last section, 2.10, deals with the characterisation techniques.

2.1 Adhesive materials

Adhesive materials are substances that have the capability of holding engineering parts together by surface attachment. This will include among others cement, glue and paste. It is well known that adhesives are used widely in manufacturing or the construction of commercial products. Consumer research within the UK in 1981 [15] revealed that 90% of the people interviewed had an adhesive available in their home; of these, 37% claimed to possess a general purpose glue.

Historically, manufactured adhesives were all made from natural products and raw materials. In the beginning of the 1700s, the first glue factory was created in Holland. At this time most adhesive materials were derived from vegetable, animal, or mineral substances. Around 1750, adhesives were first produced in Britain using fish and natural rubber [16]. By 1900, the United States had a number of factories producing glues. The industrial revolution caused a technical break-through that resulted in new materials becoming available for use in formulating adhesives. In the early-mid 1900s, the introduction of synthetic polymers allowed to the creation of a new class of adhesive materials.

During the 1920s and 1930s many new plastics and synthetically produced adhesives were produced as the technological advancements in making these materials increased [17]. Synthetic polymer chemistry offered a novel approach where epoxy resins with specific properties were made available which led to the “golden age” of adhesives beginning in the 1940’s and continuing today [18].

An uncured epoxy adhesive is a copolymer which forms from two different chemicals, the "resin" and the "hardener". The resin is a monomer or short chain polymer linked with an epoxide group at either end. The hardener is a polyamine monomer, for example Triethylenetetramine (TETA). When mixed, the amine groups react with the epoxide groups to form a covalent bond. Each NH group can react with an epoxide group, so that the resulting polymer is heavily cross linked, and is thus rigid and strong [19]. The use of polymers in producing adhesives plays an important role concerning the mechanical behaviour and durability under service conditions. Advanced technology applications of adhesives (i.e. electronics, medical device, semi-conductor and fibre optics industries) are based of the use of this copolymer material to provide good adhesive bonding.

Adhesive bonding is a general term which describes the process where an adhesive is used to join materials. The materials which are being joined are often termed substrates. The adhesive is a polymer which intimately contacts the substrate surfaces, either through chemical and/or physical forces. The chemical interactions result from atomic scale attractions between specific chemical groups of the adhesive and the substrate surface. The adhesive is a mixture of compounds which interact with the surface and each other during the bonding procedure. This process, referred to as "adhesive curing", involves the provision of energy to the adhesive system which causes a reaction of the adhesive mixture. During the early phase of the curing process the viscous adhesive will flow to enable contact with the substrates. As curing proceeds the viscous mixture becomes a rigid solid as the compounds react and cohesively link the adhesive, often referred to as cross-linking. This process enables strength to be established between the joint surfaces [20]. The significance of adhesive bonding as structure-joining technology is increasing because of its

numerous advantages compared with other methods. It offers two major benefits over mechanical bonding notably improved fatigue resistance and significant weight savings. Industry examples include aircraft structures, bridge construction and electrical and electronic applications. Moreover, adhesive joints present a homogeneous stress distribution, high corrosion resistance, easy application, and low cost [21].

2.2 Theories of Adhesion

Several adhesive theories have been developed to explain the process of bonding in adhesive structures (i.e. mechanical interlocking, diffusion, electronic, chemical bonding and adsorption). Each of these theories alone is inadequate to describe the complete process of bonding in most situations.

2.2.1 Mechanical interlocking

This theory states that mechanical keying, or interlocking of the adhesive into the irregularities surface of the substrate is the major source of intrinsic adhesion, see Figure 2.1. The adhesion usually depends on the roughness and the wetting behaviour of adhesive to the surface [22]. The surface tension of the adhesive should be similar or less than that of the substrate to achieve good adhesive bonding. Pre-treatment methods applied to surfaces may result in micro-roughness features on the substrate surface, which can improve bond strength and durability by providing mechanical interlocking.

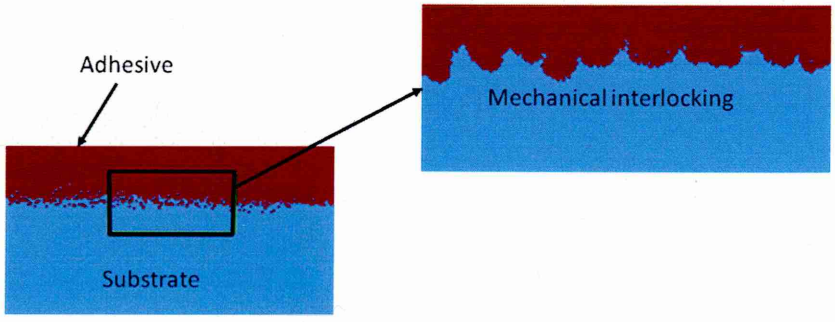

Figure 2.1 Mechanical interlocking at the interface

2.2.2 Diffusion theory

The diffusion theory of adhesion was promoted in the early 1960s by Voyustskii [23]. It suggests that the intrinsic adhesion of polymers to themselves is due to a mutual diffusion of molecules across the interface, see Figure 2.2. This can be viewed as a molecular interlock enabled adhesion. The adhesion will arise through the interdiffusion of the adherent (substrate) and adhesive. This theory is applicable only for polymers above the glass transition temperature (T_g), where the materials are more mobile. Other factors such as molecular weight of polymers, crystallinity and contact time should be considered. For example, the bonding behaviour in rubbery polymers when two surfaces coated with contact adhesives and pressed together, the interdiffusion takes place as a solvent evaporated. One application that exploits this mechanism is in the construction of plastic models.

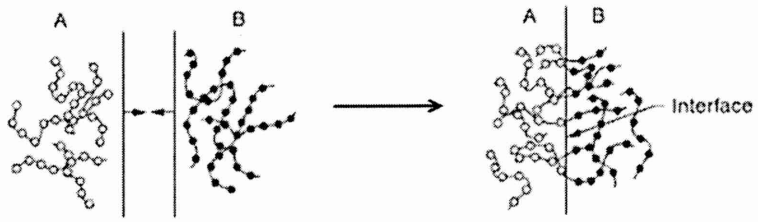

Figure 2.2 Schematic showing Inter-diffusion of polymer molecules cross the interface [23]

2.2.3 Electronic theory

This theory states that adhesion is developed through the adhesive/substrate interface due to electrostatic effects. If the adhesive and substrate have different electronic band structures, there is likely to be some electron transfer between two surfaces. The behaviour will result in the formation of a double layer of electrical charge at the interface, see Figure 2.3. Therefore, the electrostatic forces arising from such contact may contribute to the intrinsic adhesion [24].

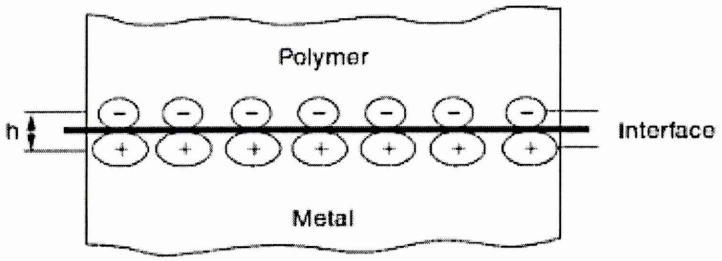

Figure 2.3 Schematic showing the electrical double layer at polymer/metal interface [24]

2.2.4 Adsorption theory

The bonding process in this theory occurs when adhesive molecules adsorb upon a solid surface and chemically react with it. It represents the most accepted general theory for explaining in the bonding mechanism. It has been demonstrated [25] that, the phenomena can be divided into two separate types: physical adsorption (or physisorption) and chemical adsorption (chemisorption or activated adsorption). The attraction forces resulting across the adhesive/substrate interface usually control the strength of a bonded joint. The forces that are involved are those that act between atoms and molecules within the material structure. The adhesive strength in this theory is attributed to the action of London dispersion forces [25], and in many instances, these are combined with contributions from other forces (dipolar, polar or primary bonding). Table 2.1 illustrates different bond types with some of their major characteristics.

Table 2.1 Bond types [24]

Bond type	Bond energy, kJ mole^{-1}	Equilibrium length nm
Primary, chemical		
Ionic	600 - 1000	0.2- 0.4
Covalent	60 - 800	0.1 -0.3
Metallic	100 - 350	0.2 - 0.6
Acid-base interactions		
Conventional Bronsted **Lewis**	< 1000 < 80	

Secondary, physical		
Hydrogen	~ 50	0.3
Van der Waals		
Dipole interactions	5 - 20	0.4
London, dispersion	1- 40	<1

In addition, the process depends on the achievement of good contact between the adhesive and substrate surface (wetting), which enhances the inter-molecular forces at the interface. For example, poor wetability results when the adhesive bridges over the surface due to the presence of solvent, air trapped and/or bubbles, which prevent full contact within the interface regions. However, good wetting results when the adhesive flows into valleys and crevices on the substrate surface, see Figure 2.4.

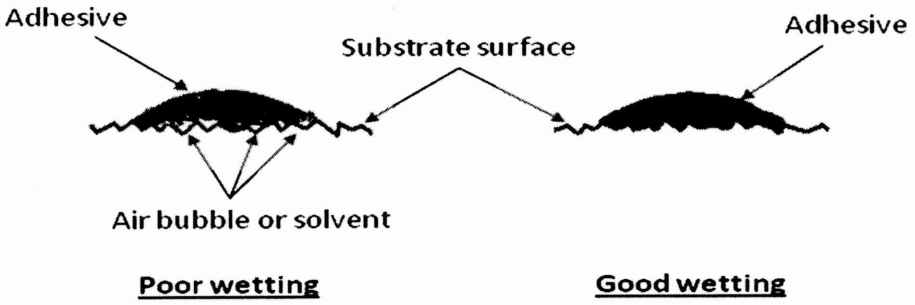

Figure 2.4 Illustration of poor and good wetting by an adhesive spreading over a surface [24]

2.3 The adhesive structures

The formation of strong and durable adhesive joints depends on complex physical and chemical phenomena. The Primary Adhesively Bonded Structure Technology (PABST) program has established that appropriate adhesive selection and the careful attention to the treatment of metal surfaces for bonding are both critical to the joint strength and long term environment durability [26]. The adhesives are normally produced from complex formulations of components that perform specially functions, and very few polymers used in producing adhesives without the addition of modified substances such as plasticiser, or fillers. Therefore, adhesive can be classified as structural or non-structural adhesives. The structural applications are adhesively bonded joints

expected to provide high strength or performance. These materials are generally formulated from thermosetting resins that are chemically cross-linked, either with the addition of a curing agent, heat, or other activators [25]. Non-structural adhesives are those requiring only low strength and durability. Epoxy structural adhesives are available in single or multi components, which may cure at either room or elevated temperatures. Epoxy molecular weight, the nature of the molecules between cross-links and the degree of cross-linking are factors that determine cohesive strength, see Figure 2.5.

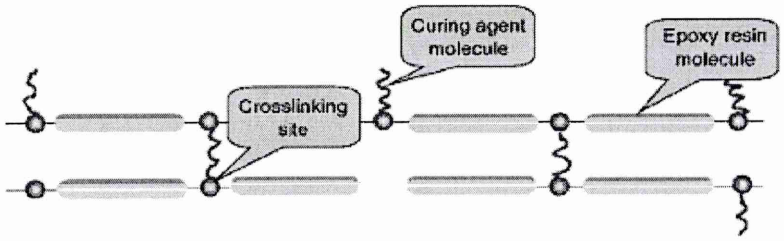

Figure 2.5 Schematic showing cured epoxy molecules [25]

Moreover, most of the epoxy formulations are formed on the use of the diglycidyl ether of bisphenol A (DGEBA) as the base epoxy resin [27]. It can be fabricated by using different chemical compounds to open the epoxy ring and set the epoxy monomers. Therefore, epoxies can undergo various chemical reactions, as shown in Figure 2.6. The amines or polyamides, present as curing agents, are used for room temperature systems, whereas anhydrides require elevated temperature curing.

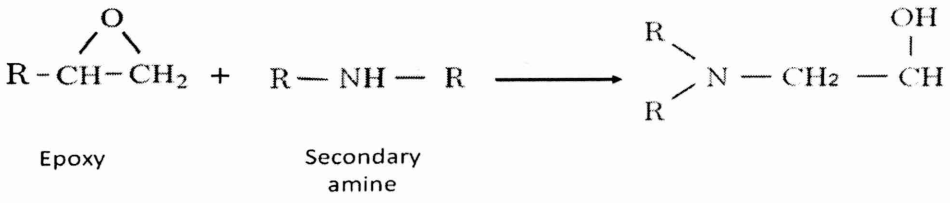

a) Epoxy/amine reaction

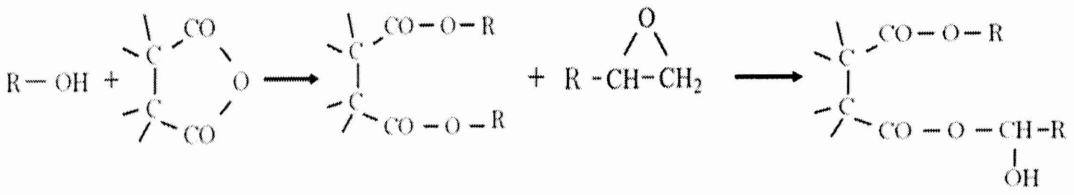

Alcohol Anhydride

b) Epoxy/anhydride reaction

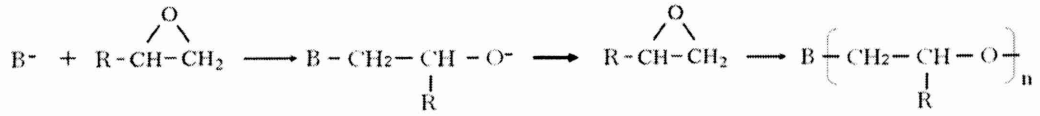

Anion **Epoxy**

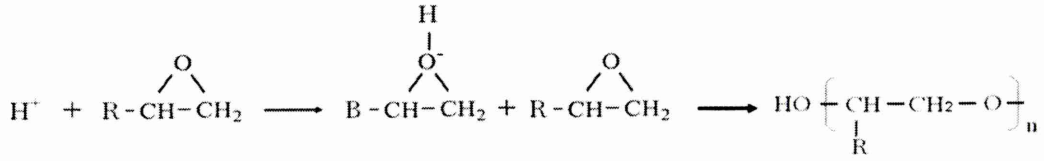

Cati **Epoxy**

C) Epoxy ring - Opening polymerization

Figure 2.6 Illustration showing common epoxy reaction mechanisms [26]

2.3.1 Adhesive toughening

The term toughening is defined as the ability of an adhesive to absorb energy without catastrophic failure (resistance to fracture). This means an enhancement of the adhesive properties, such as the impact strength. Epoxy resins have been used as adhesives since the 1950s due to their good wettability. However, when these materials are cured with stoichiometric amounts of amines, the increased degree of crosslinking makes the epoxy resin brittle. The fracture energy of these materials is low compared with that of metals (by a factor of three) or other engineering thermoplastic materials (by a factor of two) [28]. This lack of toughness causes a weakening of the peel and impact strength of epoxies and therefore limits their applications. Various approaches were developed to improve adhesive toughness, for example; common methods used to toughen adhesives include the blending of primary

resins with other polymers; such as thermoplastics or elastomers. The incorporation of thermoplastic polymers into the epoxy resin forms a crystalline structure when cooled below a certain temperature (notably the Tg), resulting in significant adhesive structural strength [29]. However, as temperature is increased, the materials tend to be elastic and gradually soften, eventually melting. Thus, thermoplastic adhesives have a limited operating temperature range and often tend to deform under load (creep) as temperature increases. The linear polymers (elastomers) which show "rubbery" behaviour provide a major improvement in toughness over a pure epoxy formulation. The cross-linked network of rubber particles, as the dispersed phase within the epoxy matrix, results in a new copolymer structure having different peel and impact strength depending on the adhesive type. For example, carboxy-terminated butadiene-acrylonitrile (CTBN) as elastomeric modified epoxy resins have improved the material crosslink density and plastic deformation by a factor of three compared with that of the unmodified matrix [30]. In addition, the incorporation of rubbers or thermoplastics into the epoxy matrix, can result in reductions of basic mechanical properties, such as a decrease in strength and modulus. Bascom et al. [31] revealed that fracture energy was increased significantly up to approximately 30 times that of the unmodified epoxy, with an increase in the volume fraction of rubber content from 4.5 to 20%. At the same time the tensile strength and tensile modulus decreased drastically in a linear relationship with the amount of rubber added to the epoxy system. Due to the poor compatibility and processability between the thermoplastic modifier and the epoxy resin, the improvement in fracture toughness by thermoplastic polymers, in some cases, was not achieved [32].

2.3.1.1 Inorganic and performed particles modifiers

Inorganic fillers have been considered as toughening agents for epoxy materials. Due to their small dimension, larger specific surface area, higher surface energy, greater proportion of atoms at the surface and better surface reaction, inorganic particles play an important role in modifying epoxy resins [33]. However, theses materials (particularly nano-size silica particles) can limit the improvement in epoxy properties as they tend to agglomerate within the epoxy resin matrix due to their highly hydrophilic surface properties leading to low dispersion of the

particles [34]. The introduction of an optimum amount of inorganic filler into the epoxy system is required in order to achieve good interaction and reduced the agglomeration within the structure. As the inorganic particles tend to agglomerate, techniques have developed and used to achieve a homogeneous particle distribution, these include; mechanical mixing using high shear forces and ultrasonic vibration. Chemical methods have also been used such as sol-gel processing to obtain nano-silica particles, in which the nano-particles are commonly formed in situ during a sol-gel synthesis and thus a homogenous dispersion can achieved. Inorganic materials such as silica or alumina nano-particles, incorporated via the sol-gel process, can noticeably improve fracture toughness and other mechanical properties of epoxies at both ambient and cryogenic temperatures.

2.4 Adhesive Joint design

The mechanical performance of the adhesive bond can be measured in a variety of ways as the maximum stress (adhesive strength) that the joint can attain before failure. Various types of loads arise in adhesive joints depending on the joint geometry and the direction of loading. The nature of stresses within the joint (i.e. shear, tensile, cleavage and peel) should be considered. Also, all of the bonded area should equally share the applied load. The following structural joints illustrate some typical designs.

2.4.1 Lap joint

Single lap joints loaded in tension are the most common joint design employed in industry and this type of joint configuration provided a convenient test for evaluating the adhesive strength. The lap joint is prepared from two plates of substrate joined by a simple overlay. For structural joint performance, the load in one substrate should be transfered through the adhesive layer to the other joint component. The strength of a lap joint is generally based on the length and width of an overlap (bonded area), higher strengths being achieved by larger bond surface areas. Lap joints or lap combinations can be fabricated as, either a single or double lap joint, as shown in Figure 2.7.

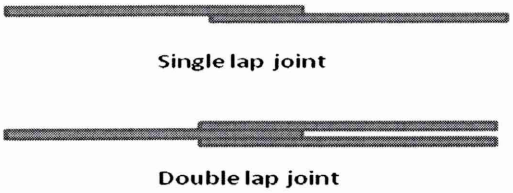

Figure 2.7 lap joints geometry

2.4.2 Butt joint

Butt joint specimens are widely used for testing the response of adhesives to shear, tensile and compressive stresses. They provide a convenient means for determining the mechanical properties of structural adhesives [35]. The joint consists of two cylindrical, or sometimes square shape sections, bonded together at the end faces and pulled by forces acting along the axis of the joint, see Figure 2.8. The achievement of a strong adhesive bond in this joint is based on the sample preparation (particularly the joint alignment). However, it has been recognised that there are significant stress concentrations at the edge of the butt joint, which limit the strength of the joint [36].

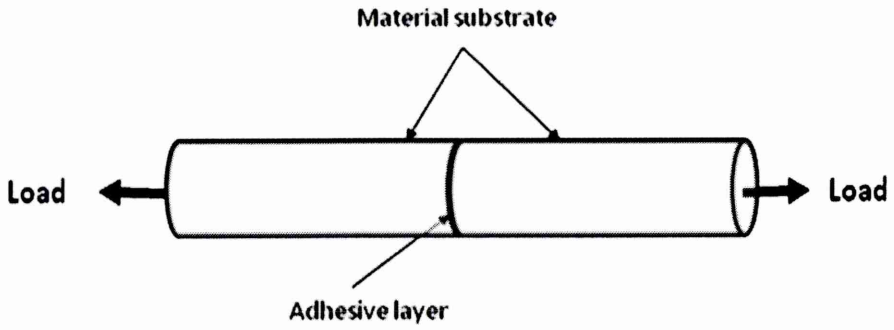

Figure 2.8 Butt joint geometry

2.5 Influence of stresses on adhesive bonded joint

In order to design the strongest possible adhesive joint, it is necessary to minimise stresses that may be generated within the joint. Stresses in adhesive materials are often classified as tensile, shear, cleavage or peel. The breakage of the adhesive bonds occurs when the local stress which is produced by an external force exceeds the local adhesive strength. In general, tensile and/or

shear loading is more desirable for most adhesives than cleavage or peel.

2.5.1 Shear stress

The design of adhesive joints usually requires a geometry such that the load experienced is predominantly in a shear mode. In this case the majority of bonds between the adhesive and the substrate experience the same load and the highest joint strength is achieved [37]. A single lap joint is a simple joint geometry used for measuring the adhesive strength. Peel and shear are the most common stresses generated in a single lap joint under longitudinal tension, affecting the adhesive strength performance [38]. Figure 2.9 shows how the shear stress varies along the length of the joint, illustrating how stress concentrations develop at the ends of the adhesive joint.

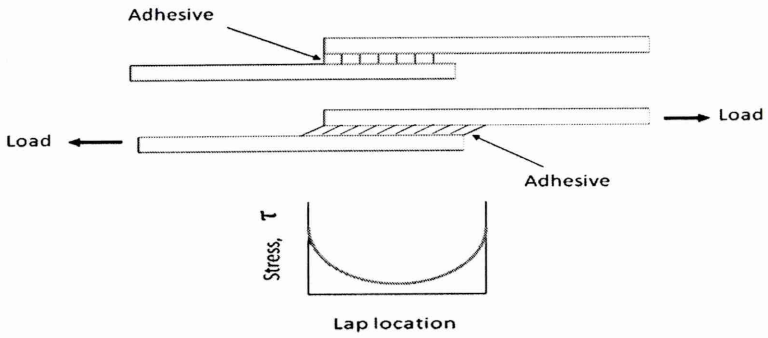

Figure 2.9 Stress distribution found in shear loading (lap joint)

During the applied load, the adhesive material will deform in shear and causing delamination at the interfacial regions or within the adhesive layer. As a result of delamination, cracks will propagate along the interface or through the adhesive and thus the joint will fail. Figure 2.10 shows the adhesive layer under shear deformation (shear stress/strain mode).

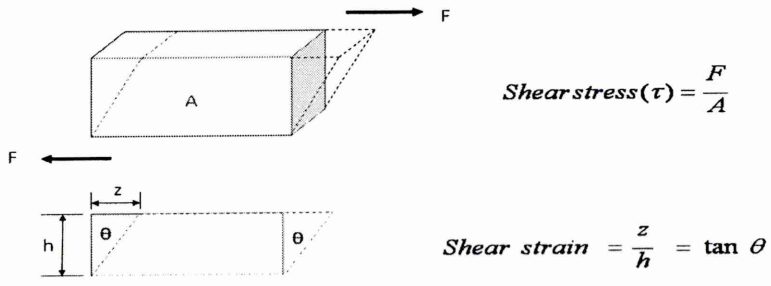

Figure 2.10 Illustration of shear stress and strain in an adhesive layer (lap joint)

2.5.2 Tensile stress

The force applied perpendicular to the adhesive layer in a tensile test specimen develops tensile stresses across the plane of the joint. The maximum stress (tensile and shear) is normally found at the outer edges of the joint, see Figure 2.11. The stress state in these regions is highly complex, varying through the thickness of the adhesive layer [39]. The cracks in the adhesive-bonded butt joints initiate at the weakest location in the joint, notably at the edges, and swiftly propagate which leads to failure of the joint. Significant bending can be induced within the joint due to misalignment of the substrates, resulting in premature failure and reducing the joint strength. However, a well designed joint will result in good resistance to tensile stress as the loading is more uniformly distributed than that in shear [40].

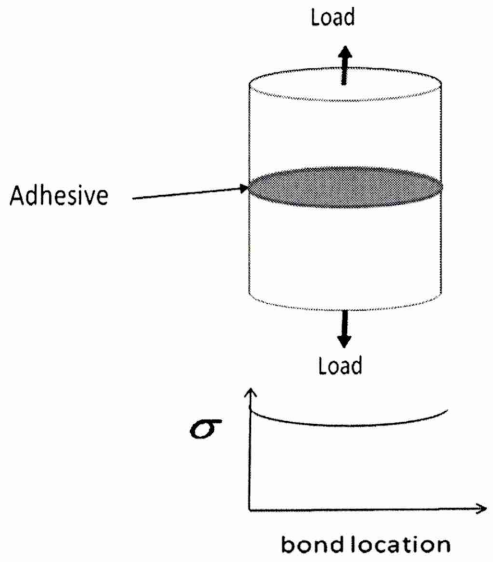

Figure 2.11 Stress distributions in tensile mode (butt joint)

The stress distribution in a butt joint subjected to a tensile load is related to varying degrees of tensile and shear stress within the adhesive layer [41]. For example, when an average tensile strength (σ) is applied parallel to the (Y) axis, see Fig 2.12, the local tensile strength (σ_y) in the (Y) direction in the adhesive is independent of (Y). However, the tensile stress (σ_x) in the (X) direction will depend on both (X) and (Y), and this stress leads the adhesive to flow toward the plane X=0. In addition, there is a shear stress acting along the slip lines (crossing each other at right angles). As local shear stresses cross the slip lines, eventually reaching the yield strength, the joint will begin to fail.

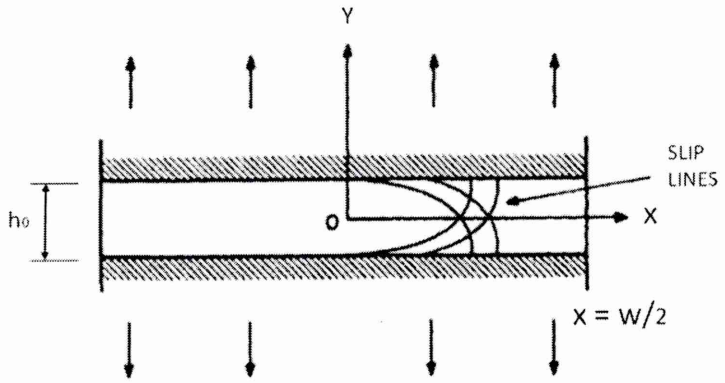

Figure 2.12 Slip lines in butt joint under tension [41]

In addition, when a structural component is subjected to several types of load, acting simultaneously, principal stresses occur. These stresses act on the principal planes, where the shear stresses are zero. Using Mohr's circle, see Fig 2.13, to analyse the stresses [42], and obtain the relationship between shear and tensile strength, the principal stresses can be obtained as maximum/minimum normal stress act on the principal plane, as follows; Equation (2-1).

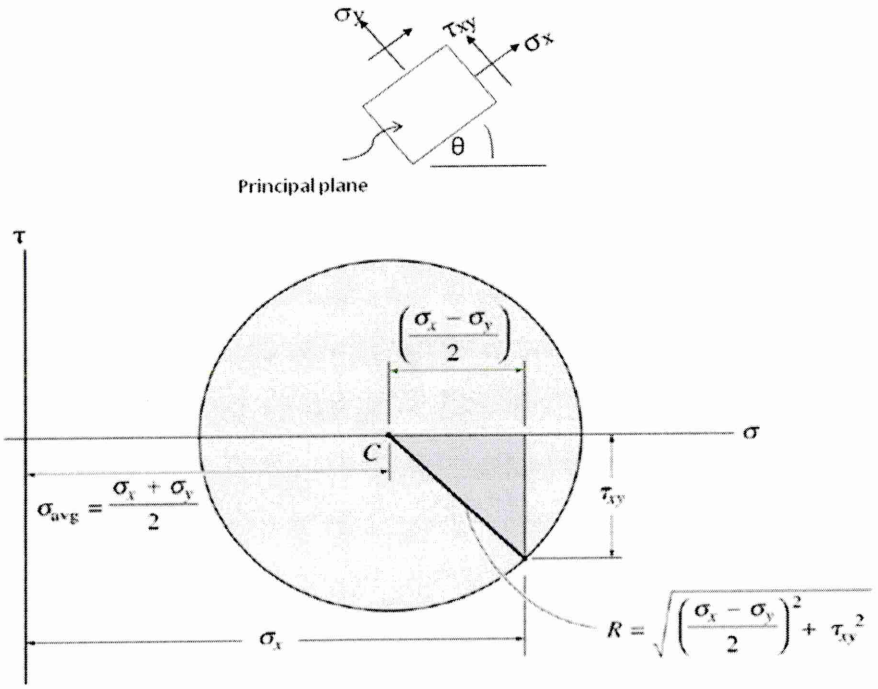

Fig 2.13. Illustration Mohr's Circle for plane stress [41]

$$\sigma = \frac{\sigma x + \sigma y}{2} \pm \sqrt{\left(\frac{1}{2}(\sigma x - \sigma y)\right)^2 + (\tau xy)^2} \qquad (2\text{-}1)$$

Where, (±) represents the maximum and minimum principal stresses, respectively. Yield strength is assumed to occur when the maximum shearing stress in the material reaches a critical value. The maximum shear stress can be obtained as following;

$$\tau_{max} = \sqrt{\left(\frac{1}{2}(\sigma x - \sigma y)\right)^2 + (\tau xy)^2} \qquad (2\text{-}2)$$

$$\tau_{max} = \frac{\sigma_{max} - \sigma_{min}}{2} \qquad (2\text{-}3)$$

$$\tau_{yp} = \frac{\sigma_{yp}}{2} \qquad (2\text{-}4)$$

Where τ_{yp} and σ_{yp} represent the yield point in shear and tensile strength, respectively [41].

The Tresca yield criterion can also be used to describe the relationship between shear and tensile strength. It demonstrates that strain deformation usually appears as a consequence of the sliding of the crystal lattice due to shear stresses. According to this criterion the material passes from the elastic to the plastic state when the maximum shear stress (τ_{max}) reaches a critical value [43,44]. When one of the principal stresses (σ_1, σ_2, σ_3) becomes smaller (or larger) than the others, the material is subject to shear. In such situations, if the shear stress reaches the yield limit then the material deforms plasticity. Yielding starts when ($\tau_{max} = \tau_y$) where τ_{max} is the maximum shear stress and τ_y represents the maximum shear at yield point.

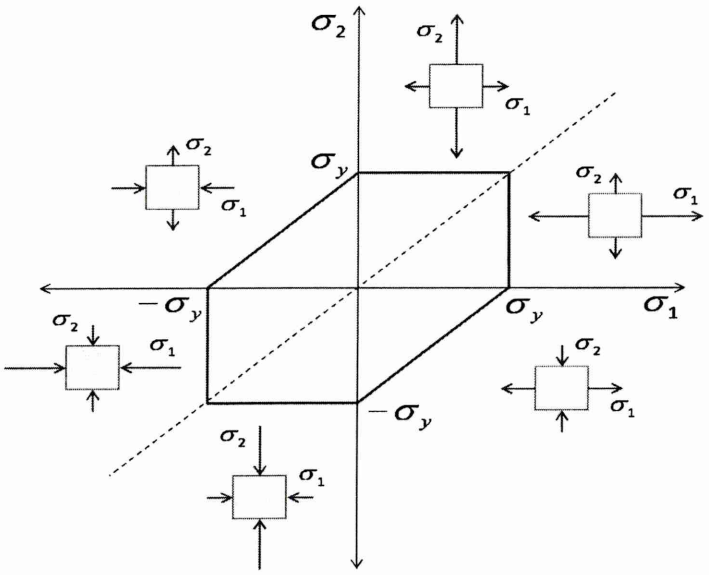

Let σ_1 , σ_2 and σ_3 be the principal stresses ($\sigma_3 = 0$):

When σ_1 and σ_2 are of opposite sign : $\tau_{max} = \frac{\sigma 1 - \sigma 2}{2}$ (2-5)

The yield condition is given by,

$$\sigma 1 - \sigma 2 = \sigma y \quad or \quad \frac{\sigma 1}{\sigma y} - \frac{\sigma 2}{\sigma y} = \pm 1 \tag{2-6}$$

When σ_1 and σ_2 carry the same sign:

If $\sigma 1 \rangle \sigma 2$ $\tau \max = \frac{\sigma 1 - \sigma 3}{2} = \frac{\sigma 1}{2}$ *and* $\sigma 1 = \sigma y$ (2-7)

If $\sigma 1 \langle \sigma 2$ $\tau \max = \frac{\sigma 2 - \sigma 3}{2} = \frac{\sigma 2}{2}$ *and* $\sigma 2 = \sigma y$ (2-8)

2.5.3 Cleavage and peel stresses

Adhesive bonds exposed to cleavage or peel stresses are undesirable; they tend to generate non uniform stress distribution throughout the bond area, see Figure 2.14. Both stresses lead to a concentration of the normal tensile stress within the adhesive layer at the edge of the joint, causing the joint to be susceptible to failure. These stresses tend to distort the joint and cause a failure.

These stresses are measured as the force per linear width of bond. These types of stress should where possible be avoided in adhesive applications. Cleavage is defined as the stress occurring when forces at one end of a rigid bonded joint act to pry the substrates apart. However, when the bonded joint, made from one or both flexible substrate materials, peel stresses are expected. Due to the angle of separation (or the orientation of the forces separating the substrates), the stress concentration is generally much greater for peel than cleavage; a little increased in cleavage strength than the joint peel strength are normally existed [24]. Stresses are confined to a very thin line at the edge of the bond, and the remaining bond area has no contribution to the strength of the joint, as shown by the stress distribution in Figure 2.14. An increase in peel strength may be achieved by increasing the width of the end of the joint, or/and from the use of stiffer materials, where the deflection of the joint is small, thus lowering the value of the peel stress.

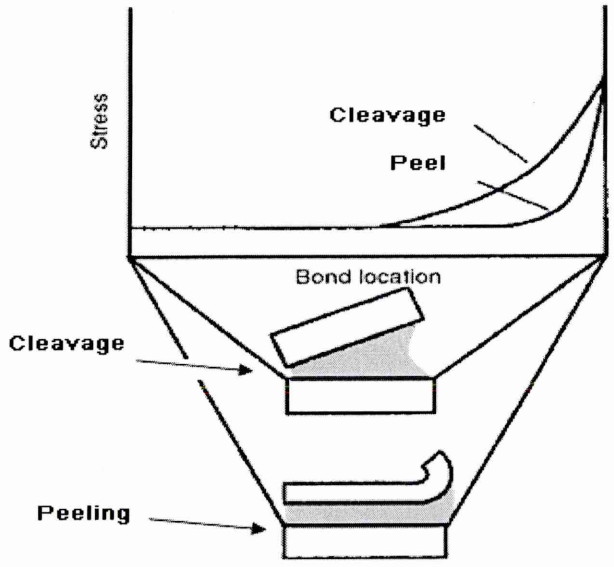

Figure 2.14 Stress distributions found in cleavage and peel tests

2.6 Adhesive failure modes

When the adhesive bonds are subjected to loading, debonding may occur at different locations in the adhesive joint. Analysis of failure mode can be an extremely useful guide to determine if the failure was due to a weak boundary layer or improper surface preparation. There are different possibilities for the occurrence of failure in adhesively bonded joint. Joints may fail by an adhesive or cohesive mode or by a combination of the two modes (adhesive/cohesive).

2.6.1 Interfacial (adhesive) failure mode

An adhesive failure is defined as interfacial bond failure between the adhesive material and the substrate surface, see Figure 2.15a. This can be attributed to surface contamination or air entrapment or some other development of a weak boundary layer [45]. If the rupture takes place at the weakest link found at the interface between materials, cracks can initiate from defects at the interface. These defects are possible loci of failures that arise because of poor wetting, and the presence of voids and dust at the interface. In addition, failure may occur within a few hundred Agstroms of the interface, which is, obviously, difficult to identify.

2.6.2 Cohesive failure mode

Cohesive failure occurs by internal failure of either the adhesive or, rarely, one of the substrates. Cohesive failure results if a crack propagates within the bulk adhesive material, see Figure 2.15b. The failed surface of both substrates is usually covered by fractured adhesive and indicates that the adhesive material in the joint reached the maximum strength. The cracks in the joint may propagate in the centre of the layer or near the interface. For this latter case, the cohesive fracture can be said to be "cohesive near the interface".

2.6.3 Mixed adhesive/cohesive failure mode

A mixed type of fracture occurs when a crack propagates within the bulk adhesive causing both cohesive and interfacial adhesive faliure, see Figure 2.15c. Mixed fracture surfaces are often characterised by quantifying the percentage or rate of adhesive and cohesive faliure. This percentage is

calculated based on the fraction of the area of the contact surface that has failed cohesively or adhesively.

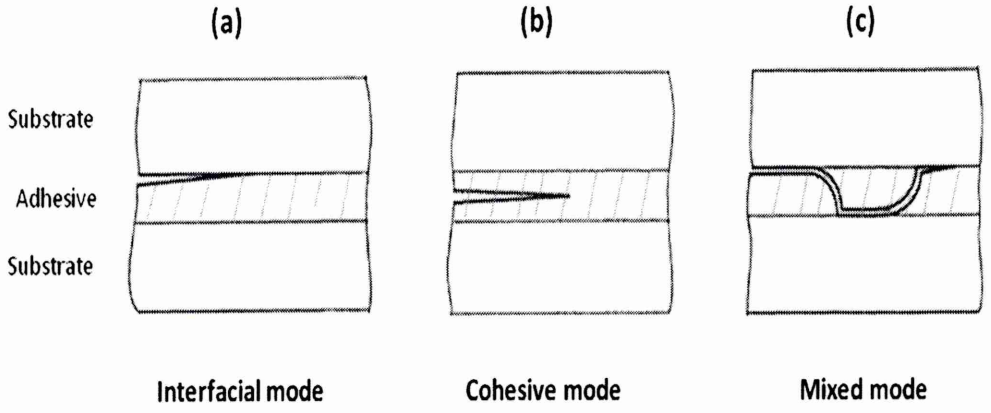

Figure 2.15 Illustration showing adhesive, cohesive and mixed failure modes

2.7 Influence of different variables on bond strength.

2.7.1 Effect of humid environments

The reduction in joint strength can be associated with two phenomena: interfacial failure due to the presence of water at the adhesive/substrate interface and physicochemical degradation of one of the components, often the adhesive. These effects can usually be distinguished by the failure mechanism. Interfacial failure is caused by adhesive separation away from the substrate at the substrate/adhesive interface and cohesive failure is due to the adhesive degradation [46]. Numerous factors govern the durability of epoxy resin bonds, such as the conditions of hydrothermal ageing, the substrate surface pre-treatment and the joint geometry. Moreover, some epoxy resins are not very durable because of their tendency to absorb water. In this case, the durability is dependent on some factors, i.e. aging condition and the pH of the electrolyte. The effect of water on adhesive joints can be variable. With some adhesives, distilled water can be a more aggressive environment than salt water. The difference is attributed to the availability of oxygen at any crack tip that forms during the wet-dry cycling [47]. It has been reported [48] that water in the natural environment is often a more severe test of a joint's durability than high humidity conditions in the laboratory. In addition, there are three factors that are important in explaining the effect of water content on the adhesive joints;

notably, the nature of the adhesive-substrate interface, the solubility of water in the adhesive and the water activity of the environment.

Although the humid environment causes a decrease in the adhesive resistance, the magnitude of damage depends upon the epoxy adhesive used. Prolongo and co-workers revealed that large amounts of absorbed water by the adhesive resulted in lower joint strengths [21]. For instance, they found epoxy/amine systems present a higher adhesive strength than homopolymerised resins. Nevertheless, the hydrothermal ageing causes more damage to epoxy/amine networks. This observation has been associated with the lower water uptake tendency of homopolymerised resins due to its lower hydroxyl group concentration. This behaviour may be explained by the structure of the adhesive network. The presence of OH groups is an important factor governing the water uptake and the subsequent damage. In addition, there are several different effects due to water uptake. For example, adhesive plasticisation results when water penetration inside the epoxy network causes rupture of the interactions, which causes stress relaxation. This relaxation gives rise to a decrease in the glass transition temperature (T_g) of the network commonly named "plasticisation effect". It has been demonstrated [49] that the absorbed water is found in the network as two different water states: bound and free water. In the network, there is some free volume, including voids, which can be occupied by absorbed water (free water). On the other hand, some molecules of water can interact with the resin, where many functional groups are present (bonded water). As the epoxy network is held together by hydrogen bonds and other secondary valence forces between adjacent polymer chains, these interactions will break by forming hydrogen bonds (a connection between two water molecules or organic molecules/water or organic/organic molecules) with water absorbed. The rupture of interchain interaction causes the T_g to decrease. Therefore, the water plasticisation effect is mainly caused by the bonded water.

In addition, the susceptibility of substrate to corrosion should be considered. The decrease in bond strength may be attributed to the corrosion product around the edges. If the substrate is corroded this creates the possibility that the failure mechanism of the joint will change, from a cohesive failure to an interfacial, or near interfacial failure mode.

2.7.2 Effect of temperature

The effect of temperature can be considered in relation to the Tg of the adhesive material. The glass transition temperature (Tg) is the critical temperature at which the adhesive material changes its behaviour from being 'glassy' to being 'rubbery'. Glassy term means hard and brittle and, therefore, relatively easy to break, while rubbery means elastic and flexible, see Figure 2.16.

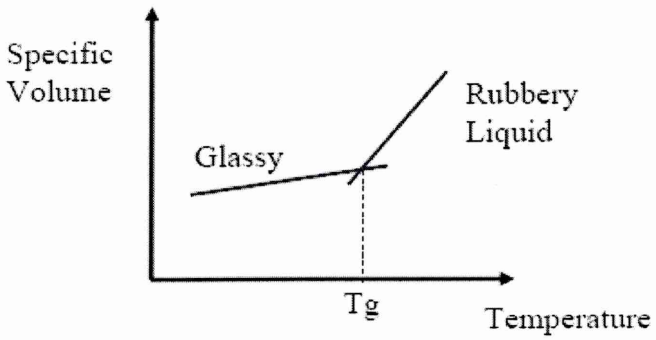

Figure 2.16 Glass transition temperature

For rigid adhesives the normal operational temperatures are below Tg, whereas for flexible adhesives they are above Tg. The effects of temperature on strength and stiffness of a single lap joint are presented in Fig 2.17. For a rubber based flexible adhesive and toughened epoxy based rigid adhesive. Rapid changes in the stiffness and strength of the joint are associated with the Tg of the adhesives. These variations indicate a Tg of -10°C for the flexible adhesive and 60°C for the rigid adhesive. Moreover, at low temperature the joint strength remained constant, but it slightly decreased at high temperature. This decrease could have two causes: a decrease of adhesive/substrate interfacial stress and the residual thermal stresses arising at the joints because of the difference in the thermal expansion coefficient (TEC) of both components [46].

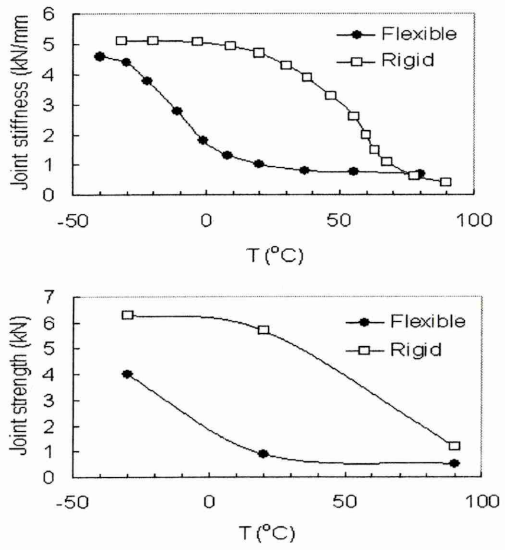

Figure 2.17 Effect of test temperature on joint stiffness and strength [46].

Characterising and understanding the properties of polymeric materials and adhesives is complex. Specific details of the various adhesive types and their toughness values can vary significantly, but some generalisations are possible. Adhesive materials are degraded to some extent by exposure to elevated temperatures. Due to its viscoelastic nature, the adhesive becomes soft and a high degree of creep may occur as temperature is increased. In addition, temperature can affect the interface by causing changes (chemical, dimensional and rheological) in the adhesive or substrate reducing the ability to absorb the external stresses.

The influence of temperature on the adhesive bond strength is based on the adhesive type. Adhesive materials with low melting points, e.g. thermoplastic adhesives, are not suitable at elevated temperature conditions. Once the service temperature approaches the Tg for the adhesive, deformation in adhesive and degradation of the cohesive strength results due to plastic flow. However, thermosetting adhesives are suitable for high temperature applications, where no melting point is exhibited, due to the highly cross-linked networks.

In addition, adhesives held above the glass transition, become flexible and their cohesive strength will decrease. The excessive temperature may also lead to

continuous cross-linking and result in bond embrittlement and shrinkage. This may cause oxidation (if oxygen or a metal oxide interface is present) resulting in a lower cohesive strength and weak boundary layers.

2.7.3 Effect of Bond-line thickness

The effect of increasing bond-line thickness in simple lap joints made with hot-cured epoxy adhesives is that of decreased joint strength. In general with hot-cured epoxy adhesives, a drop in strength occurs in the bond-line thickness range 0.1 to 0.5 mm. In thicknesses greater than 0.5 mm, shear strength is approximately constant; the optimum bond-line thickness is in the range 0.05-0.15 mm. In very thin bond-lines there is a risk of incomplete filling of the joint due to contact between high points on the joint surfaces (associated with high surface roughness, see below).

2.7.4 The Influence of Surface roughness

Surface roughness plays an important role in determining the strength of adhesive bonds. The two most prevalent mechanisms used to explain adhesion phenomena are the mechanical interlocking and adsorption theories. The mechanical interlocking theory is reviewed by Packham [50]. The mechanism suggests that the adhesive mechanically keys or interlocks with the irregularities of a roughened surface. The mechanical interlocking theory can be used to explain the influence of surface roughness in enhancing energy dissipative mechanisms to improve bond strength. However, work by Bright et al. [51] and Arrowsmith [52] suggested that the number of pores penetrated by the adhesive was linked to adhesion strength. These findings revived the mechanical adhesion theory. Nitowski [53] stated that the phosphoric acid anodising process (PAA) improved a link with surface and enhanced bond strength. The presence of long needle-like protrusions on the PAA aluminium surface was also believed to be critical in the mechanical keying mechanism. This work has contributed to making this mechanism an often quoted explanation for the observed bond performance. The adsorption theory assumes the interatomic and intermolecular interactions occurring between adhesive and substrate in intimate contact will establish adhesion forces. These interactions are classified into primary and secondary forces. The primary bonds formed are the strongest

and include covalent and ionic bonds. The secondary bonds include hydrogen bonds. In the case of epoxy adhesives bonded to metal substrates, a secondary bond is believed to exist [54]. The high strength of such adhesive joints suggests hydrogen bonding may describe the interactions which are present [55]. These interactions are believed to occur between the hydroxyl groups present on the surface of the substrate and these hydroxyl groups present in the epoxy adhesive.

2.7.4.1 Macro-Roughened Surfaces

Machining processes, such as milling and turning, provided higher bond strength than sand-blasting treatments. Gendler et al. [56] indicated that laser roughening improved the bond strength by 150% relative to flat surfaces. Formation of surface oxide nodules was believed to cause mechanical interlocking and thus explained the enhanced strength. Physical roughening of the surface by abrasion or high velocity particle impact, grit-blasting, may improve bond strength. Jennings [57] found that when comparing surface abrasion with silicon carbide paper and grit-blasting, the adhesive strength increased as a function of surface roughness relative to flat surfaces.

2.7.4.2 Micro-Roughened Surfaces

Chemical etching and anodising techniques have been used to improve the bond strength of the materials as a function of the surface produced. These surface treatments produced features less than 1μm. Using chromic acid etching process to etch surfaces to varying degrees indicated that fracture energy increased as micro-roughness developed [56]. Nitsche suggested that mechanical interlocking was a major factor leading to improved bond strength for micro-roughened surfaces [57]. Gendler and co-workers concluded that peel strength increased as a function of surface micro and macro-roughness and believed that increases in the angle of surface features enhanced the ability of the interfacial bonds to distribute load [56].

2.8 Fatigue strength of adhesives

The majority of practical engineering design applications involve fluctuating or cyclic loads well below the yield stress of the material of interest. Despite the low magnitude of these stresses, damage can accumulate and "fatigue failure" can occur. Failures occurring under conditions of dynamic loading are called fatigue. It is estimated that over 80 % of all brittle fractures involve some period of fatigue crack growth [58]. The aircraft industry is just one area of application in which the study of fatigue failure is relevant. The fatigue strength of an adhesive is obtained as the number of cycles of a known load necessary to cause failure. The point at which the smooth curve connecting the points of minimum stress crosses over a million cycle line may be reported as the fatigue strength [59]. Fatigue testing of lap joints provides useful engineering design values on the adhesive materials. S-N curve shows the relationship between stress and number of cycle to failure is shown in Figure 2.18.

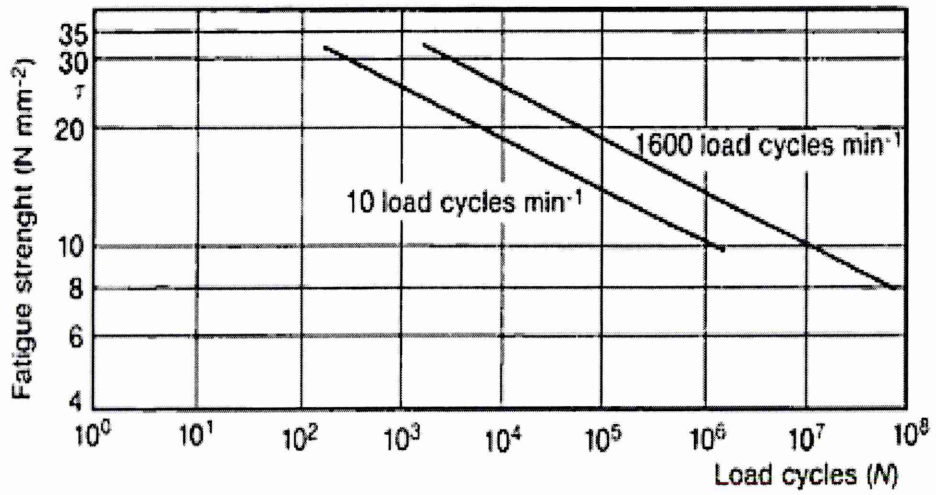

Figure 2.18 Fatigue strength of hot-setting epoxy-nitrite resin, S-N curve [59]

2.4.2 Factors influence on fatigue strength of adhesives

Many factors affect the adhesive fatigue strength, including stress level, stress state, curing conditions and loading frequency. Figure 2.19 illustrates a typical fatigue stress cycle.

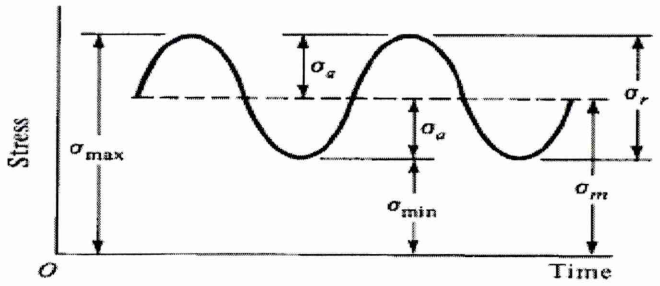

Figure 2.19 Illustration showing typical fatigue stress cycles for adhesives

Where stress amplitude σ_a is defined according to Eq 2-9.

$$\sigma_a = \frac{\sigma_{max} - \sigma_{min}}{2} \qquad (2\text{-}9)$$

In this equation, σ_{max} is the maximum normal stress during cycling, and σ_{min} is the minimum normal stress during cycling. Due to the statistical nature of fatigue, it is necessary to use the results of many fatigue experiments at a given load to find a single representative value for the number of cycles to failure. Therefore, each point on a standard S-N curve represents a series of fatigue experiments. If a large number of samples are run, confidence intervals can give accurate predictions of the fatigue life at a given load. If smaller numbers of samples are run, simply taking the average is a less precise, but acceptable alternative. In addition, fatigue behaviour of adhesives can be extremely sensitive to fatigue stress ratio, *R*, where *R* is defined according to Eq 2-10.

$$R = \frac{\sigma_{min}}{\sigma_{max}} \qquad (2\text{-}10)$$

Other factors affecting the fatigue life of adhesive bonds are the cure conditions and its exposure to the aggressive environment. Any defects on the adhesive material (i.e. voids or pores) can act as stress raisers and potentially reduce the fatigue life of the specimen. Corrosive environments can cause damage on the edges of joints. These also act as stress raisers and crack nucleation points. The frequency and peak fatigue loading is selected to be well below the ultimate short-term failure strength of the joint. Restrictions on test frequency can arise due to test equipment limitations (response time), time-dependent processes and hysteretic heating. Hysteretic heating can precipitate a rise in temperature causing thermal degradation of the adhesive material [60].

2.9 Sol-gel system

2.9.1 Background

Corrosion resistance of metallic structures is considered as a very important issue in many structural applications. For example, in modern aircraft design, components made from aluminium alloys are generally protected from corrosion by the application of protective coatings. Anodising of aluminium alloys is a well-established surface engineering alternative to form an anti-corrosion aluminium oxide barrier layer. A number of non-chromated pretreatments and primers have been developed and tested over the past years. Previous testing of non-chromate systems has focused on either replacement of the chromate conversion coating (CCC) with a non-chrome surface preparation [61,62]. Chromate conversion coatings are currently used as a pre-treatment for different aluminium alloy substrate, being based on the use of chemicals containing chromium in the so-called, 'hexavalent form'. The conversion coating provides excellent corrosion protection and good adhesion properties [63], however, the leachability and toxic nature of the chromates make them environmentally unacceptable. Skin contact, inhalation and ingestion can cause penetration of the hexavalent chromium waste into human organisms, leading to DNA damage and resulting cancer [64]. As a result, the need for the development of non-chromate environmentally friendly surface treatments is urgent. One of the prospective candidates for substitution of chromate pre-treatments is that of sol-gel derived thin films. Sol-gel technology was first discovered in the late 1800s, but it was not until the early 1970s that renewed interest in the technique was generated, when monolithic inorganic gels were formed at low temperature. The method can create a covalently bonded metal oxide-polymer interface offering improvements in surface properties [65].

A sol-gel procedure is a method that allows deposition of a thin inorganic or inorganic/organic film at room temperature upon the substrate. Sol-gel films show good adhesion to metallic substrates and organic top coats. This technology can therefore offer a variety of methods to prepare functional coatings with different properties. It has excellent potential to be used for the preparation of inorganic or organically modified protective coatings, having unique properties. For example, anti-corrosion, diffusion and oxidation barrier

and abrasion resistance [66]. Organic-inorganic hybrid materials have recently received considerable attention as a new class of composite materials through the novel properties that can arise from the combination of organic polymer (soft, flexible) and inorganic material (hard, brittle). These materials help to achieve properties that a single phase material cannot provide [67,68]. In addition, in order to achieve optimum properties, phase separation between organic and inorganic components of the hybrid must not occur. Therefore, the nature of the chemical interaction between the organic polymer and inorganic ceramic during the processing of theses materials plays an important role in avoiding such phase separation.

2.9.2 Sol-gel processing

The term " Sol-gel" is a contraction of the words, solution-gelation, which refers to a series of reactions wherein soluble metal species (a metal alkoxide or metal salt), hydrolyse to a final hydroxide. The soluble metal usually contains organic ligands tailored with the resin in the bonded structure. The metal hydroxides condense to form a hybrid organic/inorganic polymer. The sol-gel process consists of two primary steps (hydrolysis and condensation process). The hydrolysis reaction produces the sol, and then, in the condensation reaction, a macroscopic gel is formed on the substrate producing a thin film. In the sol-gel process a system of colloidal particles in a solution (sol) becomes a macroscopic material (gel), which is interpenetrated by a liquid. The sol-gel is a reaction between a metal alkoxide and water to form a metal hydroxide. This condenses into a metal- oxygen- metal sequence, with the liberation of water and alcohol. Once the liquid evaporates, a strong "glass-like" material remains.

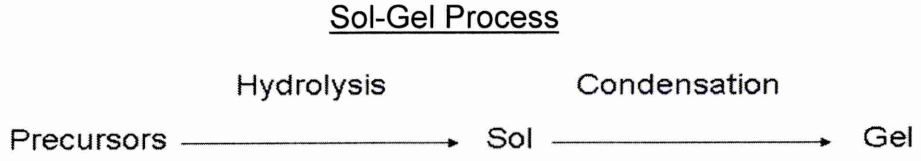

Aluminium, zirconium, tin, and cerium have been used as a metal alkoxide in these reactants. Silicon alkoxides have a more controlled and lower reactivity than the other metal alkoxides [69]. Nowadays, silica based sol-gel chemistry is

more advanced compared with other metal-organic based precursors. For example,

$$Si(OR)_4 + 4H_2O \rightarrow Si(OH)_4 + 4ROH \qquad (2\text{-}11)$$

Where R is CH_2CH_3.The metal alkoxide (tetra-ethoxy-silane or TEOS) is mixed with water; the hydrolysis reaction will be completed when all the (OR) groups are replaced by (OH) groups. This is a hydrolysis reaction which produces the sol and then the condensation reaction, where a number of (Si-O-Si) bonds increase in a process called polymerisation, produces a microscopic gel.

$$2Si(OH)_4 \rightarrow (OH)_3Si - O - Si(OH)_3 + H_2O \qquad (2\text{-}12)$$

A gel is formed on the substrate producing a thin film. The solubility of the resulting gel in a solvent depends upon the size of the particles and degree of network formation. The low reaction of sol-gel processes allows the introduction of organic groups in the inorganic material. This leads to a novel class of materials composed of both inorganic and organic components. The inorganic component helps to enhance mechanical properties while the organic component leads to an increase in the flexibility and functional compatibility with top coat organic paint systems [69]. One of the important factors that can strongly influence the kinetics of the sol-gel reaction is the nature of the solvent. Addition of a solvent, such as alcohol, is needed in order to achieve homogenization of the reaction system. Adding catalysts can lead to increased cross-link density and increasing average number of hydroxide groups on the Si atoms in the drying phase, which can be tailored by adjusting the water concentration, by using a solvent which does not cause the re-esterification of alkoxy groups on the Si atoms during drying [70]. The hydrolysis and condensation reactions are also affected by acid/base catalysis. With the existence of an acid catalyst, a weakly-crosslinked polymer is formed which can easily aggregate after drying .On the other hand, if a base catalyst is used, discrete highly branched clusters are formed and lead to a mesoporous structure after gelation. Specific processes which determine the final preparation of a sol-gel system include;

2.9.2.1 Gelation

The gel point is defined as the point at which the colloidal particles and condensed silica species link together to become a three-dimensional network. The physical characteristics of the gel network depend greatly upon the size of particles and extent of cross-linking prior to gelation [71].

2.9.2.2 Ageing

Another important factor affecting the degree of hydrolysis and condensation of the organometallic in the sol-gel film is the aging stage. Aging is an extension of the gelation step in which the gel network is reinforced through further polymerisation, possibly at different temperature and solvent conditions .During the aging stage, polycondensation continues along with localised solution and reprecipitation of the gel network, which increases the thickness of inter-particles and decreases the porosity. The strength of the gel thereby increases with aging. An aged gel must develop sufficient strength to resist cracking during drying.

2.9.2.3 Drying

During the last stages of gelation, water and the organic solvent evaporate from the glass cavities and the volume of the solid matrix gradually shrinks. In the drying phase, some of the larger pores are emptied while smaller pores remain wetted by the solvent. The final product obtained is a porous glass-like solid commonly termed as "Xerogel" [69]

2.9.2.4 Acid / base catalysts

The kinetics of hydrolysis and condensation reactions are slow and require time to reach completion. For this reason, acid or base catalysts are added to the formulation. The microstructure and properties of the final sol-gel product are more related to the amount and type of catalyst used. Hydrolysis, in acid catalyzed reactions, proceeds with an electrophilic attack of the hydrogen ion on the tetralkoxysilane, see Figure 2.20. This draws the electron density away from the silicon atom rendering it with a partial positive charge. The electronegative water molecule attacks the charged silicon and acquires its charge thus making the protonated alkoxide a better leaving group. Leaving groups are atoms or

radical groups that break away from an organic compound. Base catalyzed hydrolysis on the other hand proceeds by a nucleophilic attack on the tetralkoxysilane by the hydroxyl ion, this subsequently weakens and displaces the (OR) groups [72].

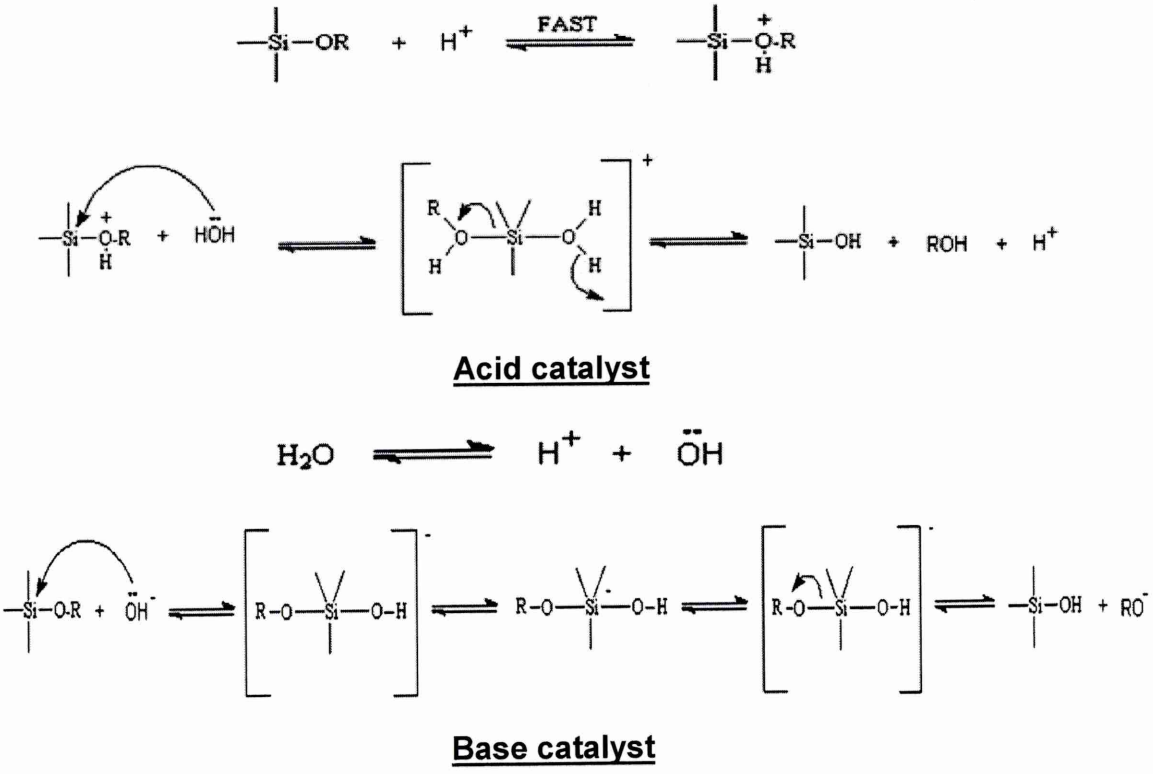

Figure 2.20 Illustration showing sol-gel acid and base reactions kinetics [73]

2.9.3 Advantages of sol-gel systems

There are several advantages of adopting a sol-gel. For instance, it is possible to produce thin bond-coatings to provide excellent adhesion between metallic substrates or thick coatings to provide corrosion protection performance. These systems can be used to shape materials into complex geometries in a gel state or produce high purity products because the organic-metallic precursor of the desired ceramic oxides can be mixed, dissolved in a specified solvent and hydrolysed into a sol and subsequently a gel, allowing excellent control of the composition. Moreover, it has low temperature sintering capability, usually 200-600°C and offers a simple, economic and effective method to produce high

quality coatings. Also, the organic/inorganic hybrid materials prepared by sol-gel process can be cured at low temperature i.e 100°C [74].

2.9.4 Limitations

Despite its advantages, sol-gels have some limitations, for example, low wear-resistance, high permeability, and poor control of porosity within the thickness limit around 0.5 μm where a crack-free film is required. The precursors are often expensive and sensitive to moisture, thus limiting large scale production for specialising applications such as optical coatings. Also, sol-gel process is time-consuming, particularly when careful ageing and drying are required. The sol-gel technique is very substrate-dependent, and the thermal expansion mismatch can also limit the application of the sol-gel technique. For example, dimensional changes on densification and of shrinkage and stress cracking during the drying stage limited the sol-gel layer performance.

2.9.5 Sol-gel coating applications

Since a coating can be applied on a variety of substrates, such as metals, glass and ceramics, it can modify and improve the mechanical and protective properties of the underlying substrate [75]. Sol-gel methods have attracted much interest in recent years and is now being widely used to prepare ceramic materials for application within the optics, electronics, automotive, aircraft and aerospace industries [76,67]. Sol-gel systems containing aluminum oxides, zinc oxides, silicon oxides, zirconium oxides and a combination of these oxides have been developed. It has been found that one of the major characteristics controlling the corrosion protection properties of the coatings is the film thickness due to the tendency for cracking to occur in single coat films greater than 200μm. A more realistic approach for defect free film formation is being taken by combining the various metal oxides with organic segments to form ceramic/polymer matrix. They are synthesized using organic functionalised metal alkoxides that promote reaction between an organic group and the inorganic alkoxide. Ceramic/polymer systems are potential chromate replacements due to the ability to tailor the systems to the specific needs of the user. The organic segment adds flexibility to the system, which lowers the

internal stresses of the system and reduces shrinkage of the coating. It was demonstrated [77] that the increased in flexibility of coating thickness for ceramic/polymer system was better than that for traditional sol-gel coatings. The Self-assembled Nanophase Particle (SNAP) surface treatment, which is a method of forming a functionalized silica nano-particle in an aqueous-based sol-gel process, followed by cross-linking the nano-particles to form a thin film is an alternative anti-corrosion non-chromate surface pre-treatment [62]. Sol-gel techniques have the potential to incorporate chemically tailored features aimed at the development of corrosion resistance through the use of structurally modified reactions. For example, incorporation of an organic group resulted in crack-free surface and chemical bonds between nano-particle and the substrate could occur to form a thin organic–inorganic hybrid film [78].

The improvements of corrosion resistance are due to the formation of protective oxide films which act as a barrier to oxygen diffusion to the metal surface. Xu Yue and co-workers [79] found that by adding some elements such as cerium, a positive and remarkable effect on the formation and properties of sol-gel coatings been achieved. Cerium has a high chemical activity thereby greatly enhanced the cohesion force between oxygen atoms and aluminum alloy substrate. As a result, the anti-corrosion potential of these coatings was promoted, and the corrosion process was consequently hindered. Hamdy and Butt [80] demonstrated that corrosion protection of sol-gel silica-based coated aluminum alloys improved due to the formation of silica rich Al-oxide film. Silicon is incorporated into the pores of the aluminum oxide film to form a high corrosion-resistant layer. Moreover, the immersion and the Electrochemical Impedance Spectroscopy (EIS) results showed that the hybrid sol–gel coatings containing ZrO_2 nano-particles are effective on corrosion performance of AA2024-T3. An increase on the amount of ZrO_2 nano-particles improves the corrosion protective properties during immersion in 3% NaCl solution.

2.9.6 Hybrid organic/inorganic sol-gel

The initial components of sol-gel synthesis are in the liquid state, and their interaction can lead to the formation of a homogeneous system. Due to modification in sol-gel parameters and development of suitable processing methods, new sol-gel approaches with interesting properties have been produced. It well know [81] that the early developments in sol-gel process were based on the potential of precursors chemically tailored. A sol-gel reaction condition at low temperatures was allowed to incorporate the organic and inorganic materials. The process led to a conceptually novel class of materials composed of both inorganic and organic components. Organic groups can improve the characteristics of the matrices, such as modification of the mechanical properties, easier processing of films and fibres, porosity control and adjustment of the hydrophilic/hydrophobic balance and electrochemical reactions. On the other hand, the inorganic part of the material improved mechanical and thermal strength and led to interesting electrochemical, electrical or magnetic properties [82]. The preparation of hybrid organic-inorganic sol-gel materials can be generated using different synthetic techniques by incorporating various starting inorganic and organic components with varied molecular structures. It has been widely described [83] that the synthesis of hybrid organic–inorganic sol-gels, is based on the basis of silicates and metal oxide materials. The use of alkoxy compounds (i.e. tetraethoxysilane, tetramethoxysilane), and organic components (i.e. polymers), having functional groups (OH) that are able to enter into specific interactions with inorganic compounds can form chemical bonds and produce hybrid network materials. The resulting hybrid material properties are mainly dependent on the chemical structure of the organic components and the composition ratio of organic to inorganic component within the matrix.

2.6.7 Sol-gel for adhesive bonding

As the performance of bonded joints improves and expectations of the bonding process become higher, the requirement for high strength adhesives becomes greater than ever. This is fuelled partially by an increasing demand for composite structures, which naturally lend themselves to fastening techniques

such as adhesive bonding. Adhesive bonding has several advantages over traditional repair approaches using mechanical methods. For example, improved structural efficiency, improved fatigue life due to elimination of fastener holes and weight savings. Metal treatment prior to bonding is a key factor for both the initial adhesion of a bonded joint and its long-term environmental durability [84]. Aluminum surface preparation techniques use phosphoric acid anodising (PAA) or chromic acid anodising (CAA) to provide a surface for adhesive bonding is utilised in many manufacturing sectors. Inorganic sol-gel system offer good adhesion between metals and organic paint. Also, introduction of an organic component to inorganic sol-gel system leads to the formation of thicker, more flexible films with enhanced compatibility to different organic top coatings [64].

2.10 Characterisation techniques

2.10.1 Scanning Electron Microscope (SEM)

The SEM is a microscope that uses high energy beam of electrons to obtain images of high magnification. The development of the SEM brought with it new areas of study, particularly in medicine [85] and the different material sciences [86,87,88]. An SEM can now produce high resolution images, which means that very small features on a selected area can be examined in detail.

The SEM generates high energy electrons from an electron gun which are condensed and focused using two or three electro-magnetic lenses into a fine spot on the sample. Scan coils located in the bore of the objective lens cage can scan the beam over a square area on the sample surface. The interactions of the electron beam with atoms at or near the surface of the sample result in emission of backscattered electrons and secondary electrons [89] see Figures 2.21and 2.22. In the most common detection mode, secondary electron alone can produce very high-resolution images of a sample surface, typically revealing details of less than 5nm in size.

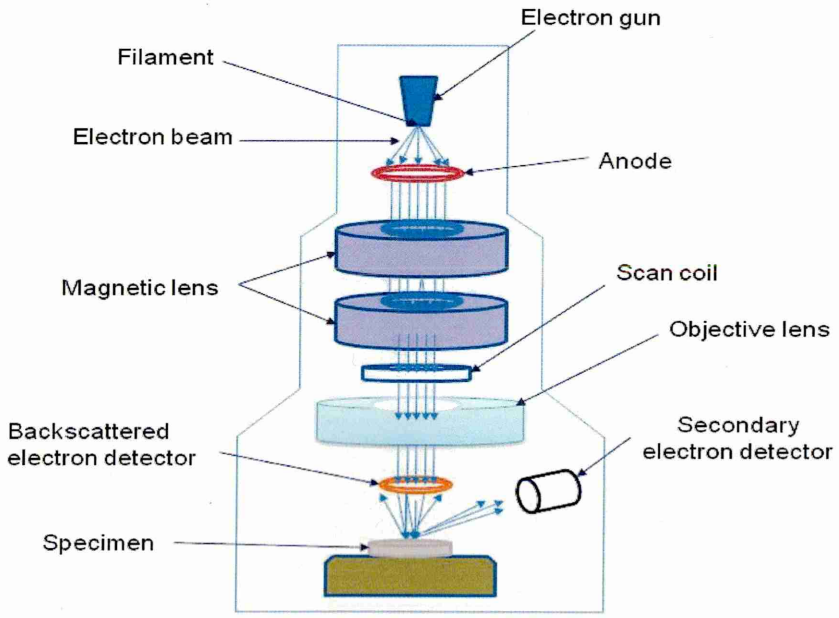

Figure 2.21 Principles of operation of the SEM [87]

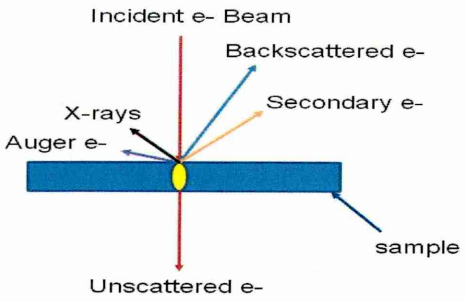

Figure 2.22 Interaction of electron beam with specimen surface

Low energy electrons produced near the specimen surface will be detected as secondary electrons, providing a predominantly topographical image. High energy electrons which are normally near to the incident path and have been scattered backward, provide information about the presence of differences in atomic number of a sample [90]. If the incident electron beam is of sufficient high energy, X-rays will be emitted from the specimen and can be measured using an energy dispersive spectrometer [91].

Figure 2.23 shows a schematic of the interaction volume of the electron beam, that is the volume inside the specimen in which interactions occur while being struck with an electron beam. The higher the atomic number of the specimen the lower the volume, the greater the energy of the beam and the more normal the angle of incidence the greater the volume. It shows that surface details will be provided by secondary or back-scattered electrons.

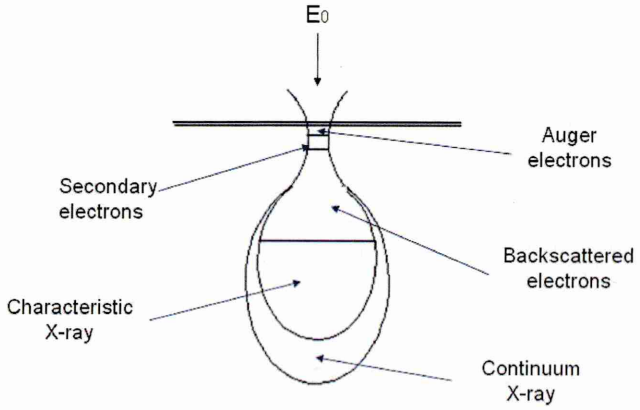

Fig. 2.23 Electron beam interaction volume

2.10.2 Infinite Focus Microscope (IFM)

The IFM is an optical device (Alicona Imaging GmbH, Austria) for the three-dimensional measurement of the surface profile of specimens, see Figure 2.24. The IFM can provide analysis of surface roughness in true colour images with a vertical resolution, in principle, of up to 20nm [92,93]. The technique is able to acquire images on surface areas as large as 50mm x 50mm and is able to merge different images (stitching) into a very good larger image.

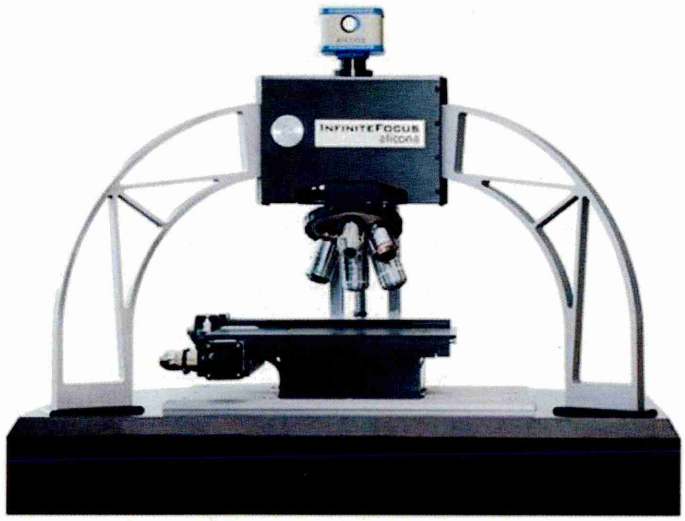

Figure 2.24 Infinite focus microscope

Rough surfaces of complex form geometries can be quantified with an IFM providing accurate measurement of an average roughness profile (R_a), mean peak to valley height of roughness profile (R_z) and maximum peak to valley height of roughness profile (R_{max}) including the bearing ratio curve [94]. Analysis includes information about gradient and spectral distribution in addition to common surface analysis and characterisation. The technique can also measure complex geometries of components. Moreover, volume analysis calculates the volume of voids and protrusions. Shufan in [95] mentioned that an IFM tool can be used in measuring the corrosion pit depth on the substrate surface. The measurement area is defined directly on the optical colour image.

2.10.3 Fourier Transform Infrared Spectrometer (FTIR)

FTIR is a common spectroscopic technique for identifying chemicals in both organic and inorganic components. In infrared spectroscopy, IR radiation is passed through a sample. Some of the infrared radiation is absorbed by the sample and some is transmitted. The resulting spectrum represents molecular absorption and transmission.

The IR radiation travelling though a sample will be incident on the atoms present in the molecules comprising the sample. When the frequency of vibration of the IR radiation is equal to one or more of the natural frequencies of the atom, the molecule absorbs energy at that frequency from the incident radiation. The absorbed infrared radiation energy is converted into vibrations (stretching and/or bending of the molecular bonds). As the atom and/or molecule returns to its original state, energy is radiated at the given frequency. This process produces a number of bands (peaks) in the IR spectrum which provide information regarding the functional groups present in the molecule [96]. The amount of relevant material present can be determined directly from the magnitude of the peak in the IR spectrum. The IR spectrum will be presented in both transmitted (T) and absorption (A) modes. FTIR can identify unknown materials in a sample, it can determine the quality or consistency of a sample, it can analyse chemical functional groups and determine the structural components of engineering materials [97,98,99].

Any FTIR spectroscopic system contains the radiation source, an interferometer, a sample, and an IR signal detector. In most FTIR systems, a Michelson interferometer is used. The interferometer consists of a beam splitter, a fixed mirror, and a moving mirror that moves back and forth very precisely, see Figure 2.25. Radiation from the source strikes the beam splitter and separates into two beams (transmitted and reflected). The beams strike the fixed and moveable mirrors and are reflected back to the beam splitter, resulting in interference at the beam splitter. The modulated IR beam which has passed through the sample has different wavelengths preferentially absorbed by the various molecules present. Finally, the IR beam is detected by a detector and Fourier transformed by the computer to obtain the IR spectrum.

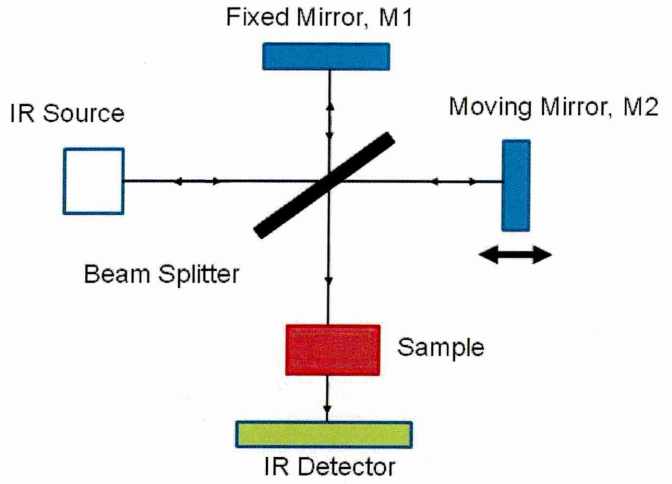

Figure 2.25 Schematic of a Michelson interferometer

The infrared radiation is an electromagnetic spectrum between the visible and microwave regions. It has wavelengths from 0.78 to 1000μm. The IR spectrum is usually presented in terms of the wavenumber:

$$\textbf{Wavenumber = 1 / wavelength (cm)} \qquad (2\text{-}13)$$

The IR region is usually divided into three ranges; near IR between 12500 – 4000cm^{-1}, mid-infrared extends from 4000–200cm^{-1} and the far-infrared region is at the lower wavenumbers 200 - 10cm^{-1}.

2.10.4 Raman spectroscopy

The Raman scattering process was first recognized in 1928 by Professor C.V Raman [100,101]. Raman spectroscopy is concerned with the measurement of incident monochromatic radiation – usually from a laser - scattered from molecules. In this technique, the sample absorbs photons from the laser light which is then re-emitted. There will be changes in photon energy due to the interaction between the laser light and the chemical bonds within the sample. The corresponding shift in the wavelength of the scattered light provides information on the vibration modes in the molecules. If the scattering is elastic

(Rayleigh scattering), the scattered light will be the same wavelength as the incident light. However, for inelastic scattering (Raman scattering), where the photons lose or gain energy during the scattering process there will be a corresponding increase or decrease in wavelength, respectively. The condition for the scattered photons in Raman measurement is divided into Stokes and anti-Stokes types, see Figure 2.26. In Stokes scattering the wavelength of the scattered light is greater than the wavelength of the incident, whereas for anti-Stokes scattering the wavelength of the scattered light is less than the incident.

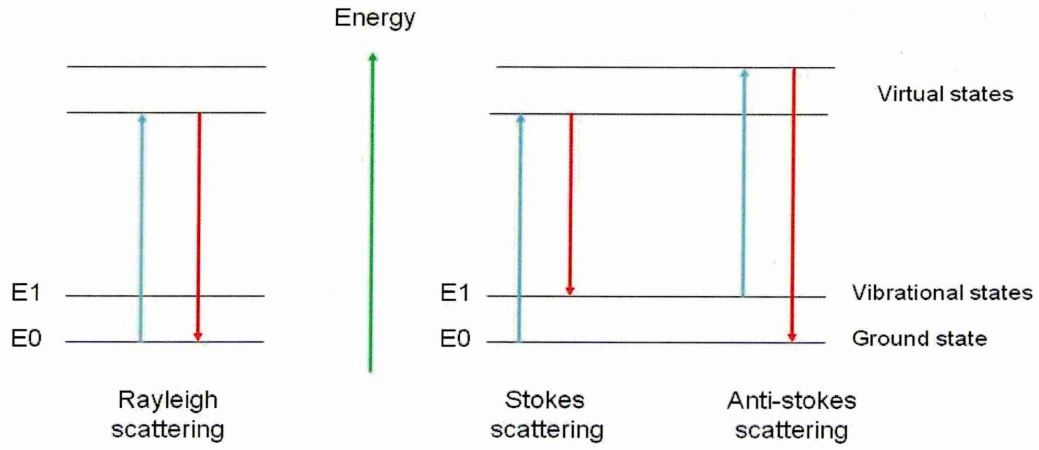

Figure 2.26 Light scattered modes in Raman spectroscopy

The difference in energy gained or lost is attributed to the vibrational energy states in the molecule. Thus, the wavenumber of Raman Stokes and anti-Stokes scattered can directly measure the vibrational energies of the molecule [102]. Raman spectroscopy is very useful in the determining chemical bonds in both liquids and solids, and can be used for both qualitative and quantitative applications. The technique also provides information on physical characteristics such as crystalline phase [103] and polymorphic forms [104].

2.10.5 X-ray Photoelectron Spectroscopy (XPS)

XPS is a photoemission technique used to measure the chemical composition and chemical state distributions at the sample surface within a depth of a few nanometres. It can also used to determine the relative quantity of each component [105]. XPS is based upon the photoelectric effect of an X-ray beam, first explained by Einstein in 1905 [106]. If a sample surface is irradiated with

photons of sufficient energy (usually Mg Kα [1.25keV] or Al Kα [1.49keV]) in a vacuum of about ~10^{-9} torr, electrons will be ejected from the surface, see Figure 2.27. The kinetic energy (KE+Φ) of the emitted photoelectrons is given by the difference between the energy of incident x-rays (hv) and the electron binding energy (BE):

$$K.E + \phi = h\upsilon - B.E \qquad (2\text{-}14)$$

Where Φ is the work function of the spectrometer, h is Plank's constant and υ the frequency of the incident X-ray beam. The XPS spectrum is presented as a graph of intensity versus the electron energy.

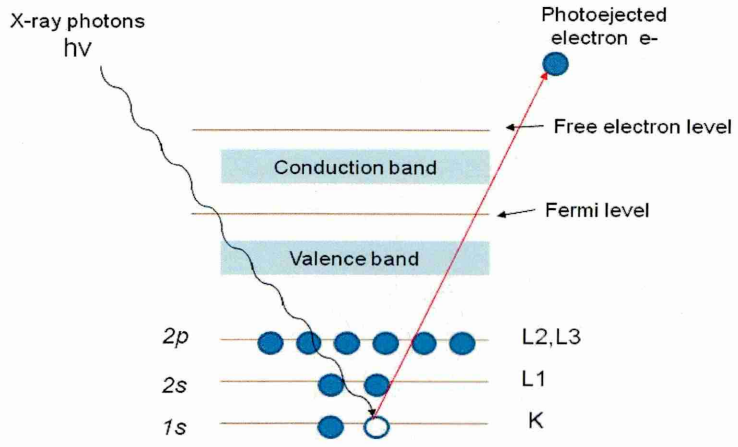

Figure 2.27 Soft X-ray incident on a surface atom ejects an electron

The binding energy is characteristic for each element in the sample and XPS spectra can be used to identify the element composition. Quantification of the relative proportions of the elements can be determined from the relative area of photoelectron peaks in the XPS spectrum. In addition, peak intensities are related to the concentration of the element within the sample. XPS has been used extensively in adhesion research for determining surface functional groups and failure modes of the joints [107,108].

2.10.6 Thermo-gravimetric analysis (TGA)

Thermal analysis techniques were conducted for evaluating physical and chemical changes in material as a result of thermal effects. TGA is a simple analytical technique to study the thermal behaviour of materials [109]. The technique measures the loss of mass of a material as a function of temperature and time while the sample is being heated at a uniform rate in an appropriate environment, i.e. nitrogen, oxygen or air [110]. Different materials can be analysed by this technique such as inorganic and organic components, ceramics, glasses, and composites. In addition, the evaporation rates of volatile products, oxidative stability [111] and the changes in decomposition reactions as temperature increases can be identified. It is a very useful technique for determining thermal stability of materials, and under different heating rates, both long and short-term thermal stability may be predicted. TGA measurement allows testing in the temperature range from 25°C to 900°C, and weight of the test sample can range from 1 mg to 150 mg.

2.10.7 Summary

This chapter reviews the most important facts, developments and techniques, which are necessary to understand this work (i.e. epoxy resin, adhesives and sol-gel technology). A sol-gel system has been used as a surface treatment to enhance adhesion for bonding metallic substrate and was found to interact strongly both with the metal substrate and epoxy-resin-based adhesive bond primers. It is possible to achieve a reproducible surface that results in durable bonded interfaces using readily available materials. Using appropriate materials and conditions, with the sol-gel pre-bond treatment and a bond primer, can yield a robust, durable bond interface system. Sol-gel coatings may also play a role for the substrate surface modification and the improvement of material properties which are affected by surface conditions.

CHAPTER 3 Experimental work

3.1 Substrate materials (Al alloy and Mild steel)

Al2024-T3 and mild steel were used as the substrate materials in testing the adhesive strength of the hybrid sol-gel materials. Table 3.1a presents the composition of Al2024-T3 and mild steel used in measuring the lap shear adhesive strength and Table 3.1b presents typical mechanical properties of the two alloys. Mild steel rods were used for determining the adhesive tensile strength. The composition of the mild steel is presented in Table 3.1c.

Table 3.1a Composition of the Al2024-T3 and mild steel used

Composition	C	P	S	Mn	Fe	Cu	Mg	Si	Cr	Ni	Zn	Ti+Zr	Al
AA2024-T3 wt%	---	---	---	0.6	0.5 max	4.4	0.45	0.5 max	0.1 max	0.05 max	0.2 max	0.2 max	Rest
Mild steel wt%	0.15 - 0.2	0.04 max	0.05 max	0.6-0.9	Rest	---	---	---	---	---	---	---	---

Table 3.1b Mechanical Properties of the Al2024-T3 and mild steel used

Materials	Tensile strength	Brinell Hardness HB500	Elongation%
AA2024-T3	485MPa	120	18
Mild steel	420MPa	140	21

Table 3.1c Composition of mild steel rods

Composition	C	P	S	Si	Mn	Fe
Mild steel wt%	0.12 - 0.18	0.05 max	0.05 max	0.1 - 0.4	0.6-1.0	Rest

3.2 Surface preparation

Aluminium 2024-T3 samples having three different surface roughness conditions were prepared. Sample A was 'as-received' from the supplier without polishing, sample B was polished with 6μm diamond paste, and sample C was polished with 1μm diamond paste (3-5 specimens were prepared for each condition). The roughness of the surfaces were then evaluated by Surface Texture Measurements (STM) using a Taylor-Hobson Laser form Talysurf Mk1. To study the influence of surface roughness on adhesive strength of the sol-gel derived adhesive, five measurements were made for samples A, B and C at random positions across the surface.

Surface roughness of the mild steel samples was also made at 3 to 5 positions using the Infinite Focus Microscope (IFM) technique prior to quantifying the effect of substrate surface condition on the adhesive strength of the hybrid epoxy/sol-gel system.

3.3 Formulation of sol-gel adhesives

3.3.1 Hybrid sol-gel derived adhesives

Different sol-gel formulations were used in this work. The designation of adhesive types and combination of components used is shown in Figure 3.1. S1# hybrid silica-based sols were first prepared from silane-based precursors supplied by Dr H Wang of Sheffield Hallam University (SHU). This hybrid sol was produced by mixing tetraethoxysilane (TEOS), methyltrimethoxysilane (MTMS), ethanol, and deionised water at a mole ratio of 2:3:40:60. Nitric acid (HNO_3) was added as a catalyst to promote the hydrolysis and condensation reactions. AD2# sols were then produced by doping the S1# sol with 0.05 wt % PANI micro-particles. AD3# and AD4# sols are listed in Table 3.2, which presents the different quantities of γ-Al_2O_3 or TiO_2 nano-particles doped into the S1# sol. AD5#, AD6#, and AD7# sols were prepared by adding both γ-Al_2O_3 nano-particles and Polyaniline (PANI) micro-particles into the S1# sol in various ratios as shown in Table 3.3.

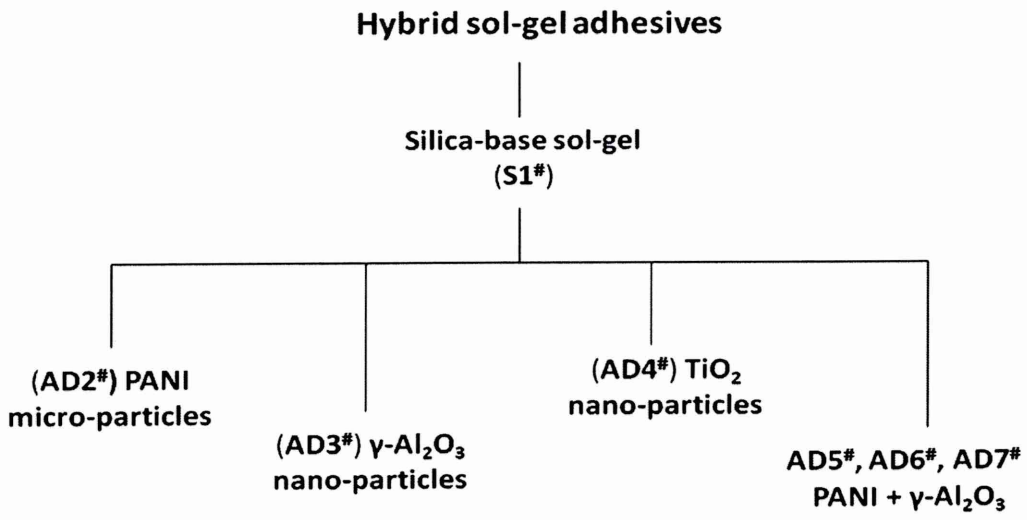

Figure 3.1 Chart showing the different sol-gel adhesive formulations prepared in this study

Table 3.2 AD3# and AD4# materials.

Hybrid sol-gel adhesives	AD3#	AD4#
	γ-Al_2O_3, wt%	TiO_2, wt%
I	0.5	0.5
II	1.0	1.0
III	2.0	2.0
IV	2.5	2.5

Table 3.3 AD5#, AD6#, and AD7# materials.

Hybrid sol-gel adhesives	AD5#		AD6#		AD7#	
	γ-Al_2O_3	PANI	γ-Al_2O_3	PANI	γ-Al_2O_3	PANI
g added to 6 ml of S1# sol-gel	0.42	0.01	0.5	0.02	0.32	0.1

3.3.2 Hybrid epoxy/sol-gel adhesives

In this system, see Figure 3.2, three different hybrid epoxy/sol-gel adhesives were produced and their adhesive performance tested on Al2024-T3 and mild steel substrates. The composition of the hybrid epoxy/sol-gel adhesives are shown in Table 3.4. The 'as-received' unmodified epoxy adhesive (designated 'pure epoxy' (PE)) was a diglycidyl ether of bisphenol-A resin (D.E.R 324, DGEBA) from Dow Chemicals with an average molecular weight of 700 g/mol, which was cured by adding a curing agent based on diethylenetriamine (DETA). The sol-gel modified epoxy adhesives were prepared by mixing the DGEBA with the as-prepared hybrid sol (ratios are listed in Table 3.4) and then left in an ultrasonic bath for 45 minutes at room temperature to ensure uniform dispersion. Note: the sol-gel systems were not formulated with a curing agent. The sol-gel epoxy adhesives were further modified by doping with 0.007g multiwall carbon nano-tubes (MWCNTs, from Sigma Aldrich) and 0.1g γ-Al_2O_3 nano-particles (99.98% metal basis, purchased from Alfa Aesar, A Johnson Matthey Company).

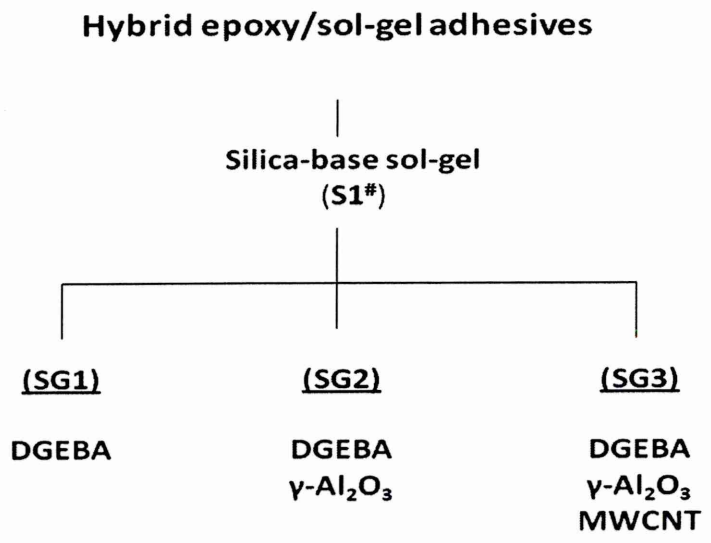

Figure 3.2 Chart show different hybrid sol-gel epoxy formulations

Table 3.4 Hybrid epoxy/sol-gel adhesive formulations

Adhesive Samples		Formulations				
		DGEBA (ml)	Sol-Gel (ml)	DETA (ml) curing agent	γ-Al_2O_3 (g) with size (10-20 nm)	MWCNT (g) with size (O.D.10-15nm, I.D. 2-6nm, length 0.1-10 μm)
PE/MS	PE/Al	1.50-2.00	---	0.5-1.00	---	---
SG1/MS	SG1/Al	1.50-2.00	12.00	---	---	---
SG2/MS	SG2/Al	1.50-2.00	12.00	---	0.1	---
SG3/MS	SG3/Al	1.50-2.00	12.00	---	0.1	0.007

PE= Pure epoxy, Al = Al2024-T3 alloy, MS= Mild steel

3.3.2.1 Dispersion of MWCNTs and γ-Al_2O_3 in hybrid epoxy/sol-gel

Due to their hydrophobic properties and the formation of stabilised bundles under the action of van der Waals forces, carbon nano-tubes (CNTs) generally aggregate together after being dispersed in water, resulting in the formation of hollow ropes [112]. Thus, uniform dispersion in a sol is one of the key issues for the application of CNTs. To achieve optimum dispersion, multiwall carbon nano-tubes (MWCNTs) and γ-Al_2O_3 nanoparticles were first added to 2-propanol. The solution was then ultrasonically dispersed for 90 minutes at 25 °C using an ultrasonic generator (Roop Telsonic Ultrasonic Ltd, TEC-40, Switzerland). After being dispered, it was mixed with the as-prepared sol–gel/epoxy solution and this mixture was then excited ultrasonically for 2 hours using the same generator, followed by continuous stirring overnight to obtain a stabilised uniform sol.

3.4 Mechanical tests

3.4.1 Shear test (Single lap joints)

This test is very common in evaluating the strength of an adhesive. Adhesive-bonded single lap joints were produced for measurement of the adhesive strength of the joints. The joint consists of two plates of substrate joined using a simple overlay. Under the applied load the joint will fail in shear mode as the

faces of the surfaces slide relative to one another. As a result, stress distributions in the lap joint change along the bonded area. Maximum stresses are located at the edges, while the minimum stresses are normally distributed within the centre of the joint [113].

3.4.1.1 Lap joint specimens tested at room temperature

3.4.1.1.1 Hybrid sol-gel adhesives

Two rectangular strips of aluminium Al2024-T3 of dimensions 100mm long x 25mm wide x 1.5mm thick were used for this test. In group A (as-received samples), a section of surface at the end of each block of the aluminium, see Figure 3.3, was first washed by tap running hot water to remove any dust on the surface, and air-dried, further immersed in acetone and ultrasonic for 15 mins at ~23°C and then air-dried, prior to application of the sol-gel adhesive at room temperature. The sol-gel adhesive was applied as a thin layer on both surfaces of the aluminium joints. The coated substrates were then left for 1 hour at room temperature to dry. Following the ASTM D1002 (Standard Test Method for Apparent Shear Strength of Single-Lap-Joint Adhesively Bonded Metal Specimens by Tension Loading (Metal-to-Metal)) [114], the aluminium samples were assembled with a single lap shear joint with 12.5 mm overlap, as shown in Figure 3.3.

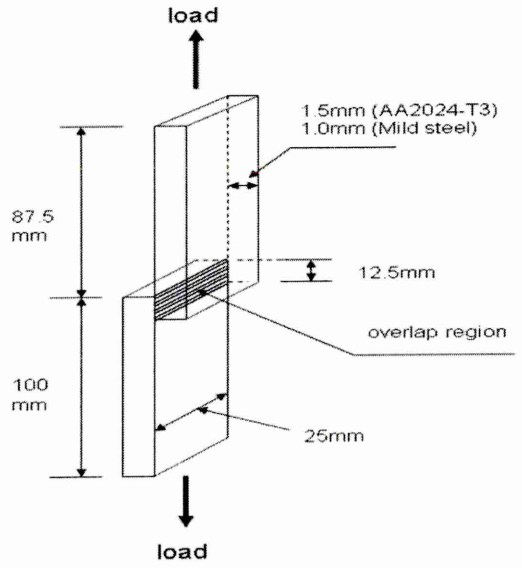

Figure 3.3 Geometry and dimensions of lap joint for experiments at room temperature

For the fixing of the lap joints and control of the adhesive bondline thickness, a simple clamping arrangement was designed and constructed, see Figure 3.4.

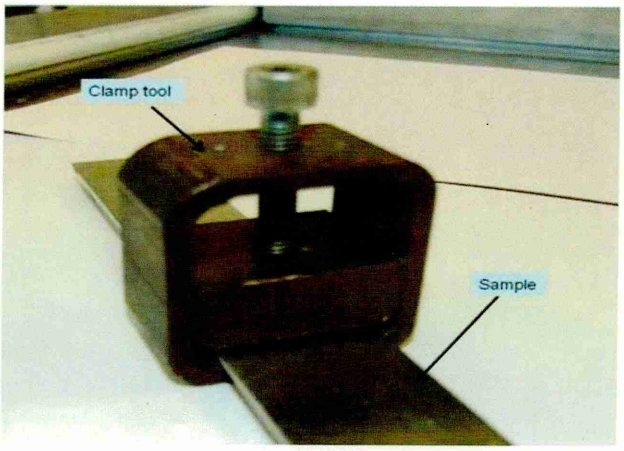

Figure 3.4 clamping tool used for preparing lap joint specimens

The bonded area was subjected to an applied pressure of 4MPa during the curing stage. This was obtained from the relationship between the applied torque and the resulting load, see Fig 3.5. The pressure was calculated from the formula; Pressure (P) = Load (F) / lap joint area (A). This procedure gave all lap joint specimens the same adhesive thickness; i.e. ~ 0.1mm. The specimen was then placed into an oven to be cured for various designated times and temperatures. The same procedures were followed with samples B and C.

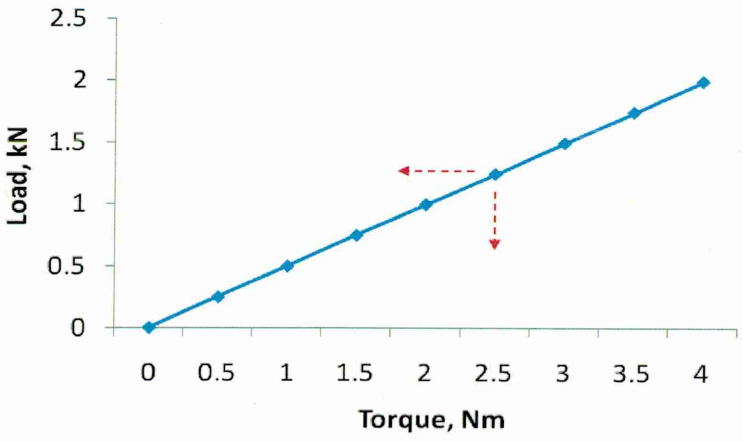

Figure 3.5 Load/torque relationship for clamping tool used with lap joint specimens

3.4.1.1.2 Hybrid epoxy/sol-gel adhesives

A slightly different procedure was used to prepare the samples for the experiments on the hybrid epoxy/sol-gel adhesive system. The surface to be adhesively joined was first washed by tap running hot water to remove any dust on the surface, and air-dried at room temperature of ~ 23°C, further immersed in acetone and ultrasonic for 15 mins at temperature of ~23°C and then air-dried. This procedure was used for both mild steel and aluminium alloys. Adhesives were then applied on the surfaces by a spray gun. Specimens were left for 30 minutes at room temperature and then pre-cured in an oven at 95±5.0°C for 40 minutes to eliminate trapped air and to evaporate the majority of solvents and water in the coating. Again following ASTM D1002, the aluminium and mild steel samples were assembled with a single lap shear joint with 12.5 mm overlap, as shown in Figure 3.3. Finally the joints were placed in a furnace at various designated times and temperatures to achieve a complete cure.

3.4.1.2 Lap joint specimens tested at high temperature

Two rectangular strips of mild steel of dimensions 100mm long x 25mm wide x 1.0mm thick were used for this test, see Figure 3.6. The mild steel was cleaned using acetone at room temperature prior to the application of the sol-gel adhesive. A hybrid epoxy/sol-gel adhesive (SG3) was applied as a thin layer on both specimen surfaces and the coated substrates were then left to dry for 1 hour at room temperature. Following ASTM D1002, the mild steel samples were assembled into a single lap shear joint with 12.5 mm overlap see Figure 3.6. The applied contact pressure was the same, about 4MPa so the lap joint specimens had an adhesive thickness of about 0.1mm. The prepared sample was then placed into an oven to be cured at 200°C for 16hours. For investigation of the SG3 adhesive shear strength at high temperature, the specimens were maintained at different temperatures (i.e. 22, 40, 60, 80, 100 and 120°C) for 40 minutes and the testing was carried out for each selected

temperature. Figure 3.7 shows the test setup for measuring lap shear strength at the desired temperature.

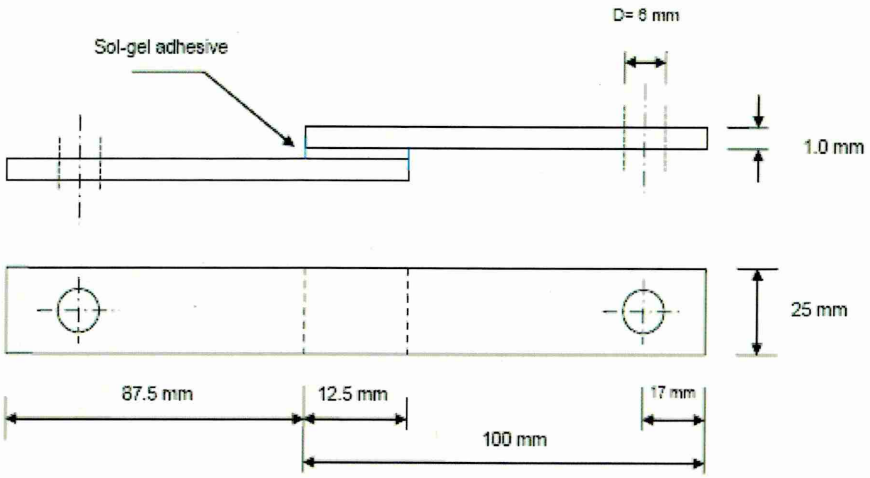

Figure 3.6 Geometry and dimensions of lap joint for experiments at high temperature

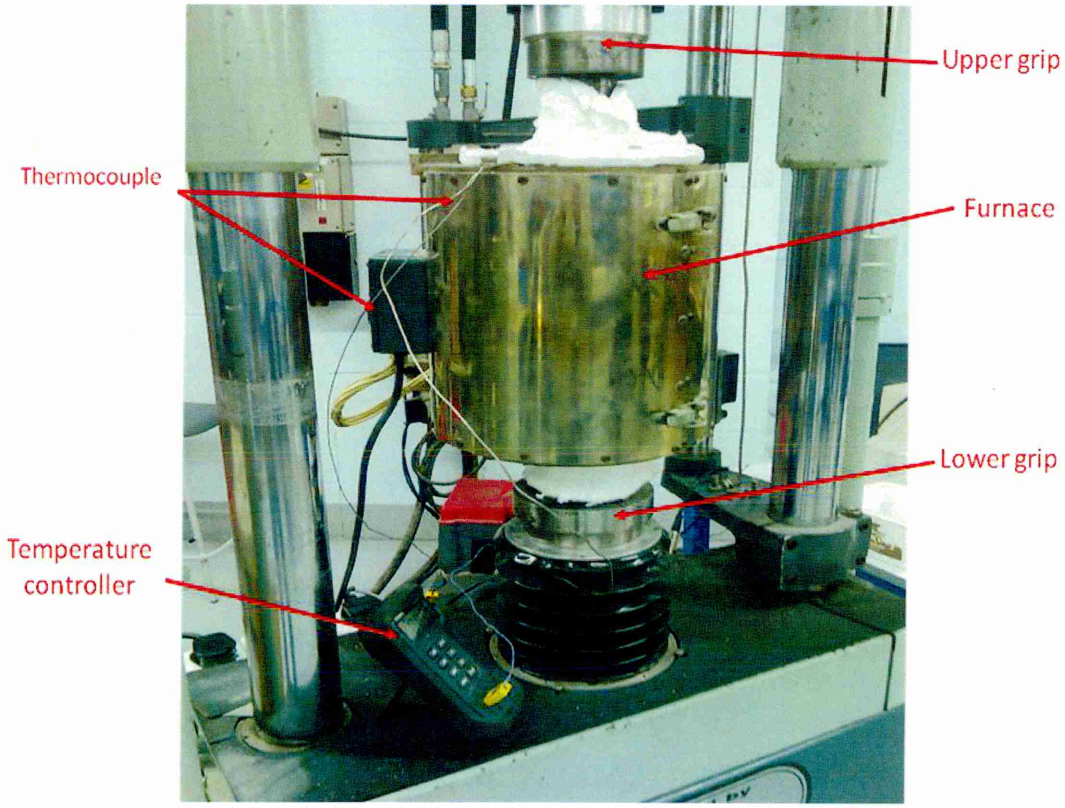

Figure 3.7 Setup for testing of lap joints at high temperature

3.4.2 Tensile test (butt joints)

The tensile strength of adhesive materials is determined as the maximum stress (longitudinal) that the joint can withstand when subjected to tension before failure. Tensile stress acts normal to the stress developed across the plane of the joint. The material used in this experiment was mild steel in the form of rods of 25mm diameter. The bonded surfaces were first washed using deionised water, then air-blow dried and then cleaned using acetone solution. Tensile strength samples, see Figure 3.8, were prepared according to ASTM D2094-00 (Standard Practice for Preparation of Bar and Rod Specimens for Adhesion Tests) [115]. The hybrid epoxy/sol-gel adhesive (SG3) was used to bond the tensile test samples. The bonded specimens were tested in a mechanically driven universal testing machine (Instron tensile machine), having a capacity of 150 KN at a constant crosshead speed of 1mm/min.

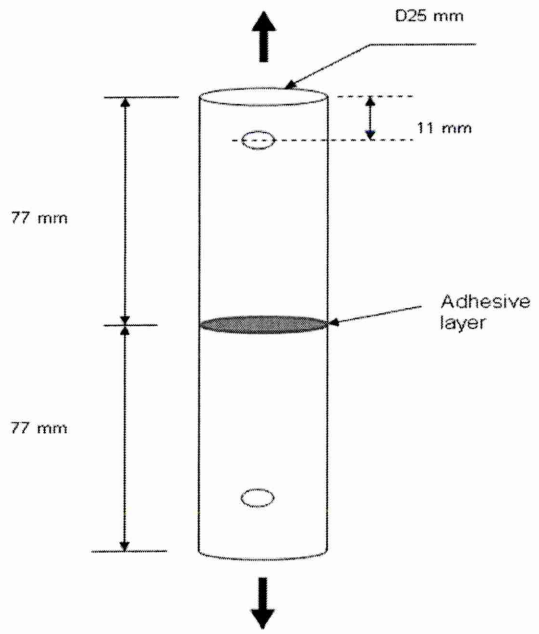

Figure 3.8 Geometry and dimensions of tensile test specimen (Butt joint)

3.4.3 Fatigue test (lap joints)

Lap joint specimens were prepared from mild steel substrates according to ASTM D1002. The hybrid epoxy/sol-gel formulation (SG3) was used as the adhesive material. Cyclic loading (fatigue) tests were performed using tension–tension sinusoidal loads at a constant load ratio of 0.1 at frequencies of 1.0 and 10.0 Hz. Attention was focused on the fatigue performance of lap joints under different maximum load levels, (P_{max}). Testing was conducted at room temperature and the relative humidity was not controlled. The influence of the load frequency on fatigue lives of both joints were studied. Table 3.5 presents the testing parameters for the fatigue experiments. Three lap joint specimens were tested at each P_{max} load for both frequencies.

Table 3.5 Fatigue testing parameters

Environment	Ambient laboratory
Load ratio	P_{min}/P_{max} = 0.1
Load type	Constant amplitude load level (sinusoidal)
Frequency	3.0 & 10.0 Hz

3.4.4 Adhesive strength measurements

Shear mode loading was used to evaluate the hybrid sol-gel and novel hybrid epoxy/sol-gel adhesive strength on aluminium alloy (Al2024-T3) and mild steel substrates. In addition a butt joint geometry was used to evaluate the novel hybrid epoxy/sol-gel adhesive tensile strength on mild steel. Lap shear strength data were taken as the average of at least three measurements with their standard deviations. Butt joint tests were also carried out in this machine on a minimum of five specimens. The joint adhesive strength was calculated using the following formula:

$$\sigma = P\max / A \qquad (3\text{-}1)$$

Where σ is the adhesive strength in (MPa), P_{max} is the maximum load at fracture (N) and A is the average cross-sectional of bond overlap area (mm^2).

3.5 Chemical and structures

3.5.1 Scanning Electron Microscope (SEM)

In this work, joint fracture surfaces were prepared and analysed using a Philips XL40 SEM with an acceleration voltage of ~20kV. A thin gold conductive film (12.5mm × 25mm and about 0.1-0.2 microns thick) was coated onto the specimens to be investigated by plasma-assisted PVD deposition at room temperature to prevent surface charging in the SEM. For some samples, a thin carbon film was coated onto specimens for the same purpose instead of the gold film. For selected samples, Energy Dispersive X-ray analysis (EDX) was applied to identify and analyse the chemical elements on selected areas. The applied current was ~ 20kA and vacuum chamber was ~ 6.3×10^{-5} mbar.

3.5.2 Infinite Focus Microscope (IFM)

Due to the ability to produce 3D images in a short time, allowing the analysis and measurement of 3D data, such as profile, area/projected area, volume, depth/height and surface roughness [116], the IFM (Alicona Imaging GmbH, Austria) was used to provide information relating to the specimen surface, notably, average roughness of the surface [117]. This technique also was used in some cases to characterise the fracture surface mode of the lap joints. The selected area was ~$200\times300\mu m^2$.

3.5.3 Fourier Transform Infrared Spectrometer (FTIR)

FTIR is a common spectroscopic technique for identifying chemical components in both organic and inorganic materials. FTIR was used in this work to determine the effect of curing on adhesive behaviour and evaluate the functional groups in the sol-gel adhesives and in the pure epoxy resin. The FTIR absorption spectrum was obtained using a Nicolet Nexus FTIR spectro-photometer. Thin film adhesive samples were used and the spectra were recorded in the range of 400–4000cm^{-1}. The influence of different cure times/temperatures on the adhesive structure were investigated.

3.5.4 Raman Spectroscopy

In order to characterize the MWCNTs in the epoxy/sol-gel adhesive, Raman spectroscopy was employed. Raman spectra were measured using a Renishaw System 2000 micro-Raman spectrometer in the backscatter configuration. The power of the laser was set to 20mW, and the spectra collection time was set to 60s to achieve a high signal to noise ratio. The spectra were acquired for wavenumbers from 100 to 5000cm^{-1} to detect all peaks in the epoxy matrix, and the D (C-C) and G (C=C) bands of the CNTs in the hybrid epoxy/sol-gel adhesive material. Spectral measurements were made at a minimum of three different locations to ensure reproducibility of peak intensities.

3.5.5 X-ray Photoelectron Spectroscopy (XPS)

XPS has been used extensively in the study of adhesives for determining surface functional groups and failure modes of adhesively bonded joints [118,119]. Measurements were performed using the Scienta instrument (VG Escalab 250 XPS) at Leeds University. A monochromatic Al kα, X-ray source operating at 1487.6 eV was used. The base pressure in the sample chamber was less than 5 x 10^{-9} Torr. Data analysis was carried out using CASAXPS software to determine atomic percentage values from the peak areas. A survey scan and high resolution scans were conducted on each sample. The high resolution scans were charge corrected to the main C 1s peak = 284.7 eV [120] and then quantified to compare the amounts of each element present. Components were fitted under the peaks to give chemical information. Survey scans were run for 10-20 minutes and high resolution scans were run for between 1 and 10 minutes depending on the signal.

3.5.6 Thermo-gravimetric analysis (TGA)

In this work, Thermo-gravimetric analysis (TGA) data was obtained on a Mettler TG-50 instrument using a nitrogen atmosphere. The technique was used to measure the amount and rate of weight change of the adhesive material as a function of temperature and time in a controlled atmosphere [121]. Typically, a sol-gel adhesive sample is examined from room temperature (RT) to above its decomposition temperature. Small amounts of cured adhesive (about 15 mg) were removed from the substrate and placed in an open aluminium sample pan.

The experiments were performed at a 10°C/min heating rate in the temperature range 35-650 °C. The apparatus consists of a microbalance within a furnace, allowing the weight of the sample to be continuously monitored while the temperature is controlled. The change in sample weight during the thermal scan is calculated as follows

$$Weight\ loss = \frac{Wi - Wt}{Wi} \times 100\% \qquad (3\text{-}2)$$

Where Wi is the initial weight and Wt is the weight at a specific temperature and/or time during the scan.

CHAPTER 4 Results

4.1 Effects of the compositions on adhesive strength

4.1.1 Lap shear strength of hybrid sol-gel adhesive

The lap shear strength of Al2024 joints using the original silica-base sol-gel S1# was studied. The results obtained were in the range of 1.38 ± 0.05 MPa. It was observed that the value of the lap shear strength was related to the heat treatment of the joint. At a curing procedure of 120^{0}C for 3 hours the shear strength was 1.38±0.05 MPa. Further increase in cure temperature (up to 170^{0}C), resulted in a shear strength of ~ 1.63±0.05 MPa, see Table 4.1. No significant change in the lap shear strength results was observed at the higher cure temperature. It was found that the effectiveness of the bonding depends on the chemical linkage of molecules across the sol-gel adhesive/Al interface, as Si-O-Al linkages, and within the sol-gel structure, as Si-O-Si bonds. Nemeth and Liu [122] reported that the chemical interaction at the interface between Si-OH in sol-gel and Al-OH on the surface within the polymerisation process led to the formation Si-O-Al bonds.

Table 4.1 Adhesive strength of sol-gel

An average shear strength, MPa	
SG cured @120°C/3Hrs	SG cured @170°C/3Hrs
1.38 ± 0.05	1.63 ± 0.05

Several absorption peaks were observed on the FTIR spectrum of the hybrid sol-gel material, indicating the presence of chemical bonds within the structure, see Figure 4.1. Generally, absorption peak regions between 400-1300 cm^{-1} are mainly associated with combinations of vibrations of silica network [123]. A strong peak at ~ 1086 cm-1 is corresponded to asymmetric stretching vibration of Si-O-Si bridges sequences within the gel structure. IR bands appeared at ~ 850-900 cm-1 is assigned to the stretching vibration of free silanol groups (Si-OH) on the surface of the amorphous solids. The absorption peak at ~ 1460

cm-1 is attributed to the combinations of vibrations of molecular water and SiO_2 network [124].

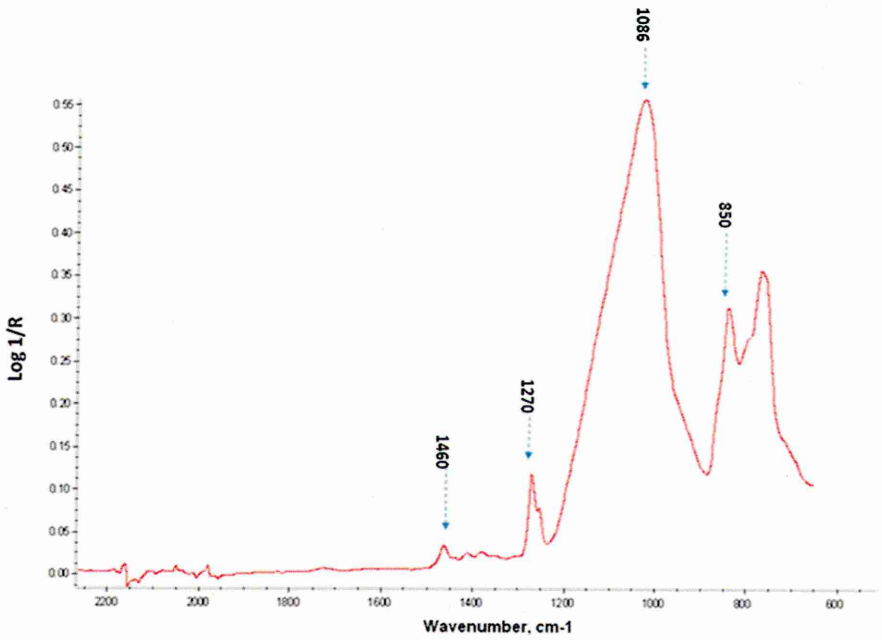

Figure 4.1. FTIR spectra of hybrid sol-gel adhesive material

Scanning electron microscopy of the fracture surface was undertaken to understand the failure mode of this sol-gel adhesive. The interfacial fracture mode was observed on the failed surface. It was found that, typically, the sol-gel system exhibited a brittle fracture that was characterised by straight line crack propagation as shown in Figure 4.2a. A strong Al peak (from the metal surface) and Si peak (from silica sol-gel) were found in the Energy Dispersive X-ray spectrum (EDX), Figure 4.2b.

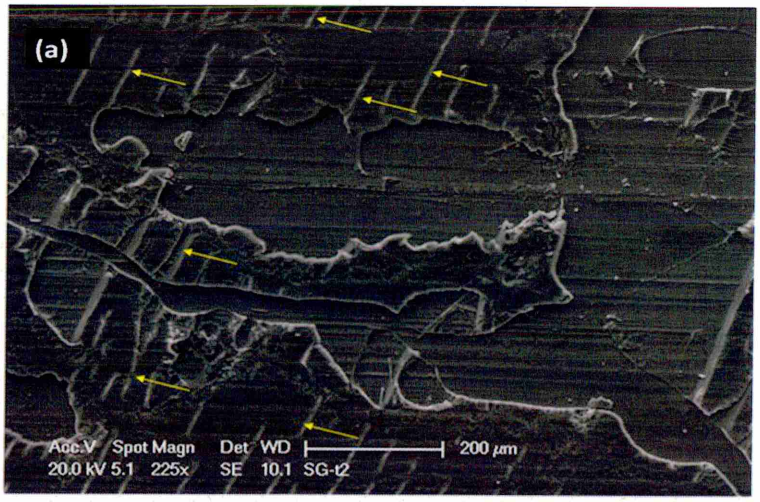

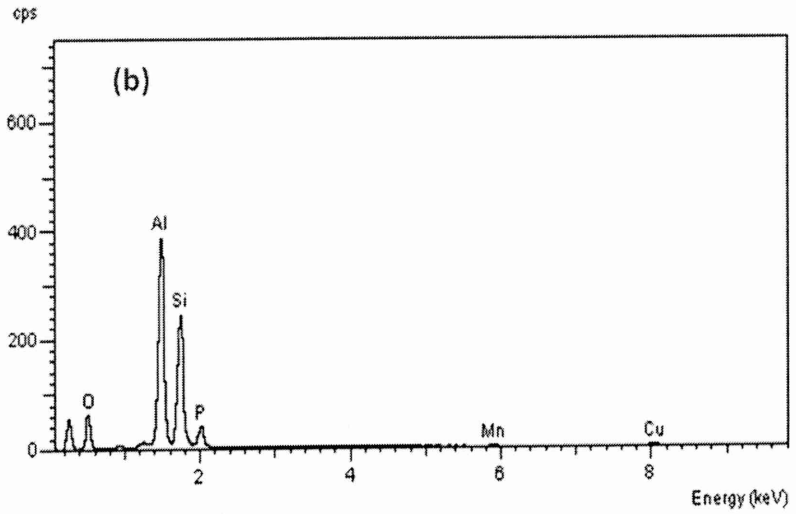

Figure 4.2 a) SEM image of sol-gel fracture surface and
b) EDX analysis

4.1.1.1 Effects of different additives on SG adhesive strength

4.1.1.1.1 Doping 0.05% PANI

The measured mean adhesive strength of sol-gel modified by 0.05 wt % of PANI micro-particles showed little improvement compared with the unmodified sol-gel bonded specimens. The average joint strength obtained was around 1.78±0.09 MPa for a sample cured at 170^{0}C for 3 hrs. This increased to ~ 2.26±0.05 MPa after the curing time was extended to 16 hrs at 170^{0}C. This slight improvement may be attributed to the removal of the residual solvent from the sol-gel during the curing procedure. The presence of polyaniline micro fillers appear to influence the matrix structure resulting in binding between PANI fillers and the sol-gel formulation, and an increase in the sol-gel adhesive strength (i.e. 2.26 MPa), compared with that of the unmodified joint (1.63 MPa). Figure 4.3 shows load/extension curves for the original silica-base sol-gel S1$^{\#}$, and the modified system by 0.05% PANI, where it can also be seen that an increase in extension at failure from ~0.15 to 0.21mm results due to the addition of PANI in the sol-gel matrix was observed.

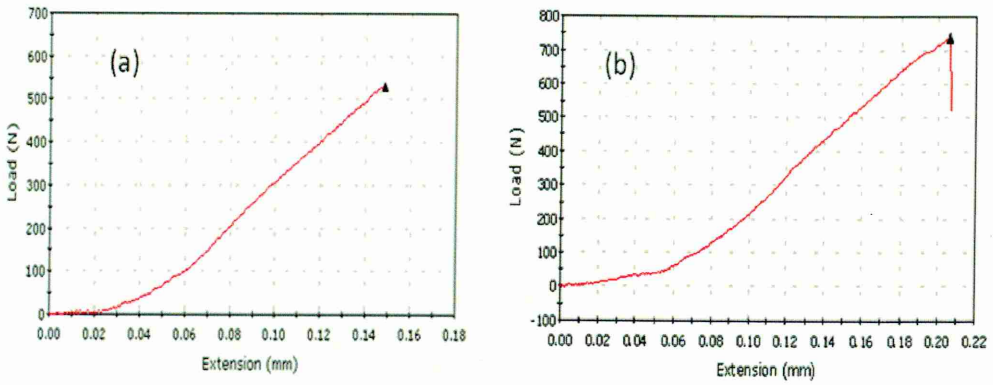

Figure 4.3 Load/extension curve for a) the original sol-gel (S1#), b) sol-gel with PANI

The surfaces of the failed joints showed a mixed cohesive and adhesive fracture, see Figure 4.4. Where the failure of adhesive joints occurs within the adhesive itself the failure is termed "cohesive" and when the failure occurs at the adherent/adhesive interface it is termed "adhesive". The changes in the fracture surfaces due to the increase of the cure time from 3 hours (a) to 16 hours (b), can be seen in Figure 4.4. For example, the changes in cohesive to adhesive fracture ratio in (a) are ~ 42:58% compared with that in (b) 48:52%. And, the distribution of adhesive remaining on both fracture sides is better in (b) compared with that in (a) sample.

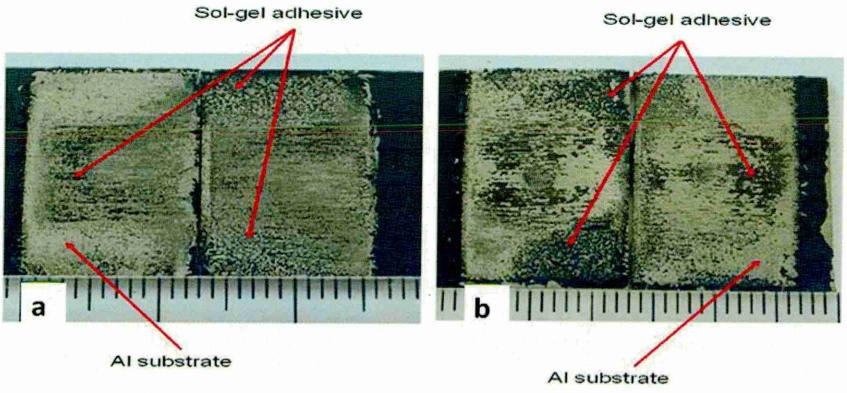

Figure 4.4 Fracture surfaces of sol-gel adhesive with PANI added, a) 3 hours cure time and b) 16 hours cure time

Figure 4.5 shows the SEM observation on the fracture surface of sol-gel adhesive modified by 0.05% PANI. The failure mode was classified as a cohesive (within the adhesive). The incorporation of the long-chain PANI polymer in sol-gel is expected to improve the flexibility of the matrix, which should reduce the stress within the adhesive, resulting in increased the lap shear strength compared with unmodified system, as shown above in Figure 4.3.

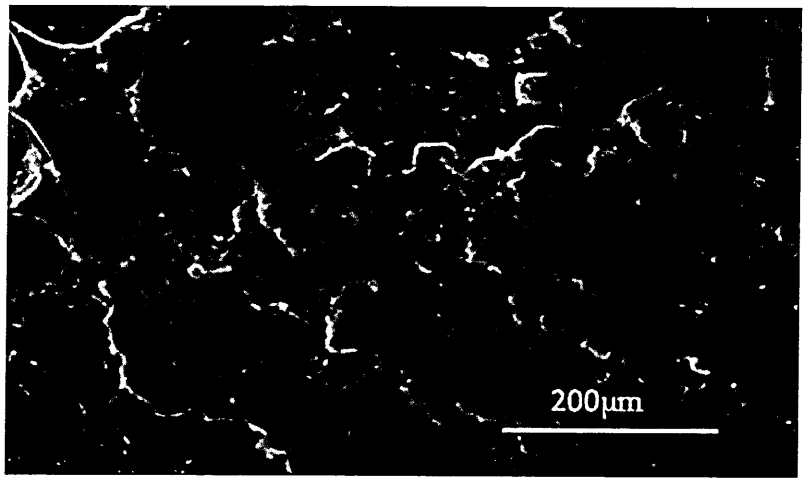

Figure 4.5 SEM sol-gel with PANI modified sol-gel

4.1.1.1.2 Effects of the addition of γ-Al_2O_3 nano-particles

The effect on the joint shear strength of adding various concentrations of γ-Al_2O_3 nano-particles to the untreated sol-gel was investigated. Measurements found that samples with added γ-Al_2O_3 showed a significantly higher adhesive strength than that of the unmodified sol-gel. The results were obtained for cure condition of 140^0C for 3 hours. The shear strength was enhanced due to the cross-linking of γ-Al_2O_3 nano-particles through the binding of -Al-O-Si- in the sol-gel coating. This interaction was demonstrated by Anggono [125] who reported that composite particles can be prepared by adsorption, hydrolysis and precipitation reactions of a component on the surface of sol particles as seen in Figure 4.6.

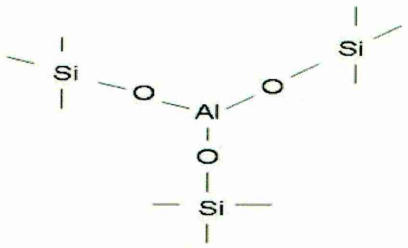

Figure 4.6 Schematic SiO_2-Al_2O_3 cross-link [125]

Figure 4.7 shows the lap shear strength of AD3# sol adhesive as a function of the concentration (weight %) of the doped γ-Al_2O_3 nano-particles. The greatest shear strength obtained was 4.48 ± 0.03MPa when 0.5% by weight of γ-Al_2O_3 nano-particles was added into the S1# sol. As the concentration of γ-Al_2O_3 nano-particles was further increased in the sol, the adhesive strength decreased gradually.

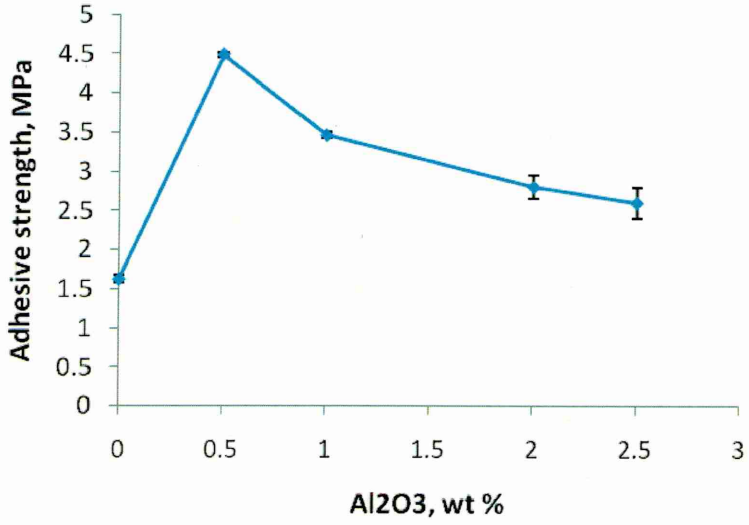

Figure 4.7 Effect of adding γ-Al_2O_3 nano-particles on lap shear strength of sol-gel adhesive

The improvement in adhesive strength by the addition of nanofiller into the matrix can be attributable to the fact that the stress distributions transfers from the matrix to the particles, causing an increase in the lap shear strength. In addition, a large increase in the effective contact area being adding nanofiller materials may improve the corrslinking within the adhesive matrix, leading to

increase the adhesive strength. The SEM image in Figure 4.8 shows the distribution of the γ-Al_2O_3 nano-particles in the sol-gel structure.

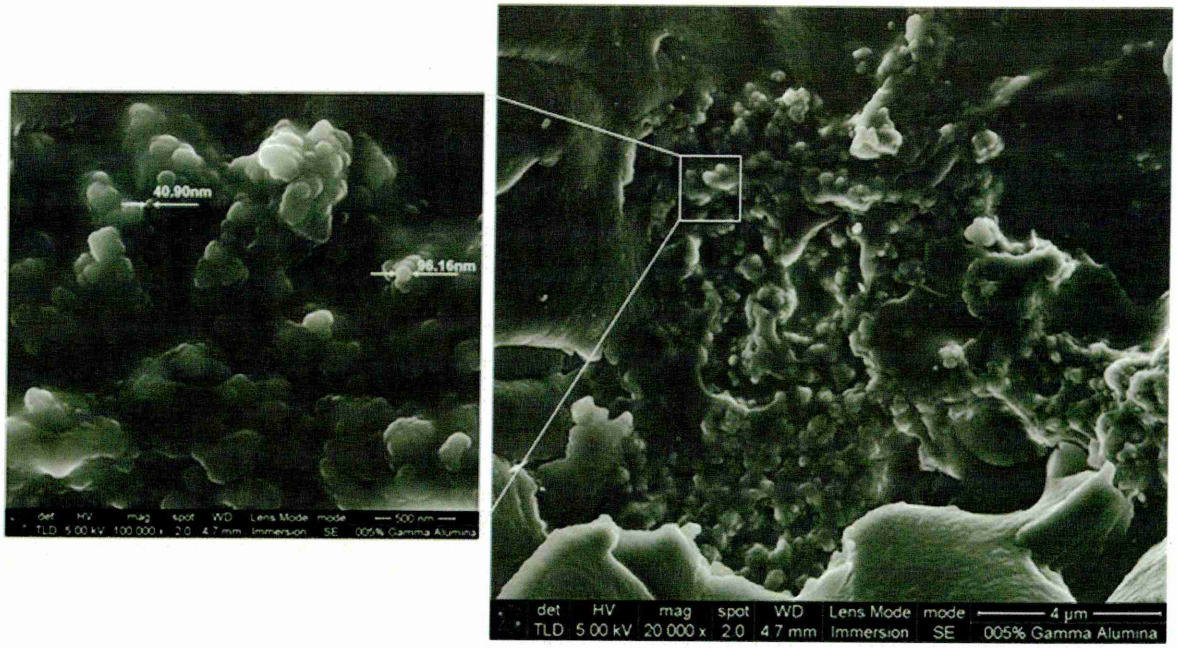

Figure 4.8 SEM of the γ-Al_2O_3 nano-particles (0.5%) within the sol-gel

Fig 4.9 shows a typical EDX analysis of the adhesive showing strong aluminium, oxygen and silicon peaks in the spectrum.

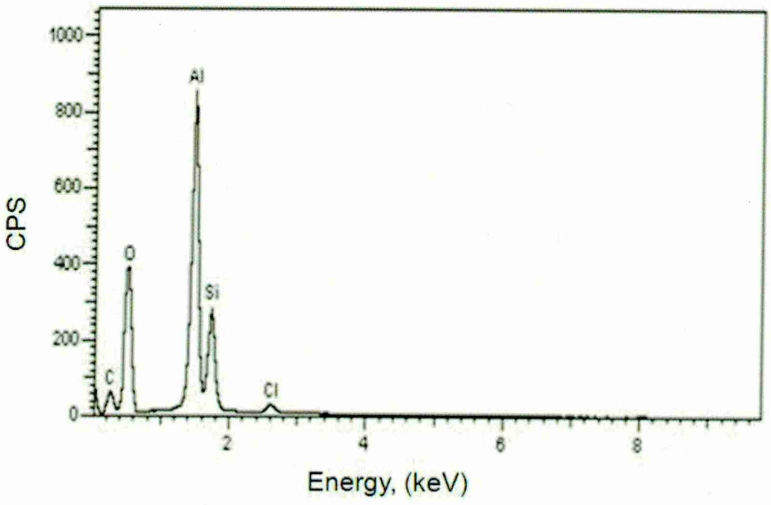

Figure 4.9 EDX analysis of γ-Al_2O_3 in silica sol-gel

The fracture profile of the failed specimen, and the bare aluminium surface of the substrate were investigated using the IFM, as the technique can produce images in 3D, see Figure 4.10 a and b. It can be seen that a large amount of the fracture surface area was covered by the adhesive and this indicates that the incorporation of γ-Al_2O_3 nano-particles into the sol-gel adhesive improved its adhesion to the surface of the substrate. The interconnections between γ-Al_2O_3 and the original sol-gel has modified the sol-gel structure and increased the bond strength at the adhesive/surface interface.

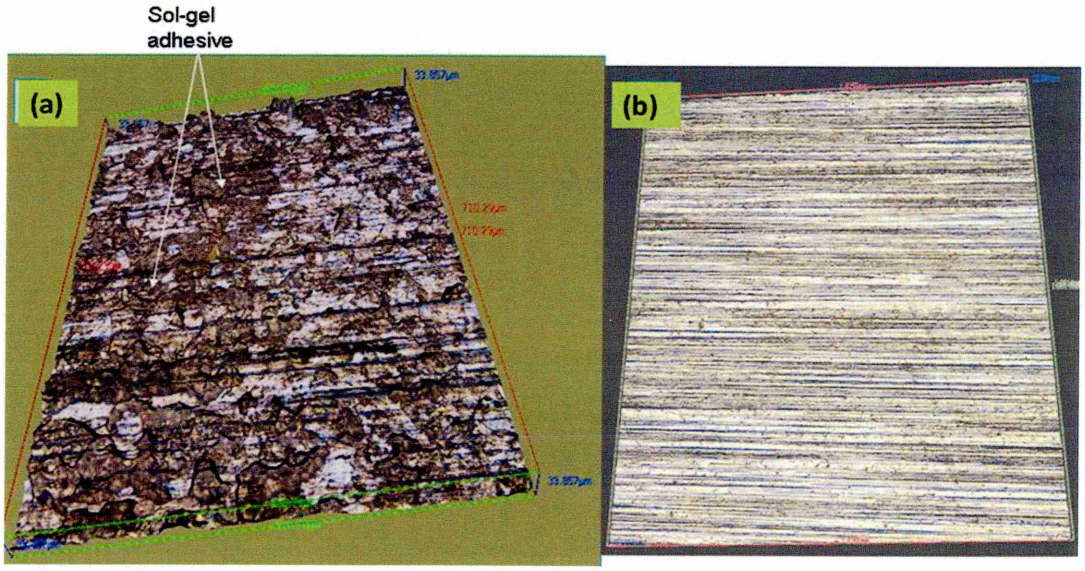

Figure 4.10 a) IFM fracture surface of 0.5 wt % Al_2O_3 modified sol-gel,
b) IFM surface of the received aluminium substrate (Ra=0.1μm)

4.1.1.1.3 Effects of the addition of TiO_2 nano-particles

The adhesive strength of AD4# was increased by the addition of TiO_2 nano-particles into the silica-based sol S1#. Different concentrations of TiO_2 nano-particles from 0.5 to 2.5%, were added into the original sol-gel system S1#. The results indicate that the AD4# joint strength was significantly increased above that of the base sol-gel system. The highest shear strength was about 4.0 ± 0.02 MPa and was achieved on addition of 2.0 wt % TiO_2 nano-particles at a heat treatment of 140^0C for 3 hours. Figure 4.11 shows the schematic diagram of the Si—O—Ti cross-linking as reported in [126].

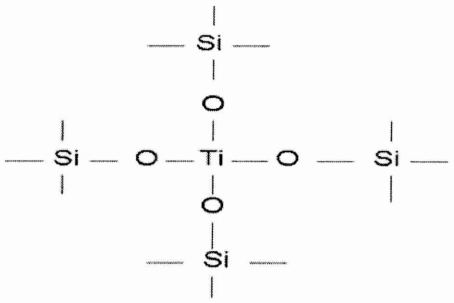

Figure 4.11 Schematic of SiO_2-TiO_2 cross-link [126]

Figure 4.12 shows the changes in sol-gel adhesive strength as a function of addition of TiO_2 nano-particles (wt %). The presence of nano-sized TiO_2 particles in the sol-gel system may increase the adhesive strength as the formation of Ti-O-Si bonds within the sol-gel structure. This is in agreement with Wu [127] who found that the incorporation of titanium and silicate phase lead to the formation of Ti–O–Si, Ti–O–Ti, and Si–O–Si bonds within the hybrid materials.

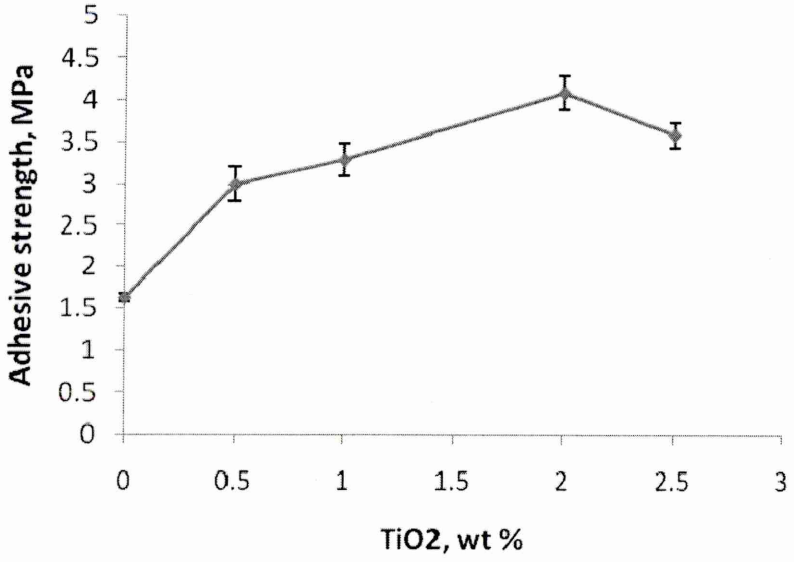

Figure 4.12 Effect of TiO_2 nano-particles
on adhesive strength of sol-gel

Figure 4.13 shows FTIR spectra for the hybrid sol-gel material (S1#) and the modified system with TiO_2 nano-partices (AD4#). The strong absorption peak at ~ 1086 cm^{-1} is attributed to the formation of Si-O-Si bonds in sol-gel matrix. A shoulder absorption peak at 927 cm^{-1}, being corresponded to the interaction between the silica matrix and TiO_2 nano-fillers as Si-O-Ti [128], confirming the cross-linking between sol-gel matrix and TiO_2, leading to the increase in the adhesive strength.

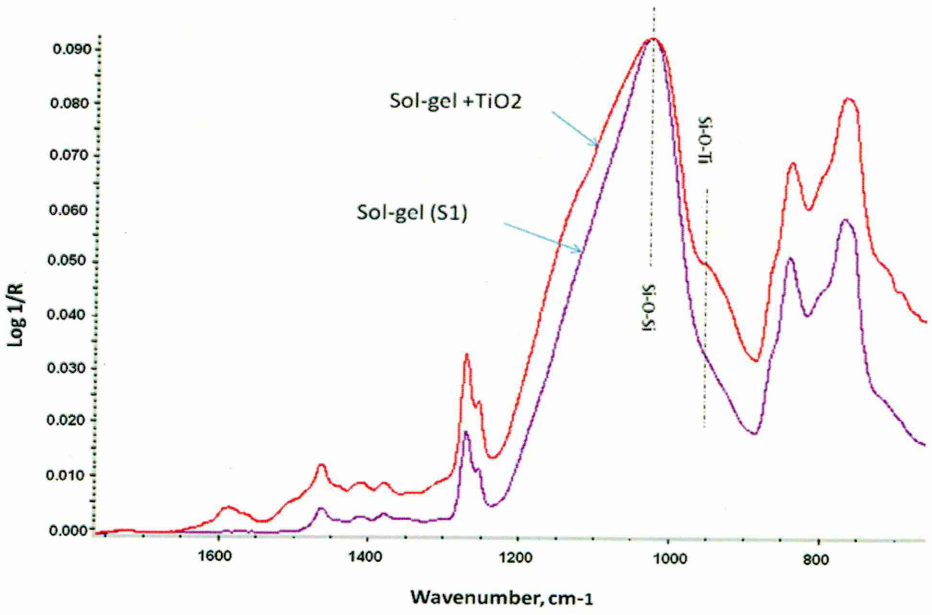

Figure 4.13 FTIR of hybrid sol-gel and modified system with TiO_2

SEM, EDX and IFM were used to investigate the surface fracture of the failed joint, see Figures 4.14, 4.15 and 4.16. Figure 4.14 shows the distribution of TiO_2 particles within the sol-gel adhesive.

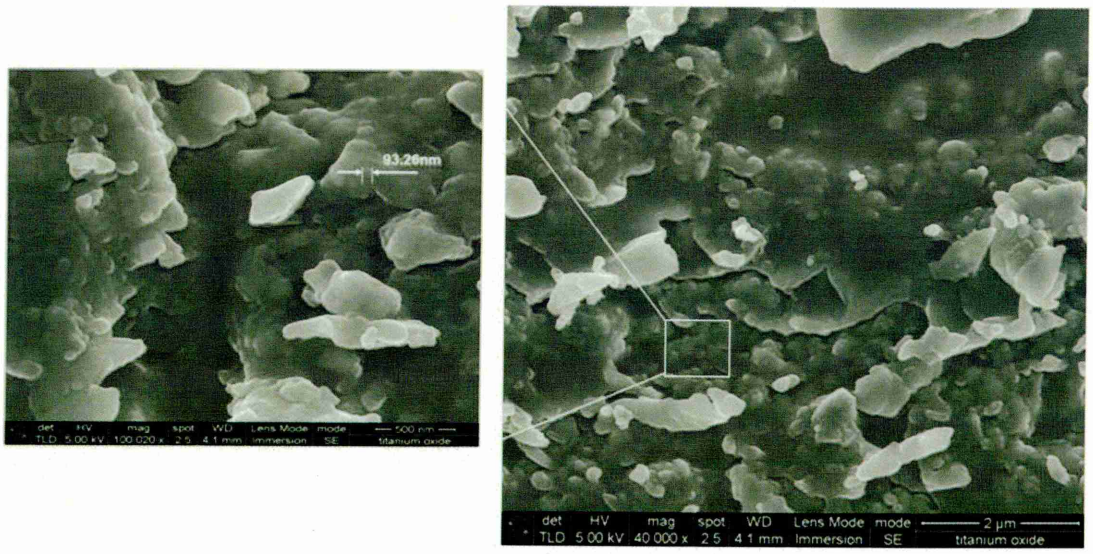

Figure 4.14 SEM and EDX of TiO_2 nano-particles in the sol-gel

The appearance of silicon, oxygen and titanium peaks in EDX spectra confirmed the presence of these materials within the adhesive formulation, see Figure 4.15.

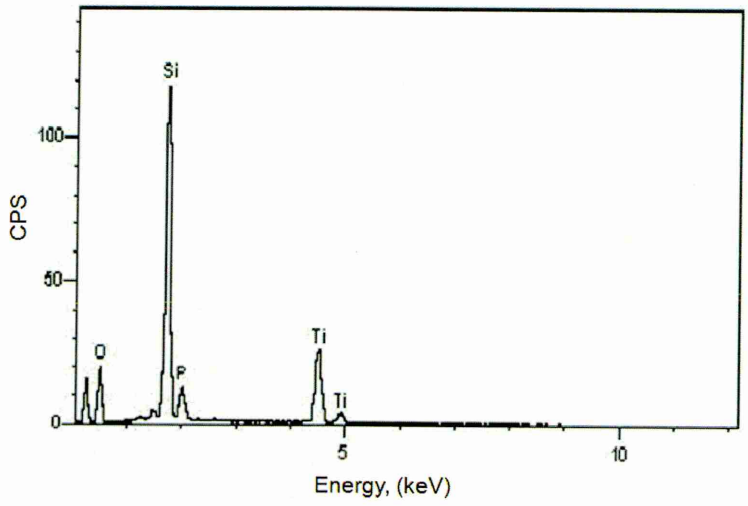

Figure 4.15 EDX analysis of TiO_2 nano-particles in the sol-gel

The 3D IFM image shown in Figure 4.16, indicates a mixed cohesive and adhesive failure mode of the sol-gel.

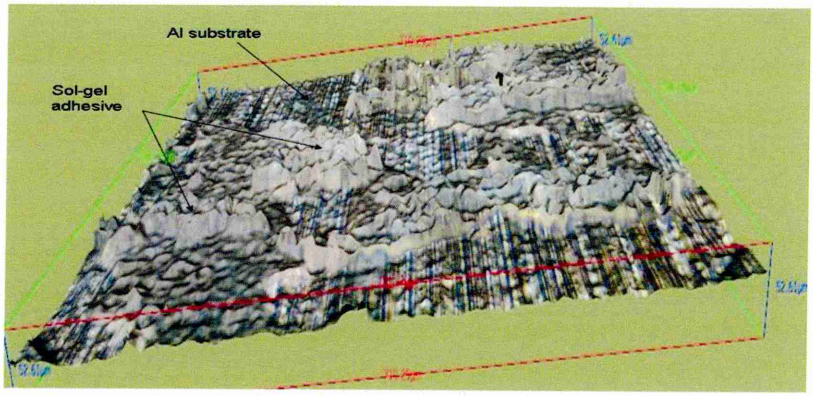

Figure 4.16 IFM fracture surface by adding 2% TiO_2 nano-particles

4.1.1.1.4 Doping PANI and γ-Al_2O_3 nano-particles

The incorporation of different amounts of PANI and γ-Al_2O_3 nano-particles in the original silica-base sol-gel as AD5#, AD6# and AD7# samples, further increased the adhesive strength from that of the unmodified system, see Figure 4.17. The maximum shear strength value was obtained using AD6# adhesive; i.e. 5.09 MPa. The increased in adhesive strength in this system compared with that in the unmodified sol-gel may be attributed to the combination of the inorganic and organic components within the sol-gel formulation, which improved the cross-linking with the matrix, thus increasing the material cohesive and interfacial forces within the joint.

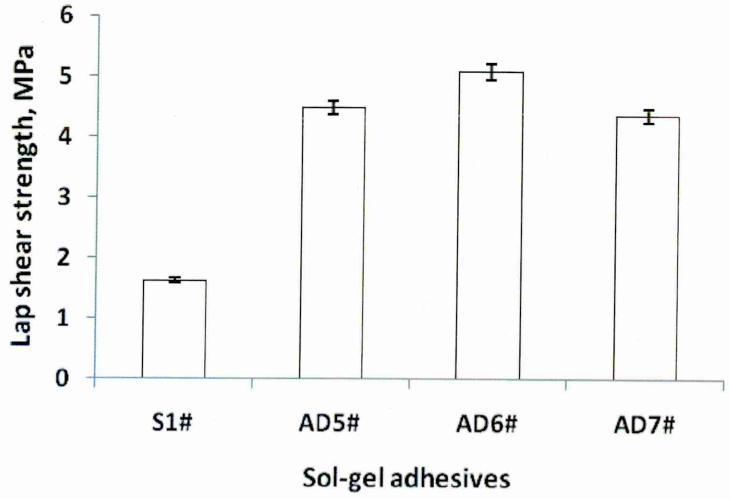

Figure 4.17 Adhesives lap shear strength for S1#, AD5#, AD6# and AD7#

Fracture surfaces were examined under an optical microscope to identify the failure mode. Examination showed that AD5# and AD6# failed by interfacial fracture mode. However, AD7# showed a more cohesive failure mode. This information was supported by digital images from (Fujifilm camera, FinePix S9500) taken on the failed surface of AD6# and AD7#, as shown in Figure 4.18 a&b. Hence, it is suggested that the adhesive formulation (notably differences in PANI/γ-Al_2O_3 ratio) may play an important role in determining the fracture behaviour.

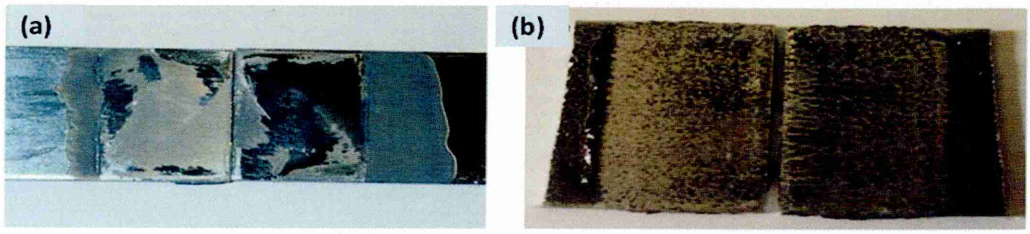

Figure 4.18 sol-gel adhesive fracture surface modes,
a) AD6# adhesive mode and b) AD7# cohesive mode.

Fracture surfaces of the AD5#, AD6# and AD7# adhesives were further characterised at high magnification using the SEM as shown in Figures 4.19, 4.20 and 4.21.

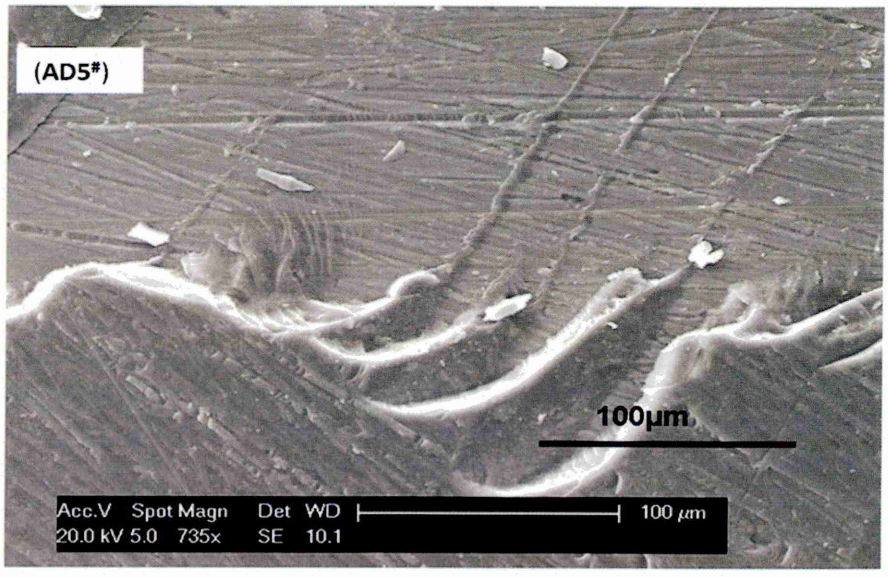

Figure 4.19 Adhesive failure surface of AD5# sol-gel adhesive cured at 120°C/16hr,
(shear strength 4.49MPa)

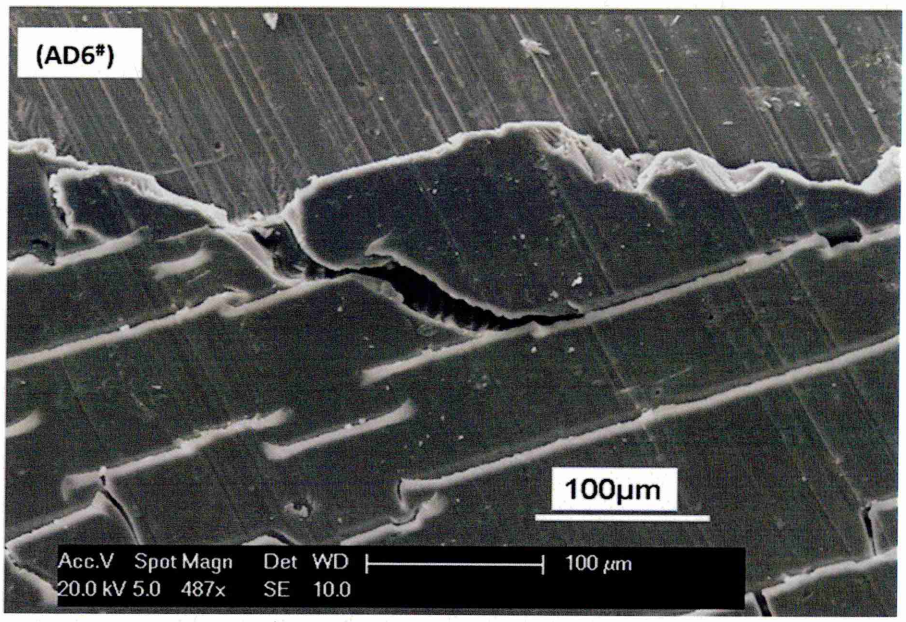

Figure 4.20 Adhesive failure surface of AD6# sol gel adhesive cured at 170°C/16hr, (shear strength 5.09MPa)

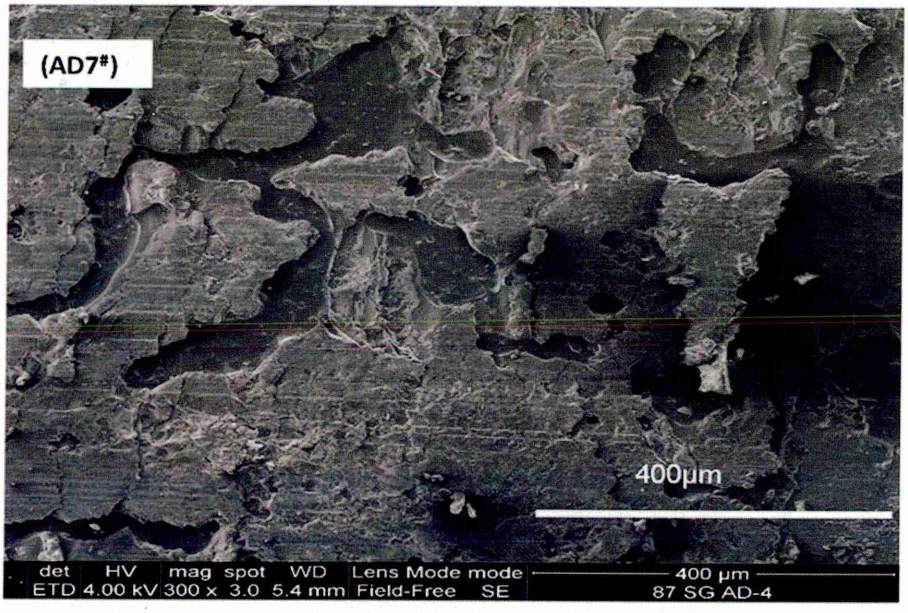

Figure 4.21 Cohesive failure surface of AD7# sol gel adhesive cured at 110°C/16hr, (shear strength 4.37MPa)

4.1.2 Lap shear strength of hybrid epoxy/sol-gel adhesives

All the results above show that the lap shear strength of the hybrid sol-gel system can be affected by the addition of different additives within the matrix. Here the formulation changes caused the lap shear strength to increase from 1.38 to 5.09MPa, depending upon the doping components. There are two key factors that affect the lap shear strength; the internal bond strength, and the adhesion between the adhesive and the substrate. This effect has been demonstrated by the improvement of the adhesive strength by the addition of γ-Al_2O_3 and TiO_2 nano-particles. However, the increase in strength may be limited by the structure of the hybrid sol-gel matrix which only consisted of hybrid SiO_2 nano-particles. Hence, further improvement of adhesive strength is expected via further modification of the sol-gel formulation; i.e. the addition of an organic polymer into the hybrid sol-gel matrix. Ellis [129] reported that the presence of reactive groups in the cured resins (long chain polymer) developed very highly branched, and promoting the cross-linking within the adhesive structure.

The development and demonstration of this novel sol-gel/epoxy adhesive is based on the combination of organic and inorganic components within the adhesive matrix. Hybrid inorganic/organic sol-gel systems are materials formed by incorporating a functional organic polymer or organic-functional silane into the matrix of an inorganic network. Organic polymers provide specific characteristics with respect to their toughness, flexibility, and processability [130] while the inorganic component enhances mechanical and thermal properties. The mechanical results of lap shear tests performed at room temperature on different hybrid epoxy/sol-gel adhesives cured at 140^0C for 16 hours on Al2024-T3 and mild steel substrates are shown in Figure 4.22.

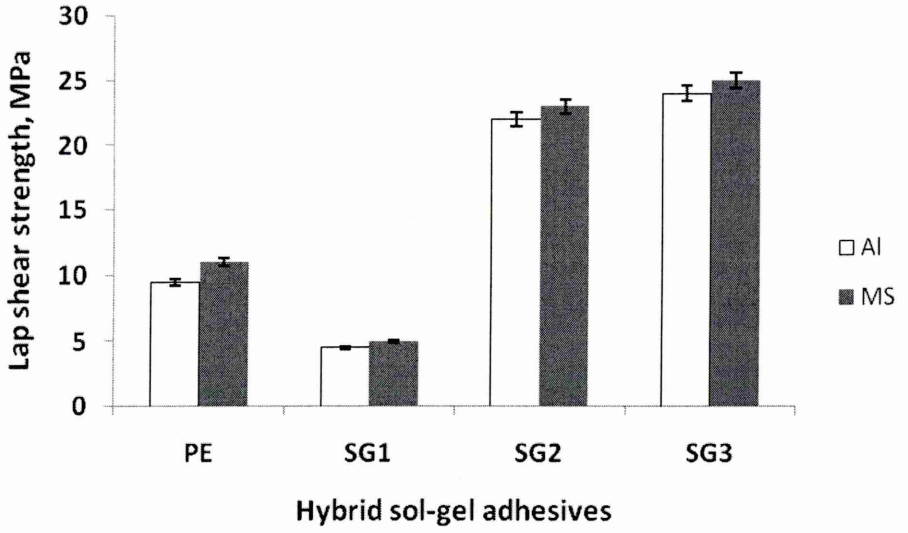

Figure 4.22 Lap shear strength of different sol-gel adhesives

The results show that the adhesive strength using a mild steel substrate was consistently slightly greater than when an aluminium substrate was used. This may be attributed to stress concentrations that occur in the curing stage. Cure condition can result in stress concentration within the joint due to the differences in thermal coefficient between the adhesive and substrate. The lap shear strength of the pure epoxy (PE), cured using an amine hardener, on aluminium and mild steel substrates were 10±0.3MPa and 11.2±0.6MPa, respectively. However, the lap shear strength of the modified system obtained by simple mixing of the PE with the sol was recorded as 3.9±0.1MPa on aluminium (SG1/Al), and 4.9±0.1MPa on mild steel (SG1/MS). A reduction in shear strength was observed with this formulation compared with that of the PE. The incorporation of γ-Al_2O_3 nano-particles into SG2, and a mixture of MWCNTs and γ-Al_2O_3 into SG3 sol-gel epoxy adhesives gave a significant improvement in the adhesive performance, where the adhesive strength increased up to 22±0.4MPa (SG2/Al) and 24±0.5MPa (SG3/Al) on the aluminium 2024-T3 substrate. Similar results were obtained for mild steel substrates where addition of nano-particle resulted in adhesive strengths of 23±0.7MPa (SG2/MS) and 25±0.8MPa (SG3/MS). The modification of an epoxy resin/sol-gel system as a result of doping small amounts of MWCNTs and γ-Al_2O_3 nano-materials

enhanced the adhesion properties (by ~ 8%) for both Al2024-T3 and mild steel surfaces.

Examination of Figure 4.22 indicates that hybrid epoxy/sol-gel adhesive modified by MWCNTs and γ-Al_2O_3 nano-particles (SG3) gave the best bond strength on both substrates. The SG3 adhesive fracture modes of mild steel and Al 2024-T3 substrates for a lap-joint cured at 140^{0}C for 16 hours are presented in Figure 4.23a&b. It can be seen that the fracture surfaces of mild steel indicated a mixed interfacial/cohesive fracture mode, ~ 70:30 %, see Figure 4.23a. The same mixed fracture mode was observed in the Al 2024-T3 failed joints, and the percentage of interfacial to cohesive mode is ~ 80:20 %, as shown in Figure 4.23b. The failure in the joints was initiated at free edges, where a maximum stresses in lap joint, further propagated along, crack paths in the interface or within the interfacial region.

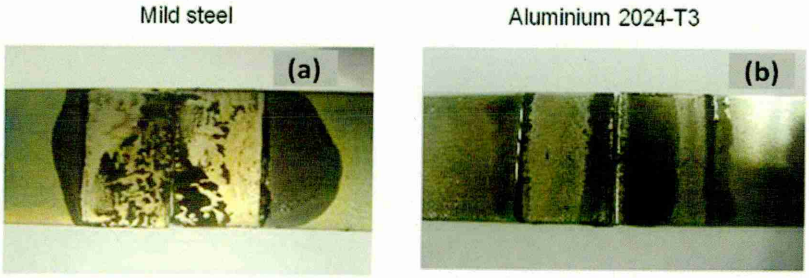

Figure 4.23 Mixed interfacial/cohesive fracture surface of lap joints

(a) SG3/MS, and (b) SG3/Al

4.1.2.1 Effects of concentration of γ-Al_2O_3 on SG3

The results presented in Figure 4.24 show that the incorporation of Al_2O_3 nano-particles increased the lap shear strength of epoxy/sol-gel adhesive material. Due to these nano-size materials, chemical interactions within the formulation such as the formation of Al-O-Al or Al-O-Si bonds increased the degree of adhesive cross-linkage. As a result, improvements in the bond strength of this system were observed. Figure 4.24 shows the measured adhesive strength

after doping the SG3 adhesive formulation with different amounts of γ-Al_2O_3. Mild steel specimens were prepared for lap joints, which were cured in an oven at 200°C for 16 hours. Initially there was an increase in SG3 adhesive shear strength with increase in γ-Al_2O_3 up to 4.0 wt%. This may be because the nano γ-Al_2O_3 increased the crosslinkage where many surface hydroxyl group on γ-Al_2O_3 materials and in silica sol-gel may react during the polymerisation stage as Al-O-Si bond and enhanced the adhesion strength per interaction area within the adhesive matrix. Lambert and Vasconcelos [131] reported that hydroxyl groups in the γ-Al_2O_3 materials can be readily reacted with silanol groups present within sol-gel structure, yielding the production of mixed bonds. The maximum adhesive strength of SG3 recorded was 23±0.4MPa. However, as the level of these inorganic materials in SG3 increased further, the adhesive shear strength gradually decreased. The reduction in the strength can be attributed to the increase in adhesive viscosity. The behaviour of the adhesive formulation changes from a liquid-like to a more solid-like state, reducing its wetting ability on the substrate surface, and thus decreasing shear strength.

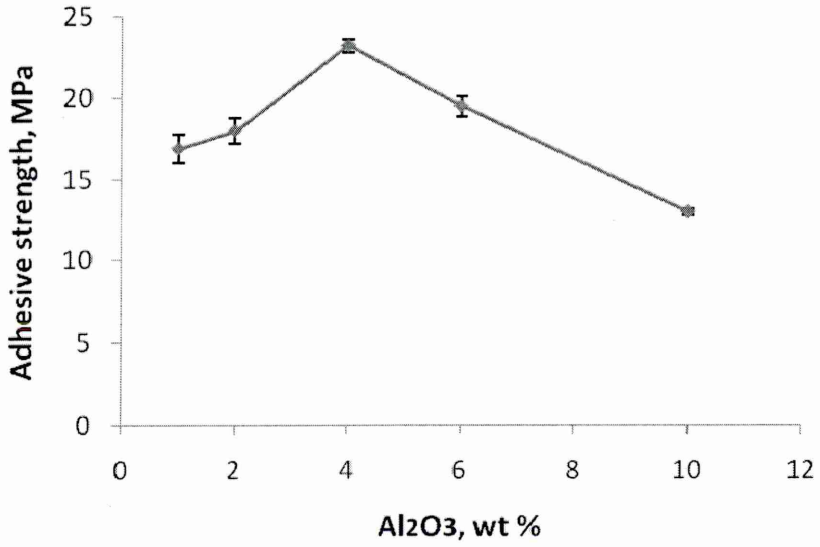

Figure 4.24 Lap shear strength of SG3/MS with addition of γ-Al_2O_3 (cure time 16 hours, cure temperature 200°C)

Figure 4.25 shows the changes in tensile stress/strain curves for the SG3 adhesive as a function of different amounts of added γ-Al_2O_3. It can be seen that the tensile strength/strain of lap joints increased with the addition of γ-Al_2O_3, exhibiting a maximum strength value of ~ 23±0.4MPa, and the highest strain value of ~ 0.015mm/mm at 4.0 %wt concentration. However, with an increase in the nano-filler content beyond 4.0 wt%, a decrease in tensile stress/strain values were observed. As the γ-Al_2O_3 increased from 4.0 to 6.0 and 10 wt%, the areas under the stress/strain curves clearly decreased, suggesting a reduction in adhesive strength. In addition, the total strain decreased as the concentration of γ-Al_2O_3 increased from 4.0% to 6.0% and 10 wt%, indicating increased brittleness. The behaviour may attribute to the presence of free non-interaction γ-Al_2O_3 nano-particles within the matrix, which promoted a higher number of stress concentration sites and reduced the adhesive's ability to absorb energy before fracture.

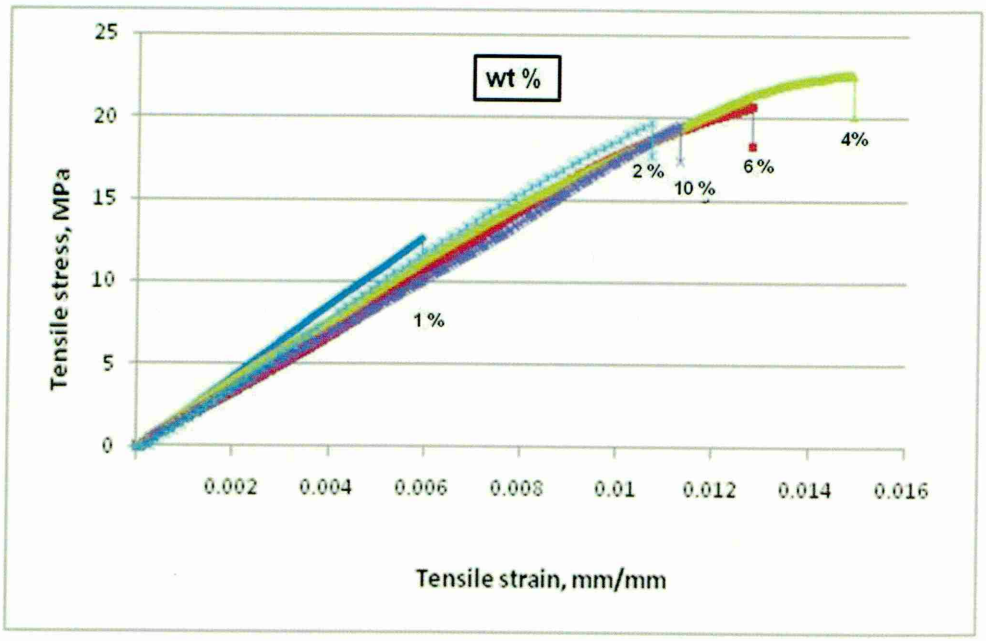

Figure 4.25 Stress/strain curve of SG3 with addition of γ-Al_2O_3 (cure time 16 hours, cure temperature 200°C)

4.1.2.1.1 SEM observations

Examination of the adhesive fracture surface of the SEM images in Figure 4.26 a, b and c, show different faliure modes. In Figure 4.26a, can be seen that doping 1.0 wt% of γ-Al_2O_3 into the SG3 adhesive produced a fracture with long cracks within the bulk adhesive, suggesting that the adhesive was brittle and the amount of γ-Al_2O_3 added was insufficient to improve adhesive ductility. The adhesive failure due to this volume of nano-fillers was a mixed adhesive/cohesive mode. Around 70% of adhesive materials were remained on the fracture surface (cohesive) and 30% were uncovered surface (adhesive).

The fracture surface of SG3 adhesive with 2.0 wt% γ-Al_2O_3 added consisted of short cracks see Figure 4.26b, indicating the crack propagation is more restricted compared with Figure 4.26a. Here the failure mode was cohesive. The addition of this amount of γ-Al_2O_3 to the formulation may increase the adhesive ductility due to the increase in adhesive cross-linking, but the addition of higher amounts γ-Al_2O_3 (10 wt%) to the SG3 adhesive decreases adhesive bonding to the substrate surface resulting from 70 to 80% an interfacial fracture mode, see Figure 4.26c. The failure at the adhesive/substrate interface results from weakness in the interface where the stress concentrations increased the local stress to levels exceeded the interfacial bonding strength.

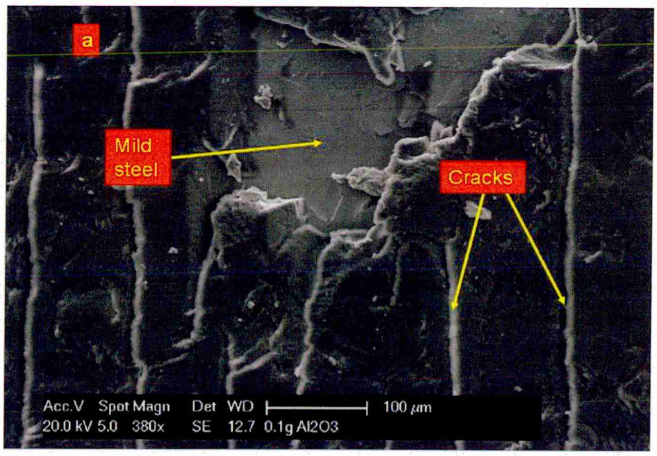

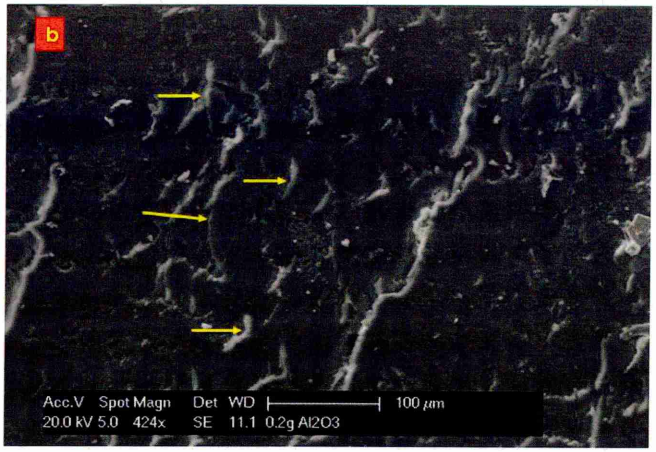

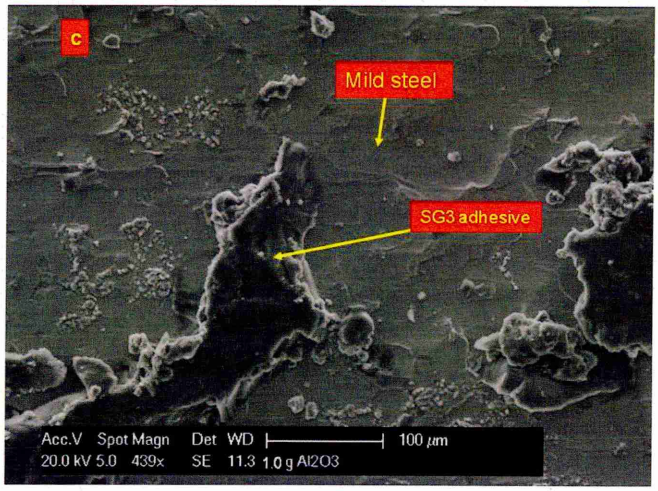

Figure 4.26 SEM images of SG3 fracture surfaces with addition of γ-Al_2O_3, (**a**) 1.0 wt%, (**b**) 2.0 wt% and (**c**) 10.0 wt% (cure time 16 hours, cure temperature 200°C)

4.1.2.2 Effects of concentration of MWCNTs on SG3

The use of CNTs as additives has been widely investigated by researchers because of the possibility of obtaining materials with enhanced mechanical and electrical properties. CNTs are dispersed in polymer matrices as reinforcement to improve strength and electrical conductivity and/or reduce thermal shrinkage and increase thermal stability [132]. The application of CNTs, however, depends on the ability to disperse them homogenously throughout the matrix.

The shear tensile strength of sol-gel/epoxy sytem modified with different ratios of MWCNTs has been determined using an Instron tensile test machine. Figure 4.27 shows the effect of doping different amounts of MWCNTs into the sol-gel/epoxy on the adhesive lap shear strength. It can be seen that the shear

strength is increased when small amounts of MWCNTs are added. However, above about 0.07 wt%, addition of MWCNTs to the epoxy/sol-gel system, decreases in the adhesive shear strength were observed. Initially adding the nano-tube fillers improved the bonding, being attributed to both the mechanical load transfer from the matrix to the MWCNTs and the high specific surface area of this material, which increase the degree of cross-linking with other inorganic fillers in the formulation. However, increasing the amount of MWCNTs above about 0. 07 wt%, decreases the adhesive strength. The reason may be attributed to the higher amount of MWCNTs within the matrix led to excessively viscous and the wetting of the substrate surfaces decreases, limiting the strength. This was supported by Loos et al. [133] who reported that the addtion of higher CNTs contents may reduce the strength of adhesive materials due to the increased in adhesive viscosity.

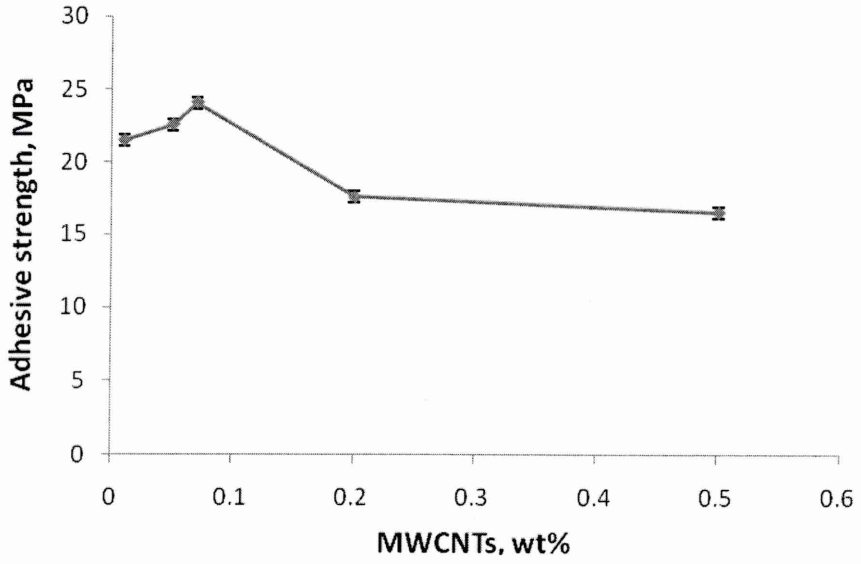

Figure 4.27 Lap shear strength with different amounts of MWCNTs added to sol-gel/epoxy sytem

Figure 4.28 shows that adding small amounts of MWCNTs (i.e. 0.01, 0.05 and 0.07 wt%) into the SG3 matrix increases the lap shear strength value. However, a higher content of MWCNTs in the adhesive matrix may result in poor interaction between the CNTs and the adhesive, and then the adhesive become excessively viscous, consequently decreasing the adhesive wettability and subsequently causing decrease the tensile strength/strain value.

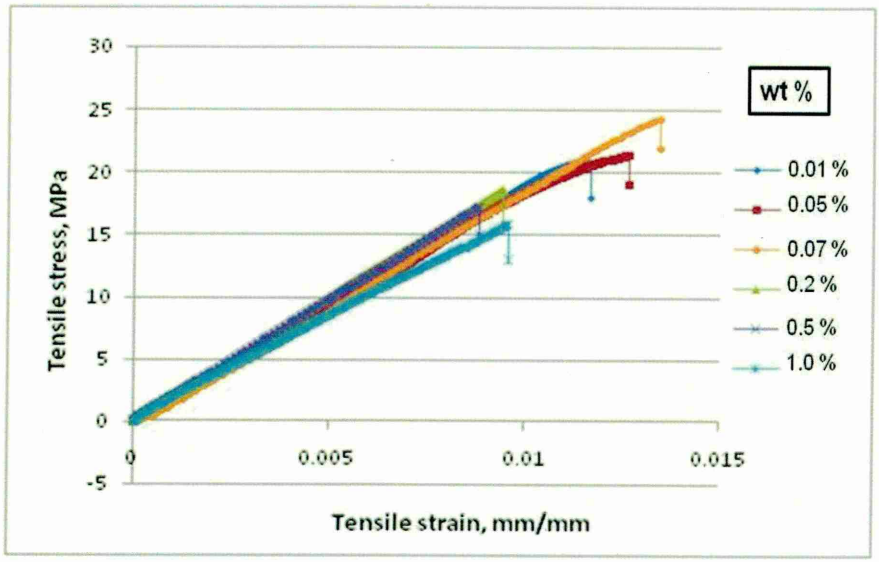

Figure 4.28 Stress/strain curves for different amounts of MWCNTs added to sol-gel/epoxy sytem

4.1.2.2.1 SEM observations

SEM images of the fracture surfaces were used to assess the fracture modes of SG3 adhesive on a mild steel substrate see Figure 4.29 a, b and c. Figure 4.29a shows the SEM micrograph of SG3 fracture surface with MWCNTs 0.01wt%. A mixed interfacial/cohesive fracture mode can be seen. This fracture mode indicates strong links at the adhesive/substrate interface, interaction between CNTs and the matrix was achieved which improved adhesion performance of SG3 to the substrate. The failure may have been initiated at the adhesive/substrate interface and then transferred within the bulk adhesive, confirming two adhesion forces controlled this system. Figure 4.29b shows the fracture surface following the addition of 0.2 wt% MWCNTs to the SG3 matrix. An interfacial fracture mode (adhesive mode) can be seen. With further increase in the amount of MWCNTs added, up to 1.0 wt%, the fracture surface mode remains interfacial with cracks in the adhesive matrix, see Figure 4.29c. The cracks may be due to the increase in MWCNTs free volume within the adhesive, which weakens interfacial bonding and reduces adhesive shear strength.

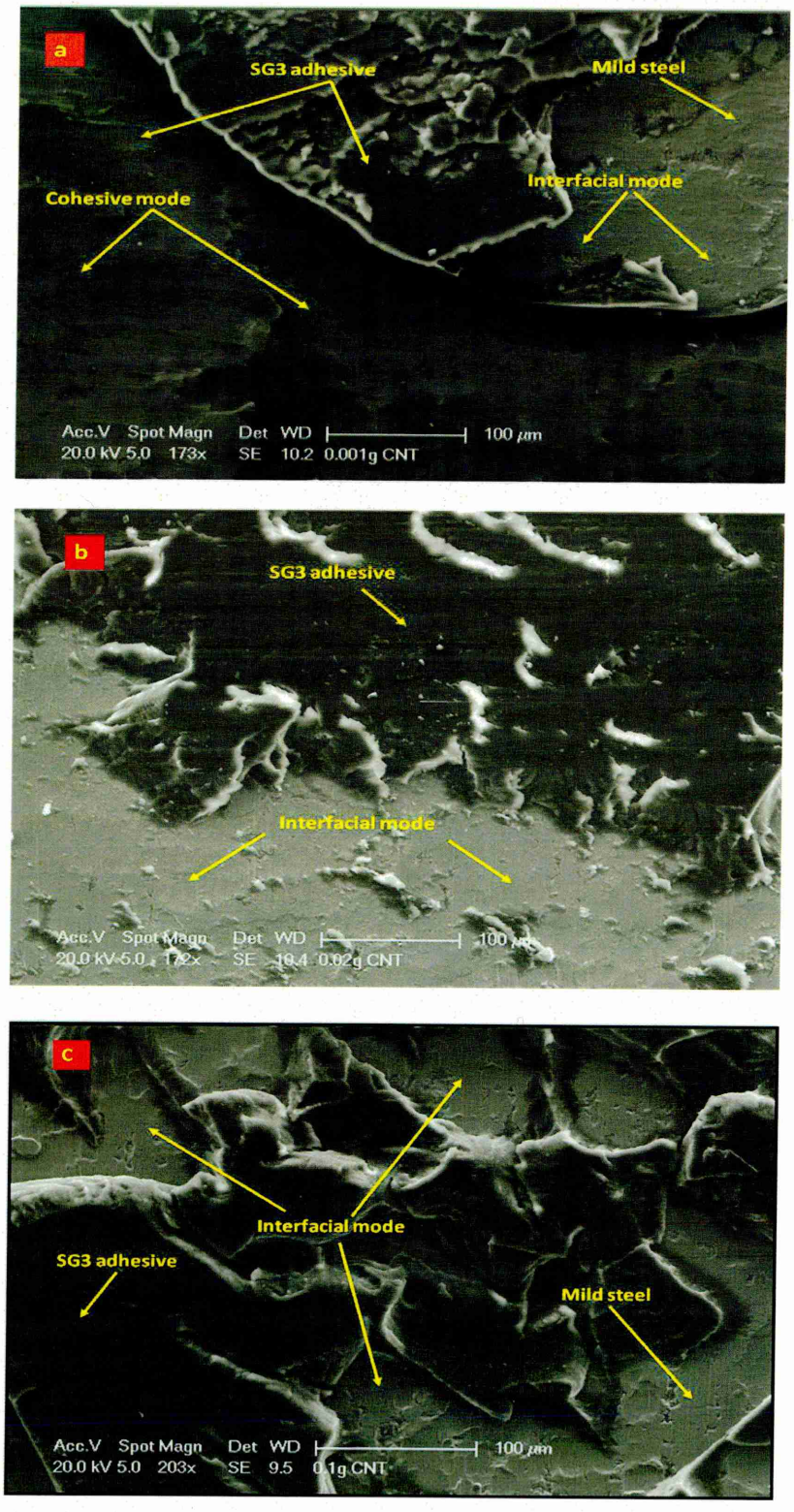

Figure 4.29 SEM images of SG3 fracture surfaces with addition of MWCNTs, (**a**) 0.01 wt%, (**b**) 0.2 wt% and (**c**) 1.0 wt% (cure time 16 hours, cure temperature 200°C)

4.2 Effects of cure conditions on SG adhesive strength

4.2.1 Effects of different cure temperatures on adhesive lap shear strength

4.2.1.1 The hybrid sol-gel adhesive

Results were obtained from lap shear tests at various cure temperatures for a cure duration of 16 hours. These are presented in Figure 4.30 in terms of the adhesive strength (shear strength). Due to the improvements observed in adhesive shear strength resulting from the incorporation of (Al_2O_3 and PANI) in the sol-gel formulation, AD7# specimens were further selected for an investigation of the effect of temperature on the adhesive strength of the hybrid sol-gel material. The shear strength of the AD7# adhesive showed an increase with temperature to 4.72 MPa at 150°C, after which there was a slight drop to 4.51 MPa at 180°C. The reduction may be attributed to the increased thermal stress at the joints arising from the difference in the thermal expansion coefficient between the sol-gel adhesive and the bonded metal substrate (Al2024-T3). The possibility that transverse and peel stress effects may also cause a reduction of the shear strength value [134] should also be considered.

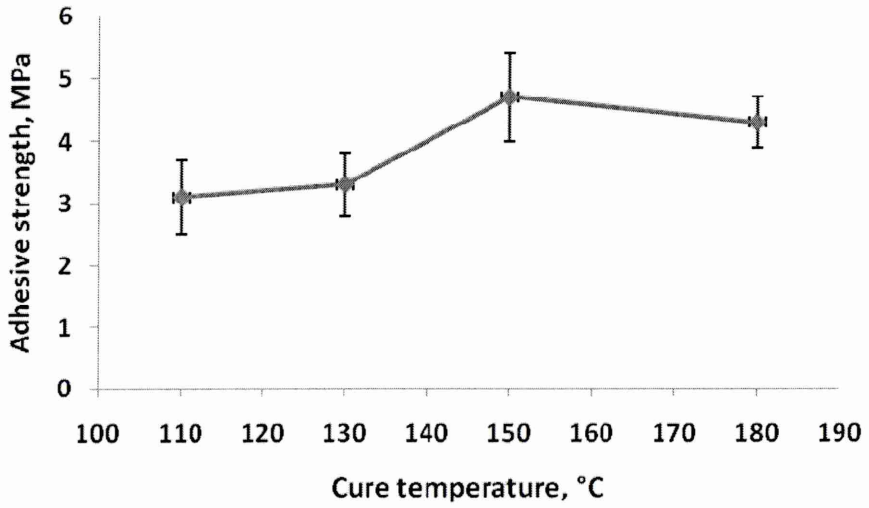

Figure 4.30 Effect of cure temperature on AD7# joint strength

Figure 4.31 presents curves of load versus extension for the tensile single-lap shear tests of the AD7# adhesive at different cure temperatures. From the curves, it can be seen that the total extension increased as the cure temperature increased, from 0.59 mm at 130°C to 0.92 mm at 150°C. This may be attributed to the polymerisation reactions or the formation of more bridges between the nano-particles Al_2O_3 and the sol-gel via the Ai-O-Si. Hence, the shear strength increased.

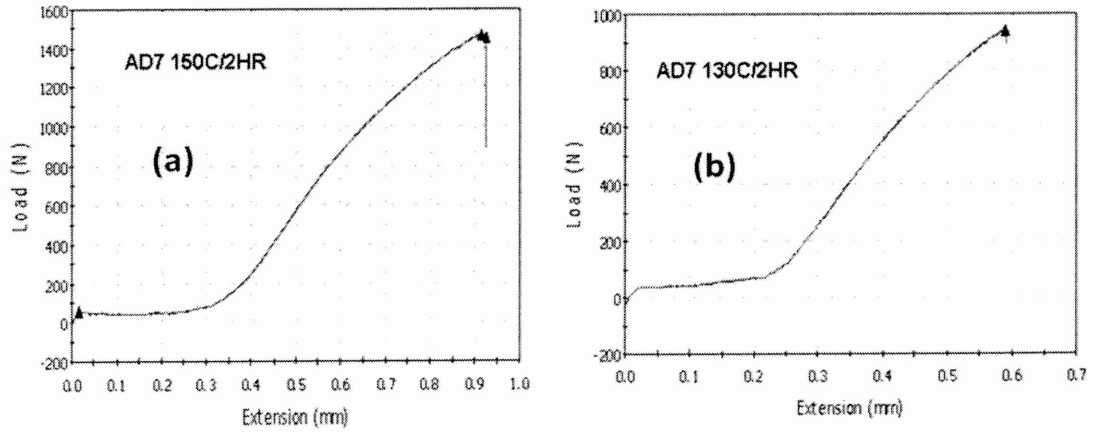

Figure 4.31 Effect of cure temperature on ductility (extension to break) for AD7# at (a) 150°C and (b) 130°C

4.2.1.2 The hybrid epoxy/sol-gel adhesive

As curing proceeds, the linear polymer chains in the epoxy resin grow and branch to form cross-links with inorganic fillers, so the cure temperature of SG3 adhesive plays an important role in determining the reliability of the lap joints. The lap shear strength of the SG3/Al and SG3/MS sol-gel epoxy adhesives were evaluated as a function of cure temperature. The adhesives were cured at 140°C, 160°C, 180°C and 200°C for 16 hours, and subsequent lap joint strengths were measured. The results for SG3/Al showed that the adhesive strength (maximum load per unit bond area) decreased as the cure temperature increased, see Figure 4.32. However, the lap joint strength of SG3/MS, showed no significant change as the cure temperature was increased from 140°C to 200°C, suggesting a stable adhesive material under the heat treatment temperatures used for curing. A different in thermal expansion coefficient between mild steel and Al alloys may play a role in this behaviour.

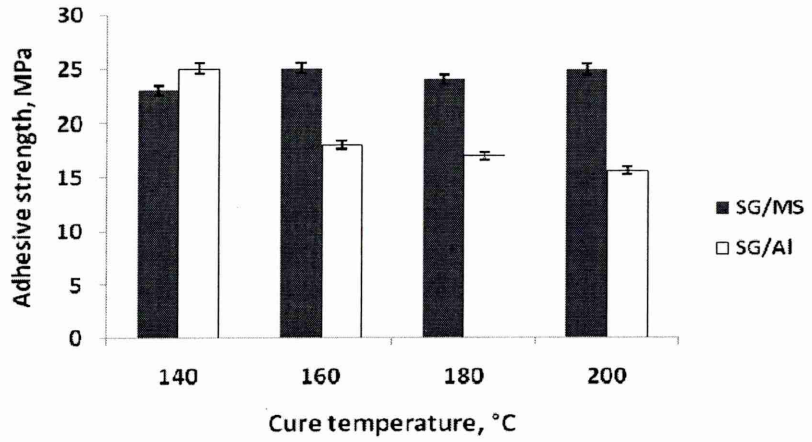

Figure 4.32 Adhesive strength of lap joints at different cure temperatures. (16 hours cure time)

4.2.1.2.1 FTIR spectra of SG3 (cure temperature changes)

FTIR spectra of SG3 at five different cure temperatures were obtained to understand the chemical changes in the epoxy/sol-gel formulation during the curing processes. Figure 4.33 shows the absorption peaks of SG3 adhesive material as a function of temperature for a cure time of 16 hours. The formation of a strong Si-O-Si band at ~1088cm^{-1} can be seen at all temperatures, with the peak increasing as the cure temperature increased. This indicates a higher density of Si-O-Si linkages and a higher degree of cross-link density in the adhesive matrix. Also, the reduction in peak at the range of ~ 800-950cm^{-1}, indicated an increase in the opening of the epoxy ring. The small peak between 3200-3500cm^{-1} (which corresponds to the O-H bond of absorbed water molecules) decreased as temperature increased. A weak absorption peak at 1680cm^{-1} related to C=C within the polymer chain also reduced as temperature increased. A new peak appears at ~ 1730cm^{-1} and is clearly visible at the cure temperature of 200°C, this corresponds to a C-O bond due to an increased polymerization reaction within the adhesive.

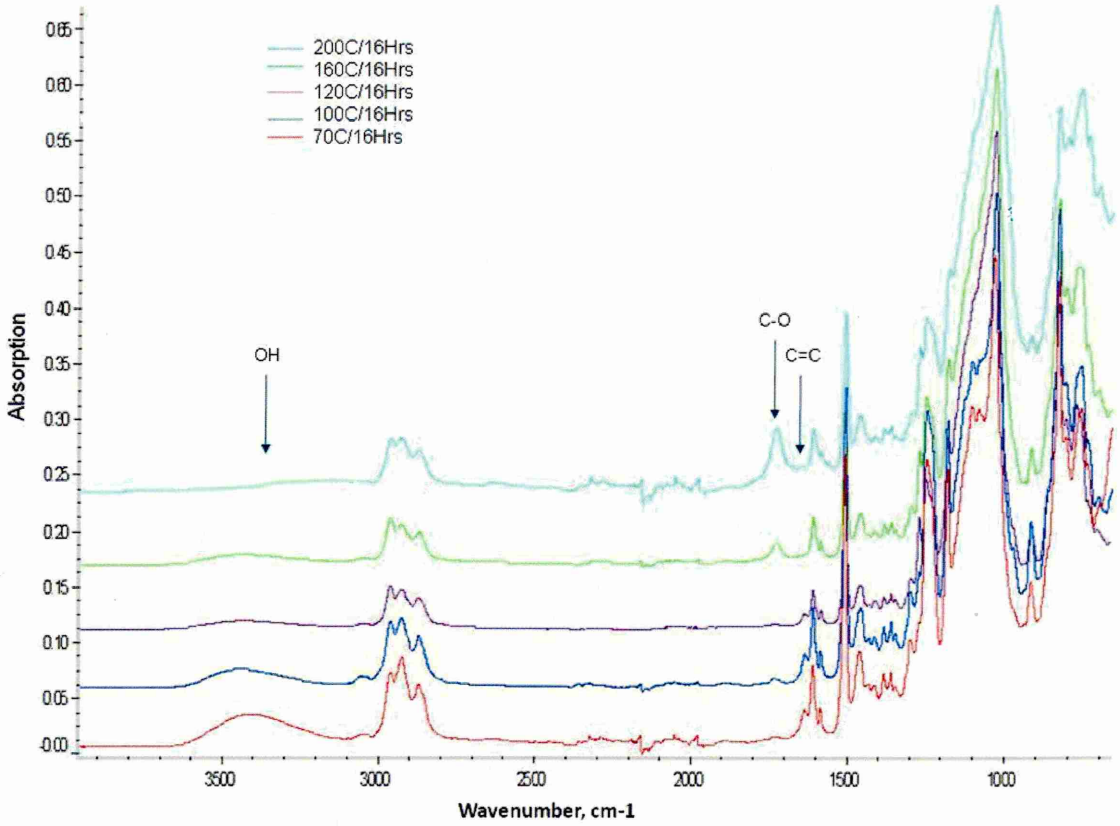

Figure 4.33 FTIR spectra of SG3 adhesive for different cure temperatures

4.2.2 Effects of different cure times on adhesive lap shear strength

4.2.2.1 The hybrid sol-gel adhesive

The shear strength of the AD7# sol-gel adhesive was evaluated for five different cure times at a fixed temperature of 150^{0}C on aluminium 2024-T3 substrate. The cure time played an important role in increasing the adhesive strength of the lap joints, see Figure 4.34. The mean adhesive strength of AD7# increased rapidly from 1.3±0.4 to 3.2±0.5 MPa as the cure time increased from 30 minutes to 2 hours. As the cure time increased to 16 hours, the adhesive shear strength of AD7# gradually increased to a maximum of 4.72±0.7 MPa. There appeared to be no further increase in the shear strength for a cure time greater than 16 hours. The reason for this may attributed to the sol-gel adhesive having attained a complete cross-linked structure.

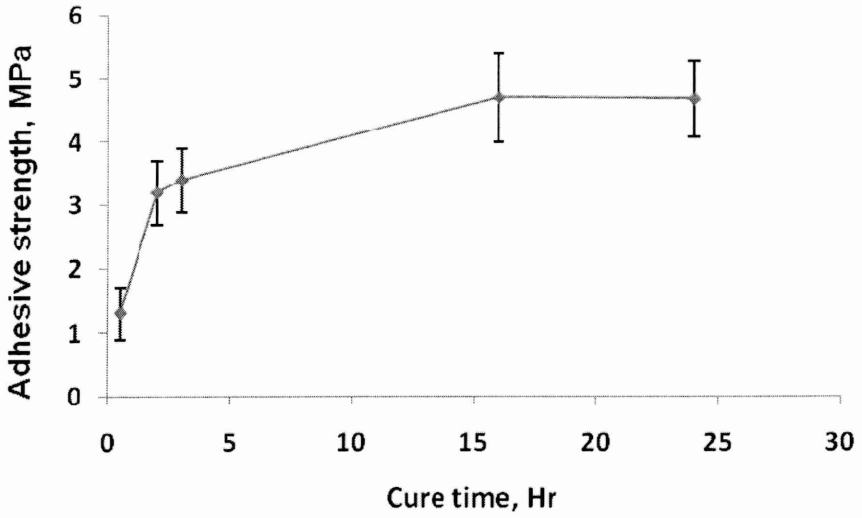

Figure 4.34 Effect of cure time on AD7# shear strength,
at constant cure temperature of 150°C

Figure 4.35 presents the effects of three different cure times on the load/extension curves of AD7#. There appears to be an increase in fracture load as the curing time is increased.

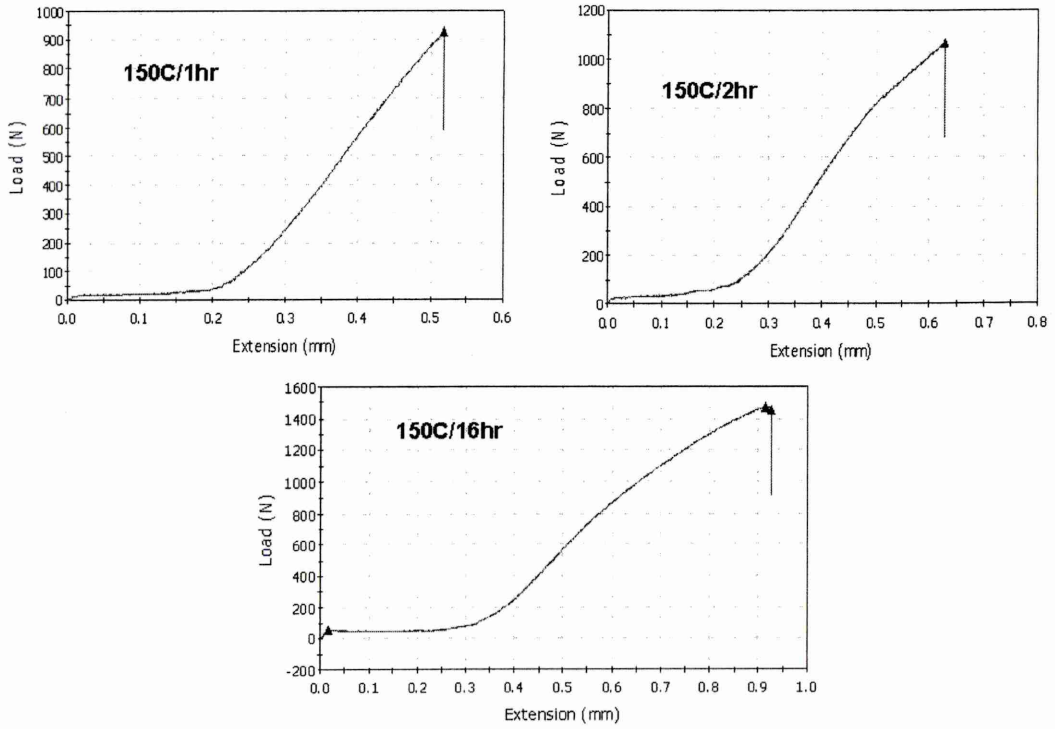

Figure 4.35 Load/extension curves of AD7# adhesive strength,
at constant cure temperature of 150°C

4.2.2.2 The hybrid epoxy/sol-gel adhesive (SG3)

Using the SG3 adhesive, the adhesive lap shear strength on mild steel samples was evaluated at different cure times. The tests were carried out for 1, 3, 7, 10, 16 and 20 hours at a constant cure temperature of 200°C. The measured adhesive shear strength is plotted against cure time in Figure 4.36. It can be seen that the SG3 adhesive strength increased with cure time, to a maximum at 16 hours, after which the curve flattened out, indicating that by 16 hours the chemical interactions within the adhesive matrix and/or at adhesive/substrate interface are complete. Thus 16 hours appears to be the optimum cure time for the adhesive to attain the maximum bond strength.

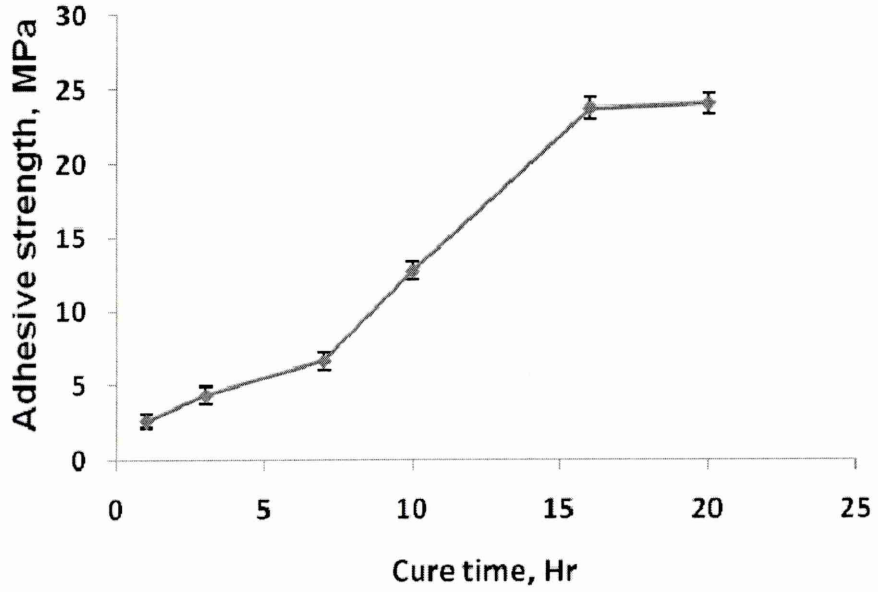

Figure 4.36 Adhesive strength of lap joint at different cure times (cure temperature 200°C)

4.2.2.2.1 FTIR spectra of SG3 adhesive

The absorption infrared spectra of SG3 as a function of cure time are shown in Figures 4.37 a and b. Figure 4.37a shows FTIR absorption peaks of SG3 adhesive over the wave number range 400-4000cm^{-1}, however, a more detailed presentation of the peaks in the range ~ 800-1800cm^{-1} is given in Figure 4.37b. The most interesting bands in the FTIR spectrum in Figure 4.37a were; the epoxy ring at ~ 950cm^{-1} which disappeared as the cure time increased, and C-O at ~ 1733cm^{-1}, which increased as cure time increased. In addition, in Figure 4.37a the broad but weak absorption peak at ~ 3200-3500cm^{-1}, which is attributed to O-H bond [135], decreased gradually as the cure time increased. This indicates that the majority of Si-OH and OH groups were reacted by condensation during curing leading to the formation of a Si-O-Si network structure.

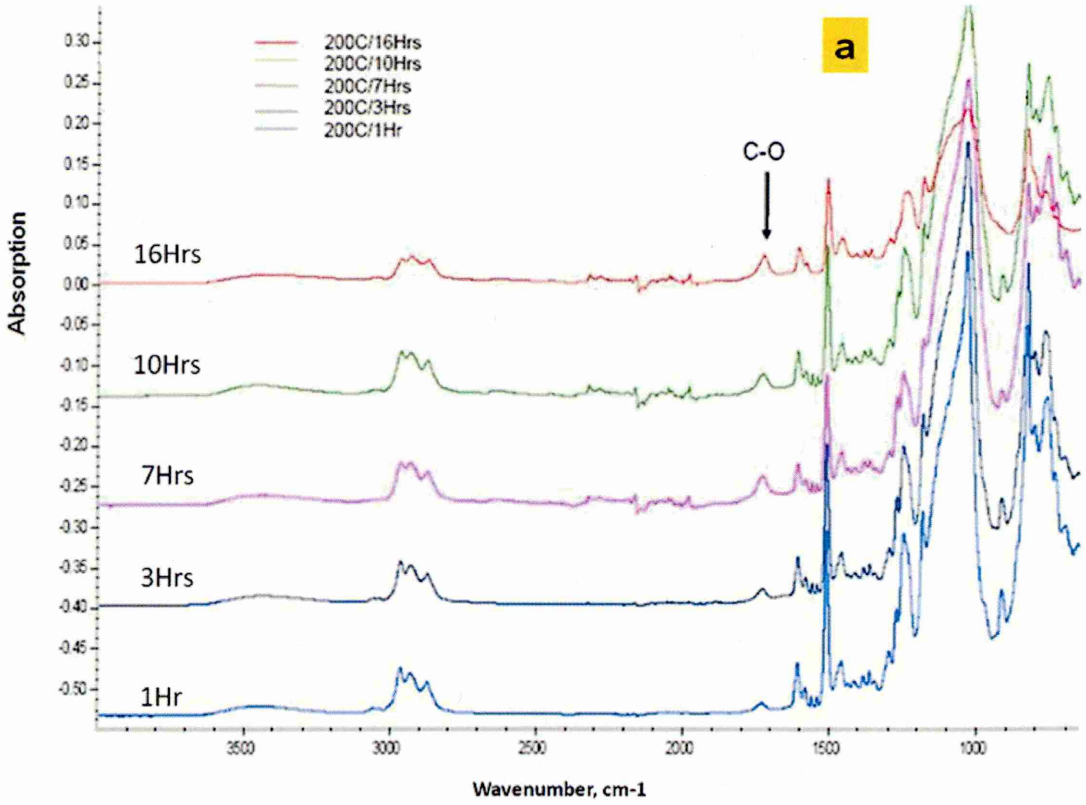

Figure 4.37a. FTIR spectra of SG3 adhesive 1000cm^{-1} to 3500cm^{-1} at different cure times (cure temperature 200°C)

An increase in cure time improved the adhesive cross-linking via the inorganic nano-filler materials (i.e. Al_2O_3, MWCNT) within the epoxy/sol-gel system. Figure 4.37b shows a clear shoulder at ~ 1165cm^{-1}, which corresponds to the Al-O-Si bond, as mentioned in [136]. The introduction of MWCNTs into the adhesive helps to prevent peeling of the adhesive by acting as a reinforcement network, restricting and reducing crack initiation or propagation within the bulk adhesive. As stated above, a strong peak related to C-O bond at ~ 1733cm^{-1} increased with increase in cure time. This peak is probably related to the cross-link between the CNT surface and silica nano-particles in the sol-gel material or epoxy matrix.

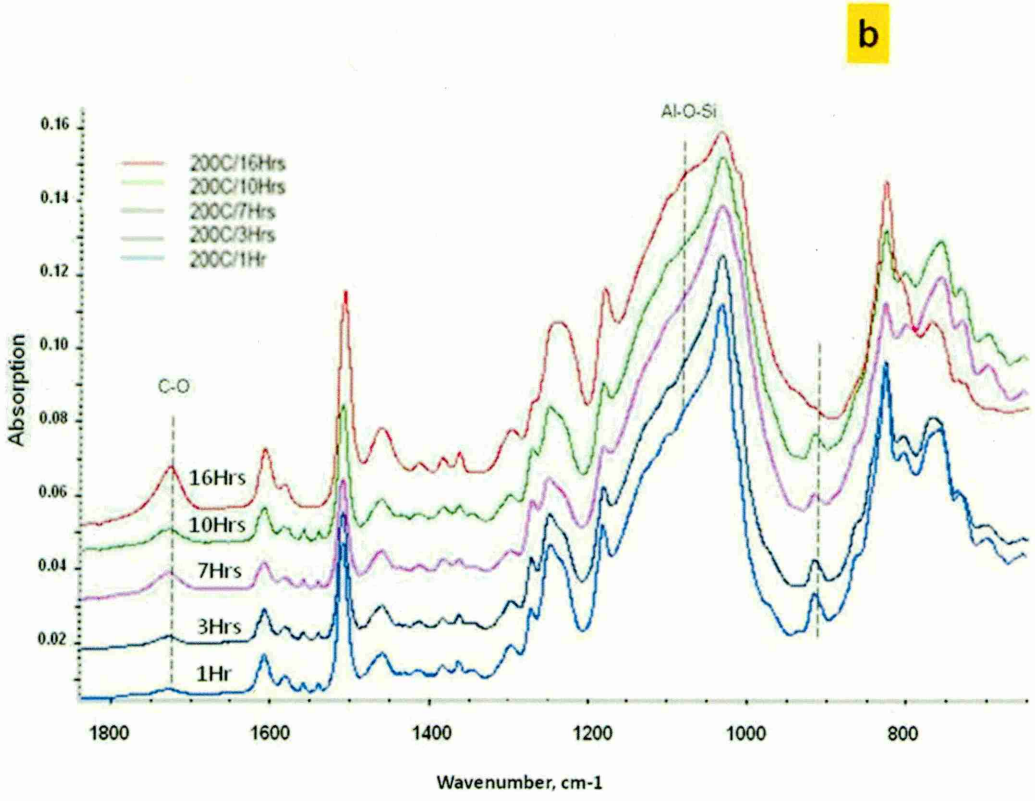

Figure 4.37b. FTIR spectra of SG3 adhesive, 800cm^{-1} to 1800cm^{-1}, at different cure times (cure temperature 200°C)

4.3 Effects of substrate roughness on adhesive strength

4.3.1 The hybrid sol-gel adhesive

The bond strength of hybrid sol-gel adhesive was measured for the lap joint on the Al alloy (2024-T3) in the as-received surface condition and for two additional surface finishes; polished 1μm diamond paste and polished 6μm diamond paste. The results obtained indicate that the adhesive strength of AD3# and AD4# decreased as the joint surface roughness decreased, see Table 4.2. It is suggested that the differences in adhesive strength are due to the mechanical interlocking between the adhesive and the substrate with the 1μm finish having smaller peak-trough features.

Table 4.2 Effect of surface roughness on bond strength

Surface preparation	Surface roughness, R_a (μm)	Adhesive strength of sol-gel modified, MPa	
		(AD3#) 0.5 wt % γ-Al_2O_3	(AD4#) 2.0 wt % TiO_2
As a received	0.102	4.43	4.0
6 μm	0.0288	3.12	2.81
1 μm	0.0191	2.62	2.36

Figure 4.38a and b shows the texture of polished surfaces. R_a represents the mean value of the surface roughness and R_z represents the sum of the height of the highest profile peak and the depth of the deepest profile valley over the same length.

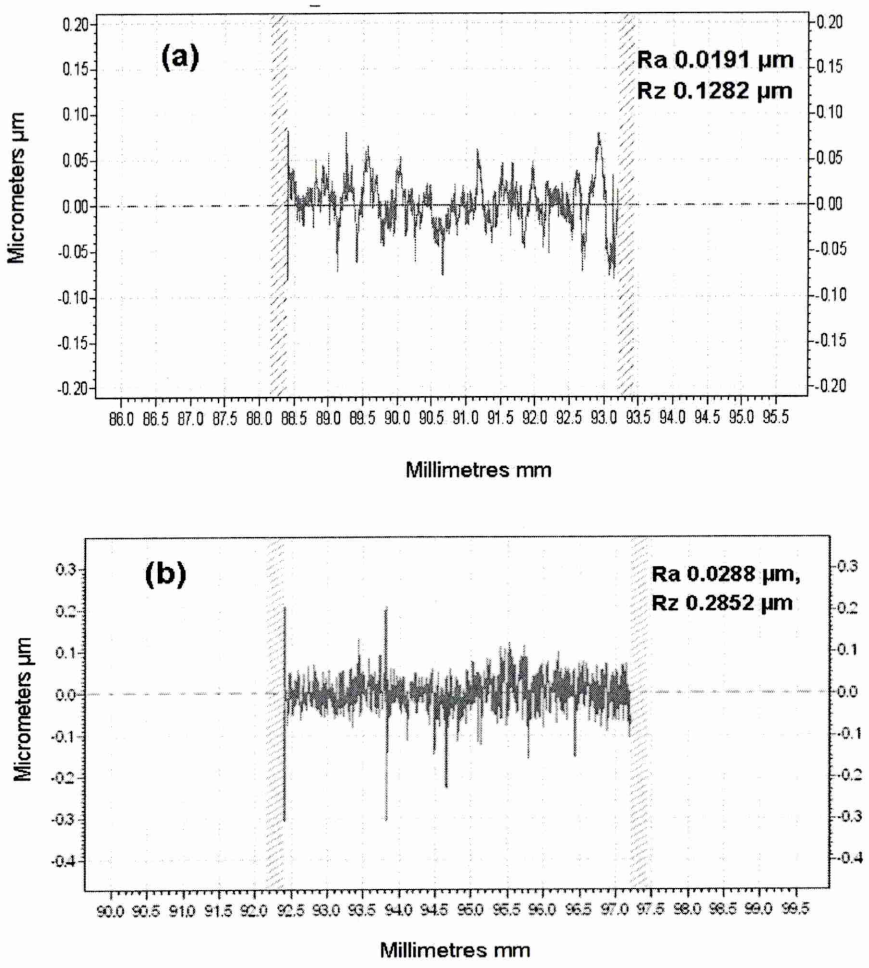

Figure 4.38 Surface roughness of Al2024-T3, (a) polished with 1µm diamond paste and (b) polished with 6µm diamond paste

4.3.2 The hybrid epoxy/sol-gel adhesive (SG3)

Figure 4.39 shows the variation in the SG3 adhesive strength due to the change of surface roughness of the mild steel substrate. In general, measured lap shear strength may reduce as surface roughness decreases [137]. Here the mild steel surfaces were abraded with abrasive paper of different degrees of roughness; fine (P120, average particle diameter 125µm), very fine (P240, average particle diameter 58.5µm) and two extra fine grades (P400, average particle diameter 35µm and P600, average particle diameter 25.8µm), where the grading is according to ISO 6344-1:1998 [138]. Between 3-5 specimens were tested for each grade of abrasive papers. It can be seen that surface abrasion with P120 abrasive paper gives the highest average shear strength value ~ 18±0.9MPa. Surfaces abraded with P240 abrasive paper gave a slightly lower shear strength

of 15±0.8MPa. Use of P400 abrasive paper decreased the surface roughness further and the adhesive strength also decreased again, to ~13±0.7MPa. Finally, abrading the substrate surfaces with P600 abrasive paper gave the lowest average shear strength value, 10.5±0.7MPa. The decrease in value of the adhesive strength is attributed to a reduction of mechanical interlocking due to less adequate penetration of adhesive on smoother surfaces. The decreasing in the actual area of contact between the adhesive and the substrate with a less rough surface may contribute in lowering the physical adsorption strength (the attractive forces at the interface, known as van der Waals forces), resulting in lower total joint strength.

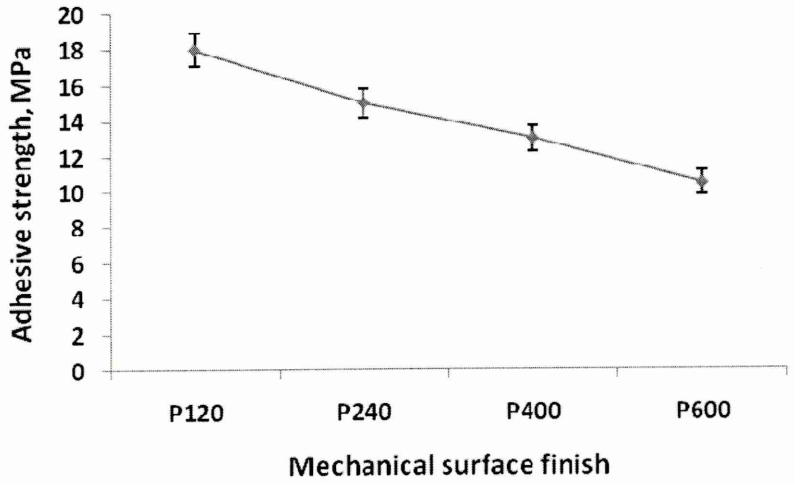

Figure 4.39 Shear strength of SG3 vs. surface roughness. Lap shear test

4.3.2.1 IFM measurements

IFM surface roughness measurements on the mild steel substrates abraded with four different abrasive papers, are presented in Table 4.3. The results obtained show that the average surface roughness values decreased as the grade of abrasive paper increased. As the surface roughness decreased with grade of abrasive paper from P120 to P600, the actual surface area (the area of contact of the liquid "adhesive" with the solid "irregular surface of the substrate") decreased, as did the depth of the surface grooves. Zhang and co-workers [139] have reported that an increase in surface area increased the physical-chemical interactions and mechanical interlocking enhanced the lap shear strength. However, if the rough surface profile has grooves which are too broad and deep, the bonding strength may decrease due to weakening of mechanical

interlocking effects (i.e. the presence of small air pockets along the interface due to limited in wetting in this case creates voids which form stress rises, leading to a reduction in overall bond strength).

Table 4.3 Surface roughness of different grades of abrasive paper.

Surface features	Abrasive paper			
	P120	**P240**	**P400**	**P600**
Ra (μm)	1.6±0.05	1.5±0.12	1.2±0.15	1.1±0.10
Rz (μm)	10.9±0.02	10.7±0.04	8.3±0.11	7.0±0.17
Rmax (μm)	12.9±0.06	12.4±0.08	9.7±0.03	7.6±0.18

Ra = Average roughness of profile
Rz = Mean peak to valley height of roughness profile
Rmax = Maximum peak to valley height of roughness profile

The surface roughness profiles for the different surface finishes measured by IFM are presented in Figure 4.40. Note the different Y-axis scales. Surface mechanical treatment with P120 abrasive paper revealed the highest depth value, and the value decreased as the surface becomes smoother i.e. P240, P400 and P600, respectively.

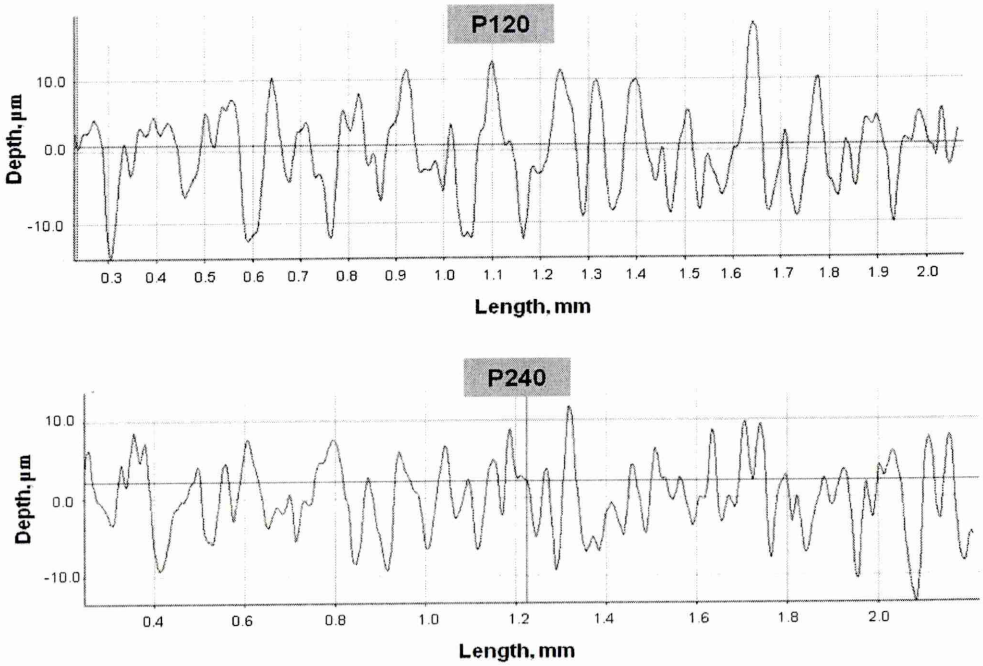

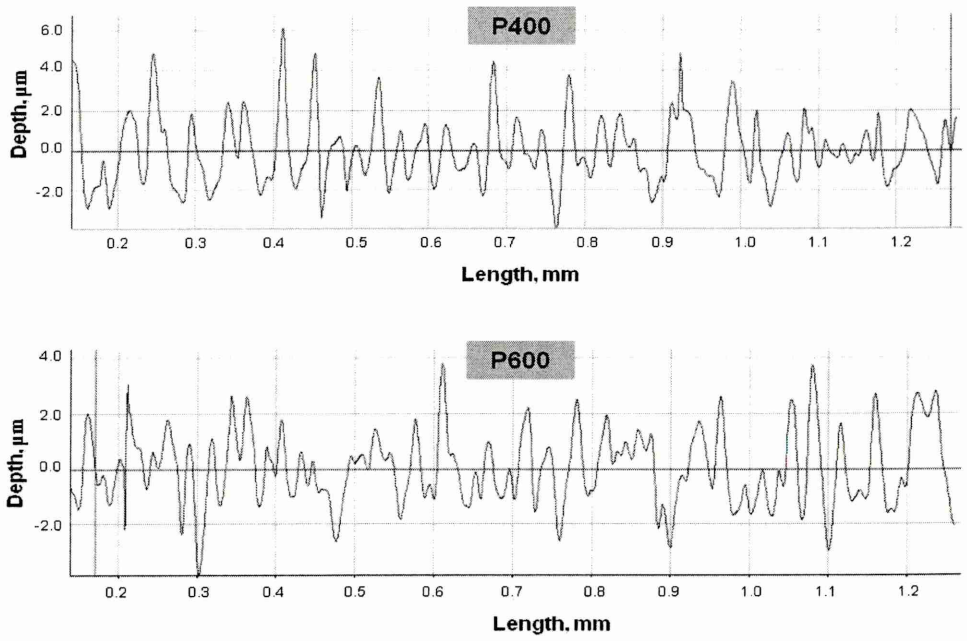

Figure 4.40 surface roughness profiles for different abrasive papers on mild steel

4.3.2.2 Fracture surface analysis

Images obtained using a digital camera were used to identify the fracture failure modes of SG3 adhesive with different surface roughness profiles, see Figure 4.41. In all four cases the failure was near the interface region and a mixed adhesive/cohesive mode was noted. The percentage of SG3 adhesive material remaining on the mild steel, when the substrate was abraded with P120 abrasive paper, was ~ 70%, and the fracture surface was a mixed adhesive/cohesive mode. This percentage changed to 50% for P240 and the failure was also mixed mode. The specimens abraded with P400 paper also had some adhesive remaining on the surfaces, ~ 35%, and the failure was again an adhesive/cohesive mode. Finally the samples abraded with P600 abrasive paper resulted in mixed failure mode and the percentage of adhesive was ~ 33%. By decreasing surface roughness, the area of adhesive adhering to the substrates decreased, suggesting a decrease in mechanical interlock and anchorage of the adhesive in pores and irregularities of the substrate as the surface become smoother.

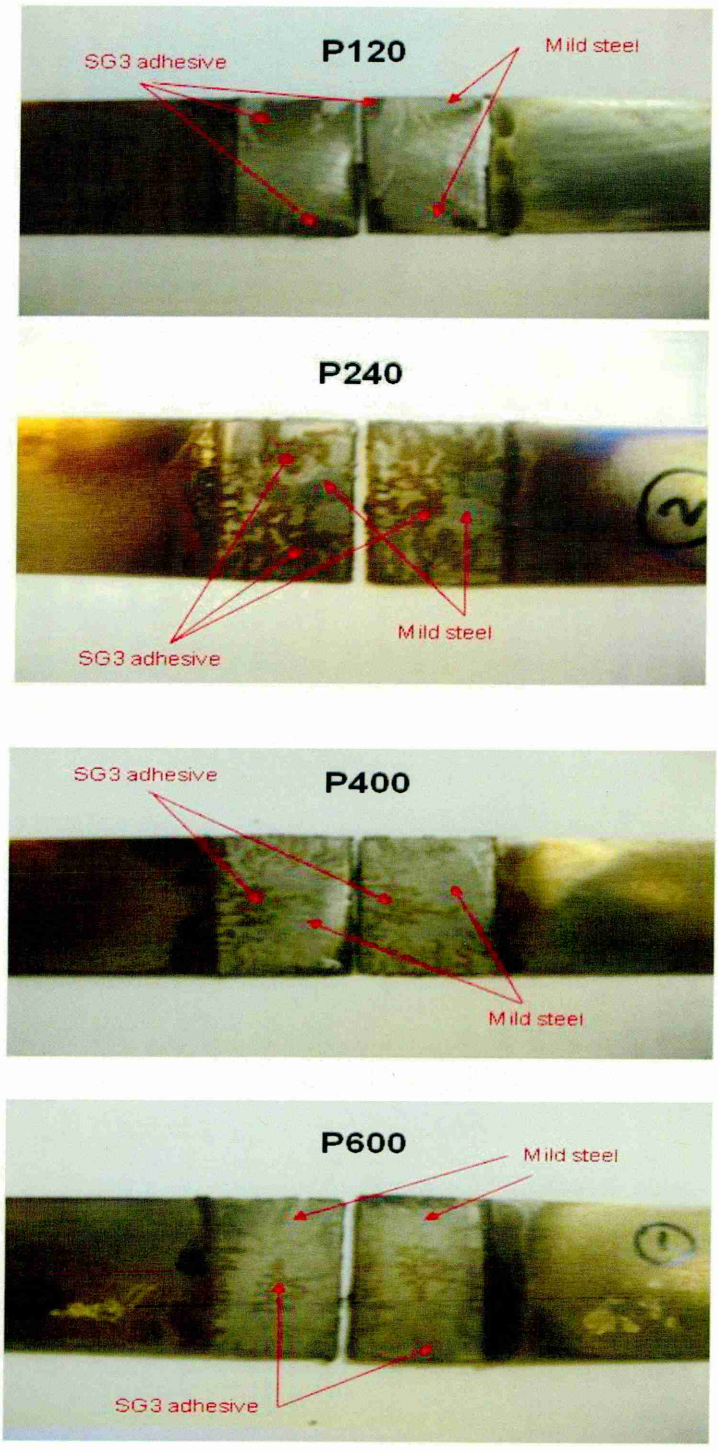

Figure 4.41. Fracture surfaces for mild steel lap joints with different initial surface roughness

4.3.3.3 SEM observations

Figure 4.42 shows SEM high resolution cross-section images of SG3 adhesive bonded mild steel, abraded with (a) P120 and (b) P240 abrasive paper. It can be seen that the adhesive wetability to the substrate surface is well achieved with the different surface roughness's. Furthermore, the difference in mechanical interlocking with P120 compared with that with P240 due to the increase in roughness can also be seen.

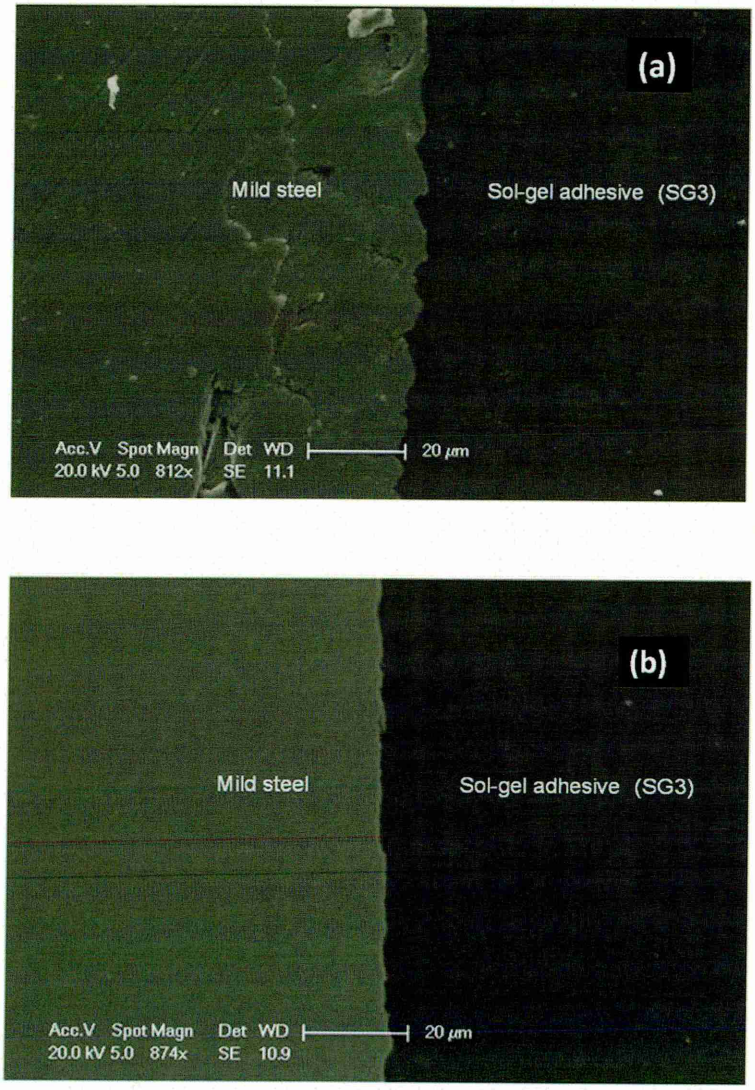

Fig. 4.42 SEM interface micrographs of mild steel substrate surface abraded with (a) P120 and (b) P240

4.4 Effect of the changes in bond geometry on SG3 adhesive strength

To determine the effect of geometrical parameters of lap shear joints on the SG3 adhesive strength, six different overlap areas (i.e. 200, 250, 375, 500, 625 and 750 mm^2) were studied. Mild steel was used as substrate for the lap joints which were cured at 160°C for 16 hours.

4.4.1 Shear strength and bonding area

It is confirmed that bonding area plays an important role in the measured shear strength of adhesives in lap joints. The measured results show that the maximum load per unit bonding area (adhesive strength) increased with increase in overlap area up to 375 mm^2, see Table 4.4. And, the maximum load carried by the joints increased as the bonding area increased.

Table 4.4 Adhesive strength at different overlap areas

Bonding dimensions			Average load at failure N	Average adhesive strength MPa
Length, mm	Width, mm	Bonding area mm^2		
8	25	200	2800	14.0
10		250	3741	15.0
15		375	6750	18.0
20		500	6850	13.7
25		625	6875	11.0
30		750	7500	10.0

However, while an increase in overlap area from 200mm^2 to 375mm^2 raised the SG3 adhesive strength from 14.0±0.5MPa to 18.0±0.7MPa, further increase in overlap area resulted in a reduction in maximum load per unit bonding area, see Figure 4.43. This result suggests that increasing the bond area to give a higher joint strength is only efficient within a limited range. This effect can be related to the different stresses that occur at the adhesive/substrate interface. The transferring of the external load during the test, around edges of the lap joint, is

higher in comparison to the inner bonded area [140]. Non-uniform distribution of stresses across the bond area from the edges to middle will increase peel and cleavage stresses, thereby decreasing the joint efficiency and the strength, see Figure 5.4 in discussion.

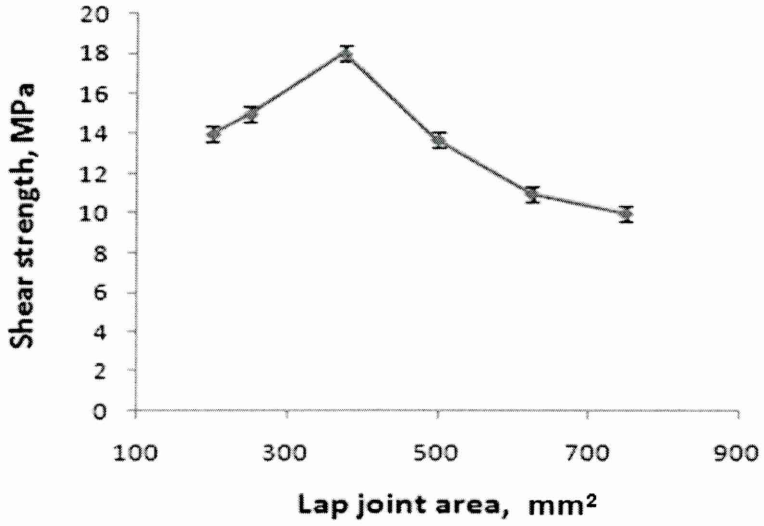

Figure 4.43 Influences of lap joint area on SG3 adhesive strength (cure temperature 160°C and cure time 16 hours)

4.4.2 Fracture surface observation

Figure 4.44 shows images obtained by digital camera of the fracture surfaces of the lap joints as a function of overlap length. In the joint with the 375mm^2 bonding area, failure was initiated at the interface and final failure was due to crack propagation. The fracture failure mode in this joint was a mixed cohesive/adhesive mode. The fracture surface of the joint with bonding area 500mm^2 shows that no more adhesive material remains at the ends of joint, suggesting cracks were mainly initiated at these points and resulted in a mixed cohesive/adhesive mode. However, the failed surfaces of the joint with bonding area of 625mm^2 show interfacial failure (adhesive) where most adhesive remained on the left side of lap joint. In the case of the joint with bonding area of 750mm^2, the major fracture type was a mixed mode.

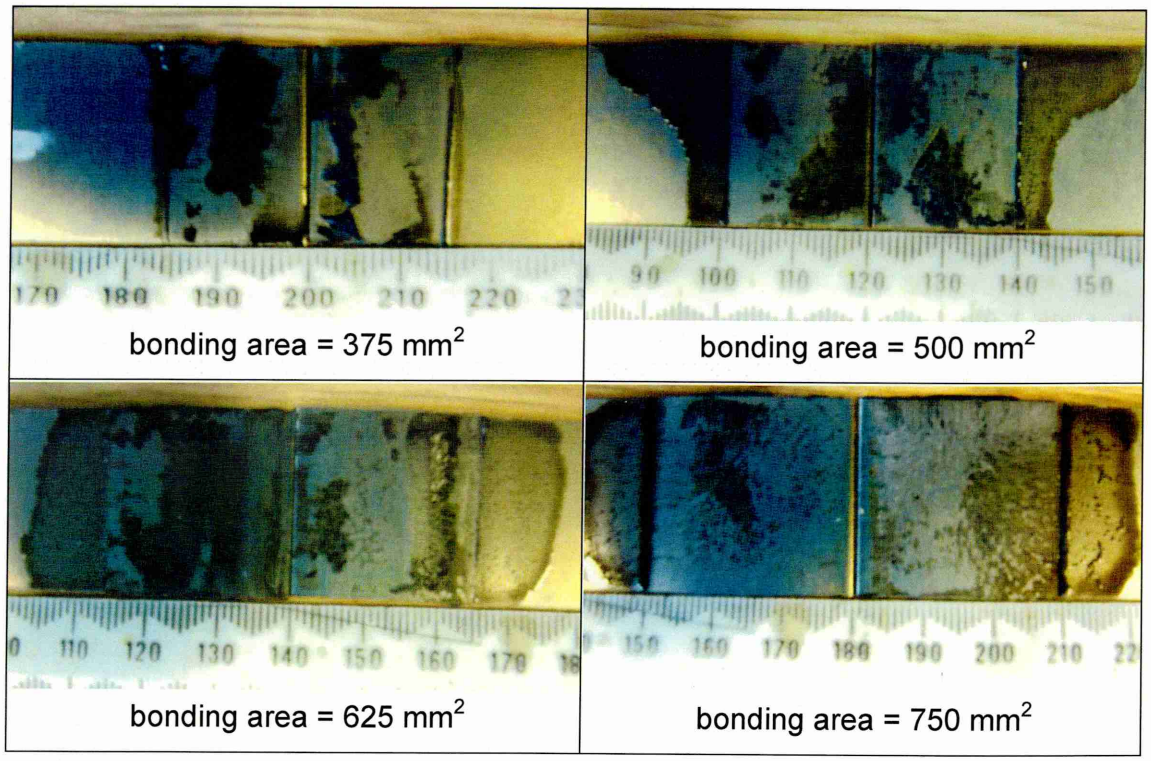

Fig. 4.44 Images of fracture surface for different overlap areas with SG3 adhesive strength (cure temperature 160°C and cure time 16 hours)

4.5 Effects of the external environment on lap shear strength

Adhesives tend to lose bond strength as their temperature increases, so the temperature response of adhesive materials plays an important role in their selection for specific applications such as aerospace, transportation and electronics. In addition, the success of an adhesive bond is related to its ability to retain an adequate level of joint strength for long periods in an operational environment. Changes in the environment can affect the way in which the adhesive performance changes with time [141]. The influence of these factors on adhesive strength is discussed below.

4.5.1 Lap shear strength of SG3 adhesive tested at (HT)

The shear strength of SG3 adhesive was investigated at six different test temperatures. SG3/MS lap joints were prepared and cured at 200°C for 16 hours. The results show a decrease in adhesive strength as test temperature increases, see Figure 4.45. An increase in temperature from room temperature 20°C to 40°C, caused a reduction in strength from ~23.0±1.0 MPa to 17.0±0.8 MPa with a further progressive decrease in adhesive strength to only about 2.0±0.4 MPa at 120°C. The decrease in adhesive strength may be attributed to the softening of the adhesive itself and the results of internal stress set up by the changes in thermal expansion coefficient between the adhesive and the substrate as the environmental temperature increased.

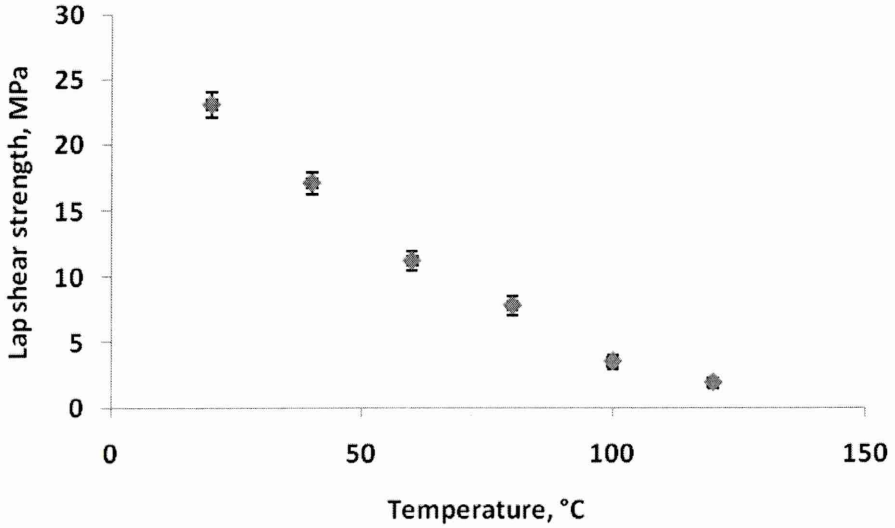

Figure 4.45 Adhesive strength of SG3/MS as a function of test temperature

The results in this study were compared with results reported by Tsui et al [142], see Figure 4.46 (dashed line) who also used a mild steel substrate. Both sets of results show that with increase in temperature a reduction in the adhesive strength is noted. The bonding strength (shear) for both adhesive materials tested is significant higher at lower temperatures. The reason may be related to the softening of the adhesive material as temperature increased.

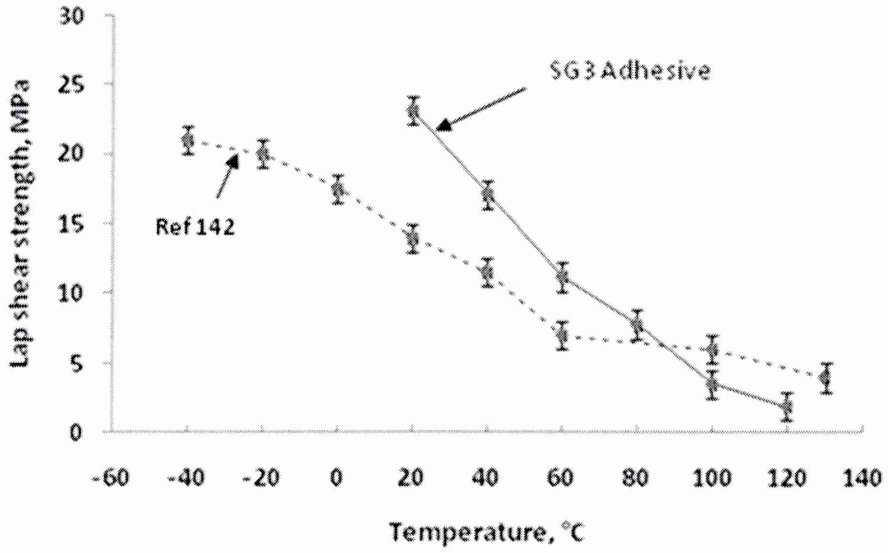

Figure 4.46 Adhesive strength as a function of test temperature: Comparsion of current study with Tsui et al [142]

4.5.1.1 Facture surface at different test temperatures

Digital images were taken for the fracture surfaces to identify possible changes in the failure mode as the temperature increased. The experimental results obtained revealed that the fracture surface gradually changes from a mixed adhesive/cohesive mode in specimens tested at low temperature to a cohesive mode as the temperature increased, see Figure 4.47. The formation of ridges or crazes through the fracture surface along the shearing direction at lower temperatures, (i.e. 40°C), may prevent nearby cracks from propagating. These crazes are attributed to the multitude of molecular motions in the deformed polymer material, based on the relaxation process of macromolecules which depends upon temperature [143]. However, as temperature increased, the SG3 adhesive formulation became soft and the ridges disappeared, so that the cross-linking within the adhesive matrix decreased and the joint failed at low applied load. In addition, the reduction in strength was relatively low in high temperature regions (i.e 80-120) compared with that at low temperature regions. The reason may be explained as a difference in the thermal expansion coefficients between the adhesive and the substrate, in both temperature regions. For example, at low temperature (i.e. 40°C) the internal stress (thermal) within the substrate increase with temperature, however, the hybrid epoxy/sol-gel structure is more stable (i.e. glassy state and below Tg) and any changes

due to thermal expansion appear to be very low, leading to a large difference in thermal stresses within the joint [144]. At high temperature, for a particular epoxy within SG3 structure, the coefficient of thermal expansion is larger (i.e. rubbery state and above Tg) and the changes in thermal stresses between the substrate and adhesive become lower (both extended), subsequently resulting in lower strength reduction rate (dσ/dT).

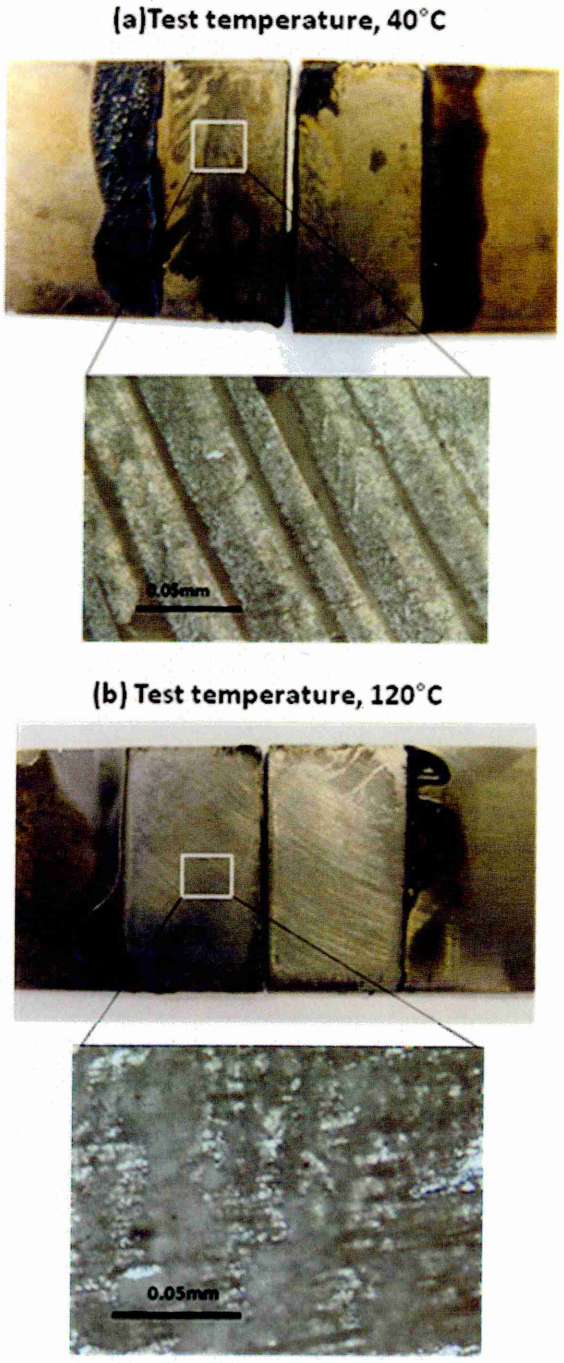

Figure 4.47 Fracture surface mode at (a) test temperature 40°C,
(b) test temperature 120°C,

4.5.2 Effects of immersion in 3.5% NaCl on the hybrid sol-gel adhesives

The lap shear strength of AD3#, AD4#, AD6# and AD7# joints aged within a corrosive environment (3.5% NaCl solution) for 7 days was measured. Results show that the bond strength of all joints decreased on immersion in the solution. The lap shear strength values after immersion were reduced from 5.1 to 3.18 MPa for AD6# and from 4.4 to 2.4 MPa for AD7# joints. A similar effect was noted for the joint strength of AD3# and AD4#, and the reduction in shear strength from 4.48 to 1.71 MPa in AD3# and from 4.0 to 1.28 MPa in AD4#. The reduction in adhesive strength may be attributed to a complex combination of damage to both the substrates and the adhesive material itself. The rate at which an aggressive solution permeates through the adhesive to the interface may affect on the shear strength of all the adhesives. Such an environment can also lead to unwanted chemical reactions in the adhesive as well as the formation of cracks within the bulk adhesive material. Figure 4.48 shows the percentage reduction in adhesive strength on exposure to a 3.5% NaCl solution.

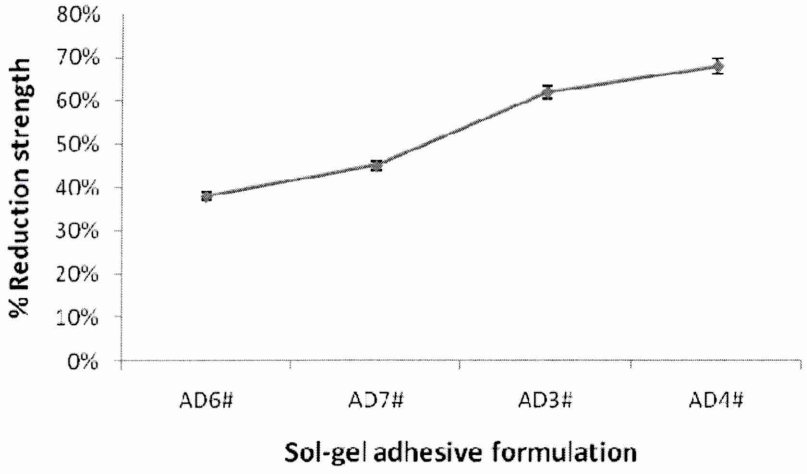

Figure 4.48 Lap shear strength reduction due to immersion for 7 days in corrosive environment (3.5% NaCl)

The SEM image in Figure 4.49 shows the effects of an aggressive environment on the fracture surface of AD3#. Cracks in the adhesive layer (arrowed) due to the wet condition were observed.

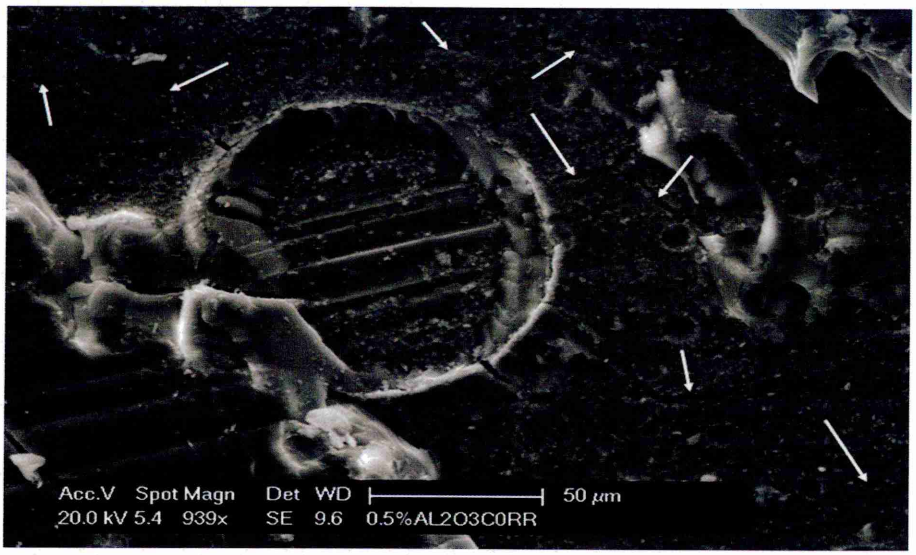

Figure 4.49 Cracks in fracture surface after immersion for 7 days in a corrosive environment (3.5% NaCl)

IFM images, Figure 4.50, of the AD3# joint edges shows damage due to the corrosive environment. Cracks and de-lamination at the substrate/adhesive interface, due to the aggressive environment also occurred, see Figure 4.51.

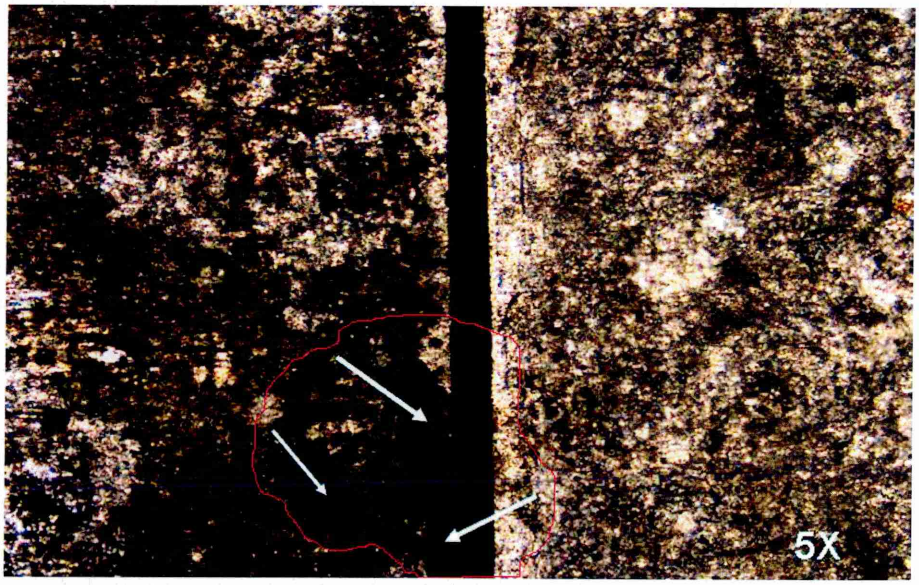

Figure 4.50 IFM images of edge joint damaged by corrosion

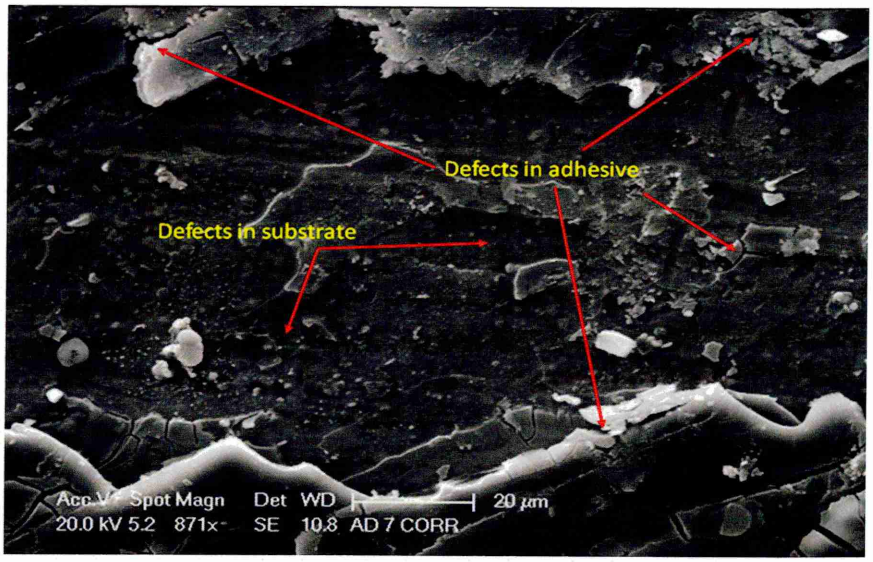

Figure 4.51 SEM image of AD3# adhesive /substrate following immersion for 7 days in 3.5%NaCl

4.5.3 Effects of immersion in 3.5% NaCl on the hybrid epoxy/sol-gel adhesive

4.5.3.1 Adhesive strength of SG3/MS vs immersion time

The adhesive strength for the SG3 adhesive on mild steel substrates aged in 3.5% NaCl solution is shown in Figure 4.52. It can be seen that following one, two, four and eight week's exposure the adhesive strength of the lap joints progressively decreased. For lap joints cured at 140°C for 16 hours the measured maximum shear strength value for dry conditions was 25±0.9 MPa, and the minimum after eight weeks exposure was 1.2±0.6MPa. This behaviour can be attributed to moisture uptake and aggressive ion ingress into the bonded joint [145], which limits the degree of bonding at the adhesive/substrate interface. In addition, if the aggressive medium reaches the interface it can break weak bonds easily (van der forces); thus, reducing any adhesive cross-linking. In addition, formation of corrosion product at the surface will cause a deterioration of the strength of the adhesive joint as a result of 'corrosion product jacking'.

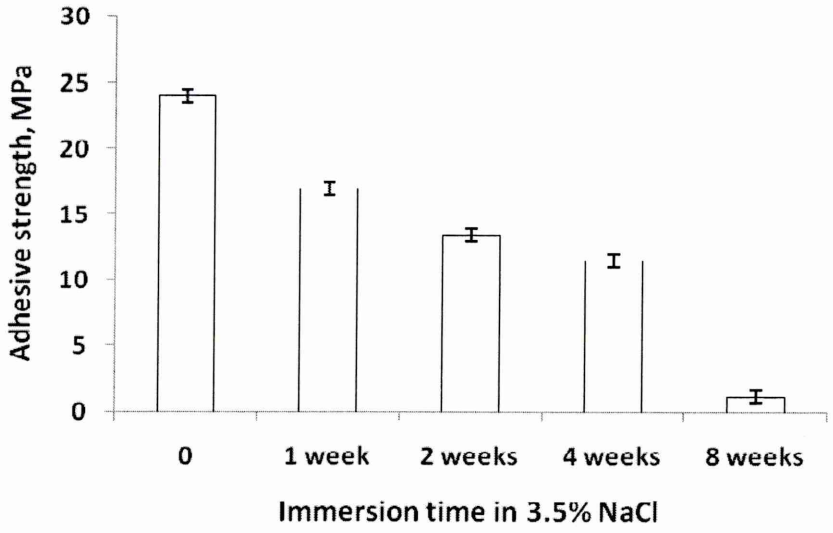

Figure 4.52 Effect of immersion times on adhesive strength of SG3/MS lap joints (cured at 140°C for 16 hours)

Figure 4.53 shows the percentage reduction in mean lap joint strength with different immersion times. It can be seen that the reduction in strength is initially relatively low but begins to drop rapidly after four weeks immersion. At eight weeks about 96% loss of adhesion was recorded.

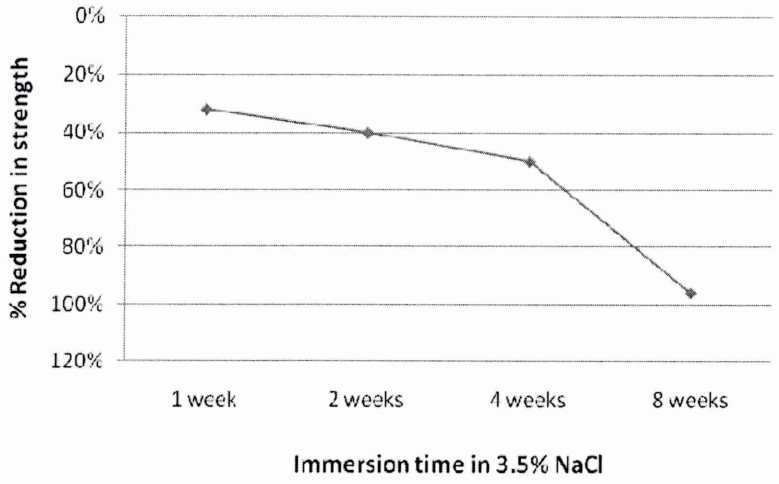

Figure 4.53 Reduction in adhesive strength of SG3/MS lap joints with duration of immersion in 3.5% NaCl (cure time 16 hours at 140°C)

4.5.3.1.1 Fracture surface

Figure 4.54 shows the fracture surface of lap joints after immersion eight weeks in 3.5%NaCl. The failed surfaces were first observed under an optical microscope (Zeiss Stemi 2000-C) which allowed magnification up to 5.0X. The delamination at the mild steel surface may be attributed to the moisture uptake with time. The failure mode can be classified as an interfacial mode (adhesive/substrate interface) and a cohesive mode in the mild steel substrate near the top surface layer. In addition, damages due to corrosion process around the bonding area also were observed.

Figure 4.54 Joint fracture surface after eight weeks immersion in 3.5%NaCl

4.5.3.1.2 SEM observations

Figures 4.55 a and b present SEM images of fracture surfaces for lap joints immersed for one and eight weeks in a 3.5% NaCl solution, respectively. The failed surface shown in Figure 4.55a revealed many cracks in the adhesive materials. This can be related to the reduction in interfacial and cohesive bonding due to the adhesive plasticization, as reported in [146]. When the immersion time increased to eight weeks, more damage in the adhesive matrix was noted, see Figure 4.55b, and cracks due to the formation of numerous voids destroyed the integrity of the adhesive material.

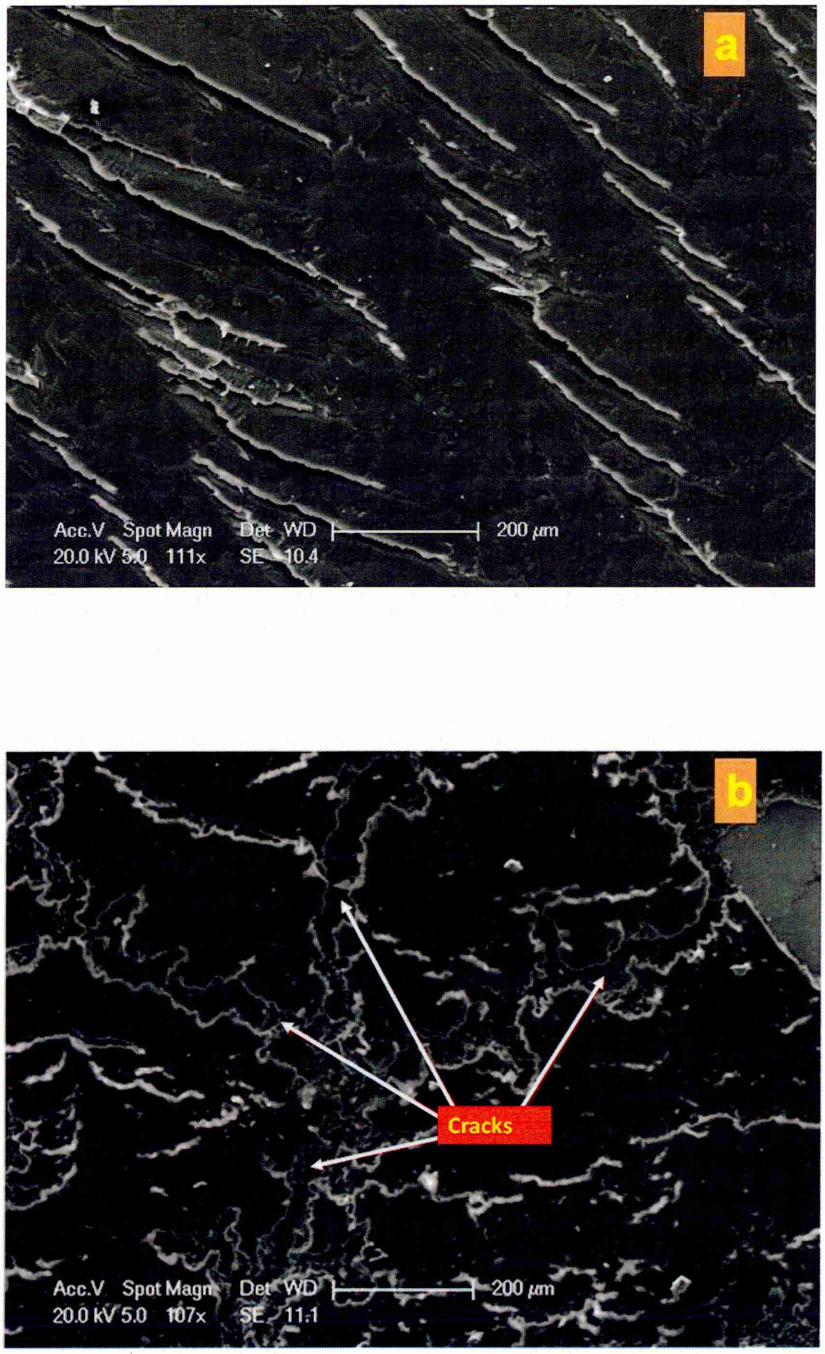

Figure 4.55 SEM images of fracture surface after immersion (a) one week, (b) eigth weeks in 3.5%NaCl (mild steel substrate)

4.5.3.2 Adhesive strength of SG3/Al vs immersion time

The adhesive strength for the SG3 adhesive on AA2024-T3 substrates aged in 3.5% NaCl solution is shown in Figure 4.56. In dry conditions the maximum shear strength value of this adhesive was 24±0.6 MPa for joints cured at 140°C for 16 hours. Similar results were obtained as for the SG3/MS lap joints: with each of one, two, four and eight week's exposure the adhesive strength of the lap joints in 3.5% NaCl solution progressively decreased. After eight weeks exposure the average shear strength was 7.8 MPa. The explanation for this trend is considered to be the same as that given for the loss of strength of the SG3/MS lap joint.

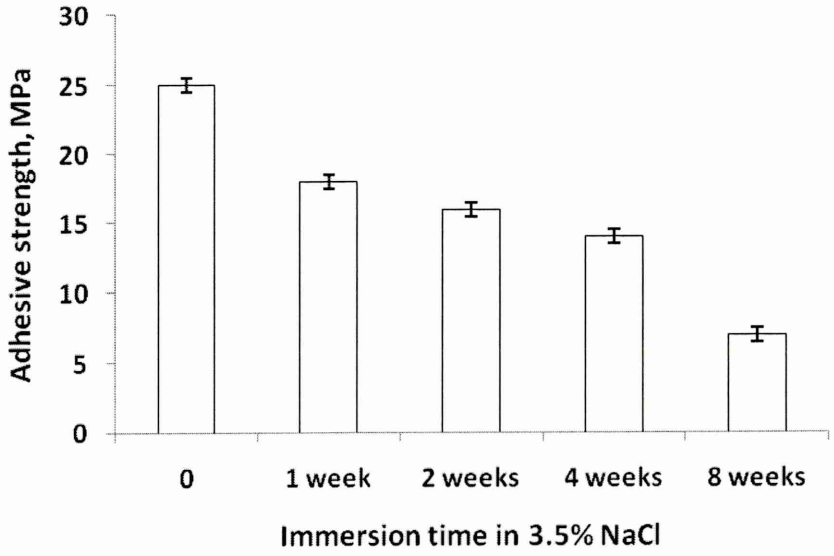

Figure 4.56 Effect of immersion times on adhesive strength of SG3/ AA2024-T3 lap joints (cured at 140°C for 16 hours)

Figure 4.57 shows the percentage reduction in mean lap joint strength with different immersion times. It can be seen that the reduction in strength is relatively low initially but begins to drop rapidly after four weeks immersion. At eight weeks about 68% of loss adhesion was recorded. The substantial reduction in the adhesion force was attributed to the increase in crack defects within the bulk adhesive.

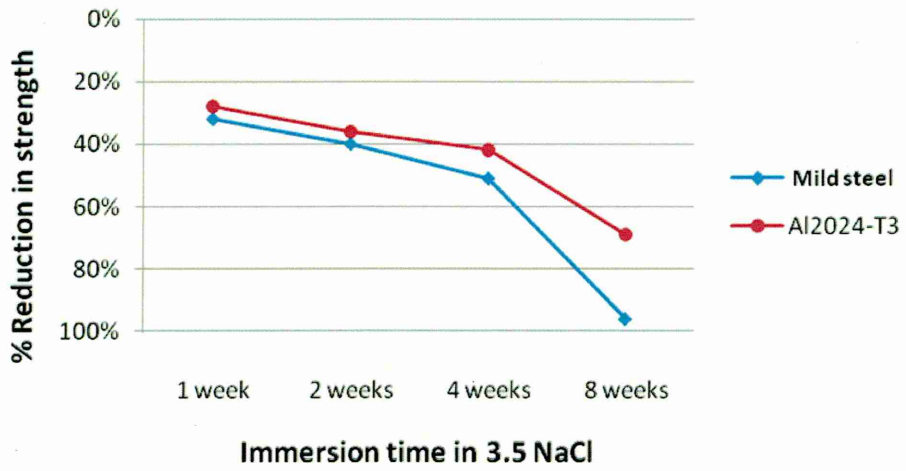

Figure 4.57 Reduction in adhesive strength of SG3/MS and SG3/Al2024-T3 lap joints with duration of immersion in 3.5% NaCl (cure time 16 hours at 140°C)

4.5.3.2.1 Fracture surface

The drop in strength after eight weeks immersion may indicate that the failure was governed by the degree of damage within the adhesive structure as the diffusion of the aggressive NaCl solution within the matrix increased with time. Comyn [147] demonstrated that the degradation in adhesive strength may be caused by diffusion of solution through the adhesive or/and along the interface or by capillary action through cracks in the adhesive. Figure 4.58 shows that adhesive material was found on both surfaces with short cracks distributed on the surface near the interface regions, indicating a mixed cohesive/adhesive failure mode.

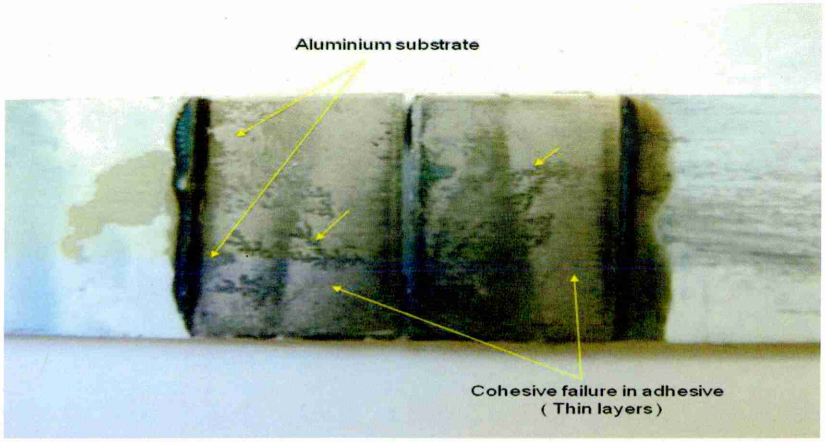

Figure 4.58 Cohesive failure mode of SG3/ AA2024-T3 lap joints after eight weeks immersed in 3.5% NaCl

4.5.3.2.2 SEM observations

Figures 4.59 a and b, respectively, show the fracture surface of lap joints immersed for one and eight weeks in the 3.5% NaCl solution. It can be seen that a mixed adhesive/cohesive mode was noted after one week, Figure 4.59a. Very short cracks in the adhesive material were observed, which may be due to a decrease in cohesive force within the adhesive matrix. This behaviour may be attributed to damage or disruption of hydrogen bonding at the molecular chains of the adhesive. Soles and Yee [148] pointed out that moisture can be transported through the unoccupied volume of adhesive and access hydrogen bonds via the nanovoids, thus decreasing the cross-linking density. In addition, no corrosion products were observed after one week on the substrate surface, suggesting the diffusion rate of moisture through the interface within this period was low compared with that after eight weeks. This is supported by the data shown in Figure 4.57 which shows the percentage reduction in strength of the SG3 adhesive to the substrate in one week (i.e. ~ 30%) was lower than that after eight weeks (i.e. ~ 70%).

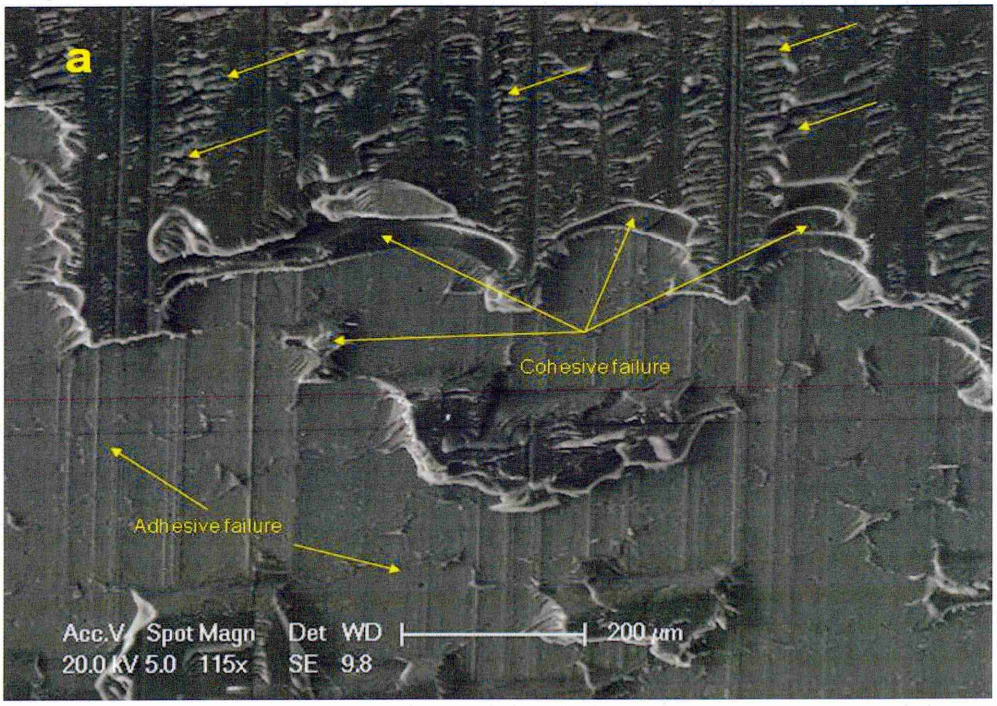

Figure 4.59a) SEM image of one week immerrsed in 3.5%NaCl
(Al 2024-T3 substrate)

However, with increase in immersion time, more damage in the SG3 adhesive material was observed due to the increase in cracks length, see Figure 4.59b. This led to higher stress intensity value at the crack tip, which reduced the adhesive's ability to resistance further crack propagation, resulting in a drop in strength of nearly ~ 70%, see Figure 4.57. With increase in immersion time the fracture surface also showed mixed adhesive/cohesive mode.

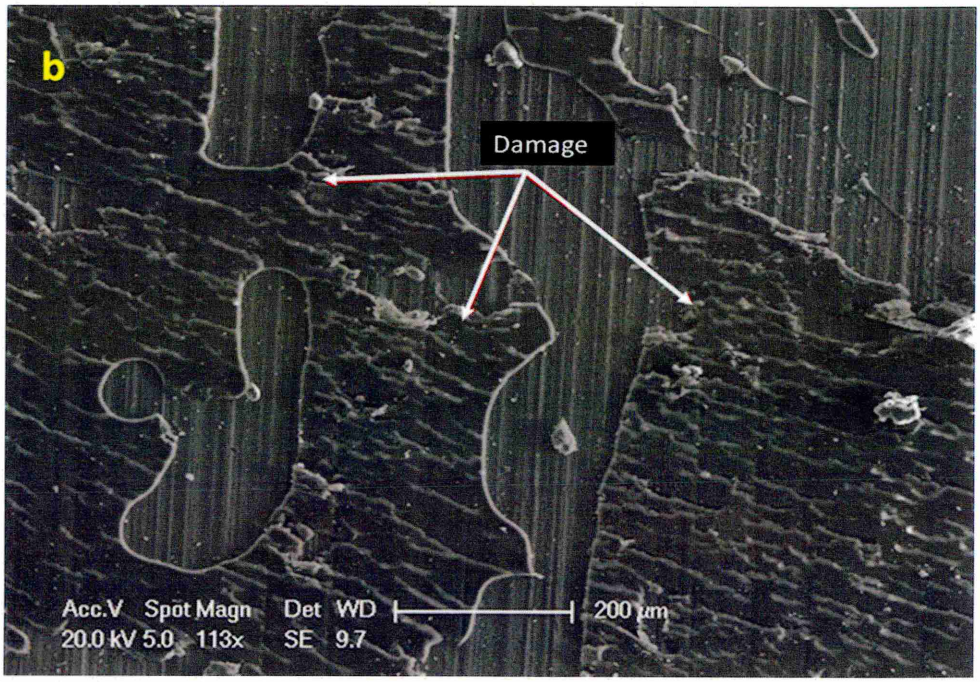

Figure 4.59b) SEM image of eigth weeks immersed in 3.5%NaCl (Al 2024-T3 substrate)

4.5.4 Tensile strength of SG3/MS adhesive (butt joint)

The adhesive strength of the butt joint is very dependent on the sample preparation due to the complex stress state existing within the adhesive layer. For example, the measured adhesive tensile strength of a butt joint can vary considerably due to small misalignments in the joint which result in cleavage stresses [149]. The SG3/MS adhesive tensile strength of five samples was measured, see Table 4.5. Due to the distribution of internal stresses within the adhesive layer a considerable variation can be seen. An average joint tensile

strength of 28.5 MPa was achieved with 16 hours cure time at 150°C, but the range was from 22.5 MPa to 35.6 MPa. These results show that the tensile strength (butt joints) of this adhesive is higher than the equivalent mild steel shear strength (lap joints) in Figure 4.22. There is indeed evidence that the shear strength (τ) of polymers is less than their tensile strength (σ) [150]. According to the Tresca criterion, shear strength in polymers is equal to half the tensile strength ($\tau_{max} = \sigma/2$) [151]. da Silva and Adams [152] have recently reported the adhesive shear to tensile strength ratios from 0.72 to 0.83 at room temperature. The measured value of SGA3/MS is relatively close to that obtained by da Silva and Adams and a shear to tensile strength ratio between 0.7 and 0.85 was observed for this system.

Table 4.5. Adhesive tensile strength of butt joints on mild steel substrates. (SG3/MS cured at 150°C for 16 hours)

Sample	Maximum Load (N)	Extension at Break (mm)	Tensile stress at maximum load (MPa)	Average tensile stress (MPa)
1	17508	1.110	35.6	28.5
2	15849	0.964	32.3	
3	13215	0.930	26.9	
4	12511	0.916	25.5	
5	11033	0.891	22.5	

For butt joints, the SG3/MS adhesive exhibited three fracture surface modes, as shown in Figure 4.60. It was found that around 50% of the fracture was via the cohesive mode (CO), about 40% via the interfacial fracture mode (adhesive fracture (AD)) and the remaining 10% via mixed failure mode (i.e. cohesive/adhesive on the surfaces (AD+CO)). The fracture behaviour can be explained in terms of an improvement in the cross-linking within the adhesive itself and at the interface. Adhesive strength is enhanced due to the incorporation of γ-Al_2O_3 nano-particles in the matrix, where the γ-Al_2O_3 is

available for catalytic epoxide ring-opening reactions. It was reported [153,154] that the opening of epoxy rings was increased with the addition of catalytically active AlOR/OH groups to the acidic silica-base sol-gel system, which supports the above.

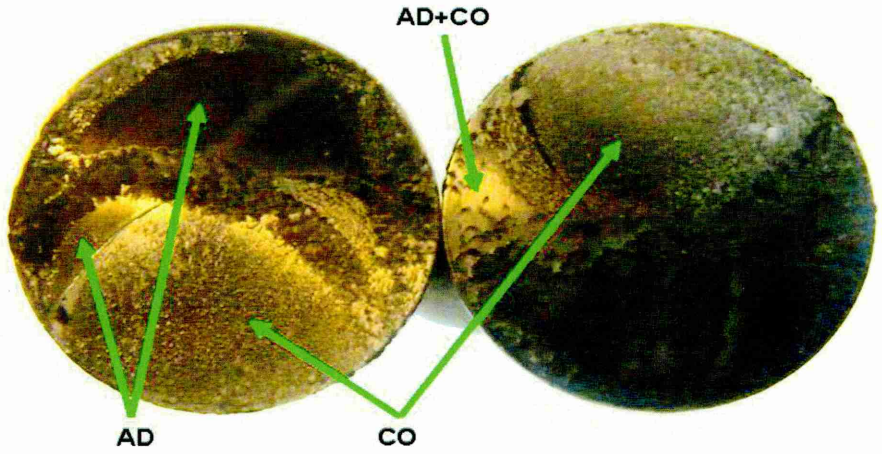

Figure 4.60 adhesive fracture surface of SG3 on mild steel (Butt joint)

4.5.5 Fatigue strength of SG3/MS adhesive (lap joint)

The fatigue strength of various adhesive materials on different metallic and non-metallic substrates has been studied extensively by many researchers [155,156,157 and 158]. It has been found that a number of variables (eg load ratio, frequency at which the load was applied, temperature and environmental humidity) have played a role in determining the performance of adhesive joints [159]. In this work, fatigue tests of a lap joint were carried out to assess the adhesive performance of SG3 under dynamic cyclic loading, with load ratio P_{min}/P_{max} = 0.1, at two different frequencies of 3Hz or 10Hz, in order to assess the working efficiency of SG3/MS adhesive. Maximum load P_{max} was varied from 3 to19 MPa.

4.5.5.1 Maximum load/cycles to failure for lap joints

Figure 4.61 presents a graph of maximum load (P_{max}) against the number of cycles to fatigue failure (N_f) for frequencies of 3 and 10Hz. It can be seen that the number of cycles to failure of the SG3 adhesive bond increased as the applied load decreased. No significant differences in the fatigue life of the lap joints were noted between the two frequencies, at any applied P_{max}. It was observed that, when P_{max} is lower than 2kN, each test sample supported more than one million cycles without failure. This may be attributed to the possibility that microscopic cracks form during cyclic load within the bulk adhesive or at the adhesive/substrate interface, but do not increase to a length critical for failure under these loading conditions. It was reported [160] that the frequency effects are related the changes in time of fatigue crack development in the material structure. This appears to be related to the adhesive formulation, where the inorganic nano-fillers played an important role in delaying adhesive rupture at the substrate surface and/or within the adhesive matrix. It should be noted that, no endurance or fatigue limit of the joints appeared at either frequency.

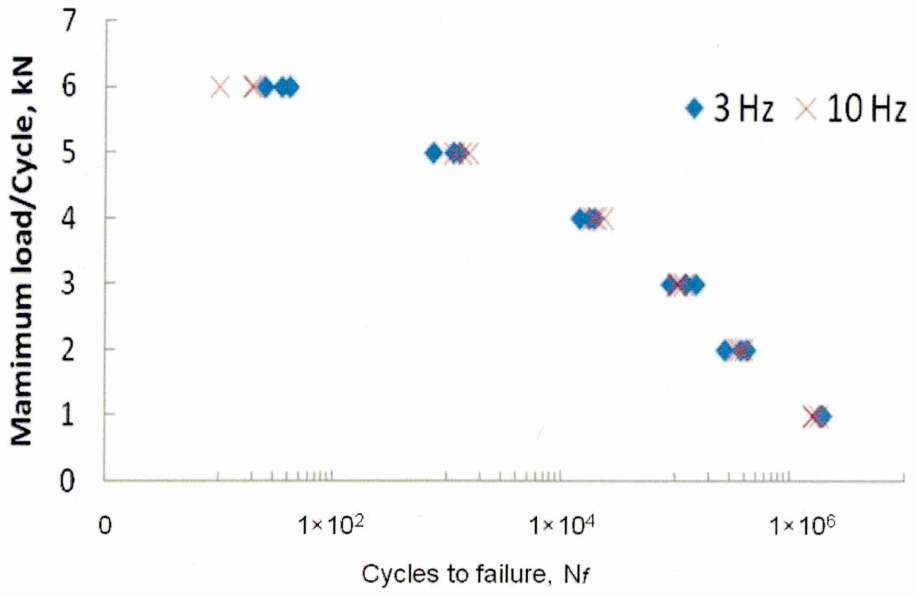

Figure 4.61 Cycles to failure for lap joints as a function of maximum applied load for SG3 adhesive

Table 4.6 presents the experimental results of SG3 adhesive for lap joints subjected to fatigue strength tests at constant load ratio, *R=0.1*. For each maximum load and tested frequency, the fatigue life results (number of cycles at failure) were obtained as average of three specimens (SG3/MS joints)

Table 4.6 Fatigue strength of SG3 adhesive

Max Load		***R (Load ratio)***	***N_f (Number of cycles to failure)***					
kN	***MPa***		***Applied frequency f = 3 Hz***			***Applied frequency f = 10 Hz***		
1	3.2	0.1	1,876,123	1,640,592	1,950,321	1,587,264	2,000,000	1,811,238
2	6.4	0.1	275,984	430,689	380,421	377,520	350,761	401,612
3	9.6	0.1	90351	152,125	123,701	119,272	105,341	100,345
4	12.8	0.1	14513	19359	17670	23702	20514	18980
5	16	0.1	754	1130	1280	1541	1350	1140
6	19.2	0.1	35	25	41	10	19	20

As the applied load increased, a reduction in fatigue life was observed. Cycling loading can result in creep failure occurring within a relatively short number of cycles due to the cumulative effect of cyclic shear strains. In addition, the decrease in the number of cycles is probably due to cracks initiated near to the ends of the overlap joint where the stress concentration is high, and which propagate within the bulk adhesive (cohesive) or near or at the adhesive /substrate interface.

4.5.5.2 Fatigue fracture surface

The fracture surface of lap joints under different cycling loading conditions was used to identify the mode of failures. Three fracture surfaces were evaluated visually as examples to highlight the failure modes obtained with fatigue testing, see Figure 4.62. The failed joints shown in this figure were tested at the same stress ratio R=0.1, and frequency *f* =10Hz. The surfaces reveal that the failure

was mixed interfacial/cohesive mode (i.e. 20/80%), under low fatigue loading, i.e. 1.0kN, and the joints failed as crack density increased with increase in the number of cycles to greater than one million, see Figure 4.62a. With further increase in loading up to 3.0kN, the joint fracture surface showed mixed adhesive/cohesive mode. It can be seen that the percentage of interfacial to cohesive is around 35/65% of the failed surfaces, see Figure 4.62b. Increasing the load up to 6.0kN resulted in a mixed failure mode with about 44% an interfacial and the remaining 56% being from cohesive fracture mode, Figure 4.62c.

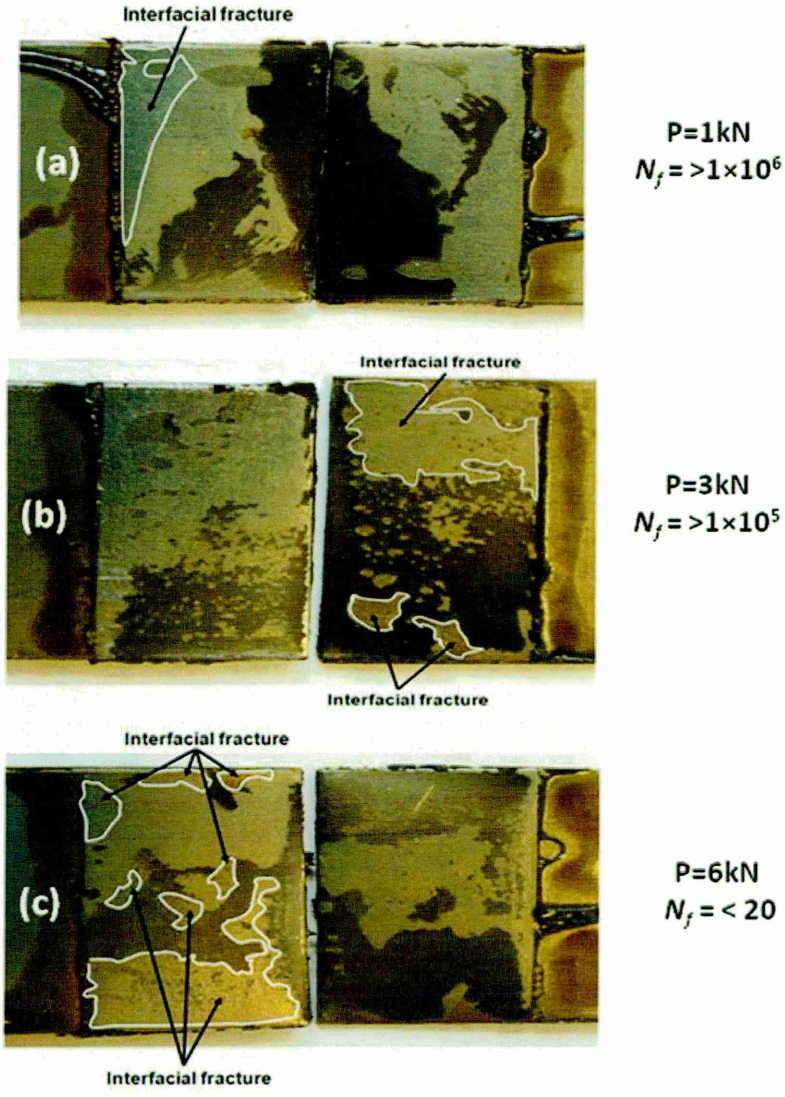

Figure 4.62 Fracture surface modes due to fatigue cycling

4.6 Hybrid epoxy/sol-gel adhesive structural (SG3)

4.6.1 SEM observations

An SEM image of the PE fracture surface of the hybrid epoxy/sol-gel system, see Figure 4.63a, shows a mixed failure mode. This image indicates that the interaction between the PE matrix and the mild steel substrate is weak, resulting in lower shear strength, see Figure 4.22, compared to SG2 & SG3 adhesives, and this is probably due to poor epoxy matrix compatibility. In addition, the area of surface covered by the epoxy resin (dark gray) is much less than that of the un-covered surface (light gray), suggesting low adhesive bonding at the interface. SEM analysis of the SG3 adhesive fracture surface, see Figure 4.63b, was also conducted to understand how the addition of γ-Al_2O_3 and MWCNTs affected the failure mode of the modified sol-gel epoxy adhesive. The introduction of inorganic fillers into the formulation increased the degree of cross-liking within the adhesive matrix and the bonding at the interface, which improved the strength and changed the failure mode to a mixed adhesive/cohesive type.

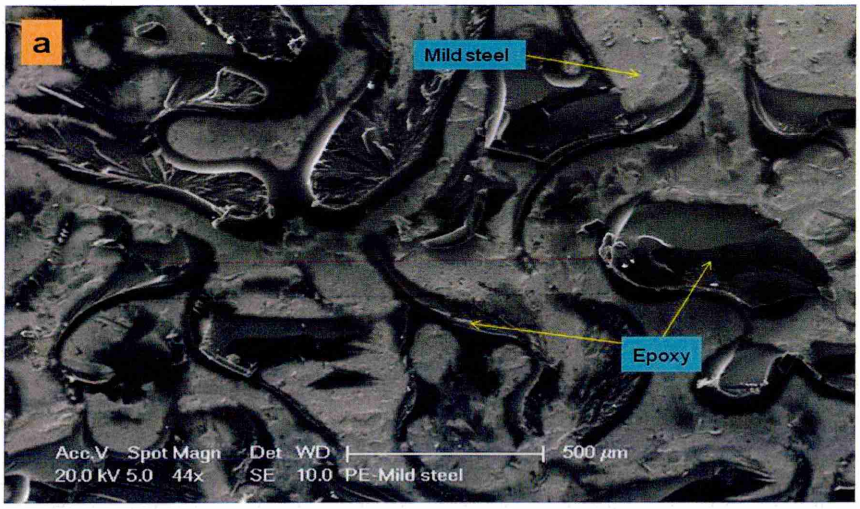

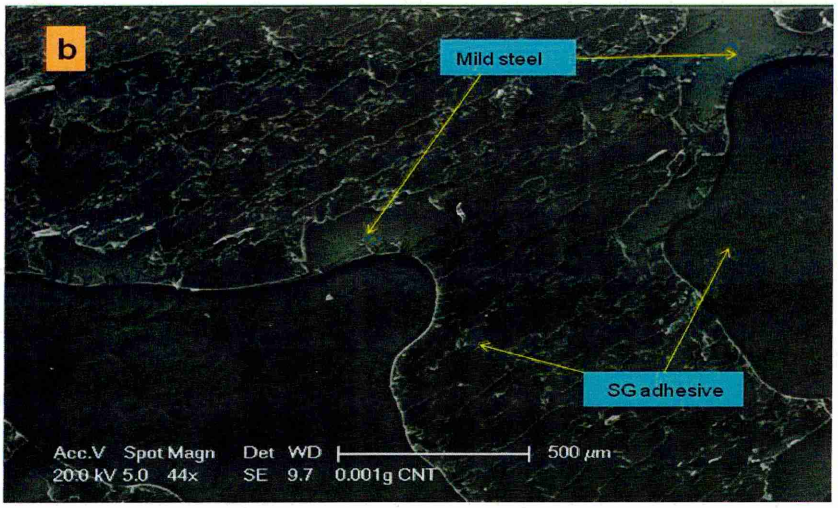

Figure 4.63 SEM of fracture surface on mild steel substrate (a) using PE adhesive and (b) epoxy/sol-gel with added γ-Al_2O_3 and MWCNTs (SG3)

Figures 4.64 a, b and c show SEM images of the SG3 fracture surface where MWCNTs and γ-Al_2O_3 have been introduced into the adhesive matrix. These appear to have a good distribution within the adhesive matrix with a consequential effect on the adhesive strength. It should be noted that the MWCNTs are quite thick and this is due to the presence of a coating of the adhesive on the MWCNTs. Achieving a good dispersion of MWCNTs introduces a positive effect on the sol-gel adhesive network and increases chemical interaction bonds [161] (i.e. hydrogen bonds) within the adhesive matrix as shown in Fig 4.64c.

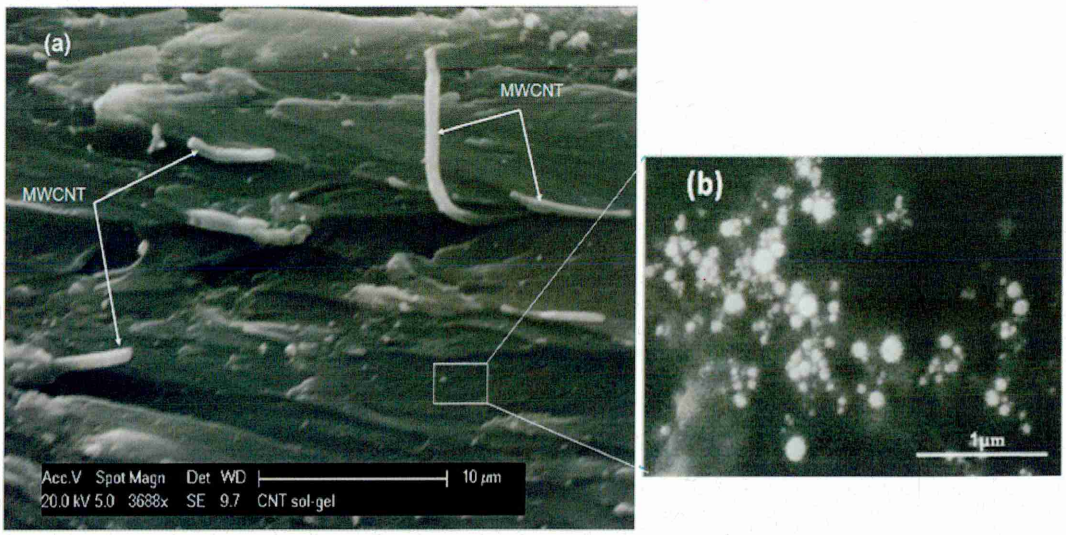

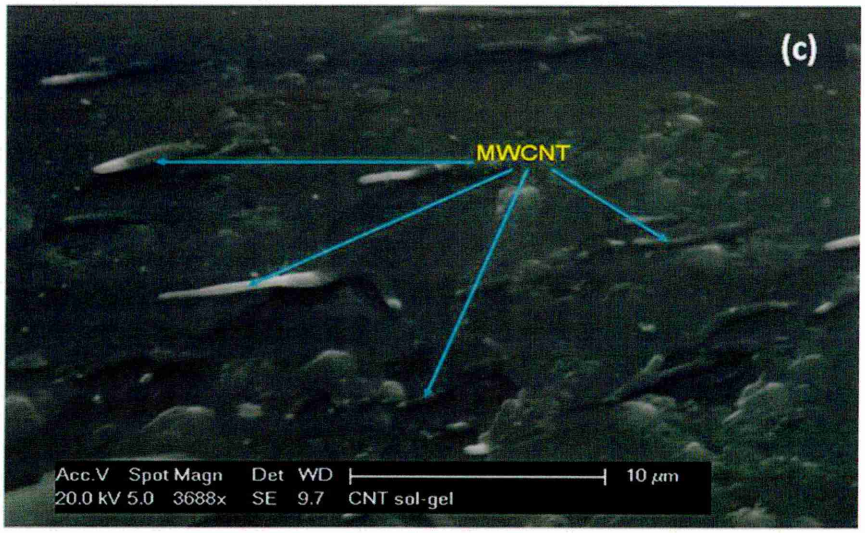

Figure 4.64 SEM images of distrribution of MWCNTs in the fracture surface

4.6.1.1 Adhesive/substrate interface

Figure 4.65 shows an SEM image of the cross-section, indicating very good bonding at the interface, with no gaps or delaminations being observed. This is attributed to the improvement in adhesive wetability on the substrate surface due to the incorporation of inorganic fillers within sol-gel adhesive formulation which consequently increased the adhesive shear and tensile strength of SG3.

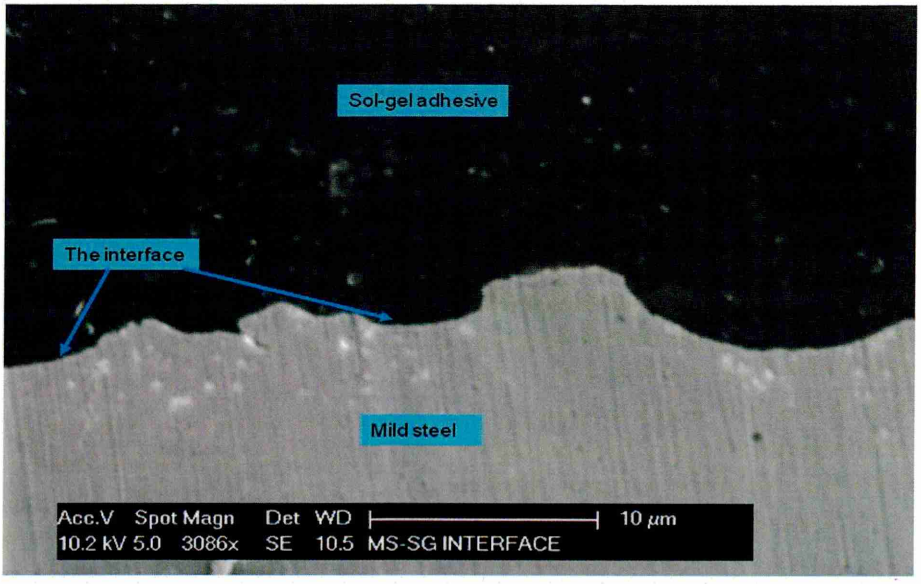

Figure 4.65 SEM image of cross-section at SG3/MS interface

Figures 4.66 a and b show SEM backscattered electron images in combination with chemical analysis obtained by using Energy Dispersive X-ray analysis (EDX) at the adhesive/metal interface and for the bulk adhesive material of SG3, respectively. It can be seen that both the interface and adhesive matrix regions (Figure 4.66a and 4.66b, respectively), were rich in carbon, oxygen and silicon elements, which are the main elements in the adhesive formulation. In addition, well-dispersed γ-Al_2O_3 nano-particles were also observed within the adhesive material, Fig 4.66b.

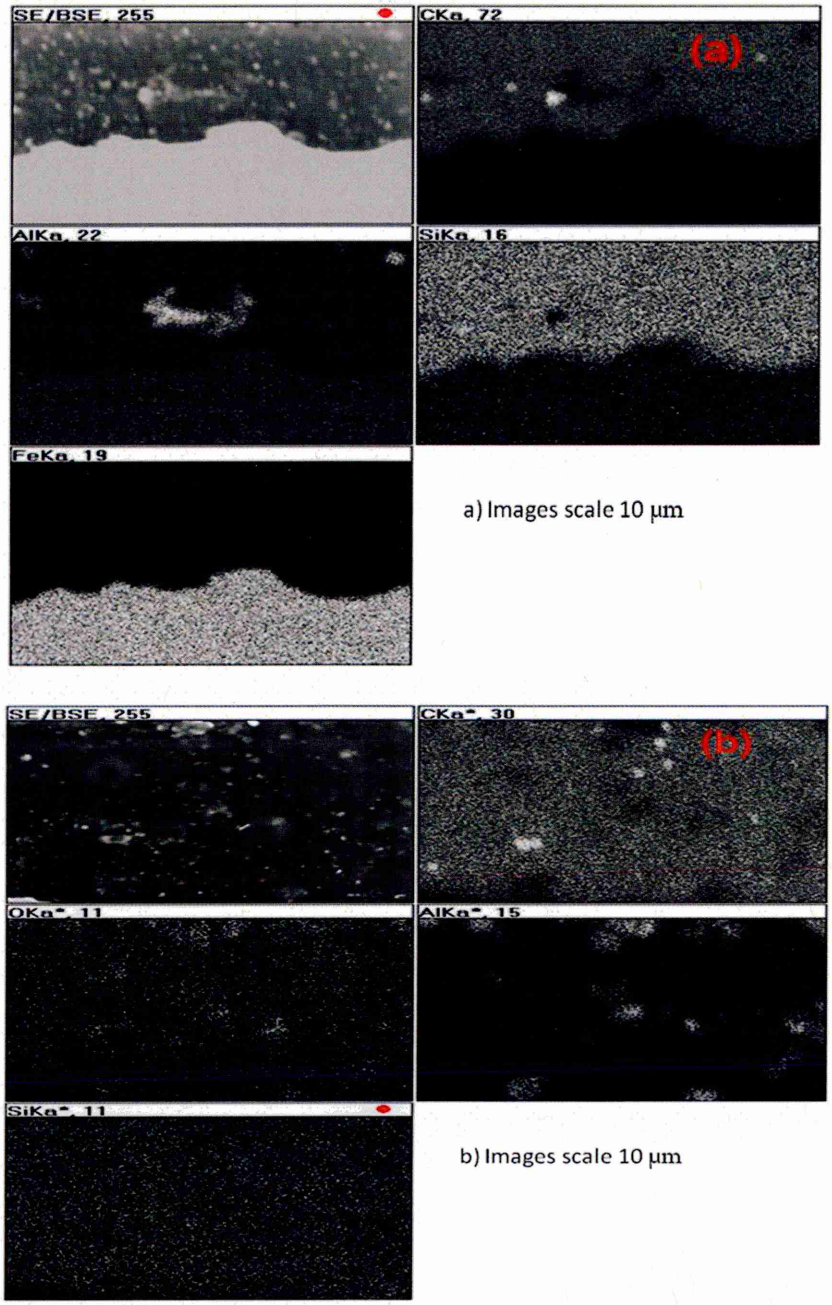

Figure 4.66 EDX maps at (a) the interface and (b) within SG3 adhesive matrix

4.6.2 FTIR analysis

FTIR measurements were used to examine the molecular structure of the epoxy resin (DGEBA) cured using the curing agent DETA, and the molecular structure of the epoxy/sol-gel adhesive (SG3). Figure 4.67 shows the FTIR spectra of the epoxy resin with DETA where the presence of an ethoxy group is shown by the appearance of a CH_2 absorption band at ~ 2950cm^{-1} and a peak at ~ 1290cm^{-1}. A C=C aromatic absorption band at ~ 1680cm^{-1} was also observed. The peak around 1580-1600cm^{-1} was attributed to a stretching vibration in a N-H bond, and confirmed the presence of the curing agent. The absorption band of the epoxy group was seen as a peak at ~ 950cm^{-1} and as a band of peaks between ~ 825cm^{-1} and ~ 3040cm^{-1} corresponded to C-H aromatic substitutions. For example, the C-H aliphatic bond appeared at ~ 1150cm^{-1} and ~ 1460cm^{-1}. Stretching vibrations in the range 3200-3500cm^{-1} correspond to the O-H bond of absorbed water molecules.

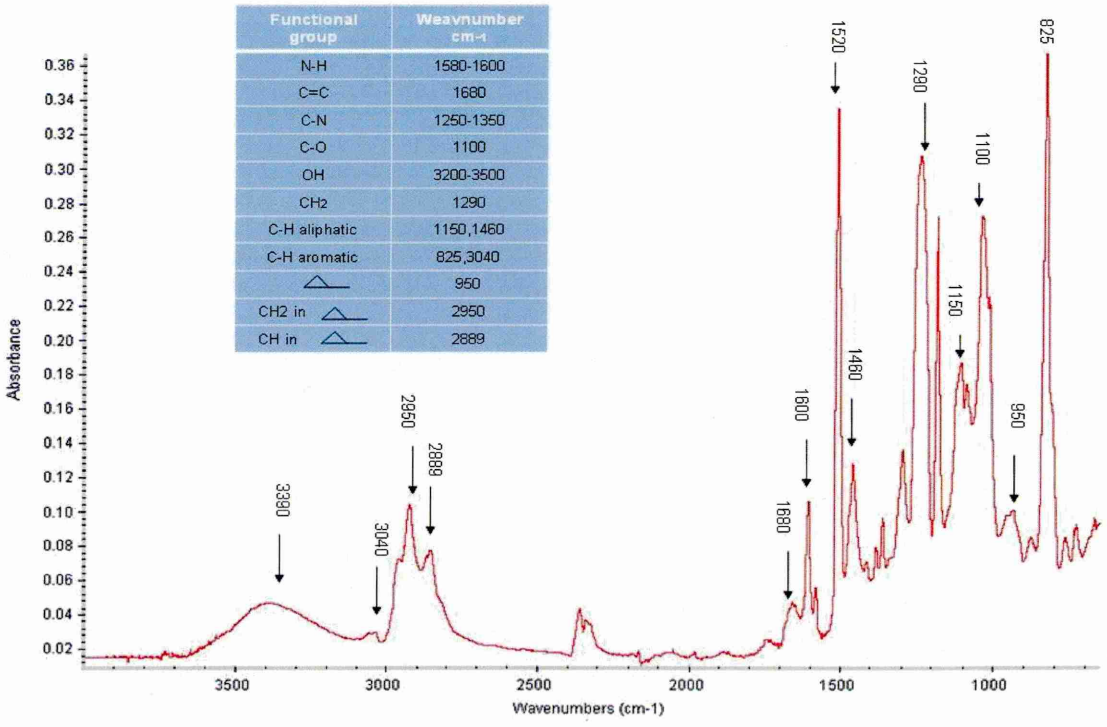

Figure 4.67 FTIR spectra of epoxy resin cured using DETA as curing agent

The characteristic peaks of the FTIR spectrum of the hybrid epoxy sol-gel adhesive (SG3) are shown in Figure 4.68. The absorption band due to water molecules at around 3200-3500cm^{-1} is smaller than in the DETA-cured epoxy resin due to sol-gel polymerisation reactions. Stretching vibrations of C-H were observed at ~ 2889cm^{-1}, and of CH_2 at ~ 2950cm^{-1}. The absorption peaks in the range ~ 1620-1680cm^{-1} and at ~ 1730cm^{-1} were related to C=C and C-O bonds, respectively. Observation of other bands in the spectra are due to the presence of inorganic phases in the adhesive material. A distinct broad absorption peak at ~ 1088cm^{-1} was attributed to Si-O-Si bond, and indicated network formation in the hybrid epoxy/sol-gel materials [162, 163]. The absorption band ~ 800-950cm^{-1} belongs to the epoxy group and the peak at 3370cm^{-1} is characteristic of -OH stretching as a result of the Si–OH, which is probably an unreative group in the inorganic networks [164]. Absorption peaks for Si-O at ~ 793cm^{-1}, Si-O-C at ~ 1198cm^{-1} and Si-C at ~ 1250cm^{-1} were also found.

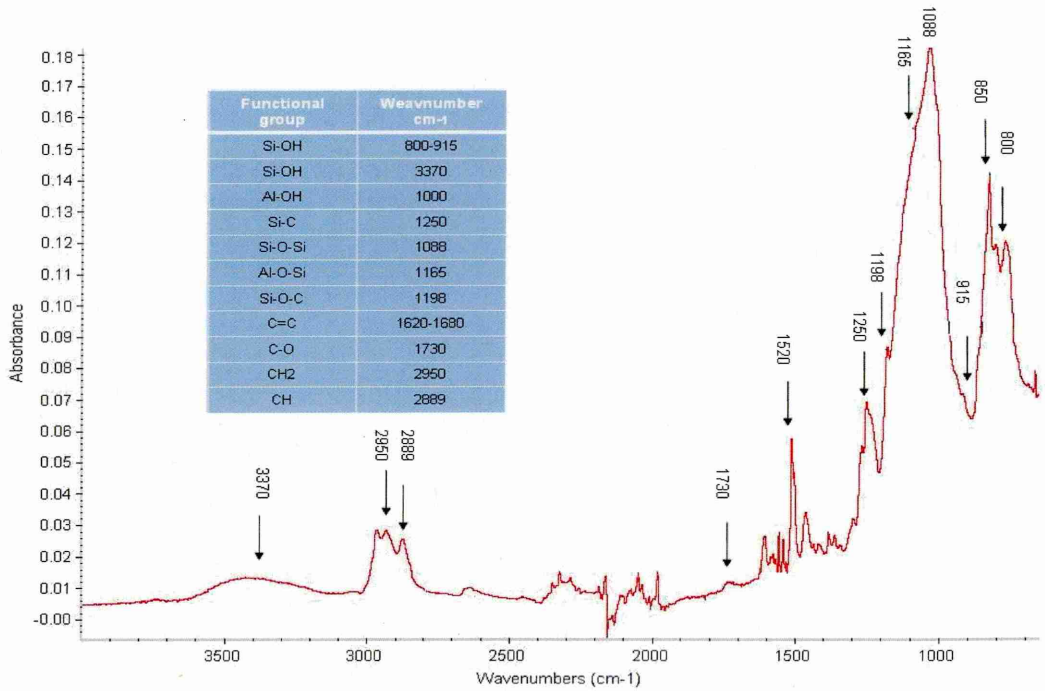

Figure 4.68 FTIR spectra of SG3 (hybrid epoxy sol-gel adhesive)

4.6.3 Raman spectra analysis

Figure 4.69 shows the epoxy resin (PE) spectrum obtained by Raman spectroscopy at room temperature and contains spectral bands associated with bisphenol A, as shown in Table 4.7. The two peaks at ~ 641cm^{-1} and ~ 3621cm^{-1} are attributed to the aromatic C-H band within the epoxy structure. The peak at ~ 1897cm^{-1} can be assigned to the asymmetric stretch of CH_2 or CH_3. A weak aromatic C=C and a strong aromatic C=C ring (phenyl) appear at 1654cm^{-1} and 1732cm^{-1}, respectively. The intense band at 1540cm^{-1} is due to CH_2 or aromatic C=C, while the band at ~1460cm^{-1} corresponds to CH_3. A strong peak at ~1270cm^{-1} is thought to be due to the C-O ether group or phenolic C-O. The peak at ~970cm^{-1} and the small shoulder at ~ 980cm^{-1} can be assigned to C-H and CH_2 within the epoxy ring, respectively.

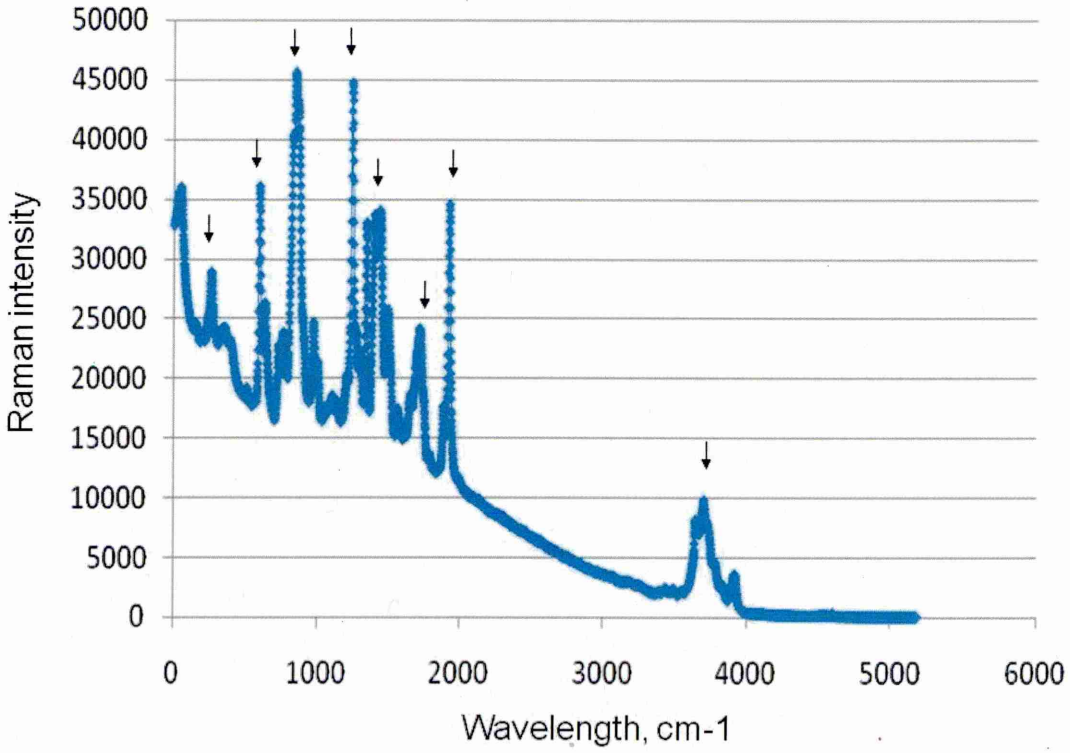

Figure 4.69. Raman spectrum of DGEBA epoxy material

Table 4.7 Raman band assignments for DGEBA [165,166]

Raman, cm-1	Assignments (BGEBA cured by DETA)
3621	C-H in aromatic ring
1897	CH_3 asymmetric stretch or CH_2
1732,1654	C=C aromatic ring
1540	CH_2 or C=C aromatic
1460	CH_3 asymmetric
1270	C-O stretch
980,870	Epoxy ring
641	C-H aromatic

Figure 4.70 shows the Raman spectral analysis of the SG3 (epoxy/sol-gel adhesive). Compared to the Raman spectra for PE adhesive there are numerous shifts in peak position or amplitude. In some cases peaks have disappeared when compared to the unmodified epoxy resin system. The results show new Raman peaks which are related to nano-filler materials in the modified system. The Raman bands of MWCNTs are clearly observed in the spectra. The spectra exhibit peaks at ~ 1275cm^{-1} and in the range ~ 1549-1590cm^{-1}. The former is the graphite G-band, and the latter is the diamond D-band. The D-band and G-band represent the C-C single bond and C=C double bond in carbon nanotubes, respectively [167]. In addition, weak Raman peaks between 400cm^{-1} and 450cm^{-1} correspond to the SiO_2 network stretch from the sol-gel structure. Spectra peaks between 830cm^{-1} and 980cm^{-1} are attributed to the Si-OH asymmetric bond or the Si-O-Si bond [168]. However, Raman spectral peaks of γ-Al_2O_3, which are normally close to the SiO_2 peak locations, are shown here between 605cm^{-1} and 610cm^{-1}, and this agrees with similar results found by in Hernandez [169] and Gnyba [168].

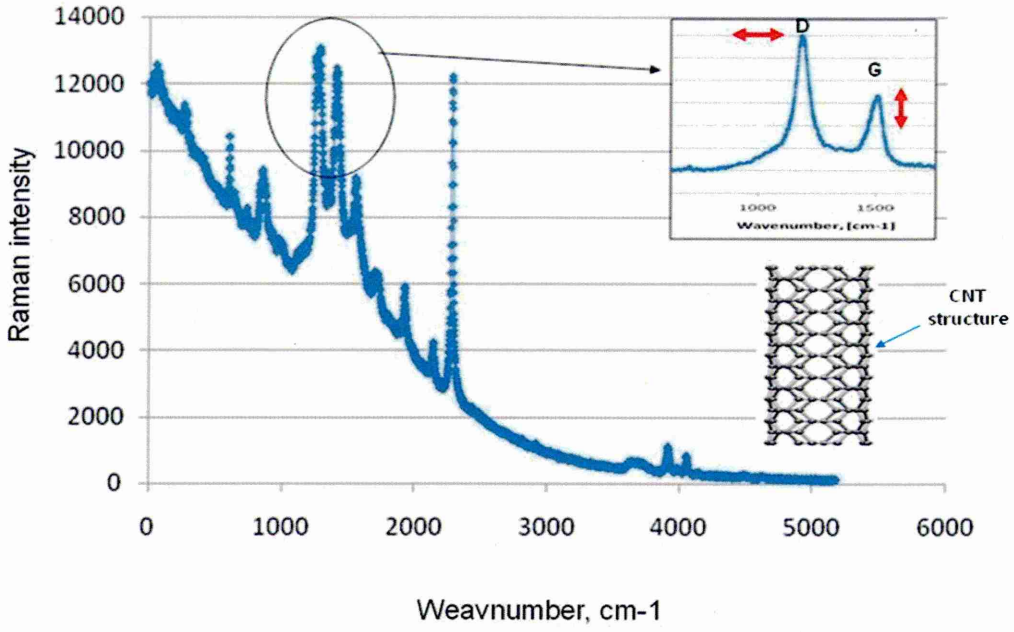

Figure 4.70. Raman spectra of SG3 (epoxy/sol-gel adhesive)

4.6.4 XPS analysis

Surface analysis has made major contributions to the study of adhesive performance on metallic and non-metallic substrates; and XPS has been used as an analytical technique to define the mode of bond failure. Here the failure mode of SG3 adhesive on mild steel and aluminium alloy substrates was investigated using XPS spectra.

4.6.4.1 XPS analysis of failed lap joint (mild steel substrate)

XPS scans were taken at two points on opposite faces of the fracture surface of the hybrid epoxy sol-gel adhesive, labelled AD1 and AD2 in Figure 4.71. Visual inspection of the opposing surfaces in Figure 4.71 clearly shows that the failure is predominantly interfacial, with some area of cohesive failure within the adhesive itself.

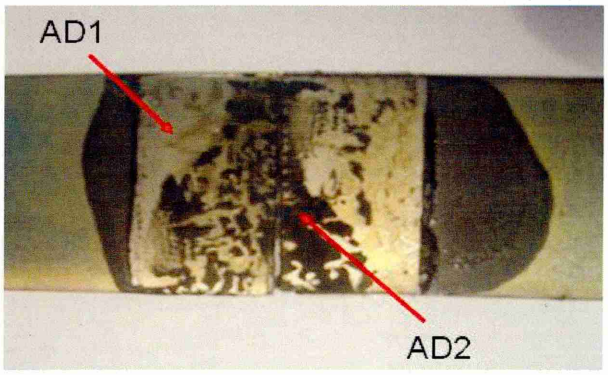

Figure 4.71 SG3 adhesive fracture surface on mild steel substrate (digital image)

The XPS spectrum recorded the following photoelectron peaks; C_{1s}, O_{1s}, Si_{2s}, Si_{2p} and a small peak of Al_{2p}, see Figures 4.72 a and b. No other elements were found in significant quantities on either side of the fracture surface. This result may be indicative that both AD1 and AD2 were covered with sol-gel adhesive material because, while the failure was mainly interfacial, there were some areas of cohesive failure within the adhesive itself. OKLL is an oxygen Auger peak and it is not relevant to this study.

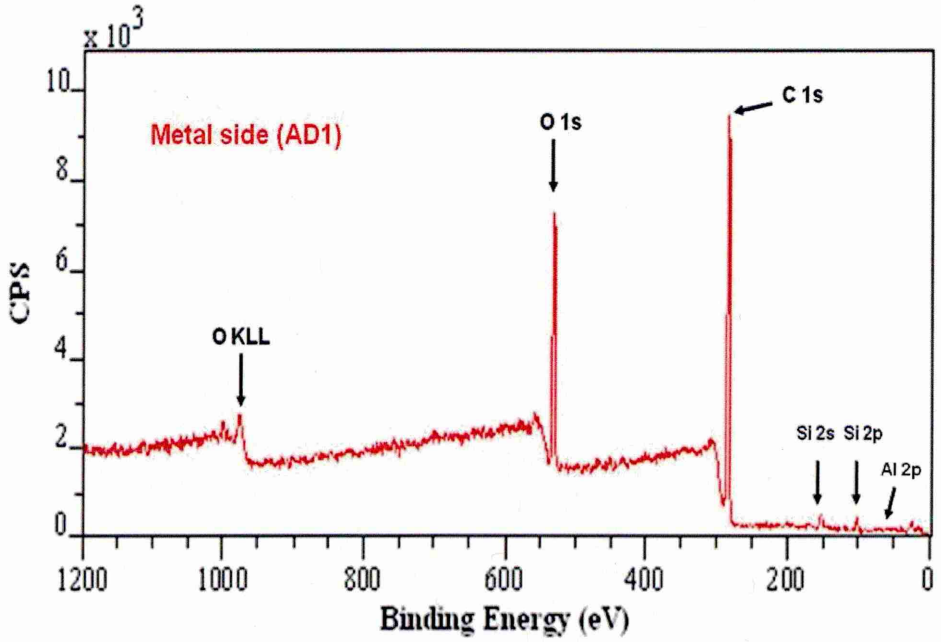

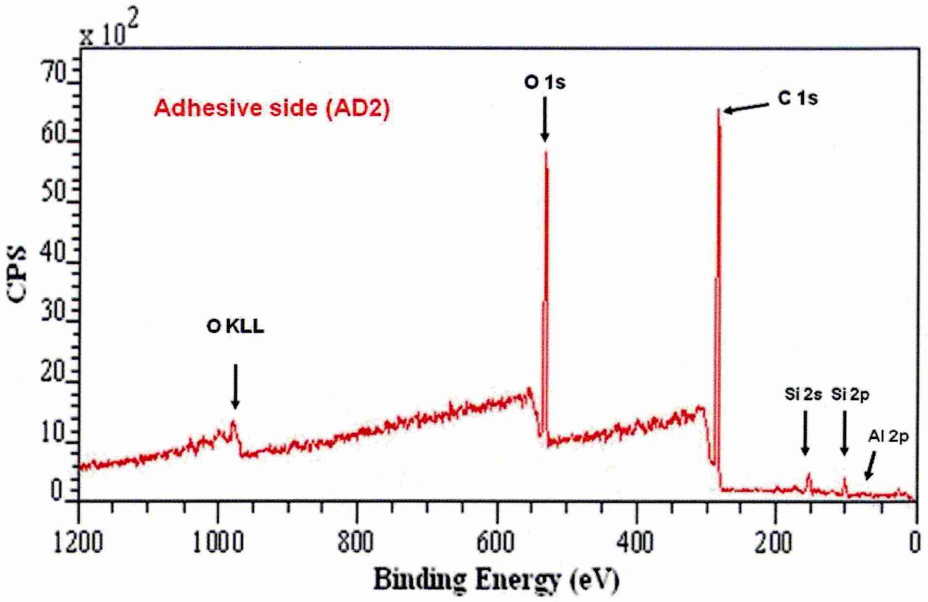

Figure 4.72. XPS survey spectra of SG3 fracture surfaces AD1 and AD2 (lap joint mild steel)

Atomic concentrations obtained from the XPS spectra on both fracture surfaces showed no significant differences in the percentage of carbon, oxygen, silicon and aluminium components, see Table 4.8. Based on these results, it is clear that the location of failure of the lap joints may be inside the adhesive film, near the interface region.

Table 4.8 Chemical analysis, Atomic % on (Mild steel)

Name	Spectral Position, eV	At %	
		AD1	AD2
C_{1s}	285.9	79.92	79.21
O_{1s}	532.4	14.96	15.33
Si_{2p}	102.1	4.11	4.31
Al_{2p}	74.1	1.01	1.24
Total	-------	100%	100%

Detailed scans were performed of the C_{1s}, O_{1s}, Si_{2p}, Cu_{2p3}, Fe_{2p3} and Al_{2p} regions. Figures 4.73 a and b show the C_{1s} XPS spectra of both fracture surfaces. The carbon peak is strong and broad, indicating that at least four different chemical states of carbon are present [170,171,172]. This includes the epoxy, MWCNTs and hydrocarbon contamination from surrounding atmosphere. After normalisation of the maximum values, the peaks exhibit a small variation in the binding energies. Each spectrum has been fitted to identify its components. In Figure 4.73a, one dominant component at 284.7±0.02eV was attributed to the C-C bond [173,174] on AD1 face, and this chemical bond appeared with the same binding energy in the AD2 face ~ 284.6±0.02eV. The weak peak at 283.1±0.01eV could be related to C=C bond on the AD1 side [174]. The peak corresponding to the same C=C bond on the AD2 face is located at 283.7±0.01eV, see Figure 4.73b. The two peaks at 284.3±0.04eV and 286.6±0.03eV in Figure 4.73a, are assigned to carbon in the C-H/C-O and C-O-C bonds on AD1 side [174]. These peaks on the AD2 side are located at 285.2±0.04eV and 286.4±0.03eV, see Figure 4.73b. The shoulders with higher binding energy peak are most probably due to the MWCNTs in the sol-gel adhesive. Meng et al. [175] found that the peak region of MWNTs can be assigned with binding energy at, 286.6eV for C-O bond and at 288 eV for C=O bond.

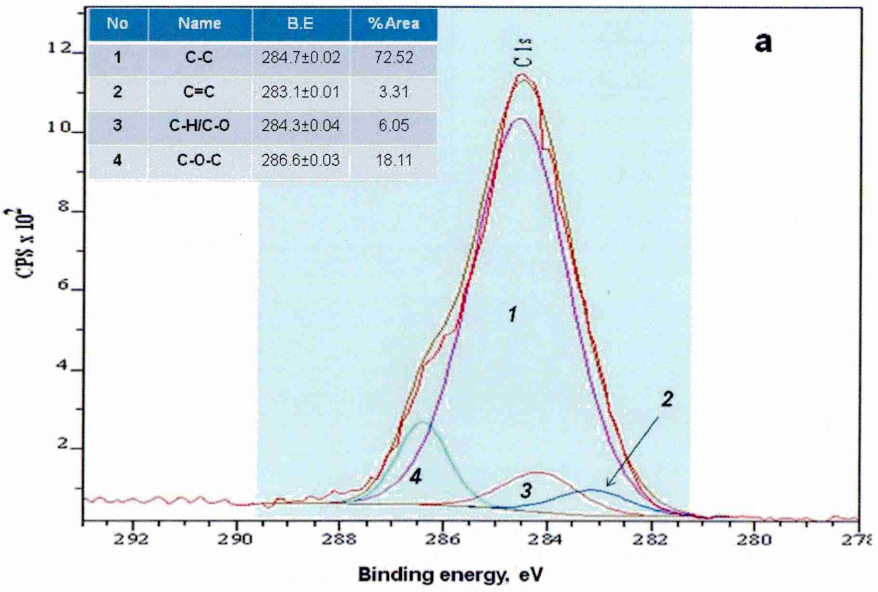

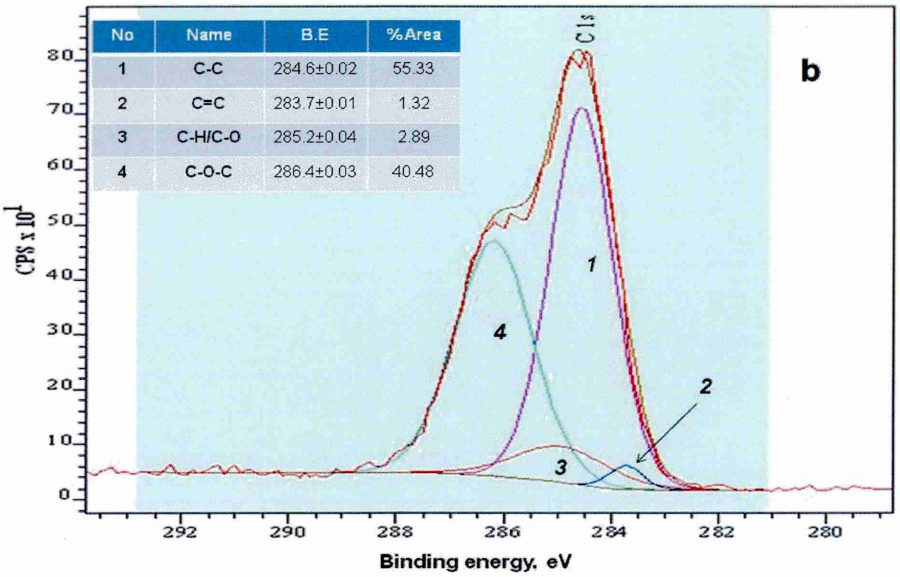

Figure 4.73 XPS spectrum of carbon component; a) on AD1 and b) on AD2

XPS spectra of oxygen also appeared with very strong peaks on both fracture surfaces as shown in Figures 4.74 a and b. The O_{1s} peak is asymmetric, indicating two different chemical states of oxygen are present. O_{1s} electrons at about 532.5±0.03eV are attributed to oxygen in SiO_2, and oxygen electrons at a slightly lower binding energy ~ 531.7±0.03eV are related to Al_2O_3. Jagadeesh and Bharat [176] showed that the oxygen spectrum at higher binding energy ~ 532 - 534eV corresponded to oxygen in the silica structure, and the lower binding energy peak of about 530.2-532.0eV is assigned to oxygen in alumina.

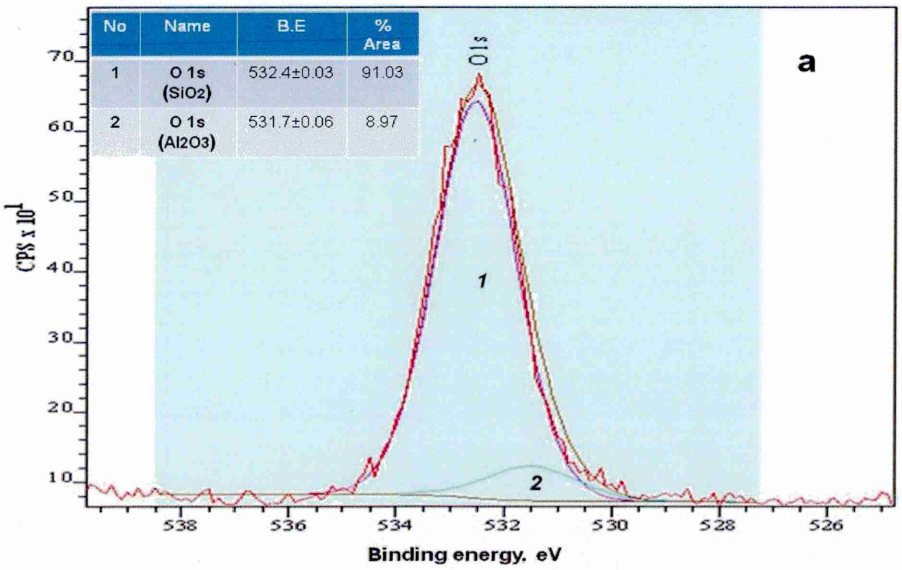

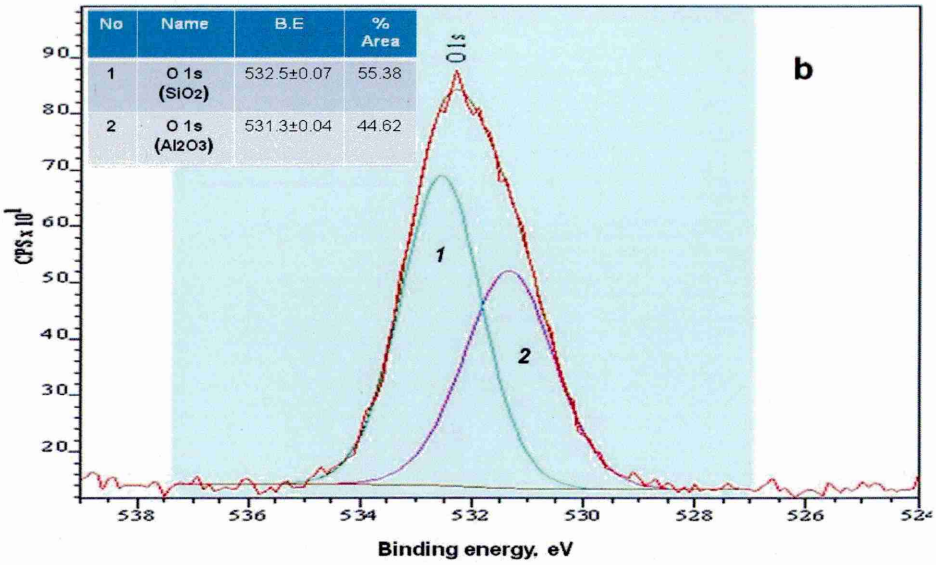

Figure 4.74 XPS spectrum of oxygen; a) on AD1 and b) on AD2

The Si_{2p} spectra for the analysis of both the AD1 and AD2 fracture faces are summarised in Figure 4.75 a and b. The silicon peak on the AD1 face consists of two regions, which can be assigned to the Si-C bond at 101.4± 0.07eV, and the Si-O bond at 102.6±0.04eV [177,178], see Figure 4.75a. However, XPS spectra of the AD2 face revealed a small silicon peak at 100.6±0.04eV due to a Si-C bond and a silicon peak for the Si-O bond centred at 102.4±0.06eV. The other spectra with a peak ~ 102.9±0.09eV may be attributed to ternary Si(C, O), see Figure 4.75b, as already proposed in the literature [179,180].

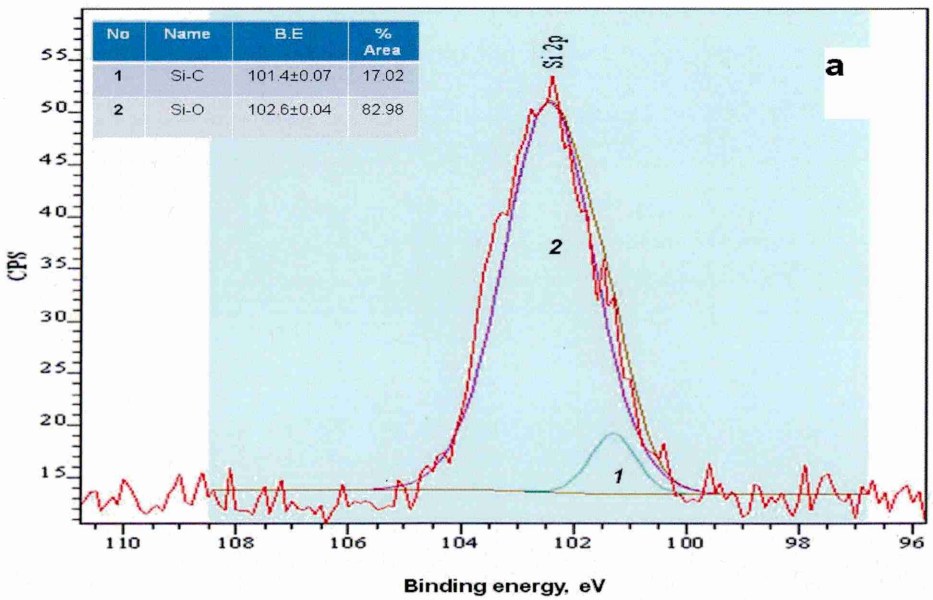

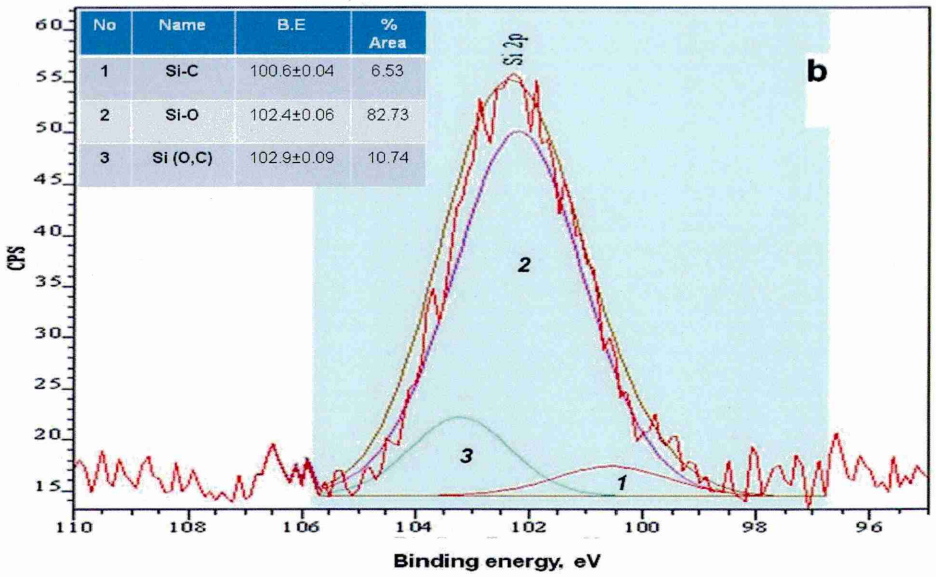

Figure 4.75 XPS spectrum of silicon element a) on AD1 and b) on AD2

The XPS spectral analysis of Al_{2p} in the surfaces AD1 and AD2 was used to identify the Al element within the adhesive material (arising from γAl_2O_3 nano-particles). Typically, the position of the Al_{2p} peak lies in the range 72-76eV [181, 182]. Figure 4.76a shows a small peak of Al_{2p} at binding energy ~ 74.9±0.03eV, which may correspond to the Al oxide form. However, the two peaks found on the adhesive face at binding energies ~ 74.4±0.03eV and ~ 75.0±0.06eV, may be attributed to bulk aluminium oxide for the first peak and the hydroxide for the second peak, see Figure 4.76b.

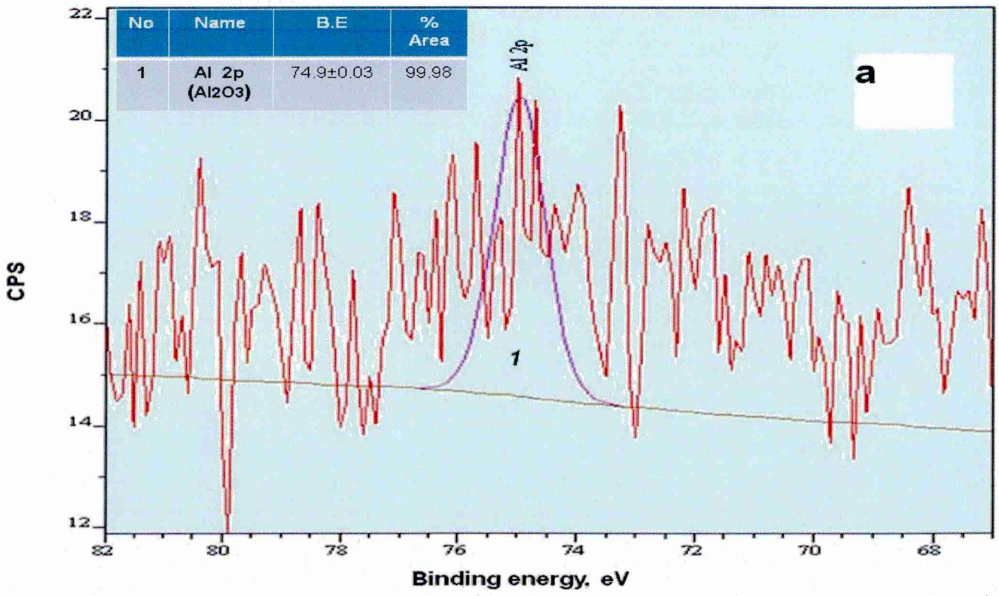

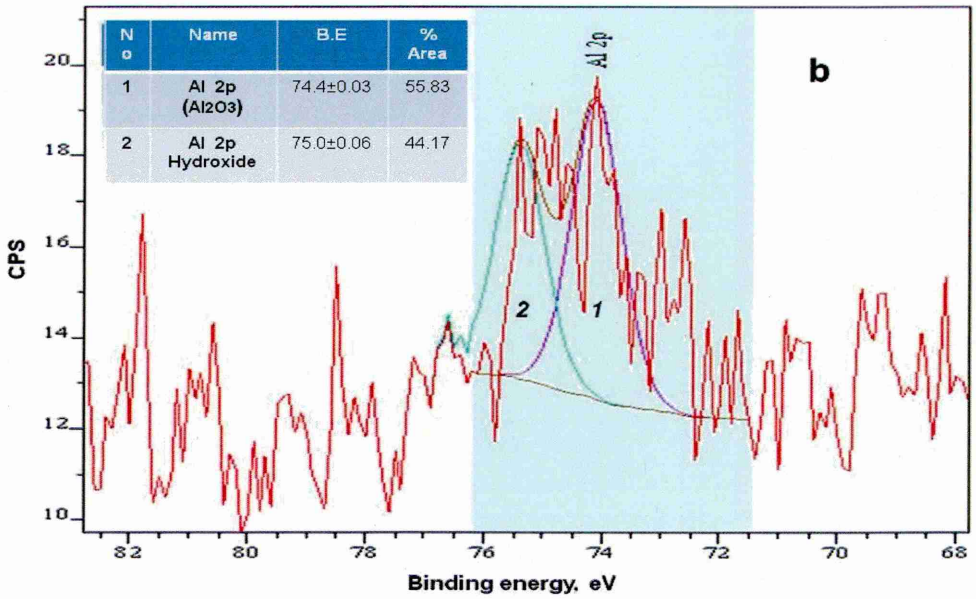

Fig 4.76 XPS spectrum of aluminium element; a) on AD1 and b) on AD2

4.6.4.2 XPS analysis of failed lap joint (Al2024-T3 substrate)

XPS scans were taken at two points on opposite faces of the fracture surface of the hybrid epoxy sol-gel adhesive, labelled F1 and F2 in Figure 4.77. Visual inspection of the fracture surfaces in Figure 4.77 shows clearly that the failure is interfacial, with some area of cohesive failure within the adhesive itself. This was an adhesive failure between F1 the aluminium alloy surface and F2 the adhesive.

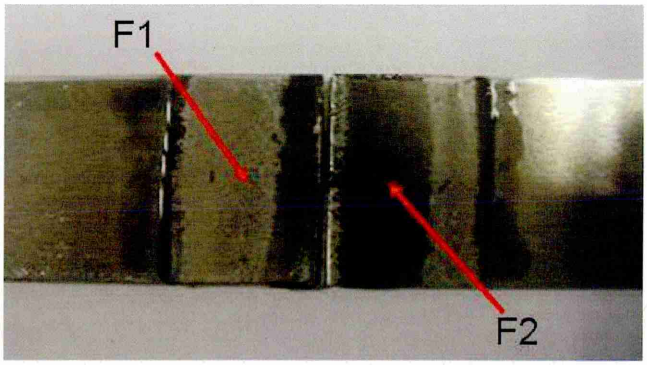

Figure 4.77 SG3 adhesive fracture surfaces on Al2024-T3 substrate

In this case, the signal to noise ratio was much better as the magnetic lens could be used. Figure 4.78 below shows the survey scans from faces F1 and F2 where the composition is overwhelmingly carbon and oxygen, with small amounts of silicon. In sample F2 (but not F1) a number of other elements are present, including sodium, nitrogen and chlorine. These elements could be related to the contamination on the adhesive surface.

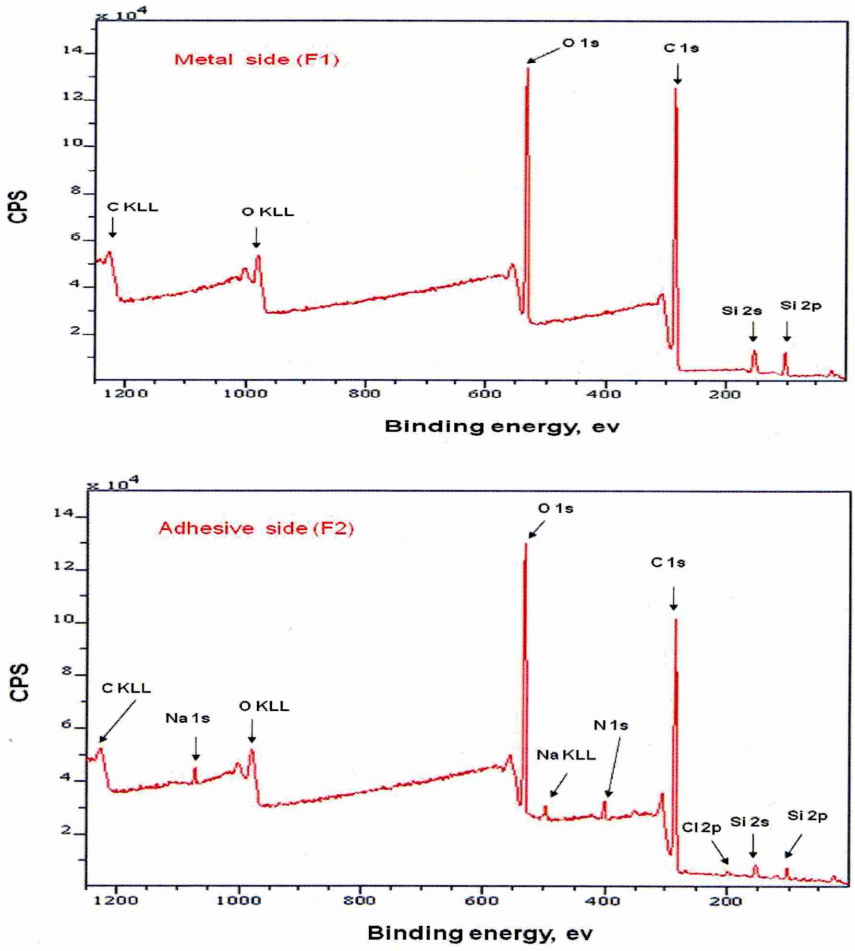

Figure 4.78. XPS survey spectra of SG3 fracture surfaces F1 and F2 (Lap joint, Al2024-T3)

Table 4.9 presents the relative atomic concentration in the lap joint fracture surfaces for the F1 and F2 faces. Clearly differences in the atomic ratio were observed. Comparing the fracture surfaces, the percentage of carbon decreased from 81.46% to 71.92%, while the oxygen increased from 13.97% to 21.88%. Small increases in silicon and aluminium were also observed. These results may indicate that the failure mode was mainly cohesive (within the

adhesive material), where the same components found on the failed surfaces. The increase in percentage atomic concentration of C_{1s} on F1 is mainly related to hydrocarbon contamination on the surface. However, the significant increase in the O_{1s} ratio on F2 compared to that on F1 may be attributed to the amount of adhesive on this side where all Al_2O_3, SiO_2 and epoxy resin included oxygen.

Table 4.9 Chemical analysis, Atomic % on (Al2024-T3)

Name	Position, eV	At %	
		F1 Aluminium	F2 Adhesive
C_{1s}	285.9	81.46	71.92
O_{1s}	532.4	13.97	21.88
Si_{2p}	102.1	3.12	4.18
Al_{2p}	74.1	1.45	2.01

The C_{1s} spectra of the F1 fracture face, see Figure 4.79a and on the F2 fracture face in Figure 4.79b show four peaks, notably; (1) A carbon peak in the range 284.3 ~ 284.5 eV, mainly related to the C-C bond in the adhesive formulation matrix on both F1 and F2. (2) A peak in the range 285.7 ~ 286.3eV attributed to C-O-C on F1 side and C-O-C and/or C-H bonds on the F2 side. (3) Carbon peaks in the range 287.6~ 288.2eV attributed to C=O bond in MWCNTs on both F1 and F2, and (4) small carbon peaks at ~288.5eV, attributed to C-H bond (F1 face), and C-O bond of MWCNT materials within the adhesive matrix (F2 face).

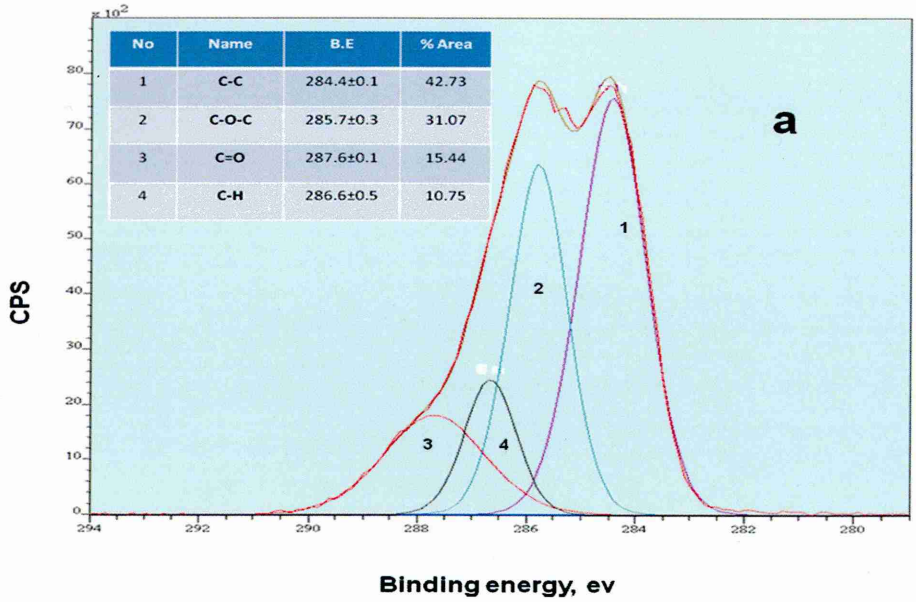

Figure 4.79 XPS spectrum of carbon (lap joint, Al2024-T3);
a) on F1 and b) on F2

The O_{1s} signal is split into two peaks as shown in Figure 4.80a. The difference in binding energies on the F1 fracture side was very small ~ 0.65eV. The strong O_{1s} peak at 533.3eV is related to oxygen from silicon dioxide. However, a weak peak around 532.7eV could be related to oxygen from the γ-Al_2O_3 nano-fillers within the adhesive matrix. The O_{1s} scan on the adhesive fracture face shows two oxygen peaks, Figure 4.80b, these peaks were wider than those for the metal face. These peaks are attributed to the oxygen in an epoxy functional group, silicon dioxide and γ-Al_2O_3 nano-particles.

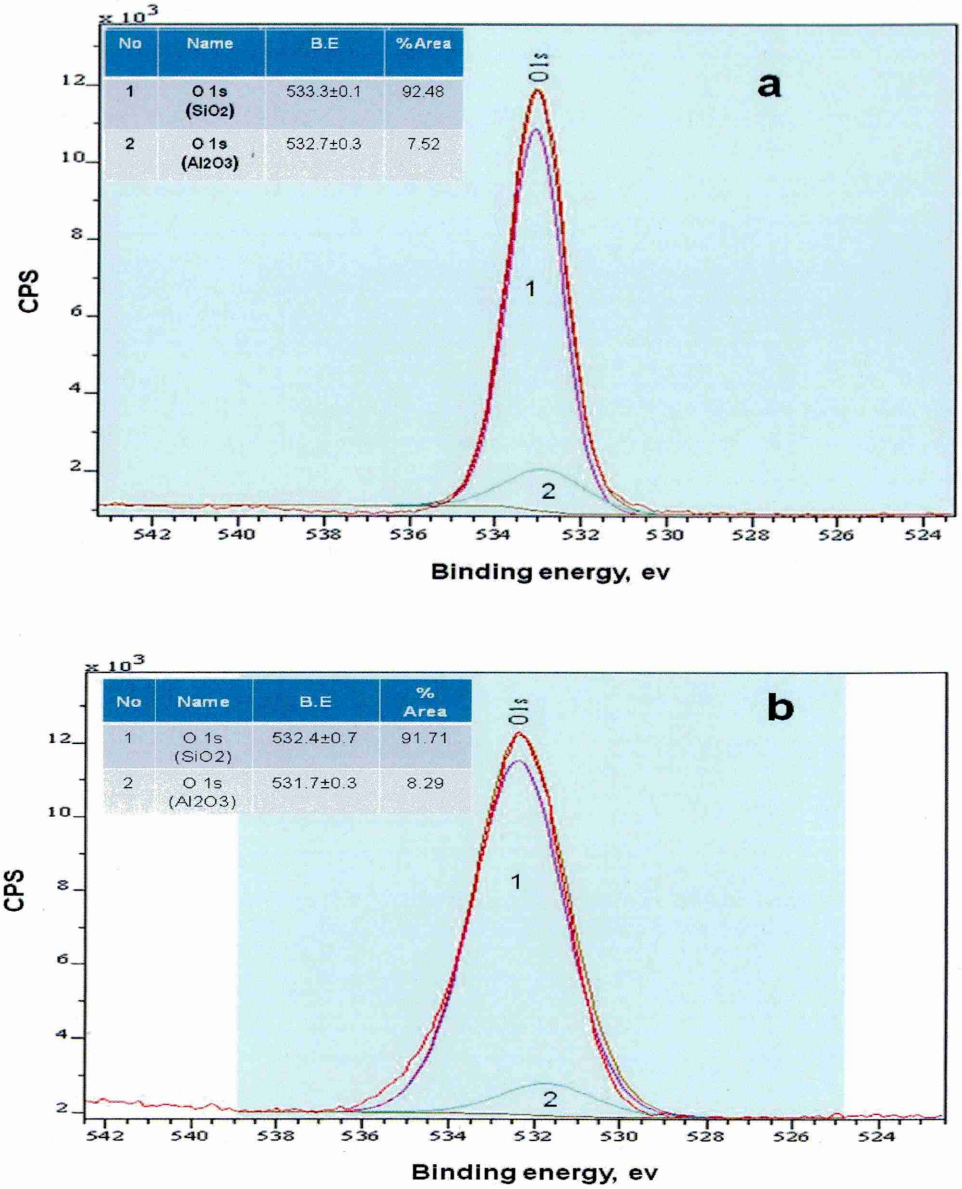

Figure 4.80 XPS spectrum of oxygen (lap joint, Al2024-T3);
a) on F1 and b) on F2

Figures 4.81 a and b shows the high resolution Si_{2p} spectra obtained for the metal and adhesive fracture faces of the lap joint. The silicon spectra in Figure 4.81a had two peaks at 102.8eV and 101.6eV that were characteristic of silicon in the fully oxidized state, as in SiO_2 and the Si-C bond. However, three peaks were revealed on the adhesive failure face, see Figure 4.81b, which corresponded to the Si-O bond at 102.4eV, Si-C at 101.5eV, and a bond at 103.8eV, intermediate between SiC and SiO_2 [183].

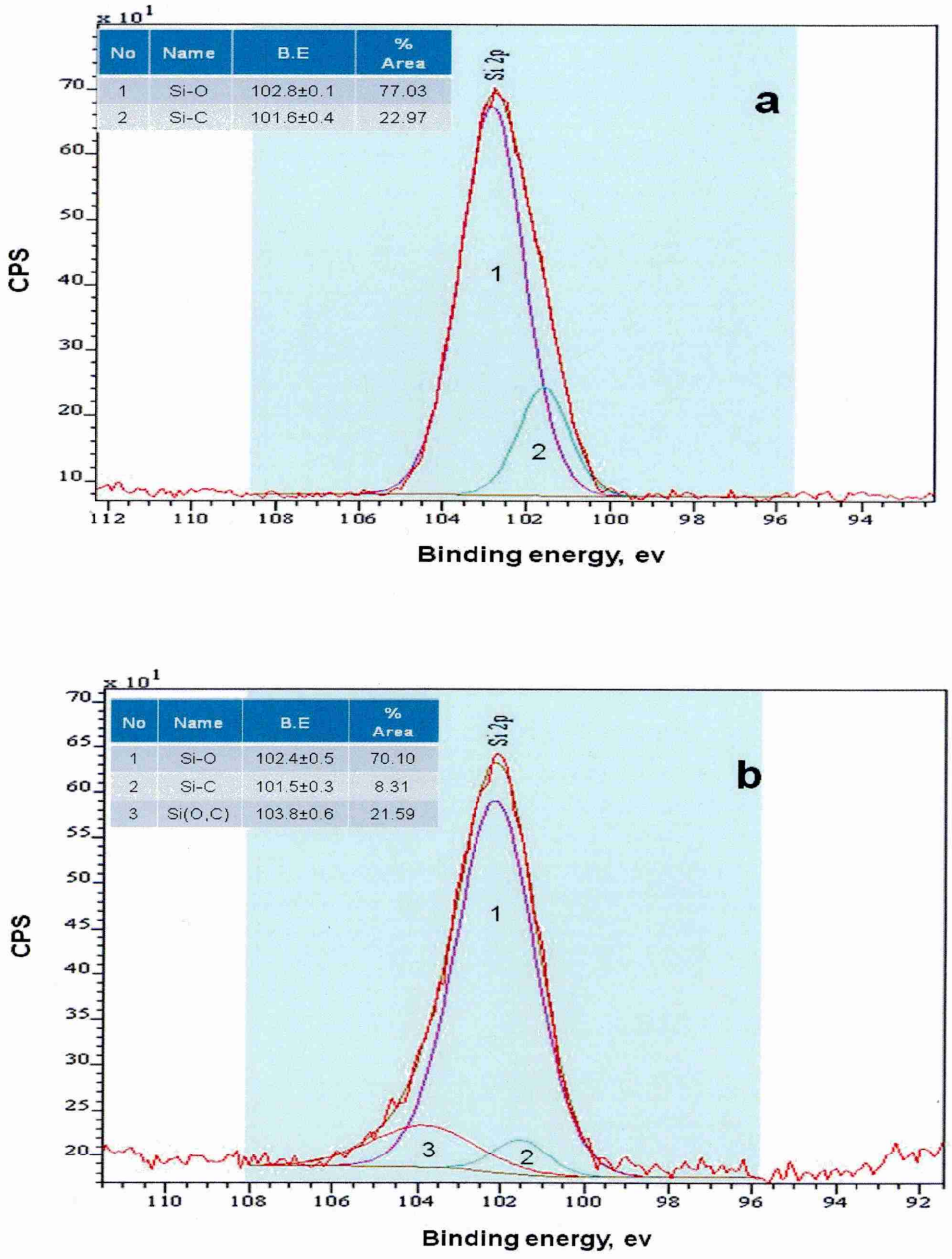

Figure 4.81 XPS spectrum of silicon (lap joint, AA2024-T3);
a) on F1 and b) on F2

Figures 4.82a and b show the XPS scan of Al_{2p} on metal and adhesive fracture faces of the lap joint. In Figure 4.82a, two peaks were found; one at a binding energy of ~ 74.5eV corresponding to Al in the γ-Al_2O_3 nano-particles and the second at ~ 72.1eV related to Al in the metallic phase. The peak intensities are much higher on the F2 face, Figure 4.82b compared with those on the F1 face, Figure 4.82a. This may indicate that the failure mode was probably near or at

the adhesive/substrate interface. However, the Al spectra on the adhesive face (Figure 4.82b) showed an Al_{2p} peak related to Al_2O_3 at ~ 74.1eV, and the binding energy ~76.2eV may be attributed to hydroxides or oxyhydroxides compounds [184].

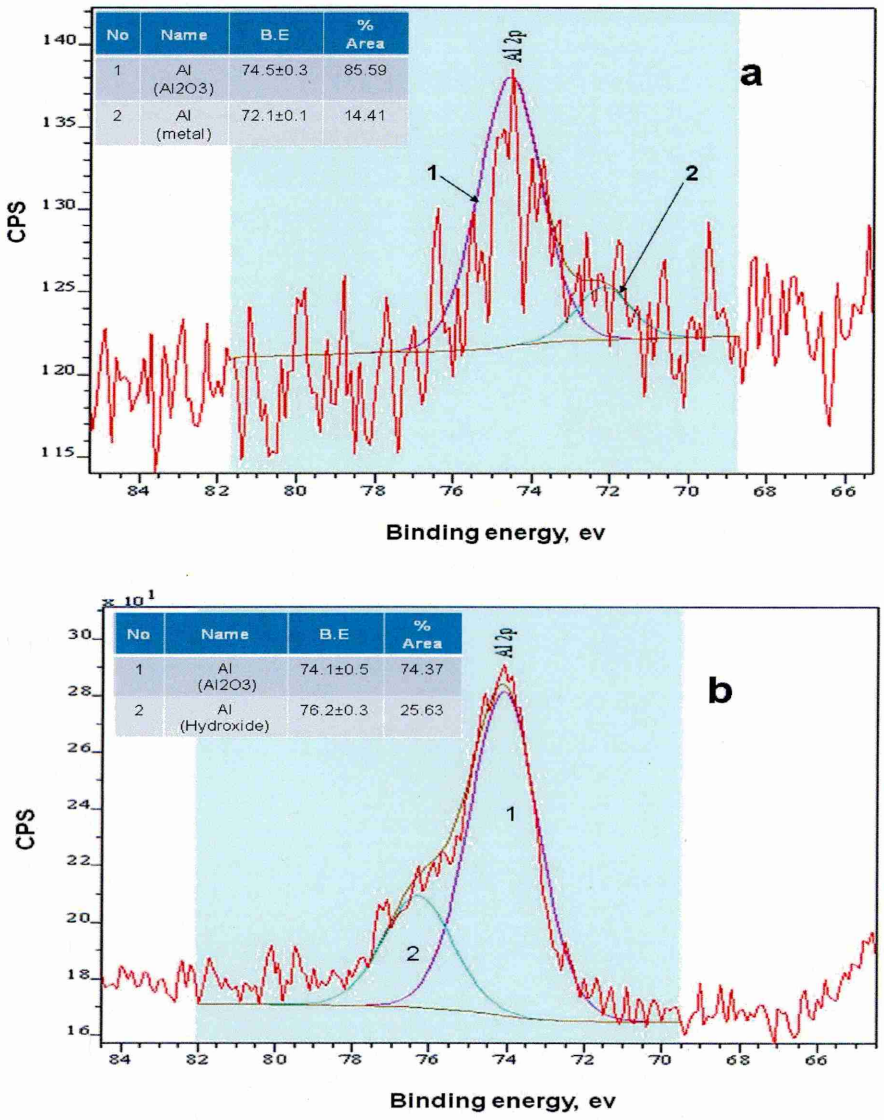

Figure 4.82 XPS spectrum of aluminium (lap joint, AA2024-T3);
a) on F1 and b) on F2

4.6.5 Thermo-gravimetric analysis (TGA)

The thermal stability of PE, SG1, SG2 and SG3 adhesives were assessed by TGA. Tests were carried out in a nitrogen atmosphere at a heating rate of 10ºC/min over a temperature range of 35-650ºC. This method measures the weight loss of the heated sample due to evaporation of volatile products. Figure 4.83 shows the changes in weight as a function of increase in temperature up to 650ºC. TGA curves for all the adhesive formulations showed very little change in weight in the temperature range of 35-200ºC. Almost all the mass loss of the PE occurred between about 350°C and 450ºC due to adhesive decomposition. The mass loss in SG1 started at a temperature of ~ 300°C, below that of the temperature at which initial weight loss changes occur for the PE sample. This may be related to phase separation in the adhesive matrix. However, the overall weight loss was lower than PE as a result of the formation of a stable 3D silica network in the formulation. The majority of the weight loss in SG2 and SG3 adhesives occurred between about 350°C and 550ºC, with SG2 losing a greater proportion of its weight at a greater rate, than SG3.

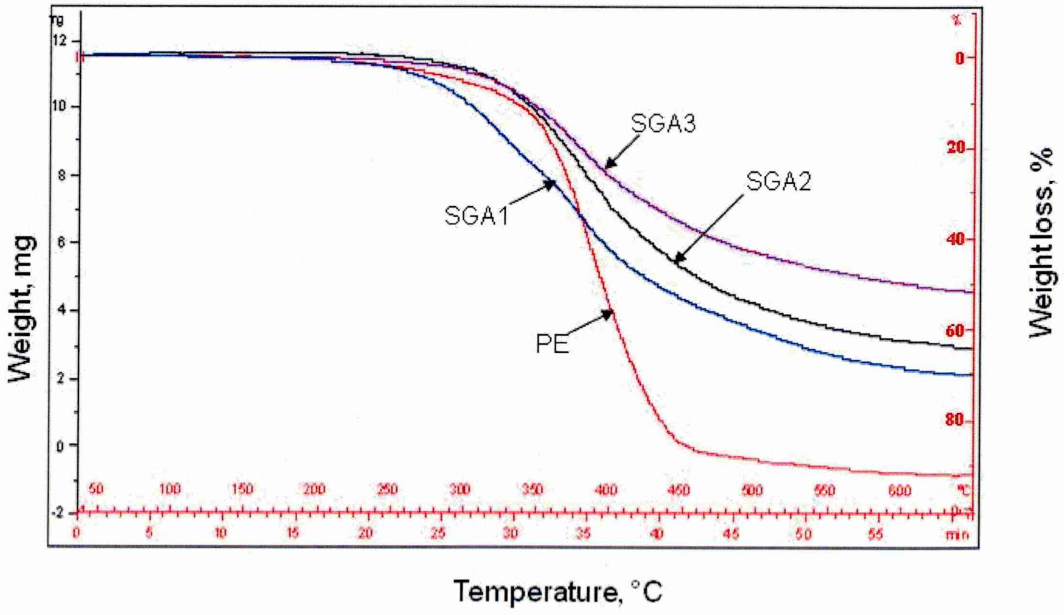

Figure 4.83 Thermo-gravimetric analysis of PE, SG1, SG2 and SG3 adhesives

CHAPTER 5 Discussion

5.1 Effects of composition on strength and structure

5.1.1 Hybrid Sol-gel adhesive formulations

The present work is concerned with assessing the capability of hybrid sol-gel derived films to act as adhesive materials for metal-metal bonding. S1# silica-based sol-gel adhesives have been investigated following curing at 120°C for 3 hours. It should be recognised that the joint strength is related to the transverse and peel stress occurring within the joint. Moreover, other stresses in the sol-gel film exist due to shrinkage during the drying process and due to the mismatch of the thermal expansion coefficients between the film and the metal substrate. The bond strength is related to the formulation of the silica-based sol-gel and the curing condition. Also, a uniform and water-free sol-gel intermediate layer plays a role in the strength of the joint. The sol-gel creates a chemically bonded, porous, and highly cross-linked coating on the substrate surface.

Joint strength was found to improve by increasing the curing temperature to activate the silanol groups on the metal surface, which provided a chemical cross-linked network between the sol-gel material and the substrate. Therefore, changing the number of silanol groups can have an effect on the adhesive strength of the sol-gel adhesive [185]. FTIR spectra in Figure 4.1 showed a very strong peak for Si-O-Si bonds, indicating a condensation reaction of the hybrid silica sol-gel material. In addition, an interaction between the sol-gel adhesive and the aluminium substrate includes two forces; i.e. a cohesive force within the sol-gel bulk material dependent upon sol-gel formulation, and an adhesive force of the sol-gel with the substrates as shown in Figure 5.1. These forces are responsible for the final joint strength.

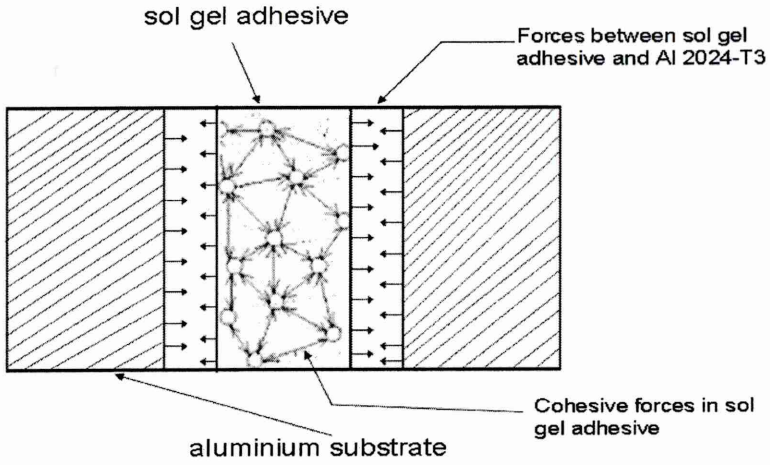

Figure 5.1 Schematic illustration of adhesive and cohesive forces

Figure 4.2a shows the results of SEM analysis on the S1# sol-gel coating cured at 120^{0}C for 3 hours where it was observed that failure was at the sol-gel/metal interface (adhesive mode), notably failure of the O-metal bond. The presence of transverse cracks in the sol-gel adhesive layer was also observed. The failed lap joint revealed brittle fracture behaviour and low interfacial forces at the adhesive/surface interface, as the ratio of covered and uncovered area with the sol-gel materials is approximately 50%. This can be explained on the basis that the bond energy value of the (Al-O-Si) at this region is lower than that within the sol-gel material (Si-O-Si). Hence, it is beneficial to remove the solvent from the sol-gel coating as soon as possible before bonding the two coated Al substrates together to form the lap shear joint. Evaporation of solvents from the sol is expected to promote the gelation stage, where the alkoxide gel precursors in aqueous solution hydrolyse, and polymerise through alcohol and/or water condensation reactions. Shear strength may also be improved by decreasing the thermal expansion coefficient mismatch between the sol-gel coating and the substrate. This may be achieved by the addition of micro/nano particles to the adhesive system.

5.1.1.1 Addition of polyaniline (PANI)

It has previously been shown that the addition of PANI to a sol-gel system causes an increase in corrosion resistance [186]. Given this benefit it was decided to investigate the addition of PANI on joint strength. AD2# sol-gel joints

modified by 0.05 wt % polyaniline appear to show a small improvement in the joint strength compared with that of the unmodified sol, see Figure 4.3. Mixed cohesive and adhesive fracture was observed on the failed surfaces of the test samples, see Figure 4.4. The adhesive strength increased as the curing time increased from one hour to 16 hours at the same cure temperature of 170 ^{0}C. This increase in strength is explained as being due to increased condensation and the removal of residual solvent from the sol-gel following extended curing. Moreover, the small enhancement in the adhesive strength may be related to the improved flexibility of the sol-gel because the long chain PANI within the sol-gel, provides additional cross-linking within the silica-based sol-gel. Fracture surfaces showed cracks within the sol-gel adhesive, resulting weakly-bonded structure, see Figure 4.5.

5.1.1.2 Addition of γ-Al_2O_3 nano-particles

γ-Al_2O_3 nano-particles have been used in the sol-gel coating to improve its mechanical properties [187]. The shear strength of the γ-Al_2O_3 nano-particle modified sol-gel was higher than that of the unmodified sol-gel as shown in Figure 4.7. Combined cohesive and adhesive fracture surfaces of the γ-Al_2O_3 modified sol-gel joints (AD3$^{\#}$) were observed on both joint sides. The highest shear strength was recorded at 4.48MPa with the addition of 0.5 wt % γ-Al_2O_3 nano-particles, improving the joint shear strength by a factor of three compared to that of the unmodified joints. The doped γ-Al_2O_3 nano-particles were well dispersed in the sol-gel and increased the cross-linking of the silica-based sol-gel adhesive. γ-Al_2O_3 nano-particles enhanced the interaction area of bonding within the adhesive matrix. Further increase of the nano-γ-Al_2O_3 content in the sol-gel led to a decrease in joint strength. It is suggested that this decrease is due to the existence of some free-bonded γ-Al_2O_3 particles in the sol-gel, which reduce the cross-linking of the sol-gel network structures and the adhesion between the adhesive and the aluminium substrate. SEM revealed that a boundary layer existed between the sol-gel adhesive and the Al substrate (Figure 4.8), where enrichment of the γ-Al_2O_3 particles was observed. These results confirmed that the nano-γ-Al_2O_3 additive was closely related to the change in the structure of the sol-gel adhesive which, in turn, may be related to the improvement of the joint strength. The γ-Al_2O_3 nano-particles were well

dispersed in the sol-gel adhesive having a typical diameter of about 40~100nm. Also, the distribution of γ-Al_2O_3 particles in the sol-gel may reduce shrinkage during the cure process compared with that of $S1^{\#}$ sol, thereby contributing to the increase of the adhesive strength. Sun and co-workers [188] also demonstrated that the addition of γ-Al_2O_3 particles not only contributes to improving the bonding between the adhesive and the metal substrate, but also compensates for the volume shrinkage of the adhesive during the curing process. The surface profile of the bare and the failed specimen were also investigated using IFM as shown in Figures 4.10a and b. It is observed that 60 ~ 75% of the failed surface was covered by the sol-gel adhesive in (a) compared with the bare Al substrate (b). This indicates that the 0.5 wt% doped γ-Al_2O_3 improves the bonding at the adhesive/substrate interface and hence increases the sol-gel joint strength.

5.1.1.3 Addition of TiO_2 nano-particles

It was expected that the addition of TiO_2 nano-particles would result in a change in the sol-gel adhesive behaviour because of their good physical (high refractive index) and chemical stability [189, 190]. Analysis of the TiO_2 nano-particle modified sol-gel adhesive samples revealed an increase in joint strength by up to three times compared with that of the unmodified system. Nano-particles of TiO_2 may play a role in improving the chemical stability due to hydroxyl groups (-OH) on the surface of the TiO_2 nano-particles which can react with hydroxyl groups in silica nano-particles enhancing the network structure in the sol-gel formulation due to the capability of Ti ions to coordinate tetrahedrally. The TiO_2 nano-particles were uniformly distributed within the sol-gel system, as shown in the SEM image in Figure 4.14, this distribution enhances cross-linking of the hybrid silica nano-particles. In addition, the drying process and the curing temperature promote the formation of a strongly cross-linked network. An increase of joint strength with increasing concentration of TiO_2 nano-particles was observed, see Figure 4.12. The addition of 2.0 wt% TiO_2 into the sol-gel adhesive increased the strength by a factor of three compared with that of the unmodified system. However, as with the addition of γ-Al_2O_3 nano-particles to the sol-gel, a reduction of the joint strength occurred with further increase of the TiO_2 concentration, notably beyond 2.5 wt%. As discussed above, this

decrease is due to the existence of some free-bonded TiO_2 particles in the sol-gel structure. The morphology of the fracture surface was investigated by SEM as shown in Figure 4.14. It can be observed that the TiO_2 nano-particles were well dispersed within the silica-based sol-gel adhesive. The improvement in adhesive strength of the modified joint was attributed to the formation of both Si-O-Si and Si-O-Ti bonds in sol-gel matrix as supported by FTIR spectrum in Figure 4.13.

5.1.1.4 Addition of PANI and γ-Al_2O_3

It was reported that the combination of PANI chains and inorganic nano-particles such as γ-Al_2O_3 as hybrid material could improve composite properties, such as thermal stability [191] and increase their application for corrosion resistance [192]. The experimental results in Figure 4.17 show a significant increased in shear strength with the doping of γ-Al_2O_3 and PANI in the original sol-gel ($S1^{\#}$). Differences in formulation chemistry notably, the different ratios of γ-Al_2O_3/PANI, led to slight changes in the adhesive bond strength. The fracture surface behaviour of $AD5^{\#}$, $AD6^{\#}$ and $AD7^{\#}$ samples showed different failure modes which may explain the variations in lap shear strength of the three adhesive formulations.

5.1.1.4.1 Adhesive strength of $AD5^{\#}$

The results show that the average shear strength of $AD5^{\#}$ specimens was 4.49±0.02 MPa and fracture surface mode was an adhesive (interfacial), see Figure 4.19. The $AD5^{\#}$ formulation was obtained by doping 0.01g PANI and 0.42g γ-Al_2O_3 into the sol-gel, see Table 3.3. The introduction of the parent polymer (PANI) and the high surface area of the inorganic component (γ-Al_2O_3) in the sol-gel system (as composite material) may provide high dispersion and easy flow of adhesive on the substrate surface. As PANI is dispersed in the sol-gel, the polymer chains may diffuse between the inorganic particles and chemical interaction within nano-composite structure may take place. These composite systems can provide new synergistic properties that can not be attained from individual materials. The adhesive strength performance in this system was significantly better compared to that in $S1^{\#}$ or $AD2^{\#}$. It was reported

that nano-fillers can improve the mechanical performance of polymers due to their adsorption capacity and high aspect ratio, which give greater possibility of energy transfer from one phase to another [193].

5.1.1.4.2 Adhesive strength of AD6#

The lap shear strength of AD6# was also significantly increased compared with that in the original sol-gel (S1#), and the strength value was ~ 5.09±0.1 MPa. The curing procedure (polymerisation), may play a role in achieving these strength levels, where monomer molecules react together to form three-dimensional networks. Note, the AD6# joint failed in an adhesive mode (interfacial). This formulation was prepared by doping 0.02g PANI and 0.5g γ-Al_2O_3 in the sol-gel material. It can be seen that the percentage of PANI and γ-Al_2O_3 is higher in this formulation than in AD5#. Increasing the concentration of functional groups of -OH and PANI chains contributed to an increase in the degree of cross-linking via O-Si-O, O-Al-O, and N-H-O-Si bridges. It was observed that for one sample the adhesive was unevenly distributed between the two surfaces resulting in fracture at the adhesive/substrate interface (Figure 4.18a). The performance of adhesive joints is strongly influenced by the interaction between the metal surface and the adhesive. Cracking was observed along both the interface and the sol-gel adhesive itself. The brittle behaviour of AD6# adhesive may also contribute in increasing the strength of joint, see Figure 4.20, compared with that of AD5# and AD7#.

5.1.1.4.3 Adhesive strength of AD7#

Formulation AD7# was produced by doping 0.1g PANI and 0.32g γ-Al_2O_3 in the original sol-gel. The ratio of PANI to γ-Al_2O_3 in the AD7# was higher than that in AD5# or AD6# formulations and the corresponding adhesive shear strength was ~. 4.37±0.1 MPa. Cohesive fracture mode in AD7# specimens were observed, see Figure 4.18b. The reduction in AD7# adhesive strength compared to that of AD5# or AD6# may be related to the increased PANI concentrations in AD7#. It was reported [194] that the PANI polymer has poor mechanical performance, the increased in amount of PANI within the adhesive may limited load transfer to the inorganic component, and therefore decreased adhesive bond strength. It

appears that the cohesive forces within the adhesive matrix may be limited as the polyaniline loading increased, resulting in an increase in free PANI chains within the sol-gel structure.

Generally, the improvement of the mechanical performance of AD5#, AD6# and AD7# over that of the unmodified sol-gel depends on the balance of PANI and γ-Al_2O_3 additions into the sol-gel structure. These materials led to an increase of the three-dimensional network within the sol-gel structure via γ-Al_2O_3 and/or two dimensional branches of PANI which enhance the adhesive cross-linking. As stated an increase of PANI may lead to free PANI chains, which would decrease the adhesive strength, while an Increase of γ-Al_2O_3 particles may cause the existence of un-bonded nano-particles which has a negative effect on the degree of cross-linking within the adhesive.

5.1.2 Adhesive strength of hybrid epoxy/sol-gel adhesives

The presence of hydroxyl groups in the sol-gel epoxy adhesive can, via condensation reactions form a strong cross-linked bond within the sol-gel epoxy adhesive, and the number of metal-oxygen (Me-O) bonds increases with the release of residual water and organic solvent during the early stages of drying. Further increase in cross-linking and Me-O bonding occurs during the high temperature cure regime. The matrix of the silica-based sol-gel played a major role in providing three dimensional networks within the adhesive. In addition, the presence of γ-Al_2O_3 nano-fillers in the adhesive may act as a coupling agent to create a link between the siloxane and the epoxy structure. This increase in cross-linking will enhance the structure of the adhesive and thus increase the lap shear strength performance.

It is well known [195] that the properties of the bisphenol-A epoxy are related to the curing agent and the opening of the epoxy groups. It has been reported that changing the amount of curing agent will have an effect on the degree of cross-linking and the formation of chemical bonds in the cured epoxy system [196]. DETA was used as the curing agent in the PE sample to open the epoxy rings via the reaction of the epoxide groups with the active hydrogen atoms in the curing agent (hardener). However, the epoxy groups can also be opened up by the nitric acid that was used as the catalyst to promote the hydrolysis and condensation reactions of the sol-gel. In this modified system, the hydroxyl

groups generated by the opening of the epoxy rings can lead to condensation with the hydroxyl groups in the sol-gel network. This reaction may create some bonding between the sol-gel and the epoxy. The difference in lap shear strength of PE and SG1, Figure 4.22, on Al2024-T3 and mild steel may be related to the lack of full cross-linking and/or phase separation between the epoxy resin and the sol-gel matrix in SG, see Figure 5.2a. The addition of γ-Al_2O_3 nano-particles further strengthen this cross-linking, greatly increasing the lap shear strength of the samples SG2/Al and SG2/MS, compared with the PE and the SG1 on both material substrates. The presence of γ-Al_2O_3 nano-fillers in the adhesive may prevent phase separation within the matrix. It was reported [197] that when nano-alumina particles are incorporated into an epoxy resin, the cure kinetics of the resin are affected due to the catalytic effect of hydroxyl groups on the particles. Changes in adhesive structure (phase separation) were observed on adding γ-Al_2O_3 nano-fillers into the epoxy/sol-gel matrix, see Figure 5.2b. A clear solution was produced indicating the high degree of miscibility and cross-linking, which enhanced the structure of the adhesive and thus increased the lap shear strength performance.

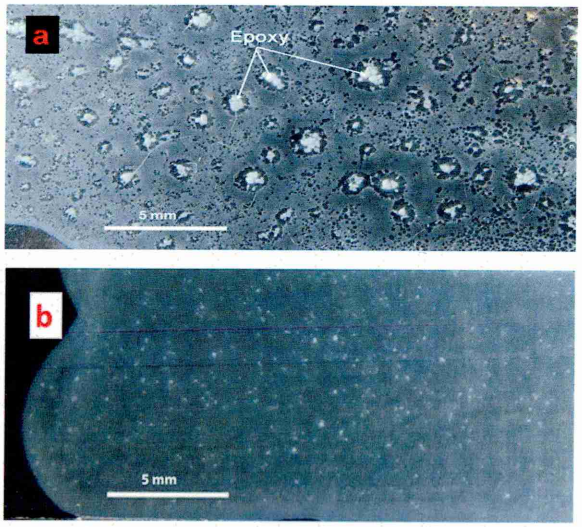

Figure 5.2a) Phase separation between epoxy and sol-gel matrix on glass slide, b) Effect of addition of γ-Al_2O_3 into epoxy/sol-gel

The doping of MWCNTs in SG3/Al and SG3/MS caused a further increase in the adhesive strength on Al2024-T3 and mild steel substrates. These improvements in lap shear strength were also related to the uniform distribution

of nano-fillers (i.e. γ-Al_2O_3 and MWCNTs) within the matrix which led to an increase of the surface contact area between the nano-particles and the polymer. The SEM image presented in Figure 5.3 shows the distribution of MWCNTs, which is thought to be coated with adhesive matrix, rich in SiO_2 nano-particles (i.e. size 40-80 nm) derived from the sol-gel matrix, and γ-Al_2O_3 (i.e size 10-20 nm). The appearance of silicon, oxygen and aluminium peaks in EDX spectra confirmed the presence of these materials.

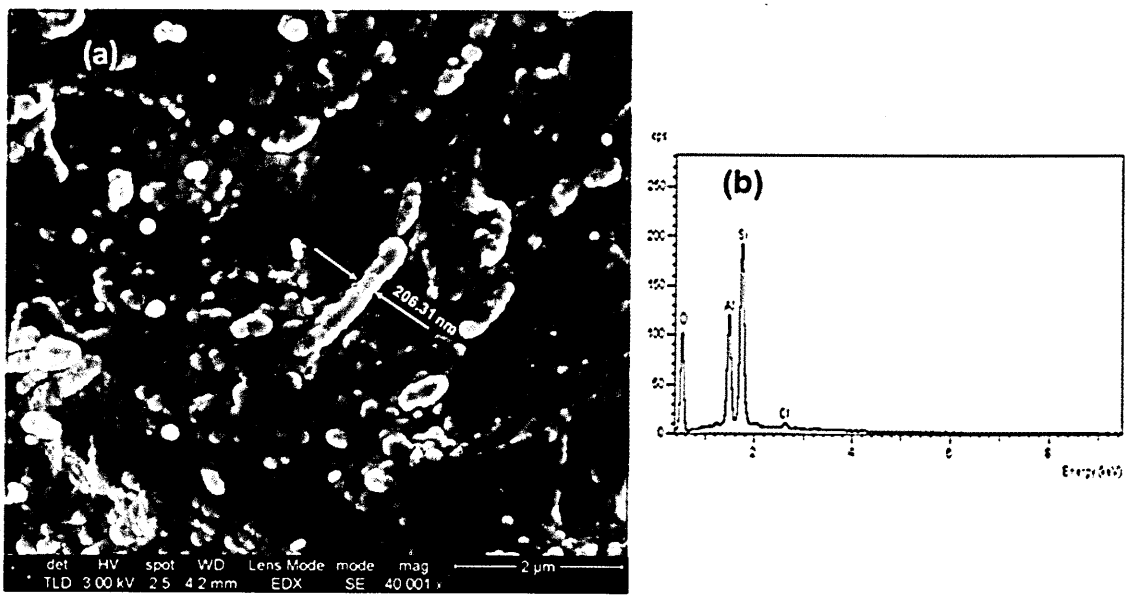

Figure 5.3. (a) SEM image of distribution MWCNT and inorganic nano-materials in SGA3/Al, (b) EDX spot analysis of surface of MWCNT

The incorporation of nano-filler materials in the epoxy/sol-gel led to an increase of the surface contact area between the nano-particles and the polymer and decreased or minimized the gap and nano-voids within the adhesive matrix compared with that of the unmodified epoxy/sol-gel system, see Figure 5.2a&b. This was also suggested by Wetzel et al. [198] who demonstrated that large contact areas between the organic and inorganic component within the matrix reduced the presence of voids; leading to an improved joint strength. Furthermore, it was found that MWCNTs act as a reinforcing phase in the epoxy/sol-gel system resulting in an increase of the joint strength. However, only a relatively small difference was observed between the adhesive strength of SG2/Al and SG2/MS compared to SG3/Al and SG3/MS samples. The reason for this might be due to the small concentration of MWCNTs added in the matrix.

5.1.2.1 Al_2O_3 effects (SG3)

The incorporation within the SG3 formulation of small amounts of spherical γ-Al_2O_3 nano-particles, up to 4.0 wt%, caused an increase in joint strength. This increase may be related to the distribution in the adhesive matrix allowing greater interaction between the γ-Al_2O_3 and silica network in the form of Al-O-Si bonds. It is also possible that, γ-Al_2O_3 in contact with the polymer segments resulted in less hindrance to the polymer [199] allowing the polymer chains to extend into the matrix and build up strong interaction, which would lower any stress concentrations at the particle/matrix interface, leading to improved adhesive toughness. The changes observed in the stress/strain curves shown in Figure 4.25 confirmed the improvements in the adhesive strength within low nano-filler volumes. In addition, γ-Al_2O_3 nano-fillers have an important influence on the curing behaviour of the SG3 formulation, including a catalytic effect of the hydroxyl groups of the particles which increased the local concentration of the activated components, thus increasing the curing reaction rate and the cross-linking density within this doping ratio [200]. However, SG3 shear strength gradually decreased as γ-Al_2O_3 nano-fillers increased beyond 4.0 wt%. At high volumes of γ-Al_2O_3 particles, poor interfacial bonding or adhesion between the filler and the adhesive matrix, or the presence of a large free volume phase (un-bonded) of these nano-fillers in the matrix, may have occurred leading to a lower bond strength with the substrate. Micrographs of fracture surfaces presented in Figure 4.26 show the presence of long flakes (Figure 4.26a) that were not seen in Figure 4.26b. A low concentration of γ-Al_2O_3 (1.0 wt %) in the sol-gel appears to limit the ability to carry the external load and long cracks appear within the matrix, see Figure 4.26a. Changes in adhesive structure occur on the addition of 4.0 wt% γ-Al_2O_3 resulting in short crack pathways, suggesting the material may act as a barrier to crack propagation and thereby increases the energy required for fracture. However, further increase of γ-Al_2O_3 (10 wt%), see Figure 4.26c, caused low interfacial bonds at the adhesive/substrate interface (interfacial fracture mode), and allowed the formation of micro-cracks in the bulk of the adhesive material which lowered its strength.

5.1.2.2 MWCNTs effects (SG3)

Figure 4.27 shows that the introduction of small amounts of MWCNTs into the SG3 adhesive improved the shear strength to a value of ~25MPa. The presence of a nitric acid catalyst within the sol-gel process may also help in creating carboxylic and hydroxyl groups on the MWCNT surface. Pitalsky et al. demonstrated [201] that chemical agents such as HNO_3 increased the density of polar functional groups on the CNT surface. This would result in strong interaction, or anchoring, of sites along the nano-tubes with the adhesive matrix, which would enhance the adhesive structure given the high relative surface area of MWCNTs. In addition, MWCNTs may play a role in minimising microcrack formation by bonding to silica nanoparticles via the interaction of the carboxylic with hydroxyl groups of SiO_2. It has been reported [202] that the increase in load transfer provided by deformed MWCNTs within the matrix give rise to Si-O-CNTs bridges and/or polymer/CNT interactions. Therefore, it would result in the development of strong interfacial bonding between the matrix and the MWCNTs. However, a decrease in bond strength of the epoxy/sol-gel hybrid system was observed with the addition of a higher volume of MWCNTs (up to 0.07 wt%). This may be attributed to the increase in internal stresses as the degree of micro cracks increased due to the presence of free CNTs during densification, leading to a decrease in bonding. Additionally, the high level of CNTs may result in their aggregation and an increase of viscosity which can lead to the formation of defects and cause the adhesive strength to deteriorate. This was also supported by Shu-quan et al. [203] who concluded that increasing the concentration of CNTs increases the viscosity of the adhesive matrix and impedes the removal of bubbles, which remain in the matrix and degrade the mechanical properties.

The results presented in Figure 4.28 show the influence of the addition of MWCNTs on the adhesive performance of SG3 in terms of stress/strain curves. At low concentrations, good CNT distribution within the matrix led to a high degree of cross-linking, which enhanced the ability of the adhesive to stretch and to carry high loads before failure [204]. However, with increasing amounts of CNTs (i.e. > 0.07 wt%) a reduction in strain was observed. The small amounts of CNTs led to a mixed fracture mode, see Figure 4.29a. Low proportions of CNTs may play a role for reinforcing the adhesive matrix, thus

improving the strength. With increase in CNTs up to 1.0 wt%, the mode of failure was interfacial, see Figure 4.29c, which could be related to the increase in adhesive viscosity and reduction in adhesive wetability on the substrate surface.

5.2. Effect of the cure temperature

5.2.1 Hybrid sol-gel adhesives

The results in Figure 4.30 indicate that the AD7# adhesive was not completely cured at 110^{0}C with an incomplete condensation due to the low temperature, resulting in a relatively high residual solvent content in the sol-gel. By increasing the cure temperature of AD7# sample from 130^{0}C to 150^{0}C, the sol-gel strength increased from 3.26 to 4.72MPa (40% increase), see Figure 4.30. The increase in the cure temperature is beneficial, because removal of residual products or solvents in the adhesive and more effective silanol condensation is promoted at higher temperature. Thus, the increase in the adhesion strength is attributed to a strong chemical bonding between the adhesive and the substrate during the drying stage. However, a further increase in the cure temperature up to 180^{0}C, for AD7# showed a decrease in the bond strength. This may be due to an increase of the residual stress in the adhesive caused by the mismatch of the thermal expansion coefficient between the adhesive and substrate. This stress may generate micro-cracks, leading to a decrease in the strength. A trend of increasing sol-gel bond strength with increasing adhesive extension was observed with increasing cure temperature, see Figure 4.31. This is thought to be due to an increase in the degree of the cross-linking within the adhesive which is improved by higher input thermal energy.

5.2.2 Hybrid epoxy/sol-gel adhesives (SG3)

It has been reported that increased curing temperature promotes physical adsorption and the diffusion between adhesive and substrate at interfaces [205]. Moreover, the curing temperature is beneficial for increasing the degree of adhesive conversion (cross-linking) during the curing reaction [206]. Thus, the peel strength should increase significantly with increase in bonding temperature.

However, Figure 4.32 shows that SG3 adhesive strength on an Al2024-T3 substrate decreased as cure temperature increased. This behaviour could be attributed to the differences in the thermal expansion coefficients at the adhesive/substrate interface, where the thermal expansion coefficient for aluminium alloys is ~ 23×10^{-6}/°C. This should be compared with the experimental results of SG3 on mild steel substrate where increasing cure temperature had little effect on shear strength, indicating good surface stability over the range of temperatures tested. It should be noted that the thermal expansion coefficient of mild steel is ~12×10^{-6}/°C, around half the value of Al2024-T3.

Changes in peak intensities in the FTIR spectra were observed as the cure temperature increased, see Figure 4.33. With increasing cure temperature for the SG3 sample, the peak which appears at 1088cm^{-1}, strongly suggests that temperature is required to promote the cure reaction (leading to improvement in epoxy/sol-gel branching). The gradual disappearance of the Si-OH silanols peak (~ 800-915cm^{-1}) as the temperature increased, confirms the improved cross-linking via a Si-O-Si bond within the matrix. In addition, the degree of formation of hydrogen bonding of neighbouring inorganic particles via the presence of Al-OH and/or Si-OH bonds increases with temperature causing an increase in the strength of the bulk material. This process is seen through the appearance of an absorption peak shoulder which appears in the range ~ 1088-1100cm^{-1} and which probably corresponds to Al-O-Si or Al-O-Al bonds as cure temperature increased. Also, the conversion of the hybrid epoxy/sol-gel adhesive from liquid-like to solid-like state and the release of solvent or water molecules from the process are enhanced. This was confirmed by FTIR in the disappearance of the -OH peak, corresponding to removal of water molecules, see Figure 4.33.

5.3. Effect of the cure time

5.3.1 Hybrid sol-gel adhesive

The experimental results shown in Figure 4.34 demonstrate that increasing cure time improves the joint strength, being due to the removal of the residual solvent from the sol-gel at the appropriate cure temperature. For example, after 30 minutes heat treatment, the AD7$^{\#}$ sol-gel adhesive was still in a "paste-like state" and the shear strength was very low. With an increase of the curing time up to 16 hours, the adhesive became solid and the shear lap strength greatly increased. The greatest shear strength obtained was 4.72 ± 0.7MPa for AD7$^{\#}$ after 16 hours heat treatment. Furthermore, the load/extension to break curves showed that the adhesive strength enhanced with increase of the cure time, as shown in Figure 4.35. Long cure time facilitates heat transfer during the process, causing a complete condensation of the sol-gel adhesive and thereby increasing the internal bond strength. Stewart and co-workers [207] stated that adhesive cross-linking will enhance as the cure level is increased in both duration and temperature; as greater thermal energy is supplied to the system more curing reactions can take place more frequently and a higher degree of cross-linking within the network can occur. It is indicated that 16 hours as an optimum cure time improved the cross-linking of the adhesive compared with 1 or 2 hours cure time. Hence the adhesive strength increased.

5.3.2 Hybrid epoxy/sol-gel adhesive (SG3)

The experimental results for the SG3 system also showed that as cure time increased the improved cross-linking had positive effects on the bond strength. When the curing time was increased from 1 hour up to 16 hours, the adhesive transformed from a low molecular viscous liquid to a dense cross-linked adhesive network due to polymerisation. Increased time at higher temperature increases the mobility of different molecules in the bulk material during the reaction and allows more monomers to react during the curing process. This occurs through two steps; the adhesive gelation time, where the formation of infinite molecular branches can increase the viscoelastic behaviour of the adhesive liquid; and the vitrification time, where the adhesive formulation changes to a more solid-like state. Increasing the exposure of the SG3

adhesive matrix to heat resulted in the production of more Si-O-Si bridges in the formulation. This is seen through the disappearance of the Si-OH peak at ~ 905cm^{-1} as shown in Figure 4.37a. Moreover, the presence of the inorganic nano-filler materials (i.e. Al_2O_3 and MWCNT) within the epoxy/sol-gel system improved the final structure linkage. Furthermore time is required to reach a fully cured state (solidification) through the formation of chemical interactions within the matrix (i.e. Si-O-C and Al-O-Si). FTIR analysis confirmed the role of cure time on degree of cross-linking between the organic/inorganic components, see Figure 4.37b.

5.4 Effects of surface roughness

5.4.1 Hybrid sol-gel adhesives

An increase in the mechanical interlocking between the adhesive and the adherent will increase the overall bond strength. This effect is well cited in the literature as the mechanical bonding or mechanical interlock theory [208,209]. Mechanical interlocking occurs when the adhesive penetrates into the pores of the adherent surface or other irregularities of the surface of the substrate and then locks mechanically to the substrate. Thus, the adhesive interlocks with the substrate on both sides, providing a simple mechanical keying effect that leads to an improvement of the bond strength. Surface roughness on the microscopic scale improved the adhesive/adherent interface. Baburaj et al pointed out that large surface roughness diverts the failure pathways from the interface to the bulk adhesive leading to lower strength [210]. Moreover, over-roughening of a surface can sometimes be detrimental because trapped air and surface contaminants can remain at the bottom of troughs and pores and hence impede bonding [211]. The experimental results in this work using AD3$^{\#}$ and AD4$^{\#}$ showed that the change in the surface of the Al alloy, polished with 6μm, led to an increase of the joint strength compared with 1μm see Table 4.2. This is related to the change in surface roughness as shown in Figure 4.38, where the polished surface leads to a low degree of mechanical interlocking.

5.4.2 Hybrid epoxy/sol-gel adhesive (SG3)

Changes in surface roughness can limit intimate contact at the interface, which can affect the final adhesion strength. It was clear from the experimental results that the strength of the single lap joints decreased with decreasing surface roughness. The magnitude of the surface roughness and adhesive viscosity determined whether the adhesive liquid is in complete contact with the substrate or only in partial contact [212]. The increase in joint strength of a metal surface treated with different grades of abrasive paper may be attributed to the availability of extra interfacial bond area. The adhesive penetrates the pores, hardens, and acts as micro interlocking wedges leading to the increase in real interfacial shear strength [213]. IFM results confirmed that a smoother surface gave a lower roughness profile, and thus decreased the interlock process. The adhesive fracture surface in all specimens treated mechanically indicated that the failure mode was mixed, that is, adhesive/cohesive. For example, the changes in average surface roughness from 1.62 microns achieved using paper grade P120, to 1.076 microns with P600, led to significant changes in the percentage (adhesive/cohesive) failure mode from ~ 70% into ~ 33%, respectively. This can be clearly observed in the SEM images, see Figure 4.42, which shows the changes in mechanical interlocking as the surfaces become rougher after being abraded with P120 and P240 abrasive papers

5.5 Bond geometry effects (SG3)

The stresses occurring within a lap joint when forces acting in the plane of the adhesive attempt to separate the two bonded surfaces, playing a major role in determining the joint's strength. The level of stress depends on the joint geometry, i.e. the width and length of the overlap. The experimental results showed that the adhesive shear strength increased with overlap area for short bond areas. However, the joint strength decreased with overlap bond area greater than 375 mm^2. During the test, the ends of the bonded joint will carry a higher proportion of the load than the interior area, see Figure 5.4 [214]. Failure will initiate and propagate from these points. Further increase in bond area does not result in an increase in load-carrying ability. This can be explained in terms

of the deformation capacity of the adhesive and stress distributions. For short bond areas, the joint will operate above the yield strength of the adhesive, Figure 5.4a, where the stress can exceed the yield adhesive strength across the joint. However, for intermediate and long bond areas, the joint will operate at stresses below the adhesive yield strength Figure 5.4b and c, where the stress in a region near the mid-point of the joint falls below the yield adhesive strength. In addition, the longitudinal stress from the direct load and the bending moment at the lap joint edges creates plastic strains which cause failure in the adhesive [215,216].

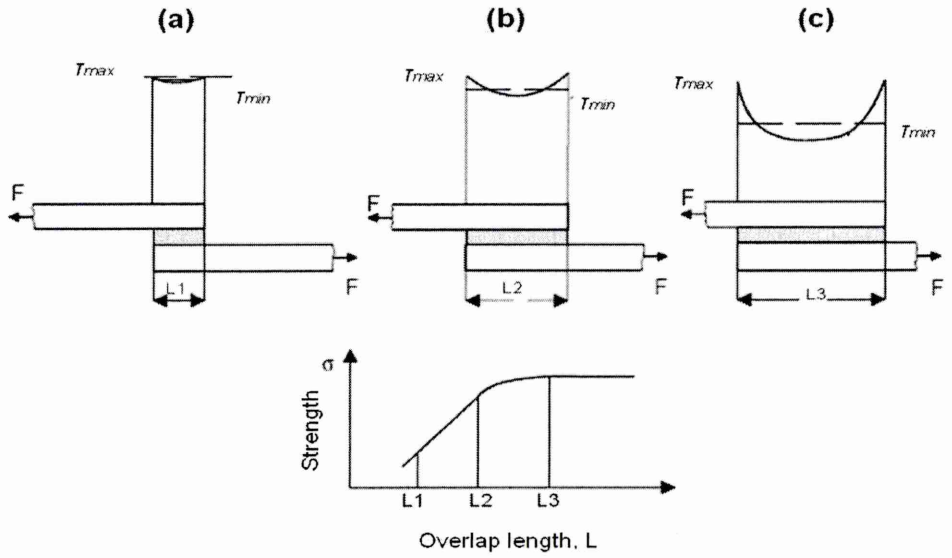

Figure 5.4 Influence of overlapping on adhesive lap joints [214]

5.6 Influence of the external environment

5.6.1 SG3 adhesive tested at high temperatures (lap joints)

The ability to use an adhesive at high temperature is mainly governed by the chemical nature of the adhesive structure. The organic polymer component in the hybrid epoxy/sol-gel adhesive formulation for this work was a DGEBA-based epoxy resin. The experimental results on the SG3 adhesive showed that at low test temperatures the adhesive was in the solid-like state due to the high degree of cross-linking which is resulting high bond strength. However, the adhesive bond strength markedly decreased as the test temperature increased, see Figure 4.45, causing the adhesive to soften and reducing its ability to

absorb energy. The results shown in Figure 4.46 indicate that the adhesive shear strength at low temperatures for both adhesives are significantly better than at higher test temperatures. The mobility of the polymer chain may increase at the elevated temperatures and facilitate the re-orientation of the organic polymer chains, therefore increasing the degree of creep and weakening the bond, both cohesively and adhesively.

The improvement in the adhesive strength of SG3, at low temperatures, compared with the value cited in [142] are attributed to the inorganic components. Zhang et al. [217] have shown that the addition of nano-particles into a polymer matrix enhances its bond strength at various stress and temperature levels. The changes in fracture mode of the lap joints, as the temperature increased, is clearly observed, see Figure 4.47. Lap joint specimens at lower testing temperatures (i.e.40°C) failed in a mixed adhesive/cohesive mode, which suggests the adhesive toughness was better in this temperature range compared to that of the higher temperature range (i.e. 120°C). On the other hand, the reduction in cohesive forces as the adhesive material being softening by temperature may be the reason for decreasing the lap shear strength in specimens tested at high temperature, see Figure 4.47.

5.6.2 Effects of immersion in 3.5% NaCl on adhesive strength

5.6.2.1 Hybrid sol-gel adhesives

The presence of nano-particulate fillers within the sol-gel system may provide a reduction in the permeability of the adhesive to water, due to their solid state nature which is unlikely to be affected by moisture. The present work indicated that the maximum shear force at failure of the adhesive joints after being subject to immersion for 7 days in "wet" conditions (3.5% NaCl solution) was less than that for dry conditions. Figure 4.48 shows the percentage reduction in shear strength on exposure to 3.5% NaCl solution. In general, AD6$^{\#}$ and AD7$^{\#}$ recorded better results than AD3$^{\#}$ and AD4$^{\#}$ sol-gel adhesives. The combination of PANI and γ-Al_2O_3 within the AD6$^{\#}$ & AD7$^{\#}$ may play a role in decreasing their environmental degradation compared with that for AD3$^{\#}$ & AD4$^{\#}$. Several studies [218,219,220] have demonstrated that the presence of PANI polymer within sol-gel systems can increased their anticorrosion performance because

of the ability to oxidise base metal to form a passive layer at the interface. However, the reduction in strength may be attributed to a decrease of the adhesive cross-linking to the surface substrate. For example, AD3# and AD4# joints failed by cohesive fracture in dry conditions, Figure 5.5a. Further, in "wet" conditions, defects in the cohesive fracture surface were also observed in AD3# and AD4#, Figure 5.5b. It can be seen that the adhesion performance is more stable in dry conditions than that in "wet" conditions.

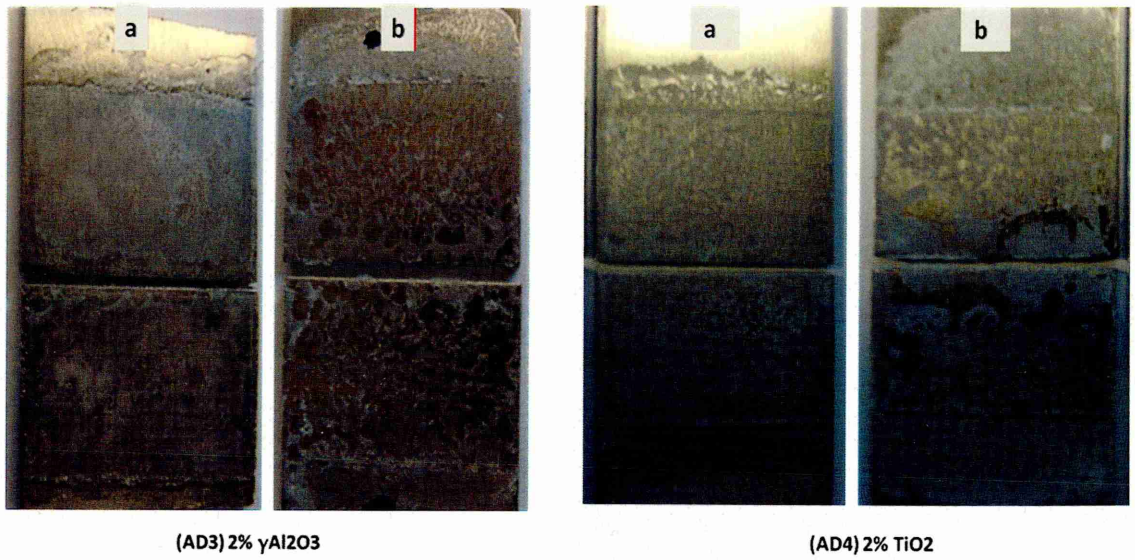

Figure 5.5 Fracture surface of AD3# and AD4#
(a) dry condition and (b) wet condition (3.5% NaCl solution)

The presence of NaCl solution caused damage associated with interfacial disbonding of the immersed specimens. Lawrence and Chau [221] reported that the changes in the adhesive properties between the substrate and the sol-gel is due to moisture absorption and trapping of water by the hydroxyl groups, resulting in the breakdown of inter-chain hydrogen-bonded structures. In considering the adhesive/substrate interface one must consider, not only the possibility of moisture disrupting the bond, but also the possibility of corrosion of the substrate. Corrosion can quickly deteriorate the bond strength due to 'jacking' forces of the corrosion products formed. It can be observed that the sol-gel joint failure started from corrosion pit initiation on the Al substrate around the edges of the bonded area, see Figure 4.50. Moreover, any cracking which develops around the pitted regions will increase the peel and transverse stress

effects during the test and lead to a decrease in strength. In Figure 4.51, it can be seen that cracks and de-lamination of the substrate surface due to the environment has occurred. The environment attacks the chemical bonds at the interface and increases water diffusion into the joint. This chemical degradation subsequently causes a reduction of the physical properties of the adhesive.

5.6.2.2 Hybrid epoxy/sol-gel adhesive (SG3)

5.6.2.2.1 Adhesive shear strength (Mild steel)

The adhesive shear strength of SG3 aged for different times in 3.5% NaCl solution decreased as the immersion time increased. The reduction in bond strength for the first, second, fourth and eighth week were recorded as 32%, 40%, 50%, and 96% respectively. For short periods of immersion (from 1-4 weeks), the adhesive structure resisted the penetration of water into the adhesive/substrate interface. The degree of disbondment from a defect in the adhesive layer was very low. The incorporation of filler materials in the adhesive matrix lowered the free volume of bonds that can be influenced by moisture. Harun et al [222] demonstrated that the presence of silane functional group bonded to a steel substrate enhanced the wet adhesion of epoxy-based adhesive. With increased immersion time, corrosion takes place at the joint edges. This in turn can increase the diffusion rate of water into the adhesive causing an increase in the area of disbondment and consequential loss of strength.

The combination of interfacial (adhesive/substrate interface) and cohesive fracture, see Figure 4.54, may indicate that the increase in moisture within the adhesive leads to a break down in the degree of cross-linking both within the adhesive and at the interface. The above factors lead to local stress concentrations thus substantially reducing the joint lap shear strength. The difference in crack behaviour in the SG3 after one and eight weeks immersion in 3.5%NaCl is clearly observed in Figure 4.55. The weakening of the interaction within the adhesive matrix with time confirmed the reduction in adhesive strength. This may be related to plasticisation in the bulk adhesive material with long term immersion due to a physical interaction of the adhesive

with ingressing water. Petrie [223] reported that polymers often absorb moisture to some extent and so become plasticised by water molecules, so changes in the bulk properties are to be expected. The diffused water can disrupt the hydrogen bonding between the molecular chains within the adhesive matrix, affecting in the adhesion performance.

5.6.2.2.2 Adhesive shear strength (Al2024-T3)

Relative to the results obtained with a mild steel substrate, Al2024-T3 showed significantly less reduction in adhesive shear strength for all immersion times. This may be attributed to aluminium oxide layers on the surface, which enhanced the corrosion resistance behaviour of Al2024-T3 substrate as stated in [224]. In addition, the formation of Al-O-Si covalent bonds at the adhesive/substrate interface during the polymerisation process (curing) reduced the moisture or water penetration at these regions and, as a result, increased the load at failure. It has previously been reported [225] that aluminium oxide and silicon oxide may form a stable mixed oxide barrier layer at the interface, which reduces pitting corrosion on the substrate surface and increases adhesion.

Nevertheless, the more time the lap joint was immersed in the NaCl solution the lower the adhesive strength. The percentage reduction in adhesive strength for one, two, four and eight week immersion periods was 29%, 39%, 42% and 68%, respectively. In this case, the adhesive performance may be influenced by water penetration within the adhesive matrix which lowered the adhesive glass transition temperature "T_g", (the temperature which the adhesive changed from rubber-like to a solid like state) by reducing the forces between adhesive molecules. Uddin et al. [226] reported that moisture effects cause a reduction in Tg and mechanical integrity of a cured adhesive. As the uptake of the aggressive medium within the matrix increased with time so the degradation in cohesive bonding increased, causing a reduction in the joint's ability to carry load. The presence of very short cracks and cohesive mode failure was observed in the fracture surface images after one week of immersion, see Figure 4.59a. More significant development in the size of cracks on the fracture surface were observed after eight weeks immersion, see Figure 4.59b,

suggesting increased moisture uptake as time increased which caused more defects within the adhesive matrix, hence a drop in shear strength, in this case of up to 70%.

5.6.3 Adhesive tensile strength of SG3 (butt joints)

From Table 4.5, it is clear that SG3/MS subjected to tensile loading showed high bonding (strength) performance for mild steel butt joints. In this test sample preparation plays an important role in achieving the high values. The sample drying process (i.e. 30 minutes at room temperature and then pre-cured in an oven at ~ 95±5.0°C for 40 minutes) improved the interfacial forces between the adhesive and the substrate surface. Once the adhesive was applied on both substrate faces, the initial interactions (molecular attractions) at the interface started to increase as the adhesive gradually changed to a solid-like state. This is due to the condensation reactions at the interface and increase in the number of -O- bridges as the degree of solvent evaporation increased. In addition, the presence of three fracture modes for the butt joint samples as shown in Figure 4.60, may be attributed to the improvement in the cross-linking within the adhesive itself and at the adhesive/substrate interface. However, with butt joints any inequality in the lateral deformation of the adhesive and the substrate can introduce a complex stress distribution with both shear and tensile stresses being generated within the adhesive layer during the test. Hence, the bond strength of the joint may be highly sensitivity to the butt joint alignment.

Adams et al. [227] reported that typical stress concentrations in loaded butt joints resulted from two different regions. Firstly, the central region of the adhesive, where the tensile stresses are uniform and the shear stress is zero. Secondly, from around the periphery of the joint, where both shear and tensile stresses are present. Here, on the mid-plane of adhesive, the tensile stress decreases to low values and the shear stress is zero, however, there are significant stress concentrations (mainly tensile stress) at the adhesive-substrate interface at the joint edges.

5.6.4 Fatigue strength of SG3 adhesive (lap joints)

The performance of hybrid epoxy sol-gel adhesively bonded mild steel lap joints under cyclic-fatigue loading in dry conditions using two different test frequencies (3Hz and 10Hz) was assessed. Typical fatigue behaviour, notably increasing fatigue life-time with decreasing fatigue load was observed, see Figure 4.61. No significant affects in the fatigue behaviour of the lap joints were noted for two applied load frequencies. The results appear to be related to the adhesive formulation. Cracking in adhesive materials subject to cyclic loading at different test frequencies is related to the creep behaviour of the adhesive. Zeng and Sun have demonstrated [228] that the crack opening times which occur near the peak of each load cycle, at which creep damage develops in the adhesive material, is relatively longer at low-frequencies compared to the time available at high-frequencies.

The improvement in viscoelastic properties of the hybrid epoxy sol-gel adhesive due to the combination of organic polymer chains and inorganic nano-particle materials may also play an important role in fatigue behaviour. It has been reported [229] that, for elastic materials, the energy stored in the sample during loading is returned when the load is removed. However, a viscous material does not return any of the energy stored during loading. All the energy is lost as “pure damping” once the load is removed. In this case, the stress is proportional to the rate of the strain, and the ratio of stress to strain rate is known as viscosity [230]. These materials have no stiffness component, only damping and the combination of both viscous and elastic behaviour produce viscoelastic materials. In this system, some of the energy stored in the viscoelastic system is recovered upon removal of the load, and the remainder is dissipated in the form of heat. The modulus of elasticity of these materials is represented by two quantities. The first part, known as the "storage modulus" relates to the elastic behaviour, and defines "stiffness". The second component is "loss modulus" and relates to the material’s viscous behaviour, and defines the "energy dissipative ability of the material". In the present work, strong chemical bonds formed in the adhesive, due to the presence of Si-O-Si, Si-O-Al and Si-O-MWCNTs bridges, resulted in good material stability which reduced the time for cracks to open/close during the cyclic load and decreased the creep damage at

both load frequencies. Moreover, due to the increase in the degree of cross-linking within the adhesive matrix, the adhesive elasticity was increased. It was reported [231] that the difference in load frequency corresponds to different strain rates in the adhesive layer. This could affect the fatigue strength and fatigue failure mechanism involving micro-cracking or/and void nucleation's around the inorganic filler particles within the adhesive matrix. Also, the initiation of failures under fatigue cycling in the lap joints may be expected to occur at the edges of bonded areas, which present higher stress and strain levels. Mixed adhesive/cohesive mode in the samples was also noted. These fracture behaviour may be attributed to the adhesive cross-linking due to the presence of inorganic materials within the matrix.

5.7 Adhesive structural characterisation of SG3

5.7.1 SEM observations

Figure 4.63, shows that the adhesive failure of SG3 on mild steel occurs by a mixed interfacial/cohesive fracture mode. Cracks in lap joints were initiated from the ends of the joint overlap, a site that is associated with local stress concentrations. From examination of the pairs of failed lap joints, the degree of interfacial/near-interfacial and cohesive failure in a mixed mode fracture was estimated. The PE/MS specimen, see Figure 4.63a showed far fewer features in the SEM fracture surface than those of the modified system. However, the fracture surface morphology of SG3/MS showed many ridges, dimpled patterns, and crevices on the fracture surfaces, which are mainly related to the existence of MWCNT and Al_2O_3 nano-materials in the adhesive matrix, see Figure 4.63b. It is possible that the fracture features observed in SG3/MS are related to the introduction of the inorganic materials in SG, as reported in [232]. The addition of nano-fillers may increase the adhesive matrix crosslinking, and reduce the formation of voids within the adhesive. Therefore, good distribution of these nano-fillers in the matrix is important, see Figures 4.64a and b. Such features allow load transfer between the adhesive matrix and the CNT and increase the adhesive's ability to absorb energy during the tensile load, thereby improving the joint strength. Also, good contact between the fillers and the adhesive

resulted in improved bonding and a restriction of the crack propagation pathways compared with that in unmodified systems.

5.7.2 Adhesive/substrate interface

The strength of an adhesive material is not simply governed by the mechanical or physical properties of the adhesive matrix and/or reinforcing phases. The small region or phase between the adhesive and substrate plays an importance role in determing the adhesive's strength. The adhesive properties of this region may arise from different forces (i.e van der Waals forces, chemical bonding and mechanical interlocking) [233]. In addition, good interfacial bonds between the sol-gel material and nanotubes aids in increasing the bond strength in this region due to the amount of energy required to break this bond. Moreover, joint strength is also related to the nature of the substrate surface (surface energy) and the adhesive's wetability. Figure 4.66 shows elemental maps for a cross-section of an SG3/MS sample. The map for carbon exhibited high-density, as well oxygen and silicon in this region. The result suggests that these elements are related to the formation of different chemical bonds in the matrix, being due to the cross-linking adhesive structure. The map for aluminium showed a lower distribution over the interface region and a better distribution in the adhesive matrix, Figure 4.66, which may be attributed to the formation of Si-O-Al in the adhesive structure.

5.7.3 FTIR analysis

The FTIR spectra of the two adhesive systems were compared in order to identify the changes that have taken place during curing, notably changes in the crosslink networks of the epoxy-amine and the hybrid sol-gel adhesive (SG3). The results shown in Figure 4.67 indicate the presence of amine links, as characterised by vibration peaks in the range 1580-1600cm^{-1}.The band at 950cm^{-1} is attributed to the epoxide groups (asymmetrical ring stretching bands). The chemical pathway for the DGEBA epoxy cured with DETA amine curing agents is presented in Equations 1 and 2 [234,235]. The reaction can be

controlled by the reactivity of the amine, temperature, and the equivalent mole ratio of epoxy and amine agent.

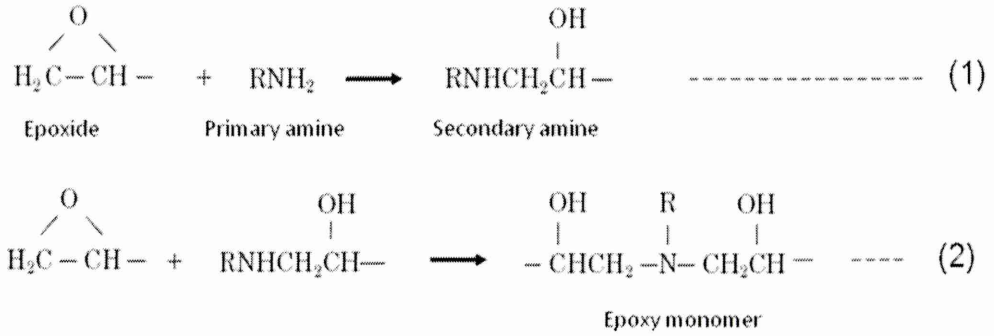

The addition of primary amine active hydrogen to the epoxide group produced secondary hydroxyl group and secondary amine (Equation 1). This is followed by the resulting secondary amine, which can react with another epoxide group to provide polymer formation with poly-functional epoxy monomers (Equation 2). The increase in formation of a three-dimensional network in the epoxy-amine sample is due to the opening of the epoxy ring during the curing process which causes an increase in the molecular weight of the material. This is known as vitrification, where the chains in the epoxy matrix tended to branch, causing reduced mobility, see Figure 5.6.

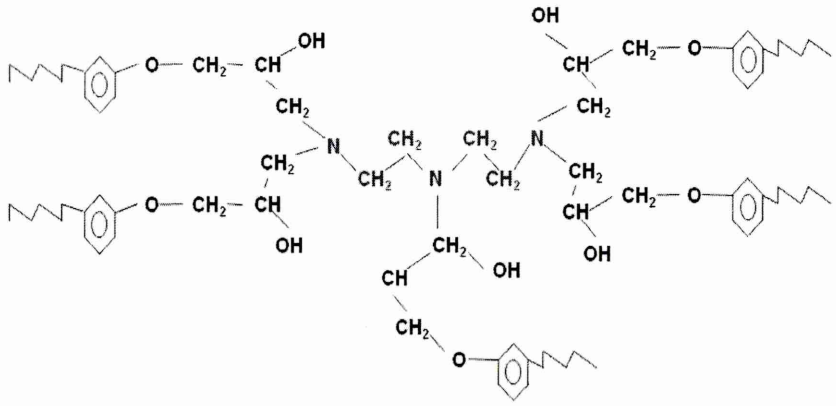

Figure 5.6 Schematic of cross-linking (an epoxy and DETA)

The presence of methoxy groups (-OCH_3) in TEOS and ethoxy groups (-OC_2H_5) in MTMS in the sol-gel produce silanol (Si-OH) groups. The presence of acid media (HNO_3) can be used to catalyze the opening of the epoxy ring.

Furthermore, the silanol groups can react with the hydroxyl (-OH) group on epoxy resins to form Si-O-C bonds, see Figure 5.7. The characteristic FTIR peaks of the hybrid epoxy sol-gel adhesive (Figure 4.71) indicate that the disappearance of the peak of epoxy group and the formation of Si-O-C bond during the reaction, results from opening of the epoxy ring.

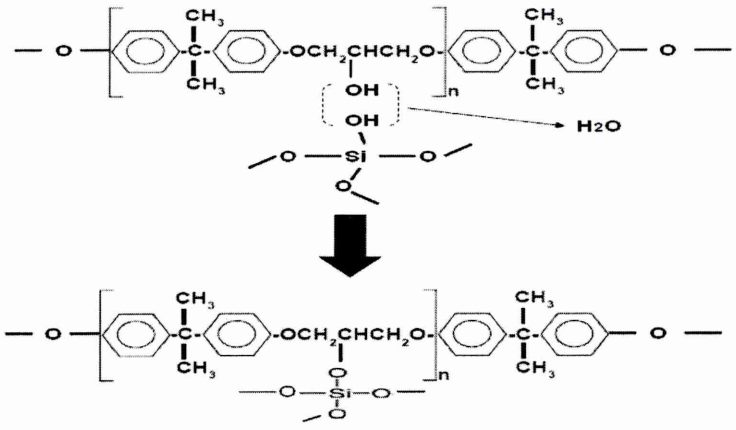

Figure 5.7 Schematic of linkage (epoxy/sol-gel material) [236]

The incorporation of inorganic phases (i.e. γ-Al_2O_3 and MWCNT) in the adhesive material lead to the introduction of other potential covalent bonds between the inorganic and organic components. The FTIR analysis in Figure 4.68 show a strong absorbance peak at 1088cm^{-1}, which is characteristic of the Si-O-Si bond, resulting from the reaction of silica sol-gel with the polymer. The appearance of a stretching vibration belonging to Si-OH, Si-O-C, and Al-OH confirmed the changes in the adhesive network compared to that in PE sample. According to many researchers [237,238,239] the surface of CNTs can be chemically modified to impart a specific desired property, for example, either covalent or through physical adsorption. Using a strong acid solution, some stable chemical functional groups, such as -OH, -C=O and -COOH can be generated on the surface of the CNTs. Nitric acid in this system was used to oxidise the CNTs surface for the generation of –COOH groups on the sidewalls. Due to the –OH group in sol-gel system and the C–O, C=O and O–C=O groups on CNTs, SiO_2–CNTs linkages formed through some physicochemical actions such as van der Waals force or/and hydrogen bonding among the groups on the two surfaces. More details on the modification process of CNTs surface using

HNO_3 is explained in [240]. Figure 5.8 illustrates a silica network crosslinked with polymer, MWCNT and γ-Al_2O_3 in the SG3 adhesive material.

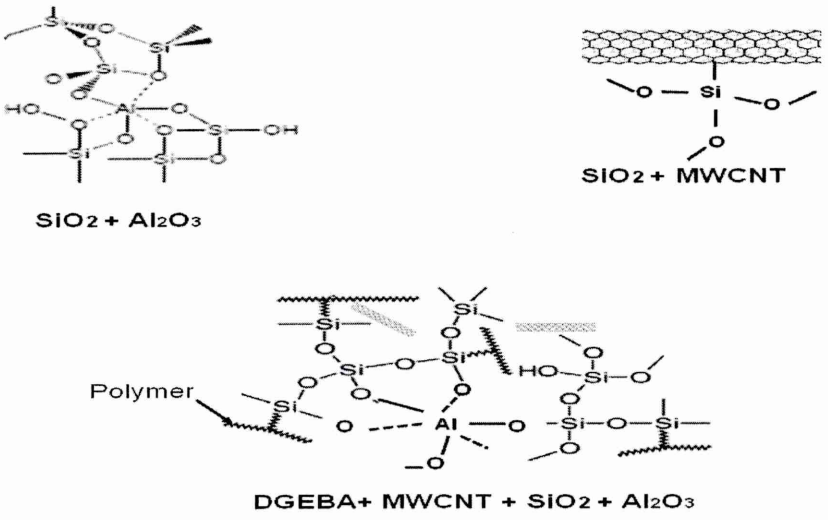

Figure 5.8 Schematic hybrid epoxy/sol-gel material [241,242]

5.7.4 Raman spectroscopy analysis

The changes in the intensity of Raman bands for an epoxy resin toughened by DETA and the hybrid epoxy/sol-gel adhesive were observed, see Figures 4.69 & 4.70. The Raman spectra of a hybrid epoxy/sol-gel adhesive (SG3), see Figure 4.70 highlighted the presence of inorganic components, i.e. MWCNTs, in the epoxy/sol-gel adhesive matrix. The main bands at 3621cm^{-1} (C-H) and 1897cm^{-1} (CH_2 or CH_3) in the epoxy resin disappeared in the SG3 adhesive system while the appearance of a peak at ~ 431cm^{-1}, is related to the bending of Si-O-Si bonds. In addition, the peaks in the range 820 -1076cm^{-1} are related to the stretching mode of Si-OH, which indicating the presence of some free silanol groups in the hybrid epoxy/sol-gel system. Shift and width changes in the peaks of the D (C-C bond) and G (C=C bond) bands reflect the interaction of CNT materials with the polymer matrix. MWCNTs in this system enhanced the adhesive linkage and interacted with other inorganic materials as observed through the formation of Si–O–MWCNT [243].

5.7.5 XPS analysis of failed lap joint

XPS analysis of selected areas revealed no traces of iron on either side of the mild steel fracture faces, AD1 or AD2, see Figure 4.71. The absence of this element on both fracture surfaces, is due to the presence of a thin layer of sol-gel adhesive, which indicates the fracture is within the adhesive matrix. This thin layer is sufficient to prevent detection of the iron element as XPS only samples the first few nanometres of depth. In addition, no significant changes in the atomic concentrations of C_{1s}, O_{1s}, Si_{2p} and Al_{2p} on the fracture surfaces were detected, see Table 4.8, suggesting good adhesion between the substrate and hybrid epoxy/sol-gel adhesive.

The presence of the Si-O and Si-O-C bands is evidence that the silane was attached to the surrounding organic and inorganic materials in the adhesive matrix. The amount of Al detected on metal AD1 and adhesive AD2 fracture sides was almost identical, which reflects good cross-linking of Al_2O_3 within the matrix. This may be the reason why a cohesive failure in SG3 adhesive matrix is the main failure mechanism on the mild steel sample. Moreover, the lack of the Mg and Cu signals on both fracture surface faces for the aluminium lap joint suggests that failure still in adhesive. XPS elemental analysis results (in at %) for the F1 and F2 fracture surfaces indicated the locus of failure is within the adhesive layer near the interfacial region. The high amount of C detected on the metal side F1 compared with that in adhesive side F2 indicates high levels of hydrocarbon contamination from the surrounding atmosphere.

5.7.6 Thermo-gravimetric analysis TGA

Figures 4.83 shows that the differences in percentage total weight loss in the adhesives at 650°C were 91% for PE compared with 71% for SG1, 64% for SG2, and 50% for SG3. The reduction in weight loss for SG1, SG2 and SG3 is attributed to the addition of the inorganic components. The addition of the nano-fillers significantly improved the thermal stability of the sol-gel epoxy adhesive and shifted any major changes in the structure of the adhesive matrix to higher temperatures. The adhesive cross-link density increased with strong covalent bonds between the polymer chain and the inorganic network, thereby reducing

the chain mobility. Further the addition of nano-materials appears to cause thermal stability and slows down the rate of degradation of the adhesive.

CHAPTER 6 Conclusions

This research reports on a new application of a sol-gel system to produce a novel adhesive material. The adhesive formulation was first prepared based on the use of a hybrid silica-base sol-gel derived system and further developed by introducing an epoxy resin as the organic component and inorganic nano-particles into the adhesive formulation. Aluminium alloy 2024-T3 and mild steel substrates were used to evaluate the adhesive strength under different conditions. Selected techniques such as SEM, IFM, FTIR, Raman, XPS and TGA were used to identify the adhesion performance mechanism of these adhesive materials. Consideration of various sol-gel formulations guided this research to the following conclusions.

6.1 Adhesive strength of hybrid sol-gel material as a function of composition.

1. The bond strength of the hybrid silica-base sol-gel is found to be related to the Si-O-Si network in the adhesive.

2. Sol-gel joints modified with 0.05% PANI micro-particles have a slightly enhanced adhesive strength compared with that of the unmodified joints. This is due to the improved flexibility of sol-gel because of the presence of PANI within the sol-gel formulation.

3. The presence of 0.5% γ-Al_2O_3 nano-particles in the sol-gel formulation led to a significant increase in joint strength. The reason is attributed to the enhanced cross-linking among the hybrid SiO_2 based nano-particles through the bonding of -Si-O-Al- in the sol-gel system.

4. The incorporation of TiO_2 nano-particles into the sol-gel plays a role in increasing the cross-linking among the hybrid SiO_2 based nano-particles through the bonding of -Si-O-Ti-, which resulted in an improvement in the joint strength.

5. The combination of PANI and γ-Al_2O_3 into the sol-gel structure led to a further increase in adhesive strength compared with that of the unmodified system. This is considered to be related to the formation of three-dimensional network within the sol-gel structure via γ-Al_2O_3 and/or via two dimensional branches of PANI which enhanced the adhesive cross-linking.

6. A novel adhesive based on a sol-gel and epoxy system has been developed incorporating the use of nano-fillers (γ-Al_2O_3 and MWCNTs). The adhesive lap shear strength of the sol-gel epoxy was increased on both Al2024-T3 and mild steel substrates up to 24±0.6MPa and 25±0.9MPa, respectively compared with 10±0.5MPa in the pure epoxy.

7. The increase in the proportion of nano γ-Al_2O_3 (up to 4.0 wt%) within the SG/epoxy adhesive resulted in an increase in shear strength. However, additions above 4.0 wt% caused a decrease in shear strength. This increase is due to this material enlarging the interaction area and enhancing the bonding within the adhesive matrix.

8. An increase in the proportion of MWCNT (up to 0.07 wt%) within the SG/epoxy adhesive resulted in an increase in shear strength. This increase can be attributted to mechanical load transfer from the matrix to the MWCNTs and the high specific surface area of this material, which increases the degree of cross-linking with other inorganic fillers in the formulation. Further increase in MWCNT beyond 0.07 wt% led to a decrease in shear strength.

6.2 Role of cure conditions and surface roughness on adhesive strength

1. The adhesive strength of hybrid sol-gel material and hybrid epoxy/sol-gel (SG3) increased as the curing time and temperature increased. The improvement in the joint strength is primarily related to the removal of residual solvent from the sol-gel adhesive.

2. The optimum cure time to achieve the highest bond strength on Al alloys and mild steel substrates for this adhesive system was found to be 16 hrs.

3. The adhesive strength of hybrid sol-gel adhesive increased as the specimen surface roughness increased. The adhesive interlocks with the substrate on both sides, providing a simple mechanical keying effect that leads to an improvement of the bond strength.

4. Increasing surface roughness resulted in a increase in adhesive strength, suggesting better mechanical interlocking on a rougher surface compared with finer surface finshes.

6.3 Role of bond geometry and external environment on adhesive strength

1. A gradual increase in lap joint geometry, notably bond area, increased the hybrid epoxy/sol-gel adhesive strength to a maximum at an area of ~ 375mm^2 (i.e. 18.0±0.7MPa). With further increase in bond area, a reduction in adhesive strength per unit area was observed, the reason being related to the increase in non-uniform shear stresses across the joint.

2. A decrease in hybrid epoxy/sol-gel adhesive strength on mild steel was observed as test temperature increased. It was noted that the adhesive became softer as the temperature increased, causing a reduction in adhesion performance.

3. The adhesive strength of the hybrid sol-gel and hybrid epoxy/sol-gel (SG3) gradually decreased as immersion time in 3.5%NaCl increased. The reduction is due to water absorption and the formation of corrosion products along the interfacial bond line.

4. A study of the adhesive performance of SG3 adhesive subjected to cyclic loading showed typical fatigue behaviour, notably increasing fatigue life with

decreasing fatigue load. No significant affects in the fatigue behaviour of the lap joints were noted for different loading frequencies, e.g. 3Hz and 10Hz.

6.4 Adhesive structural characterization

1. FTIR, Raman and XPS analysis confirmed that the improvements in strength of the hybrid epoxy/sol-gel materials were related to the formation of different covalent bonds in the adhesive matrix, i.e. Si-O-Si, Si-O-Al and Si-O-C.

2. The sol-gel/epoxy adhesive showed a greater thermal stability than the conventional PE adhesive tested; suggesting this novel adhesive could be used for moderately high temperature environments.

3. The high strength and thermal stability of this novel sol-gel/epoxy adhesive were attributed to the addition of inorganic nano-components; i.e. silica-based sol-gel, γ-Al_2O_3 nano-particles and MWCNTs. These components play a role in increasing the adhesive matrix ductility and reducing the formation of voids within the adhesive.

6.5 Summary

The original aim of the project was to synthesise and assess the structural performance of a hybrid sol-gel adhesive, as modified through the combination of organic/inorganic, nano/macromolecular materials. The overall conclusions of this work indicate that the maximum adhesive strength obtained, namely 25 MPa, was achieved after 16 hrs cure time at 200°C.

When compared to commercially available adhesives for structural use, it was concluded that the current novel sol-gel/epoxy adhesive system has some processing and property limitations. For example, the cure time is very long and the cure temperature is above that accepted by industry. In addition it has lower lap shear strength and fatigue response. The results of this study also indicate that prolonged exposure to 3.5%NaCl, and severe temperature changes significantly decrease the shear strength of sol-gel/epoxy adhesive However, despite these limitations it is recognised that a sol-gel route for the production of adhesives is extremely attractive due to the versatility of hybrid sol-gel

technology. In the first instance it is recognised that the adhesive strength of the system is very good and that the cohesive strength would benefit markedly by the introduction of suitable surface treatments.

CHAPTER 7 Future work

Possible future work based on the presented results in this research can be summarised as follows;

1- The experimental investigation could be extended to obtain material data on other mechanical properties (i.e. toughness, modulus and yield strength) to understand how the hybrid epoxy/sol-gel adhesive perform under these conditions.

2- Chemical surface pre-treatment methods (i.e etching and PAA) can be used to study the effects of initial substrate surface morphology on the mechanical properties of the bonded joints. It would be beneficial to determine the optimum surface condition for forming a strong bond that can help to prolong the lifetime of a bonded joint.

3- The optimisation of hybrid epoxy/sol-gel system by modifying the sol-gel formulation or organic/inorganic additives for achieving a strong bonding to the substrate surface within low cure time/temperature conditions.

4- The optimisation of hybrid epoxy/sol-gel system for enhancing the adhesive performance at high temperature conditions (i.e. 200°C).

5- Study the interaction at adhesive/substrate interface by using transmission electron microscopy (TEM) to identify the nature of the adhesive/metal interface.

6- The fatigue work programme could be extended to study the effect of fatigue crack propagation in adhesively bonded joints using double-cantilever beam (DCB) samples.

References

[1] J. T. Cherian, D.G. Castner and R. M. Fisher, 2002 " Surface analysis of disbonded titanium/sol-gel/polyimide joints" J. Materials Engineering and Performance. Vol 11, No 6, pp 603-609.

[2] M. Keranen, M. Gnyba, P. Raerinne, T. Kololuoma, A. Maaninen and J. T. Rantala, 2004 "Synthesis and characterization of optical sol–gel adhesive for military protective polycarbonate resin" J. Sol-Gel Science and Technology. Vol 31, pp 369–372.

[3] E. Moncada, R.Quijada and J. Retuert, 2007 " Nanoparticles prepared by the sol–gel method and their use in the formation of nanocomposites with polypropylene" Nanotechnology, Vol 18, No 33, pp 335606 (7).

[4] S. R. Lu, C. Wei, J. H. Yu, X. W. Yang and Y. M. Jiang, 2007 " Preparation and characterization of epoxy nanocomposites by using PEO-grafted silica particles as modifier " J. Mater. Sci, Vol 42, pp 6708–6715.

[5] H. Wang and R. Akid, 2008 " Encapsulated cerium nitrate inhibitors to provide high-performance anti-corrosion sol–gel coatings on mild steel" Corrosion Science, Vol 50, No 4, pp1142–1148.

[6] F. Andreatta, P. Aldighieri, L. Paussa, R. Di Maggio, S. Rossi and L. Fedrizzi, 2007 "Electrochemical behaviour of ZrO_2 sol–gel pre-treatments on AA6060 aluminium alloy" Electrochimica Acta 52, pp7545–7555.

[7] S. V. Lamaka, D. G. Shchukin, D. V. Andreeva, M. L. Zheludkevich, H. M. Hwald, and M. G. S. Ferreira, 2008. " Sol-Gel/polyelectrolyte active corrosion protection system " Adv. Funct. Mater. Vol 18, pp 3137–3147.

[8] D.R. Uhlmann, T.Suratwala, K.Davidson, J.M.Boulton and G.Teowee, 1997 "Sol-gel derived coatings on glass" Journal of Non-Crystalline solids, Vol.218, pp 113-122.

[9] A. S. Hamdy, 2006 "Advanced nano-particles anti-corrosion ceria based sol gel coatings for aluminium alloys" Materials Letters, Vol 60, pp 2633–2637.

[10] S. Kumar, 2009 "Analysis of tubular adhesive joints with a functionally modulus graded bondline subjected to axial loads" Int. J. Adhesion & Adhesives, Vol 29, No 8, pp785–795.

[11] N. Choupani, 2009 " Characterization of fracture in adhesively bonded double-lap joints" Int. J. Adhesion & Adhesives Vol 29, pp 761–773.

[12] S. J. Park, F. L. Jin and J. R. Lee, 2005 "Synthesis and characterization of a novel silicon-containing epoxy resin" Macromolecular Research, Vol. 13, No. 1, pp 8-13.

[13] B. C. Samanta, T. Maity, S. Dalai and A. K. Banthia, 2008 "Toughening of epoxy resin with solid amine terminated poly (ethylene glycol) benzoate and effect of red mud waste particles" J. Mat. Sci. Technol, Vol 24, No.2.

[14] P. Innocenzi, T. Kidchob and T. Yoko, 2005 "Hybrid organic-inorganic sol-gel materials based on epoxy-amine systems" J. Sol-Gel Science and Technology, Vol 35, pp 225–235.

[15] B. Jack, 1981 "International news products equipment meetings publications" International Journal of Adhesion and Adhesives, Vol. 1, No 6, pp275.

[16] BSA Educational Services Committee, 1991 "History of Adhesives" Vol. 1, Issue 2, pp 1-4.

[17] S. D. Goddard, , 2008 "A History of Adhesives" Retrieved December 5, 2009, from http://ezinearticles.com/?A-History-of-Adhesives&id=1253855

[18] R. W. Smith, 2002 "Adhesives From Natural Sources, Workshop, Cleveland, OH - sponsored by Adhesives Age and The Adhesive and Sealant Council " The Chem Quest Group, Inc. 8150 Corporate Park Drive, Suite 250, Cincinnati, Ohio, USA, pp1-4.

[19] C. A. May, Second edition, 1988 "Epoxy resins: chemistry and technology" Marcel Dekker, INC, 270 Madison Avenue, New York, pp3-4.

[20] A. Rider, PhD thesis, 1998 "Surface properties influencing the fracture toughness of aluminium-epoxy joints ". University of New South Wales.

[21] S. G. Prolongo, G. D. Rosario and A. Urena, 2006 "Comparative study on the adhesive properties of different epoxy resins " International Journal of Adhesion & Adhesive, Vol. 26, pp125-132.

[22] J. D. Minford, 1993 "Handbook of aluminium bonding technology and data" Marcel Dekker, INC, 270 Madison Avenue, New York, USA, pp 17-18.

[23] A. Pizzi, 1994 " Advanced wood adhesive technology" Marcel Dekker, INC, 270 Madison Avenue, New York, USA, pp 4-5.

[24] E. M. Petrie, Second edition, 2007 "Handbook of adhesives and sealants" McGraw - Hill companies, INC, New York, pp 53.

[25] D. E. Packham, Second Edition, 2005 "Handbook of Adhesion" John Wiley & Sons Ltd, The Atrium, Southern Gate, Chichester, UK, pp39-40.

[26] J. Mazza. "Adhesive bonding surface preparation qualification considerations " Materials & Manufacturing Directorate. Air Force Research Laboratory

[27] K. D. Kumar and B. Kothandaraman, 2008 "Modification of (DGEBA) epoxy resin with maleated depolymerised natural rubber" Express Polymer Letters Vol.2, No.4, pp302–311.

[28] D. Ratna and A. K. Banthia, 2000 "Toughened epoxy adhesive modified with acrylate based liquid rubber" Polymer International, Vol. 49, pp281-287.

[29] W. Zhao, K. Ramani and B. E. Mueller, 2000 "Processing and fracture behavior of a polyethylene-based thermoplastic adhesive and a glass-fiber filled epoxy adhesive" International Journal of Adhesion & Adhesives, Vol. 20, pp 409-413.

[30] M. Imanaka, Y. Nakamur, A. Nishimur and T. Iida, 2003 "Fracture toughness of rubber-modified epoxy adhesives: effect of plastic deformability of the matrix phase" Composites Science and Technology, Vol. 63, pp41–51.

[31] W. D. Bascom, R. L. Cottington, R. L Jones and P. Peyser, 1975 "The fracture of epoxy-and elastomer-modified epoxy polymers in bulk and as adhesives" Journal Applied Polymer Science, Vol 19, pp 2545–2562.

[32] J. H. Hodgkin, G. P. Simon and R. J. Varley, 1998 "Thermoplastic Toughening of Epoxy Resins: a Critical Review" Polymers for Advanced Technologies, Vol. 9, No1, pp. 3–10.

[33] H. Wang, W. Han, H. Tian, Y. Wang, 2005 "The preparation and properties of glass powder reinforced epoxy resin" Materials Letters, Vol. 59, pp 94– 99.

[34] Y. Sun, Z. Zhang and C. P. Wong, 2006 "Study and Characterization on the Nanocomposite Under fill for Flip Chip Applications" IEEE, Transactions on components and packaging technologies, Vol. 29, No. 1, pp 190-197.

[35] K. L. Mittal, 2002 "Adhesive joints: formation, characteristics, and testing" VSP BV, P.O Box 346, 3700 HA Zeist, The Netherland, Vol. 2, pp 179.

[36] T. Yokoyama, 2003 "Experimental determination of impact tensile properties of adhesive butt joints with the split Hopkinson bar" J. Strain Analysis Vol. 38, No.3, pp233-245.

[37] N. J. De lollis, 1970 "Adhesives for metals: theory and technology " Industrial Press, New York.

[38] G. N. Rao, M. V. Rao, K. M. Rao, V. R. Raju, V. B. K. Murthy and V. V. S. Raju, 2009 " Analysis of adhesive bonded single lap joints in hybrid composites subjected to transverse load with S-S end conditions" International Journal of Mechanics and Solids, Vol. 4, No. 1, pp 85-94.

[39] A. A. Neves, E. Coutinho, A. Poitevin, J. V. der Sloten, B. V. Meerbeek and H. V. Oosterwyck, 2009 " Influence of joint component mechanical properties and adhesive layer thickness on stress distribution in micro-tensile bond strength specimens" Dental Materials, Vol. 25, No. 1, pp 4-12.

[40] D. Y. Wang, 2006 "Influence of stress distribution on fatigue strength of adhesive-bonded joints" Experimental Mechanics, Vol. 4, No. 6, pp173-181.

[41] S. Wu, 1982 "Polymer interface and adhesion- analysis and testing of adhesive bonds" Marcel Dekker, INC, 270 Madison Avenue, New York, USA, pp 497.

[42] W. A. Nash, Chapter 16, Fourth Edition, 1998 "Schaum's outline of theory and problems of strength of materials" McGraw - Hill companies, INC, New York, pp420.

[43] A. Andriyana, 2008 "Failure Criteria for Yielding" http://andriandriyana.files.wordpress.com/2008/03/yield_criteria.pdf

[44] R. M. Jones, 2009 " Deformation Theory of Plasticity" Bull Ridge Publishing, Virginia, USA, pp146.

[45] W. D. Bascom, C. O. Timmons and R. L. Jones, 1975 "Apparent interfacial failure in mixed-mode adhesive fracture" Journal of material science, Vol. 10, No. 6, pp 1037-1048.

[46] S. G. Prolongo and A. Urena, 2007 "Durability of aluminium bonded with a homopolymerised epoxy resin " The journal of adhesion, Vol. 83, pp1-14.

[47] R. A. Dicliel, L. P. Haack, J. K. Jehwaba, A. J. Kinloch and J. F. Watts, 1998 " The Fatigue and Durability Behaviour of Automotive Adhesives. Part II: Failure Mechanisms, The Journal of Adhesion, Vol. 66, pp. I - 37.

[48] K. B. Armstrong, 1997 "Long-term durability in water of aluminium alloy adhesive joints bonded with epoxy adhesives" Int. J. Adhesion and Adhesives, Vol. 17, pp 89-105.

[49] A. Lekatou, S. E. Faidi, D. Ghidaoui, S. B. Lyon and R. C. Newman, 1997 "Effect of water and its activity on transport properties of glass/epoxy particulate composites " Composites Part A: Applied Science and Manufacturing, Vol. 28, No. 3, pp 223-236.

[50] D. E. Packham, 1992 "The mechanical theory of adhesion. Changing perceptions " J. Adhes, Vol. 39, No. 2, 3, pp 137 - 144.

[51] K. Bright , B. W. Malpass , D. E. Packham, 2006. "Adhesion of polyethylene to high energy substrates" British Polymer Journal, Vol. 3, pp205 - 208.

[52] D. J. Arrowsmith , 1970 "Adhesion of electroformed copper and nickel to plastic laminates " Trans. Inst. Metal Finish., Vol. 48, pp 88–92.

[53] G. A. Nitowski, PhD thesis, 1998 "Topographic and surface chemical aspects of the adhesion of structural epoxy resins to phosphorus acid treated aluminium adherends " Blacksburg, Virginia.

[54] R. G. Schmidt and J. P. Bell, 1986 "Epoxy adhesion to metals " Advances in Polymer Science, Vol. 15, pp33.

[55] B. D. Bhatt and V. Radhakrishnan, 1989 "Evaluation of Some Machining Processes as Adherend Surface Treatments in Bonding Aluminium " J. Adhes. Sci. Technol, Vol. 3, No. 5, pp383.

[56] Z. Gendler, A. Rosen, M. Bamberger, M. Rotel, J. Zahavi, A. Buchman and H. Dodiuk, 1994 " Improvement of adhesive bonding strength in sealed anodized aluminium through excimer laser prebond treatment " J. Mater. Sci. Vol. 29, pp1521.

[57] C. W. Jennings, 1972 "Primary-tertiary diamines mixed with polyamines as epoxy resin" J. Adhes, Vol. 4, pp25.

[58] J. M. Goetz, Honors, Thesis, 2005 "Investigation of Coating Cracking and Fatigue Strength of 7050-T74 Aluminium Alloy with Different Anodize Coating Thicknesses" The Ohio State University Columbus, OH, USA College of Engineering, Department of Mechanical Engineering.

[59] W. Brockmann, P. L. Geiss, J. Klingen, K. B. Schroder, 2005 "Adhesive Bonding: Materials, Applications and Technology" Wiley-VCH, GmbH &Co. KGaA, Weinheim, Germiny. pp164-165.

[60] ASTM D 3166, 1999, "Standard Test Method for Fatigue Properties of Adhesives in Shear by Tension Loading" (Metal/Metal).

[61] H. Wang and R. Akid, 2007 "A room temperature cured sol–gel anticorrosion pre-treatment for Al 2024-T3 alloys" Corrosion Science, Vol. 49, pp4491–4503.

[62] N. Voevodin, D. Buhrmaster, V. Balbyshev, A. Khramov, J. Johnson, R. Mantz, 2005 "Non-chromated coating systems for corrosion protection of aircraft aluminum Alloys" Air Force Research Laboratory, Materials and Manufacturing Directorate, AFRL/MLBT, Coatings Research Group, Wright Patterson AFB, OH, USA.Tri-service corrosion conference.

[63] M. L. Zheludkevich, R. Serra, M. F. Montemor, I. M. Miranda Salvado and M. G. S. Ferreira, 2006 "Corrosion protective properties of nanostructured sol-gel hybrid coatings to AA2024-T3 " Surface & coatings technology, Vol. 200, pp3084-3094.

[64] M. L. Zheludkevich, I. Miranda Salvado, and M. G. S. Ferreira, 2005 "Sol-gel coatings for corrosion protection of metals" Journal of materials chemistry, Vol. 15, pp5099-5111.

[65] K. Masaru, S. K. Kumiko and T. Toyoka, 2005 "Silica sol-gel monolithic materials and their use in a variety of applications " J. Sep. Sci. Vol. 28, pp1893-1908.

[66] D. C. L. Vasconcelos, J. A. N. Carvalho, M. Mantel and W. L. Vasconcelos, 2000 "Corrosion resistance of stainless steel coated with sol-gel silica " Journal of non-crystalline solids. Vol. 273, pp135-139.

[67] Y. H. Han, A. Taylor, M. D. Mantle and K. M. Knowles, 2007 "Sol-gel derived organic-inorganic hybrid materials " Journal of non-crystalline solids, Vol. 353, pp313-320.

[68] N. Ljubica and R. Ljiliana,1997 "Alumina strengthening by silica sol gel coating " Thin Solid Films. Vol. 295, pp101-103.

[69] K. Jordens, PhD thesis, 1999 "Novel poly (propylene oxide) based ceramers, abrasion resistant sol–gel coatings for metals, and epoxy–clay nanocomposites " Blacksburg, Virginia.

[70] C. Mutter, T. N. M. Bernards, M. P. J. Peeters, J. H. Lammers and M. R. Bohmer, 1999 "The effect of the solvent on the cross-link density of SiO2 coatings" Vol. 351,pp95-98.

[71] S. V. Aurobind K. P. Amirthalingam and H. Gomathi, 2006 "Sol-gel based surface modification of electrodes for electro analysis " Advances in Colloid and Interface Science. Vol.121, pp1–7.

[72] P. K. E. Frederick, MSC thesis, 2004 "Fabrication of random hole optical fiber performs by silica sol-gel processing " Materials Science and Engineering, Blacksburg, Virginia.

[73] K. A. Mauritz "Organic/inorganic hybrid materials via polymer in situ sol-gel chemistry " Available at http://www.psrc.usm.edu/mauritz/rshsum.html.

[74] B. Y. Ahn, S. Seok, S. Hong, J. S. Oh, H. K. Jung and W. J. Chung, 2006 "Optical properties of organic/inorganic nanocomposite sol-gel films containing LaPO4:Er,Yb nanocrystals" Optical Materials, Vol. 28, pp374–379.

[75] L. Nikolic and L. Radonjic, 1998 "Effect of silica sol-gel coatings on the properties of glass substrate " Ceramics international, Vol. 24, pp547-552.

[76] A. Conde, J. De Damborenea, A. Duran and M. Menning, 2006 "Protective properties of a sol-gel coating on zinc coated steel" Journal of Sol-Gel Science and Technology, Vol. 37, pp79-85.

[77] R. L. Twite and G. P. Bierwagen, 1998 "Review of alternatives to chromate for corrosion protection of aluminum aerospace alloys" Progress in Organic Coatings, Vol. 33, pp 91–100.

[78] J. Liu, G. Gong and C. Yan, 2006 "Enhancement of the erosion–corrosion resistance of Dacromet with hybrid SiO2 sol–gel " Surface & Coatings Technology, Vol. 200, pp 4967 – 4975.

[79] X. Yue, L. Yingjie and L. Sha, 2007 "Preparation and Characterization of Sol-Gel Coatings Doping with Cerium Ingredients on Aluminum Alloy Surface ". Journal of Rare Earths. Vol. 25, pp 193.

[80] H. Abdel Salam and D. P. Butt, 2006 " Environmentally compliant silica conversion coatings prepared by sol–gel method for aluminum alloys ". Surface & Coatings Technology, Vol. 201, pp 401–407.

[81] U. Schubert, N. Huesing, and A. Lorenz, 1995 "Hybrid Inorganic-Organic Materials by Sol-Gel Processing of Organo-functional Metal Alkoxides" Reviews, Chem. Mater, Vol. 7, pp 2010-2027.

[82] C. Sanchez and E. Ribot, 1993 "Molecular design of hybrid organic-inorganic materials" Journal de physique III, Vol. 3, pp1349-1355.

[83] I. N. Tsvetkova, O. A. Shilova, V. V. Shilova, A. Yu. Shaulov, Y. P. Gomza and S. V. Khashkovskii, 2006 "Sol–Gel Synthesis and Investigation of Hybrid Organic–Inorganic Borosilicate Nanocomposites" Glass Physics and Chemistry, Vol. 32, No. 2, pp 218–227.

[84] I. Stewart, A. Chambers and T. Gordon, 2007 "The cohesive mechanical properties of a toughened epoxy adhesive as a function of cure level" International Journal of Adhesion & Adhesives, Vol. 27, pp 277–287.

[85] I. B. Rozanova, T. T. Daurova and G. N. Dudnikova, 1982 "Investigation of dressing material by scanning electron microscopy" J. Bulletin of Experimental Biology and Medicine, Vol. 94, No. 6, pp1762-1764.

[86] A. H. Susin, L. S. Alves, G. P. deMelo and T. L. Lenzi, 2008 "Comparative scanning electron microscopic study of the effect of different dental conditioners on dentin micro morphology" J. Appl. Oral. Sci, Vol. 16, No. 2, pp100-5.

[87] S. Macari, M. Goncalves, T. Nonaka and J. M. Dos-Santos, 2002 "Scanning electron microscopy evaluation of the interface of three adhesive systems" Braz Dent J, Vol. 13, No. 1, pp33-38.

[88] I. Alli and B. E. Baker, 2006 "Constitution of leguminous seeds. Scanning electron microscopy of proteins prepared from Phaseolus beans" J. Science of Food and Agriculture, Vol. 32, No. 11, pp1069 - 1073.

[89] L. C. Sawyer and D. T. Grubb, Second edition, 1996 "Polymer Microscopy" Chapman & Hall, London.

[90] R. Gauvin, K. Robertson, P. Horny, A. M. Elwazri and S. Yue, 2006 " Materials characterization using high-resolution scanning-electron microscopy and x-ray microanalysis" JOM J. Minerals, Metals and Materials Society, Vol. 58,No. 3, pp20-26.

[91] K. D. Vernon-Parry, Review, 2000 "Scanning electron microscopy: an introduction" III-Vs Review, Vol. 13, No. 4, pp40-44.

[92] http://www.schaefer-tec.it/NanoTech/EN_prodotti.cfm?id_prodotto=28.

[93] H. Schroettner, M. Schmied and S. Scherer, 2006 " Comparison of 3D surface reconstruction data from certified depth standards obtained by SEM and an infinite focus measurement machine (IFM)" Microchim Acta, Vol. 155, pp279–284.

[94] M. Ramezani, Z. M. Ripin and R. Ahmad, 2009 "Computer aided modelling of friction in rubber-pad forming process" J. Materials Processing Technology, Vol. 209, pp 4925–4934.

[95] S. Wang, Msc Thesis, 2009 " Effect of oxygen on CO2 corrosion of mild steel " Ohio University, Chemical Engineering (Engineering and Technology), USA.

[96] C. Sherman Hsu, 1997, "Handbook of instrumental techniques for analytical chemistry" Prentice-Hall International, London, pp247-277.

[97] C. Fernandez, S. F. Ausar, R. G. Badini, L. F. Castagna, I. D. Bianco and D. M. Beltramo, 2003 "An FTIR spectroscopy study of the interaction between αs-casein-bound phosphoryl groups and chitosan" Int. Dairy Journal, Vol. 13, pp897–901.

[98] L. Mariey, J. P. Signolle, C. Amiel and J. Travert, 2001 "Discrimination, classification, identification of microorganisms using FTIR spectroscopy and chemometrics" Vibrational spectroscopy, Vol. 26, No. 2, pp151-159.

[99] B. J. Hunt and M. I. James, 1993 "Polymer characterisation", Blackie Academic & Professional, an imprint of Chapman & Hall, London.

[100] N. B. Colthup, L. H. Daly, S. E. Wiberley, Third Edition 1990 "Introduction to Infrared and Raman Spectroscopy" Elsevier Science, (Boston), USA

[101] P. Vandenabeele and L. Moens, 2006 "Introducing students to Raman spectroscopy" Anal Bioanal Chem, Vol. 385: pp209–211.

[102] H. G. M. Edwards and J. M. Chalmers, 2005 "Raman spectroscopy in archaeology and art history" The Royal Society of Chemistry, Cambridge, pp17-40.

[103] M. J. Pelletier, 1999, "Analytical applications of Raman spectroscopy" Blackwell Science Ltd, Oxford, pp114-117.

[104] J. J. Laserna, 1996, "Modern techniques in Raman spectroscopy" John Wiley & Sons Ltd, UK.

[105] D. M. Brewis and I. Mathieson, Report 143, 2001 "Adhesion and bonding to polyolefins" Rapara Technology Ltd, Vol. 12, No. 11, UK.

[106] J. F. Watts and J. Wolstenholme, 2003 "An Introduction to surface analysis by XPS and AES" John Wiley and Sons Ltd, UK.

[107] A. Pizzi and K. L. Mittal, Second edition, 2003 "Handbook of adhesive technology" , USA.

[108] A. J. Kinloch, 1986 "Durability of structural adhesives" Elsevier Science Publishing Co, New York.

[109] S. Ahuja and N. D. Jespersen, 2006 "Modern instrumental analysis" Elsevier, UK, Vol. 47, pp92-105.

[110] J. D. Menczel and R. B. Prime, 2009 "Thermal analysis of polymers, fundamentals and applications" Wiley & Sons Ltd, USA, pp241-256.

[111] A. Riga, R. Collins and G. Mlachak, 1998 "Oxidative behaviour of polymers by thermogravimetric analysis, differential thermal analysis and pressure differential scanning calorimetry" Thermochimica Acta , Vol. 324, pp135-149.

[112] H. S. Kim, S. H. Yoon, S. M. Kwon, and H. J. Jin, 2009 "pH-sensitive multiwalled carbon nano-tube dispersion with silk fibroins", Biomacromolecules, Vol. 10, pp82–86.

[113] R. D. Adamas and N. A. Peppiatt, 1974 " Stress analysis of adhesive-bonded lap joints" Journal of Strain Analysis, Vol. 9, No. 3, pp185-196.

[114] ASTM D1002 - 05, " Annual Book of ASTM Standards".

[115] ASTM D2094 - 00, 2006 "Annual Book of ASTM Standards".

[116] H. Schroettner, M. Schmied and S. Scherer, 2006 "Comparison of 3D Surface Reconstruction Data from Certified Depth Standards Obtained by SEM and an Infinite Focus Measurement Machine (IFM)" Microchim Acta, Vol. 155, pp279–284.

[117] S. Scherer "Analysis of fractured surfaces with topomicroscopy" Alicona Imaging GmbH, Teslastrasse 8 A-8074 Grambach/Graz, Austria, www.alicona.com.

[118] A. Pizzi and K. L. Mittal, Second edition, 2003 "Handbook of adhesive technology", USA.

[119] A. J. Kinloch, 1986 "Durability of structural adhesives" Elsevier Science Publishing Co, New York.

[120] J. Watts, J. Wolstenholme, 2003, "An Introduction to surface analysis by XPS and AES," John Wiley & Sons Ltd, UK, pp212.

[121] M. P. Sepe, 1997 "Thermal analysis of polymers" Rapra Review Reports, Vol. 8, No. 11.

[122] S. Nemeth and Y.C. Liu, 2009 "Mechanical properties of hybrid sol–gel derived films as a function of composition and thermal treatment" Thin Solid Films, Vol. 517, pp 4888–4891.

[123] G. Orcel, J. Phalippou and L.L. Hench, 1986 "Structural changes of silica xerogels during low temperature dehydration" Journal of non-crysalline solids, Vol. 88, No. 2, pp 114-130.

[124] R. F. S. Lenza and W.L.Vasconcelos, 2001 "Preparation of Silica by Sol-Gel Method Using Formamide" Materials Research, Vol. 4, No. 3, pp189-194.

[125] J. Anggono, 2005 "Mullite Ceramics: Its Properties, Structure, and Synthesis" Journal Teknik Mesin, Vol. 7, No. 1, pp1 – 10.

[126] T. Gunji, I. Sopyan and Y. Abe, 2003 "Synthesis of polytitanosiloxanes and their transformation to SiO2-TiO2 ceramic fibers" Journal of Polymer Science Part A: Polymer Chemistry, Vol. 32, No. 16, pp 3133-3139.

[127] C. S. WU, 2005 "Synthesis of Polyethylene-Octene Elastomer/SiO2-TiO2 Nanocomposites via In Situ Polymerization: Properties and Characterization of the Hybrid" Journal of Polymer Science: Part A: Polymer Chemistry, Vol. 43, pp1690–1701.

[128] Q. Chen, C. Boothroyd, A. M. Soutar and X. T. Zeng, 2010 "Sol–gel nanocoating on commercial TiO2 nanopowder using ultrasound" J. Sol-Gel Sci. Technol., Vol. 53, pp115–120.

[129] B. Ellis, First Edition, 1993 "Chemistry and technology of epoxy resins" Chapman & Hall, London, UK, pp 5.

[130] M. Ochi, R. Takahashi and A. Terauchi, 2001 "Phase structure and mechanical and adhesion properties of epoxy/silica hybrids" Polymer, Vol. 42, No.12, pp 5151-5158.

[131] R. Lambert and W. L. Vasconcelos, 1997 "Sol-Gel Transition and Structural Evolution on Multi component Gels Derived from the Alumina-Silica System" Journal of Sol-Gel Science and Technology, Vol. 9, No. 3, pp239–249.

[132] J. Sandler, M. S. P. Shaffer, T. Prasse, W. Bauhofer, K. Schulte and A. Windle, 1999 "Development of dispersion process for carbon nanotubes in epoxy matrix and the resulting electrical properties" Polymer, Vol. 40, pp 5967-5971.

[133] M. R. Loos, L. A. F. Coelho, S. H. Pezzin and S. C. Amico,2008 "Effect of Carbon Nanotubes Addition on the Mechanical and Thermal Properties of Epoxy Matrices" Materials Research, Vol. 11, No. 3, pp347-352.

[134] A. Baldan, 2004 "Review, adhesively-bonded joints in metallic alloys, polymers and composite materials: Mechanical and environmental durability performance" J. Mater. Sci., Vol. 39, pp 4729-4797.

[135] M. Muller, P. Hrabe, R. Choteborsky and D. Herak, 2006 "Evaluation of factors influencing adhesive bond strength" Res. Agr. Eng., Vol. *52*, No.1, pp30–37.

[136] C. Hernandez and A. C. Pierre, 2000 "Influence of the sol-gel acidic synthesis conditions on the porous texture and acidity of SiO2-Al2O3 catalysts with a low Al proporation" Langmuir, Vol. 16, pp530-536.

[137] A. J. Kinloch, First Edition,1987 " Adhesion and adhesives: science and technology" Chapman & Hall, London, UK, pp 59.

[138] ISO 6344-1998, coated abrasives, Grain size analysis, Part 1, Grain size distribution test.

[139] J. Zhagn, X. Zhao, Y. Zuo, J. Xiong and X. Zhang, 2008 "Effect of surface pretreatment on adhesive properties of aluminum alloys" J. Mater. Sci. & Tech., Vol. 24 No.2, pp236-240.

[140] T. H. Kim, J. H. Kweon and J. H. Choi, 2008 "An experimental study on the effect of overlap length on the failure of composite-to-aluminum single-lap bonded joints" J. Reinforced Plastics and Composites, Vol. 27, No. 10, pp1071-1081.

[141] G. Doyle, R. A. Pethrick, 2009 "Environmental effects on the ageing of epoxy adhesive joints" Int. J. of Adhesion & Adhesives, Vol. 29, pp77–90.

[142] S. W. Tsui, H. M. White and A. F. Johnson, 2009 "Enhanced bonding of polypropylene to polypropylene and other materials with novel thermoplastic heat activated adhesives" School of Chemistry, University of Leeds, http://www.speautomotive.com/SPEA_CD/SPEA2002/pdf/f04.pdf

[143] M. C. Gutierrez, S. Henning and G. H. Michler, 2003 "Craze Formation in Long Chain Branched Poly (Styrene) as Revealed by In Situ Transmission Electron Microscopy: Influence of Deformation Temperature" Journal of Macromolecular Science, Part B-Physics, Vol. B42, No. 1, pp 95–105.

[144] P. E. Cassidy, J. Johnson and C. E. Locke, 1972 " The Relationship of Glass Transition Temperature to Adhesive Strength" The Journal of Adhesion. Adhesion, Vol. 4, pp183-191.

[145] R. Kahraman and M. Al-Harthi, 2005 "Moisture diffusion into aluminium powder-filled epoxy adhesive in sodium chloride solutions" International Journal of Adhesion & Adhesives, Vol. 25, pp 337–341.

[146] Zhi-Cheng, D. Hayward, R. Gilmore and R. A. Pethrick, 1997 " Investigation of moisture ingress into adhesive bonded structures using high frequency dielectric analysis" Journal of Materials Science, Vol. 32, pp 879- 886.

[147] J. Comyn, 1983 "Kinetics and mechanisms of environmental attack. In: Kinloch, J. (ed.) Durability of Structural Adhesives. Applied Science, London (1983).

[148] C. L. Soles and A. F. Yee, 2000 "A Discussion of the Molecular Mechanisms of Moisture Transport in Epoxy Resins" Journal of Polymer Science: Part B: Polymer Physics, Vol. 38, pp792–802.

[149] A. B. de Morais, A.B. Pereira, J. P. Teixeira and N. C. Cavaleiro, 2007 "Strength of epoxy adhesive-bonded stainless-steel joint" Int. J. Adhesion & Adhesives, Vol 27, No. 8, pp 679–686.

[150] W. Souheng, 1982 " Polymer Interface and Adhesion" Published by CRC Press.

[151] I. M. Ward, Second edition 1983" Mechanical properties of solid polymers,, John Wiley &Sons, Bristol, UK, pp430.

[152] L. F. M. da Silva and R. D. Adams, 2005 "Measurement of the mechanical properties of structural adhesives in tension and shear over a wide range of temperatures", J. Adhes. Sci. Technol., Vol. 19, No. 2, pp109-14.

[153] T. H. Lee, E.S. Kang and B.S. Bae, 2003 "Catalytic Effects of Aluminum Butoxyethoxide in Sol-Gel Hybrid Hard Coatings" Journal of Sol-Gel Science and Technology; Vol. 27, pp23-29.

[154] D. Hoebbel, M. Nacken and H. Schmidt, 2001 "On the Influence of metal alkoxides on the epoxide ring-opening and condensation Reactions of 3-Glycid-oxypropyltrimethoxy-silane" Journal of Sol-Gel Science and Technology; Vol.21; pp177–187.

[155] W. C. de Goeij, T. Van and A. Beukers, 1999 "Composite adhesive joints under cyclic loading" Mater. Des., Vol. 20, pp213–221.

[156] J. Mackerle, 1997 "Finite element analysis and simulation of adhesive bonding, soldering and brazing" Modelling Simul. Mater. Sci. Eng., Vol. 5, pp159–185.

[157] A. J. Kinloch and S. O. Osiyemi, 1993 "Predicting the fatigue life of adhesively-bonded joints" J. Adhes., Vol. 43, pp79–90.

[158] A. D. Crocombe and G. Richardson, 1999 "Assessing stress state and mean load effects on the fatigue response of adhesively bonded joints" Int. J. Adhesion & Adhesives, Vol. 19, pp19–27.

[159] Q. Zeng and C. T. Sun, 2004 "Fatigue performance of a bonded wavy composite lap joint" Fatigue & Fracture of Eng. Mat. & Structures, Vol. 27, No. 5, pp413 - 422.

[160] L. I. Domozhirov,1978 "Effect of loading frequency upon fatigue crack development" Strength of materials, Vol. 10, No. 9, pp 1022-1025.

[161] Y. Yan, S. Qiu, W.Cui, Q. Zhao, X. Cheng, R. K. Yiu Li, X. Xie and Y. W. Mai, 2009 "A facile method to fabricate silica-coated carbon nanotubes and silica nanotubes from carbon nanotubes templates" J. Mater. Sci., Vol. 44, pp4539-4545.

[162] N. Farhadyar, A. Rahimi, and A. E. Langroudi, 2005 "Preparation and characterization of aromatic amine cured epoxy-silica hybrid inorganic-organic coating via in situ sol-gel process" Iranian Polymer Journal, Vol. 14, No. 2, pp 155-162.

[163] J. Choi, J. Harcup, A.F. Yee, Q. Zhu, and R. M. Laine, 2001 "Organic/inorganic hybrid composites from cubic silsesquioxanes" J. Am. Chem. Soc., Vol. 123, pp 11420-11430.

[164] S. R. Lu , C. Wei, J. H. Yu, X. W. Yang and Y. M. Jiang, 2007 "Preparation and characterization of epoxy nanocomposites by using PEO-grafted silica particles as modifier" J. Mater. Sci., Vol. 42, pp 6708–6715.

[165] W. Araki and T. Adachi, 2008 "Viscoelasticity of Epoxy Resin/Silica Hybrid Material Prepared via Sol–Gel Process: Considered in Terms of Morphology" Journal of Applied Polymer Science, Vol. 107, pp253–261.

[166] J. K. F. Tait, H. G. M. Edwards, D. W. Farwell and j. Yarwood, 1995 "Fourier transform Raman spectroscopic examination of two amine-based epoxy resin crosslinking agents" Spectrochimica Acta, Part A, Vol. 51, pp2101-2106.

[167] S. M. Yuen, C. C. M. Ma, C. C. Teng, H. H. Wu, H. C. Kuan and C. L. Chiang, 2008 "Molecular motion, morphology, and thermal properties of multiwall carbon nanotube/ polysilsesquioxane composite" J. Polymer Science: Part B: Polymer Physics, Vol. 46, pp 472–482.

[168] M. Gnyba, M. J. Szczerska, M. Keranen and J. Suhonen, 2003 "Sol-gel materials investigation by means of Raman spectroscopy" XVII IMEKO World Congress, Metrology in the 3rd Millennium, June 22−27, Dubrovnik, Croatia.

[169] C. Hernandez and A. C. Pierre, 2000 "Influence of the Sol-Gel Acidic Synthesis Conditions on the Porous Texture and Acidity of SiO2-Al2O3 Catalysts with a Low Al Proportion" Langmuir, Vol. 16, pp 530-536

[170] H. E. Szwarckopf, 2004 "XPS photoemission in carbonaceous materials: A 'defect' peak beside the graphitic asymmetric peak" Carbon, Vol. 42, No. 8-9, pp 1713-1721.

[171] C. Morant, J. Andrey, P. Prieto, D. Mendiola, J. M. Sanz, and E. Elizalde, 2006 "XPS characterization of nitrogen-doped carbon nanotubes" Phys. Stat. Sol., Vol. 203, No. 6, pp1069–1075.

[172] W. He, Z. Guo, Y. Pu, L. Yan and W. Si, 2004 "Polymer coating on the surface of zirconia nano-particles by inductively coupled plasma polymerization" Appl. Phys. Lett., Vol. 85, No. 6, 9.

[173] J. Binner and Y. Zhang, 2001 "Characterization of silicon carbide and silicon powders by XPS and zeta potential measurement" J. Mat. Sci. Lett., Vol. 20, pp 123-126.

[174] S. M. Yuen, C. C. M. Ma, C. L. Chiang, C. C. Teng and Y. H. Yu, 2008 "Poly(vinyltriethoxysilane) modified MWCNT/polyimide nanocomposites preparation, morphological, mechanical, and electrical properties" J. Pol. Sci., Part A: Polymer Chemistry, Vol. 46, pp 803–816.

[175] H. Meng, G. X. Sui, P. F. Fang and R. Yang, 2008 "Effects of acid- and diamine-modified MWNTs on the mechanical properties and crystallization behavior of polyamide 6 " Polymer, Vol. 49 , pp 610-620.

[176] J. Bhatarai and B. R. Bhattarai, 2001 "X-ray photoelectron spectroscopy investigation on sintered bodies of porcelain raw materials of nepal" Analytical Sciences, Japan Society for Analysis Chemistry, Vol.17 , pp 361-363.

[177] Y. A. Teterin, K. E. Ivanova, A. Yu. Teterina, A. M. Lebedeva, I. O. Utkina and B. L. Vukchevich, 1999 "Auger and X-ray photoelectron spectroscopy study of the density of oxygen states in bismuth, aluminium, silicon and uranium oxides" J. Electron Spectroscopy and Related Phenomena, Vol.101–103, pp 401–405.

[178] L. G. Gosset, J. F. Damlencourt, O. Renault, D. Rouchon, P. Holliger, A. Ermolieff, I. Trimaille, J. J. Ganem, F. Martin and M. N. Semeria, 2002 "Interface and material characterization of thin Al2O3 layers deposited by ALD using TMA/H2O" J. Non-Crystalline Solids, Vol. 303, pp17–23.

[179] J. Ma, Q. Y. Feng, L. H. Shi and J. Xu, 2002 "Preliminary Study on Pyrolysis of Polymethylsilsesquioxane by FT-IR and XPS" Chinese Chemical Letters, Vol. 13, No. 1, pp 75 – 78.

[180] S. Y. Jing, H. J. Lee and C. K. Choi, 2002 "Chemical Bond Structure on Si-O-C Composite Films with a Low Dielectric Constant Deposited by Using Inductively Coupled Plasma Chemical Vapor Deposition" J. Korean Physical Society, Vol. 41, No. 5, pp. 769-773.

[181] D. G. Georgiev, K. Kolev, and L. D. Laude, 1998 "X-ray photoelectron spectroscopy study of excimer laser treated alumina films" Appl. Phys. Lett., Vol. 72, No 1, pp 31-33.

[182] A. Franquet, M. Biesemans, H. Terryn, R. Willem and J. Vereecken, 2006 "Study of the interaction of hydrolysed silane solutions with pre-treated aluminium substrates" Surf. Interface Anal., Vol. 38, pp172–175.

[183] P. Schreck, C. V. Guterl, P. Ehrburger and J. Lahaye, 1992 "Reactivity and molecular structure of silicon carbide fibres derived from polycarbosilanes" Part II XPS Analysis, J. Mat. Sci., Vol. 27, pp 4243-4246.

[184] S. Thomas and P. M. A. Sherwood, 1992 "Valence Band Spectra of Aluminium Oxides, Hydroxides, and Oxyhydroxides Interpreted by X-alpha Calculations" Anal. Chem., Vol. 64, pp 2480-2495.

[185] G. Li, X. Wang, A. Li, W. Wang and L. Zheng, 2007 "Fabrication and adhesive properties of thin organosilane films coated on low carbon steel substrates" Surface & Coatings Technology, Vol. 201, pp 9571–9578.

[186] M. Mostafa, PhD thesis, 2009 " Hybrid Sol-Gel/Polyaniline Coating for the Corrosion Protection of AA2024" Sheffield Hallam University.

[187] W. Zhang, W. Liu and Q. Xue, 2001 "Characterization and tribological investigation of Al2O3 and modified Al2O3 sol-gel films" Materials Research Bulletin, Vol. 36, pp1903–1914.

[188] H. Sun, X. Quan, S. Chen, H. Zhao and Y. Zhao, 2007 "Preparation of well-adhered g-Al2O3 washcoat on metallic wire mesh monoliths by electrophoretic deposition" Applied Surface Science, Vol. 253, pp 3303–3310.

[189] M. Sabzi, S. M. Mirabedini, J. Zohuriaan-Mehr and M. Atai, 2009 "Surface modification of TiO2 nano-particles with silane coupling agent and investigation of its effect on the properties of polyurethane composite coating" Progress in Organic Coatings, Vol. 65, pp 222–228.

[190] Y. U. Ahn, E. J. Kim, H. T. Kim, and S. H. Hahn, 2003 "Variation of structural and optical properties of sol-gel TiO2 thin films with catalyst concentration and calcination temperature" Materials Letters, Vol. 57, No. 30, pp 4660-4666.

[191] Y. N. Qi, F. Xu, L. X. Sun, J. L. Zeng and Y. Y. Liu, 2008 " Thermal stability and glass transition behaviour of PANI/Al2O3 composites" Journal of Thermal Analysis and Calorimetry, Vol. 94 ,No. 2, pp553–557.

[192] D. Zhang, 2006 "Preparation of Core–Shell Structured Alumina–Polyaniline Particles and Their Application for Corrosion Protection" Journal of Applied Polymer Science, Vol. 101, pp 4372–4377.

[193] J. K. Pandey, K. R. Reddy, A. P. Kumar and R. P. Singh, 2005 "An overview on the degradability of polymer nanocomposites" Polymer Degradation and Stability, Vol. 88, pp234-250.

[194] S. Ebrahim, 2009 "Electrical Transport Mechanism in Polyaniline/Formvar Blend Films" High Performance Polymers, Vol. 21, pp468–483.

[195] Z. Zhang, X. Wang, J. Xie and G. Liang, 2007 "Using Octa (aminpropyl) silsesquioxane as the Curing Agent for Epoxy Resin" Journal of Reinforced Plastics and Composities, Vol. 26, No. 16, pp1665-1670.

[196] C. P. Wong, 1998 "Polymers for encapsulation: Materials Processes and Reliability" Georgia Institute of Technology. Chip Scale Review, Vol. 2, No. 1, pp 30-7.

[197] Q. L. Ji, M. Q. Zhang, M. Z. Rong, B. Wetzel and K. Friedrich, 2004 "Tribological properties of surface modified nano-alumina/epoxy composites" Journal of materials science, Vol. 39, pp 6487 – 6493.

[198] B. Wetzel, F. Haupert and M. Q. Zhang, 2003 "Epoxy nanocomposites with high mechanical and tribological performance" Composites Science and Technology, Vol. 63, No14, pp2055-2067.

[199] M. C. Kuo, C.M. Tsai, J. C. Huang and M. Chen, 2005 "PEEK composites reinforced by nano-sized SiO2 and Al2O3 particulates" Materials Chemistry and Physics, Vol. 90, pp185–195.

[200] Q. Ji, M.Q. Zhang, M.Z. Rong, B. Wetzel, K. Friedrich, 2004 "Tribological properties of surface modified nano-alumina/epoxy composites" J. Mater. Sci., Vol. 39, pp6487 – 6493.

[201] Z. S. Pitalsky, C. Aggelopoulos, G.Tsoukleri, C. Tsakiroglou, J. Parthenios, S. Georga, C. Krontiras, D. Tasis, K. Papagelis and C. S. Galiotis, 2009 " The effect of oxidation treatment on the properties of multi-walled carbon nanotube thin films" Materials Science and Engineering B, Vol. 165, pp 135–138.

[202] I. Sridhar and K. R. Narayanan, 2009 "Processing and characterization of MWCNT reinforced aluminium matrix composites" J. Mater. Sci., Vol. 44, pp1750–1756.

[203] L. Shu-quan, J. Chun-yan, T. Yan, Z. Yong, Z. Jie and P. An-qiang, 2007 "Mechanical and electrical properties of carbon nanotube reinforced epoxide resin composites" Trans. Nonferrous Met. Soc. China, Vol. 17, pp 675-679.

[204] M. F. Yu, M. J. Dyer and R. S. Ruoff, 2001 "Structure and mechanical flexibility of carbon nanotube ribbons: An atomic-force microscopy study " Journal of applied physics, Vol. 89, No. 815, pp 4554-4557.

[205] M. A. Uddin , M. O. Alam , Y. C. Chan and H. P. Chan, 2004 "Adhesion strength and contact resistance of flip chip on flex packages - effect of curing degree of anisotropic conductive film" Microelectronics Reliability, Vol. 44, No. 3, pp505-514.

[206] M. Inoue and K. Suganuma, 2009 "Influential factors in determining the adhesive strength of ACF joints" J. Mater. Sci. Mater. Electron, Vol. 20, pp1247–1254.

[207] I. Stewart, A. Chambers and T. Gordon, 2007 "The cohesive mechanical properties of a toughened epoxy adhesive as a function of cure level". Int. J. Adhesion and Adhesives, Vol. 27, pp 277–287.

[208] G. W. Critchlow and D. M. Brewis, 1995 "Influence of surface macroroughness on the durability of epoxide-aluminium joints" Int. J. Adhesion and Adhesives. Vol. 15, pp173-176.

[209] A. Rathke, Y. Tymina and B. Haller, 2009 " Effect of different surface treatments on the composite–composite repair bond strength" Clin. Oral. Invest., Vol. 13, pp317–323.

[210] E. G. Baburaj, D. Starikov, J. Evans, G. A. Shafeev and A. Bensaoula, 2007 "Enhancement of adhesive joint strength by laser surface modification" Int. J. Adhesion and Adhesives. Vol. 27, pp268-276.

[211] R. A. Difelice, PhD Thesis, 2001 "An investigation of plasma pretreatments and plasma polymerized thin films for titanium/polyimide adhesion" , Blacksburg, Virginia

[212] B. N. J. Perssona and E. Tosatti, 2001 "The effect of surface roughness on the adhesion of elastic solids" J. Chem. Phys., Vol. 115, No. 12, pp5597- 5610.

[213] T. Komatsu, 1996 "Effects of surface treatments of super drawn polyoxymethylene fibers on adhesion to epoxy resins" J. App. Polymer Science, Vol. 59, pp1137-1143

[214] R. W. Messter, 2004 "Joining of materials and structures" Elsevier Butterworth-Heinemann, Linacre House, Oxford, UK, pp177-227.

[215] F. M. da-Silva , R. J. C. Carbas, G. W. Critchlow, M. A. V. Figueiredo and K. Brown, 2009 "Effect of material, geometry, surface treatment and environment on the shear strength of single lap joints" Int. J. Adhesion and Adhesives, Vol. 29, pp621-632.

[216] G. Fessel, J. G. Broughton, N. A. Fellows, J. F. Durodola, A. R. Hutchinson, 2007 "Evaluation of different lap-shear joint geometries for automotive applications" Int. J. of Adhesion and Adhesives, Vol. 27, pp574–583.

[217] W. Zhang, A. Joshi, Z. Wang, R. Skane and N. Koratkar, 2007 "Creep mitigation in composites using carbon nanotube additives" Nanotechnology,Vol.18, No 185703, 5pp.

[218] M. T. Galkowski, P. J. Kulesza, K. Miecznikowski, M. Chojak and H. Bala, 2004 " Protective properties of redox polymer film deposited on stainless steel" J. Solid State Eletrochem, Vol. 8, pp 430–434.

[219] R. Vera, R. Schrebler, P. Cury, R. Del Rıo and H. Romero, 2007 "Corrosion protection of carbon steel and copper by polyaniline and poly(ortho-methoxyaniline) films in sodium chloride medium. Electrochemical and morphological study" J. Appl. Electrochem, Vol. 37, pp519–525.

[220] S. Sathiyanarayanan, S. S. Azim and G. Venkatachari, 2008 "Performance Studies of Phosphate-Doped Polyaniline Containing Paint Coating for Corrosion Protection of Aluminium Alloy" Journal of Applied Polymer Science, Vol. 107, pp 2224–2230.

[221] C. M. Lawrence Wu and M. L. Chau, 2002 "Degradation of flip-chip-on-glass interconnection with ACF under high humidity and thermal aging" Soldering and Surface Mount Technology, Vol. 14/2, pp 51–58.

[222] M. K. Harun, J. Marsh and S. B. Lyon, 2005. "The effect of surface modification on the cathodic disbondment rate of epoxy and alkyd coatings" Prog. in Organic Coatings, Vol. 54, pp317–321.

[223] E. M. Petrie, Second Edition, 2007 "Handbook of adhesives and sealants" Chapter 25, Effects of the environment, McGraw-Hill companies, pp736-804.

[224] L. Domingues, J. C. S. Fernandes, M. Da Cunha Belo, M. G. S. Ferreir and L. Guerra-Rosa, 2003. "Anodising of Al 2024-T3 in a modified sulphuric acid/boric acid bath for aeronautical applications" Corrosion Science, Vol. 45, pp149–160.

[225] X. F. Yanga, D. E. Tallmana, V. J. Gellinga, G. P. Bierwagenb, L. S. Kastenc, J. Berga, 2001 "Use of a sol-gel conversion coating for aluminium corrosion protection" Surface and Coatings Technology, Vol. 140, pp44-50.

[226] M. A. Uddin, H. P. Chan and C. K. Chow, 2004 " Thermal and Chemical Stability of a Spin-Coated Epoxy Adhesive for the Fabrication of a Polymer Optical Waveguide" Chem. Mater., Vol.16, pp4806-4811.

[227] A. J. Kinloch, First Edition, 1987 "Adhesion and adhesives: science and technology" Chapman & Hall, London, UK, pp 206-210.

[228] Q. Zeng and C. T. Sun, 2004 "Fatigue performance of a bonded wavy composite lap joint" Fatigue Fract. Eng. Mat. Struct., Vol. 27, No. 5, pp413–422.

[229] O. H. Varga, 1966 "Stress-strain behavior of elastic materials: selected problems of large deformations" polymer review, New York; Inter-science Publishers, USA.

[230] R. O. Ebewele, 2000 "Polymer science and technology" Chapman & Hall/CRC, pp390.

[231] B. Harris, First edition, 2003 "Fatigue in composites: science and technology of the fatigue" Woodhead publishing limited, Cambridge, UK, pp630-631.

[232] S. Ganguli, H. Aglan and D. Dean, 2005 "Microstructural origin of strength and toughness of epoxy nanocomposites" J. Elastomers Plast, Vol. 37, No. 1, pp19–35.

[233] A. J. Kinloch, 1997 "Adhesives in engineering" Proc. Instn. Mech. Engrs., Vol. 211, Part G, pp307-335.

[234] I. Hamerton, 1997 "Recent developments in epoxy resins" Report 91, Rapra Technology Limited, Shawbury, UK.

[235] B. L. Denq , Y. S. Hu, L. W. Chen, W. Y. Chiu and T. R. Wu, 1999 "The curing reaction and physical properties of DGEBA/DETA epoxy resin blended with propyl ester phosphazene" J. Applied Polymer Science, Vol. 74 No.1, pp 229-237.

[236] N. Farhadyar, A. Rahimi, and A. E. Langroudi, 2005 "Preparation and characterization of aromatic amine cured epoxy-silica hybrid inorganic-organic coating via in situ sol-gel process" Iranian Polymer Journal, Vol. 14, No. 2, pp 155-162.

[237] Y. Wang, Z. Iqbal and S. V. Malhotra, 2005 "Functionalization of carbon nanotubes with amines and enzymes" Chemical Physics Letters, Vol. 402, pp 96–101.

[238] D. R. S. Jeykumari and S. S. Narayanan, 2007 "Covalent modification of multiwalled carbon nanotubes with neutral red for the fabrication of an amperometric hydrogen peroxide sensor" Nanotechnology, Vol.18 ,No.125501, 10pp.

[239] R. J. Chen, Y. Zhang, D. Wang and D. Hongjie, 2001 "Non-covalent Sidewall Functionalization of Single-Walled Carbon Nanotubes for Protein Immobilization" J. Am. Chem. Soc., Vol.123, pp3838-3839.

[240] W. M. Chiu and Y. A. Chang, 2008 "Chemical modification of multiwalled carbon nanotube with the liquid phase method" Journal of Applied Polymer Science, Vol. 107, pp1655–1660.

[241] A. Gomathi, S. R. C. Vivekchand, A. Govindaraj, and C. N. R. Rao, 2005 " Chemically Bonded Ceramic Oxide Coatings on Carbon Nanotubes and Inorganic Nanowires" Adv. Mater., Vol. 17, pp2757–2761.

[242] K. Balani and A. Agarwal , 2008 "Wetting of carbon nano-tubes by aluminium oxide" Nanotechnology, Vol. 19, pp165701/8.

[243] H. B. Zhang, G. D. Lin, Z. H. Zhou, X. Dong and T. Chen, 2002 "Raman spectra of MWCNTs and MWCNT-based H2 -adsorbing system" Carbon, Vol. 40, pp 2429–2436.